# EFFECT OF ADMIXTURES, CHLORIDES, AND MOISTURE ON DIELECTRIC PROPERTIES OF PORTLAND CEMENT CONCRETE IN THE LOW MICROWAVE FREQUENCY RANGE

By

Kiran Pokkuluri

Thesis submitted to the Faculty of the

Virginia Polytechnic Institute and State University

In partial fulfillment of the requirements for the degree of

MASTER OF SCIENCE

In

Civil Engineering

APPROVED

______________________

Dr. Imad L. Al-Qadi, Chairman

Professor of Civil Engineering

______________________ ______________________

Dr. Sedki M. Riad
Professor of Electrical Engineering

Dr. Gerardo W. Flintsch
Assistant Professor of Civil Engineering

October, 1998

Keywords: Nondestructive Evaluation, Portland Cement Concrete, Electromagnetic waves, Transmission lines, Dielectric properties

# Effect of Admixtures, Chlorides, and Moisture on Dielectric Properties of Portland Cement Concrete in the Low Microwave Frequency Range

**Kiran S. Pokkuluri**


## (ABSTRACT)

The use of electromagnetic waves as a nondestructive evaluation technique to evaluate Portland cement concrete (PCC) structures is based on the principle that a change in the structure, composition, or properties of PCC results in a change in its dielectric properties. The coaxial transmission line is one of the few devices that can measure the dielectric properties of PCC at a frequency range of 100-1000 MHz. A coaxial transmission line developed at Virginia Tech was used to study the effect of moisture, type of aggregate, water/cement ratio, curing period, admixture type (microsilica, superplasticizer, and shrinkage admixture), and chloride content on the dielectric properties of PCC.

Measurements were conducted in the time domain and converted to the frequency domain using Fast Fourier Transform. The research found that an increase in the moisture content of PCC resulted in an increase in the dielectric constant. Mixes containing limestone aggregate had a greater dielectric constant than those containing granite. The dielectric constant decreased with curing period due to the reduction in free water availability. Mixes containing higher water/cement ratios exhibited a higher dielectric constant, especially in the initial curing period. The admixtures did not significantly affect the dielectric constant after one day of curing. After 28 days of curing, however, all three admixtures had an effect on the measured dielectric constant as compared to control mixes. Chloride content had a significant effect on the loss part of the dielectric constant especially during early curing. A relationship was also established between the chloride permeability (based on conductance measurements) of PCC and its dielectric constant after 75 days of moist curing.

# ACKNOWLEDGEMENTS

I would like to thank my advisor Dr. Imad L. Al-Qadi for his support and encouragement during the duration of my study. This work would not have been possible without his guidance and input. I would also like to thank my committee members, Dr. Sedki M. Riad, and Dr. Gerardo W. Flintsch for their advice and assistance during the completion of this work.

Special thanks are due to Amara Loulizi for his invaluable comments and help throughout this work. The assistance of Dr. Robert Marshall, Raqibul Mostafa, and Jason Yoho is greatly appreciated.

Finally, I want to thank my colleagues in the Materials Engineering, Agata, Alex, Amara, Brian, Erin, James, Mike, Mostafa, Ramzi, Salman, Stacey, and Walid whose encouragement and support made my stay in Blacksburg a pleasant and enriching experience.

# TABLE OF CONTENTS

# LIST OF FIGURES

# LIST OF TABLES

# CHAPTER 1. INTRODUCTION

## 1.1 Background

Portland Cement Concrete (PCC) is the most popular building material and accounts for a large part of the infrastructure system. Roads are an important part of the infrastructure system and concrete pavements constitute 6% of the total pavement length in the United States. There are also about 575,000 bridges in the United States, a majority of which are built with concrete. Unfortunately, the transportation infrastructure in the United States is currently deteriorating at an alarming rate. Before any repairs can be undertaken on a PCC structure, its condition needs to be evaluated to determine the existing conditions and understand the mechanisms of deterioration. Nondestructive testing is one of the techniques that can be used for assessing the structural condition. Nondestructive techniques are becoming increasingly popular due to their ability to provide information not discernible to the unaided eye and conventional assessment techniques. While nondestructive techniques are not perfect, they have great potential for in-situ applications.

Among the nondestructive evaluation techniques is the use of electromagnetic waves. Electromagnetic properties of materials show the interaction of a material with applied external electric and magnetic fields. The main property of interest related to applications in PCC is the complex dielectric constant. Changing properties and deterioration in PCC results in a change in its electromagnetic properties. The amplitude and the phase measurement of the reflected and the transmitted electromagnetic waves can provide information about internal flaws, material compositon, porosity, state of curing, and moisture content of PCC. Therefore, electrically characterizing PCC would allow for a better knowledge of its internal structure. In addition, changes in dielectric properties of PCC at different frequencies may assist in optimizing the frequency at which deterioration can be detected. The coaxial transmission line device is one of the few techniques that can measure the dielectric properties of PCC at frequencies greater than 100 MHz.

The coaxial transmission line is mainly used for low loss transmission of power. However, it has also been used as a tool for the dielectric characterization of materials, including PCC. Coaxial transmission lines developed by various organizations have been used to test for the effect of such factors as curing time, aggregate type, chlorides, and moisture content on the complex dielectric constant. The transmission lines developed for testing PCC have larger than normal dimensions to accommodate the size of the aggregates in the PCC mixes.

## 1.2 Problem Statement

Currently there is little information on the electrical characterization of PCC in the frequency range of 100-1000 MHz. The only studies carried out in this frequency range are the ones done by Al-Qadi and Riad (1996), Al-Qadi *et al.* (1994), Shaw *et al.* (1993), and Robert *et al.* (1996). In addition, except the studies at Virginia Tech and the one by Robert *et al.* (1996), most of the research on electrical characterization of PCC by transmission lines has been confined to specimens having a maximum aggregate size of 10 mm or on cement pastes and mortar specimens due to the size limitations of the transmission line. The previous research conducted at Virginia Tech did not address the effect of moisture and chemical admixtures on the electrical properties of PCC.

## 1.3 Objective

The main objective of this research is to study the effect of moisture, aggregate type, time of curing, water to cement (w/c) ratio, microsilica, high range water reducer, shrinkage admixture, and presence of chlorides on the dielectric properties of PCC using the Virginia Tech coaxial transmission line. A secondary objective is to establish a relationship between the chloride permeability (based on conductance measurements) and the dielectric constant.

## 1.4 Scope

To achieve the aforementioned objectives, the Virginia Tech coaxial transmission line was used to measure the dielectric properties of different PCC mixes. Portland cement concrete mixes with varying parameters such as type of aggregate, w/c ratio, chloride content, and admixture type were cast. The effect of curing time on the complex dielectric constant was studied by taking measurements until 90 days of moist curing. To evaluate the effect of moisture content on the dielectric constant, measurements were taken at five different moisture levels. The chloride permeability was determined at 75 days of curing.

Chapter 2 describes the constituents of cement and its hydration. It discusses the permeability of PCC and the admixtures used in this research. Chapter 3 presents the electromagnetic properties of materials and the features of the different currently researched coaxial transmission lines including the modes of propagation and their parameters.

Chapter 4 focuses on the experimental program. It describes the materials used in preparing the specimens, dielectric and chloride permeability measurements (based on conductance measurements), and the rationale behind choosing the different mixes. Data analysis and results are presented in Chapter 5. In this chapter, the procedure used to analyze the measurements, the time window used for the measurements, and the factors affecting the measured dielectric properties are discussed. Chapter 6 summarizes the findings and conclusions of this study.

# CHAPTER 2. STRUCTURE AND PROPERTIES OF PORTLAND CEMENT CONCRETE

## 2.1 Portland Cement Concrete

For over a hundred and fifty years, Portland cement concrete (PCC), which is a mixture of cement, water and aggregate, has been the most commonly used building material because it is durable, cheap, and readily available and can be cast into almost any shape. The main components of PCC are the hydrated cement paste, aggregates, water, and the transition zone.

### 2.1.1 Hydrated cement paste (HCP)

The main constituent of PCC is cement, which is made up of calcium, silica, alumina, and iron oxide. Calcium carbonate materials like limestone provide the calcium, while clay is usually the source for silica, alumina, and iron oxide. The manufacture of cement involves the crushing and grinding of the raw materials to about 75 microns in size and then mixing them together in the kiln. This mix is then heated to about 1000°C. The reactions inside the kiln produce Tricalcium silicate ($3CaO.SiO_2$), Dicalcium silicate ($2CaO.SiO_2$), Tricalcium aluminate ($3CaO.Al_2O_3$), and Tetracalcium aluminoferrite ($4CaO.Al_2O_3.Fe_2O_3$). In order to simplify the usage of these terms, they have been abbreviated as $C_3S$, $C_2S$, $C_3A$, and $C_4AF$, respectively. The composition of these compounds ranges from 45-60%, 15-30%, 6-2% and 6-8%, respectively (Mehta, 1986). These compounds do not exist in a pure form. The $C_3S$ phase is a solid solution containing magnesium and aluminum and is called alite. The phase containing $C_2S$ along with aluminum, magnesium and potassium dioxide is called belite. The $C_3A$ phase is called aluminate phase and consists of magnesium, sodium, potassium, and silica along with the $C_3A$. The $C_4AF$ phase is called the ferrite phase.

The chemical reaction of cement with water is called hydration. The hydration of silicates produces a calcium silicate hydrate gel that accounts for 60-70% of the volume of solids in the HCP (Ramachandran, 1995). The reaction of the $C_3S$ with water is the following:

$$2C_3S+6H \rightarrow CSH+3CH \qquad 2.1$$

where CSH stands for $3CaO.2SiO_2.3H_2O$ and CH stands for $Ca(OH)_2$.

This gel is poorly crystalline and contains particles of colloidal size. Although its exact structure is not known, it is believed that the gel has a layer structure with a very high surface area of the order of 100-700 $m^2/g$ (Powers, 1958). The distance between the layers is of the order of 18A°. The layers are bound together by van der Waals forces, which imparts strength to the paste. The gel does not have a fixed composition and the C/S ratio keeps on decreasing as hydration progresses. The gel is also referred to as the CSH gel because the composition is not fixed.

Since hydration is an exothermic reaction, it can also be explained by calorimetric studies. There are five stages in the hydration of $C_3S$ (Ramachandran, 1995). In the first stage, $C_3S$ reacts with water and releases CSH, calcium, and hydroxyl ions into the solution while liberating a large amount of heat (equation 2.1). This stage, called the pre-induction stage, usually lasts about 15 to 20 minutes. The second stage, called the dormant or induction period, lasts a few hours. The hydration slows down considerably during this stage and there is little evolution of heat. The next stage finds the reaction accelerating and the amount of heat reaching a maximum level at its end. This peak corresponds to the final set. A deceleration in the rate of reaction occurs in the fourth stage which might take place over a few days. In the fifth stage which lasts for a few years, there is almost no reaction and very little evolution of heat.

When hydrated, $C_2S$ also gives out CSH. The reaction is given by:

$$2C_2S+4H \rightarrow CSH+CH \qquad 2.2$$

Calorimetric studies have shown similar results to that of hydration of $C_3S$, but with less heat evolution. According to stoichometric calculations, the hydration of $C_3S$ would produce 61% of CSH gel and 39% of CH, while the hydration of $C_2S$ would produce 82% of CSH gel and only 18% of CH (Mehta, 1986) Therefore, a higher quantity of $C_2S$ in the cement would result in more strength. For early strength, however, more $C_3S$ is needed, because its reaction rate is higher.

The other major component in the hydration of silicates is calcium hydroxide, which is crystalline with a hexagonal prismatic shape. It occupies 20-25% of the volume of solids in the hydrated paste (Ramachandran, 1995). It does not contribute to the strength of the PCC since it has a lower surface area than the CSH. In fact, the presence of CH may be a liability, because it is highly soluble and susceptible to acidic and sulfate attack.

Tricalcium aluminate ($C_3A$), the compound responsible for the early setting of cement, has the highest rate of reaction with water among the constituents of cement. Gypsum is added to cement to retard this rapid reaction. Tricalcium aluminate reacts with gypsum and water to form needle shaped prismatic crystals, called ettringite. The reaction is given by:

$$C_3A + 3C\overline{S}H_2 + 26H \rightarrow C_6A\overline{S}_3H_{32} \qquad 2.3$$

where $C\overline{S}H_2$ stands for $CaSO_4.2H_2O$ and $C_6A\overline{S}_3H_{32}$ stands for $3CaO.Al_2O_3.3CaSO_4.32H_2O$.

After the consumption of all gypsum into ettringite, the excess $C_3A$ reacts with ettringite to form sulfoaluminate hydrate. This reaction is given by:

$$C_6A\overline{S}_3H_{32} + 2C_3A + 4H \rightarrow 3C_4A\overline{S}H_{12} \qquad 2.4$$

where $C_4A\overline{S}H_{12}$ stands for $3CaO.Al_2O_3.CaSO_4.12H_2O$.

$C_4AF$ hydrates to give structurally similar products as $C_3A$. However, gypsum retards the reaction more effectively than it does with $C_3A$. In the first stage of the reaction, it forms a high calcium sulfoaluminate form that reacts with the excess $C_4AF$ to give a low sulfoaluminate form. These sulfoaluminates occupy about 15-20% of the volume of solids in the paste and influence the early setting and hardening reactions of the cement paste.

### 2.1.2 Aggregates

Aggregates occupy 60 to 80% of the volume of PCC (Mehta, 1986). The role of aggregate in PCC is as a filler. Aggregates can be classified on the basis of their size. Aggregates greater than 4.75 mm are called coarse aggregate and those smaller than 4.75 mm are called fine aggregate. Aggregates play a significant role in the physical properties of PCC. They affect the unit weight, elastic modulus, absorption, and the durability of PCC. The properties of PCC are also affected by the shape, texture and gradation of the aggregate. Aggregates are usually stronger than cement paste and therefore do not play a significant role in the strength of PCC. Aggregate reaction with cement may be detrimental such as alkali-silica reaction.

### 2.1.3 Water

Portland cement concrete has a number of voids that are usually filled with water. Depending on the type of voids and the degree of firmness with which the water is held in these voids, water can be classified as capillary water, adsorbed water, and interlayer water. Capillary voids are spaces in PCC that are not filled by the products of hydration. The water in these voids, called capillary water, can be further subdivided into free and bound water. Free water is the water present in voids greater than 50 nm in size, while the water in voids in the 5-50 nm range constitutes bound water. As will be explained later, bound water is crucial from the point of view of shrinkage. Free water, on the other hand is responsible for the electrical conductivity of PCC. Adsorbed water is the water bonded to the surface of the CSH gel. The water present between the layers of the CSH gel is called interlayer or zeolitic water. Adsorbed water and interlayer water do not have an impact on the conductivity.

### 2.1.4 Transition zone

The transition zone, the region that exists between the hydrated cement paste and the aggregate, is very thin, with a thickness on the order of 10 to 50 μm. The transition zone is important in that it is the weakest zone in the PCC and thus influences its stiffness and durability. In the early stages, the transition zone is made up of ettringite and calcium hydroxide, both of which contain large crystals that result in more voids in the zone. Due to the larger size and high number of voids, the van der Waals force of attraction with the aggregates is low compared to the HCP, resulting in lower strength. Hydration takes place slowly in the transition zone; thus strength increases when the voids start getting filled with CSH along with a decrease in calcium hydroxide. Cracking may start at 70% of the ultimate strength of PCC. The properties affecting the strength of the transition zone are the capillary voids, the amount of calcium hydroxide, and the presence of microcracks. The transition zone also affects the durability of PCC; the microcracks present in the transition zone increase the permeability of the PCC, thus making it easy for corrosion to take place.

## 2.2 Admixtures

Portland cement concrete by itself does not possess all the required properties. Hence admixtures are added. An admixture, as defined by ASTM, is a material other than water, aggregates, hydraulic cements, and fiber reinforcement, that is used as an ingredient of PCC or mortar and added to the batch immediately before or during mixing. There are hundreds of admixtures currently in use and it is reported that about 71% of the PCC placed in the United

States contains at least one admixture (Mehta, 1986). Admixtures fall into two categories: admixtures that act by changing the surface tension of water (e.g., superplasticizers) and those that break up into their ionic constituents and affect the chemical reactions between cement compounds and water (e.g., fly ash). In this thesis, only admixtures related to this research are discussed.

### 2.2.1 Pozzolans

Pozzolans are defined as noncementitious materials that contain constituents which combine with the calcium hydroxide in the hydrated cement paste in the presence of water to form stable insoluble compounds possessing cementing properties (Lea, 1971). Pozzolans can be divided into two groups, natural and artificial. The natural pozzolans include materials of volcanic origin and certain diatomaceous earths. Artificial pozzolans are the more commonly used types and include burnt clay and shales, fly ash, blast furnace slag, and microsilica. The pozzolan on combination with the lime forms a hydrated calcium silicate similar to the CSH gel and tetracalcium aluminate hydrate. When calcium sulphate is present, ettringite is formed initially and later transforms into the monosulphate as gypsum is removed from the solution.

Microsilica is being used more and more as a pozzolan. It is a by-product of electric arc furnaces used to reduce high purity quartz with coal in the production of elemental silicon and ferrosilicon alloys. This process produces SiO vapors that oxidize and condense into minute spherical particles of the order of 1 μm, which are called microsilica or silica fume. Microsilica particles react with the calcium hydroxide in the transition zone and form a large number of small crystals. This results in a significant improvement in the microstructure of the hydrated cement paste in the transition zone. With an increase in the amount of microsilica, there is a reduction in thickness of the transition zone and also the amount of water bound to the aggregate. This translates to increased strength and reduced permeability due to reduction in porosity. A reduction in bleeding has also been reported.

An added advantage is that microsilica, which is a waste product, can be put to good use. It is superior to fly ash (obtained by combustion of powdered coal in power plants and comes in many types) in that it does not exhibit the variability in composition and heterogeneity in mineralogical character which fly ash does. Because of its higher surface area, the rate of reaction with calcium hydroxide is significantly higher than it is with fly ash. This results in earlier attainment of higher strength. Typical addition rate of microsilica in the state of Virginia is 7% by weight of cement. Because of the increased surface area, more water is needed. Therefore, super plasticizers are also required.

### 2.2.2 Superplasticizers

Water reducing admixtures are chemicals that increase workability of PCC and allow reduction of water. Superplasticizers or High range water reducers differ from conventional water reducers in that they are capable of reducing the water requirement by up to 30% (Mehta, 1986). They can also increase the slump by up to 250 mm (Mehta, 1986). More significant than the increase in workability is the fact that PCC having lower w/c ratios can be used. Theoretically a w/c ratio of 0.27 is adequate for hydration and any water greater than this ratio lowers the potential compressive strength that can be achieved (Cement and Concrete Association Publication 45.030). It has also been observed that PCC containing superplasticizers have high ultimate strengths, excellent durability, and water proofing characteristics.

The three commonly used superplasticizers are sulfonated melamine formaldehyde, sulfonated naphtalene formaldehyde, and modified lignosulfates. Superplasticizers work on the principle of dispersion of cement particles. They are composed of long chained organic molecules that are hydrophobic at one end and hydrophillic at the other. The superplasticizer is adsorbed onto the cement particles where its anionic nature imparts a negative charge to the cement particles that results in their mutual repulsion. Thus, less water is required. Figure 2.1 shows the working of superplasticizers. It has been observed that superplasticized PCC exhibits an acceleration of the hydration process that might be attributed to the good dispersion of the cement particles. Due to the higher rate of hydration, superplasticized PCC show higher compressive strengths at one, three, and seven days than PCC containing no super plasticizer (Mehta, 1986). Superplasticizers are also needed when pozzolanic materials like microsilica and fly ash are used because of the higher water requirement due to an increased surface area.

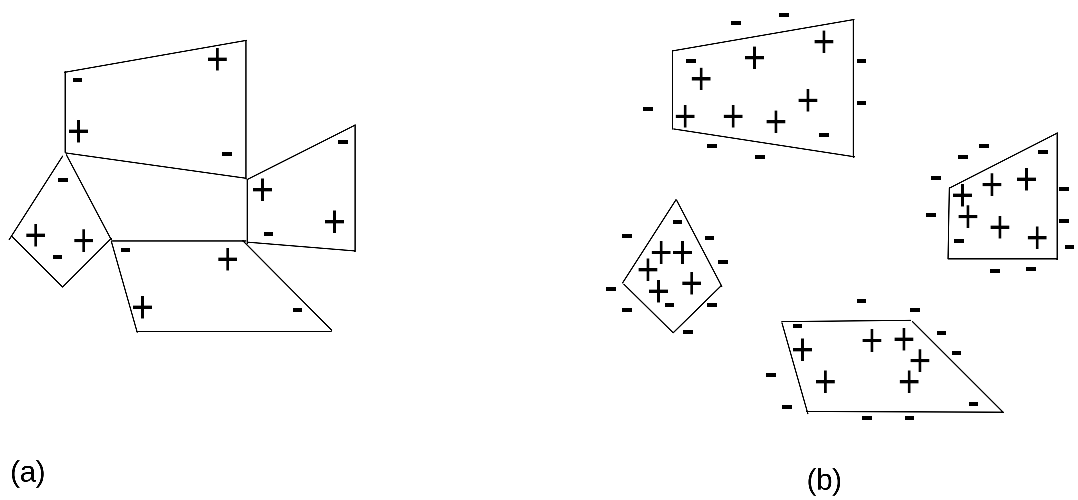


Figure 2.1. Effect of superplasticizers on cement; (a) cement particles before the addition of superplasticizers; (b) cement particles after the addition of superplasticizers; (After Kreigger, 1980).

### 2.2.3 Shrinkage admixture

Volume changes that may occur in the PCC after it has been cast are called shrinkage. There are two types of shrinkage, drying and thermal. Drying shrinkage is associated with the loss of water by either evaporation or hydration. When exposed to the environment, the cement paste will lose moisture since the humidity is normally lower than 100%. The loss of free water, the water in the larger capillary pores, does not result in shrinkage because the water is not under the influence of any adhesive forces to the cement paste. However, the water held in the capillary voids, which are of the order of 5-50 nm, is retained by capillary tension. The drying up of this water would result in a reduction of volume. When the structure is restrained and the PCC shrinks, tensile stresses form in the structure. When these stresses exceed the tensile strength of the PCC, the structure cracks. Thermal shrinkage is associated with the expansion and contraction of PCC. The heat of hydration results in the expansion of PCC after it has been placed. As it cools down, shrinkage strains develop. If the structure is restrained, stresses develop that may crack the structure.

Shrinkage reducing admixtures have been introduced recently. They have been found to be more effective for controlling drying shrinkage rather than thermal shrinkage. These admixtures work on the mechanism of the reduction of surface tension of water. As specified earlier, in voids less than 50 nm in size, as the water evaporates, curved menisci are formed and the surface tension of water pulling the walls of the voids results in shrinkage. The use of the shrinkage admixtures reduces the surface tension, resulting in reduction of the force pulling in the walls of the voids. A reduction in shrinkage of up to 80% has been observed at 28 days. The addition of these admixtures has also been found to reduce the heat of hydration. However, the use of shrinkage admixtures has been found to reduce the compressive strength by about 10%. Manufacturers therefore recommend the use of super plasticizers to reduce w/c ratio of the mix.

## 2.3 Permeability of Portland Cement Concrete

According to the ACI, permeability of water in PCC is defined as the rate of discharge of water under laminar flow conditions through a unit cross-sectional area of a porous medium under a unit hydraulic gradient and a temperature of 20°C. It is one of the most important properties of PCC relating to its durability. This is because the durability of the PCC structure is affected by the transport of water containing chloride and sulfate ions through its pore system.

While permeability depends on the porosity to a large extent, it does not depend just on the level of porosity. It also depends on the size of the pores and how well they are interconnected. While the permeability is mainly due to the capillary pores, the gel pores are also responsible. However, their permeability is only $7\times10^{-16}$ compared to $10^{-14}$ for the capillary pores (Powers, 1958). The permeability of PCC is due to both the cement paste and the aggregate. The addition of low permeable aggregate to the cement paste should decrease the permeability. However, according to Mehta (1986), the opposite is true. He attributes this increase in permeability to the presence of micro cracks in the transition zone. Also, the porosity and pore sizes are greater in the transition zone. According to Mehta (1986), there are two components of pores. One is the same for PCC with different w/c ratios, while the other changes as a function of the w/c ratio. The two pore ranges are divided at 1320A° with the pores greater than 1320A° being responsible for permeability. Permeability of the cement paste is almost zero for capillary porosities less than 10%. This level is assumed to be a transition stage between a system of interconnected pores and a system of isolated pores. The permeability also depends on the w/c ratio, the age of the PCC, and the use of pozzolans. For the same level of hydration, permeability is reduced as the w/c ratio decreases. This happens because, as the w/c ratio decreases, the cement content in PCC increases. More of the products of hydration can be formed, thereby reducing both the amount and size of voids.

The flow space in the cement paste is confined to distinct flow channels. As hydration progresses, the products of hydration subdivide the spaces between the cement particles into smaller channels. This reduces porosity and changes the pore size distribution, thereby reducing permeability. From the permeability point of view, where the CSH gel forms is more important than the amount of gel produced. If the gel formation results in blockage of capillary pores, permeability is reduced.

Portland cement concrete containing pozzolans such as fly ash, microsilica, or slag has been found to have lower permeability than PCC without these pozzolans, because the fine pozzolan particles react with the calcium hydroxide in the cement paste to form more CSH gel that fills up the voids. Ozyilidrim and Halstead (1994) have shown that PCC containing fly ash and silica fume has less permeability than PCC without fly ash and silica fume. They also observed that increasing the curing temperature up to 38°C and duration of moist curing reduces the permeability.

## 2.4 Effects of Chlorides on Portland Cement Concrete

Corrosion of the steel in reinforced PCC is a major problem and millions of dollars are spent every year to repair the deterioration it causes. Corrosion of steel is an electrochemical process. The nonuniformities in the steel, such as in the welds and in the physical and chemical properties of the surrounding PCC can produce electrical potential differences and cause corrosion. However, corrosion is prevented by a passive film of iron oxide, which is formed during the hydration of the cement. The high alkalinity of the PCC due to calcium hydroxide prevents the breakup of this film. In some cases, the presence of sodium and potassium oxides increases the pH to about 13.2 (Mehta, 1986).

There are two mechanisms responsible for reducing the alkalinity of PCC and breaking the passive layer: the carbonation of PCC and the presence of chloride ions (Weyers *et al*, 1993). Chlorides may be present in the PCC due to deicing salts, aggregate, or seawater. In the corrosion process, the pore water acts as the electrolyte. The corrosion process can be explained by the reactions that take place at the anode and the cathode. At the anode, the iron is oxidized and the chloride ions react with it to form iron chloride, which ultimately forms iron oxide. At the cathode, the oxygen reacts with the water to form hydroxyl ions.

Anode:

$$Fe \rightarrow Fe^{++} + 2e^- \qquad 2.7$$

$$Fe^{++} + 2Cl^- \rightarrow FeCl_2 \qquad 2.8$$

$$FeCl_2 + H_2O + OH^- \rightarrow Fe(OH)_2 + H^+ + 2Cl^- \qquad 2.9$$

$$4Fe(OH)_2 + 2O^- \rightarrow 2Fe_2O_3 + 4H_2O \qquad 2.10$$

Cathode:

$$O_2 + 2H_2O + 4e^- \rightarrow .4OH^- \qquad 2.11$$

The iron oxide formed increases in volume up to six times, resulting in tensile stresses in the PCC. If these stresses are greater than the tensile strength of the PCC, it spalls and cracks. There is a certain level of chlorides below which their presence does not result in corrosion. Called the threshold value, this value has been reported to be in the range of 0.6 to 0.9 kg of chlorides for every cubic meter of PCC (Mehta, 1986) at the reinforcement level.

# CHAPTER 3. ELECTROMAGNETIC WAVES AND COAXIAL TRANSMISSION LINES

## 3.1 Electromagnetic Waves

The generation of electromagnetic waves depend on the relationship between the electric and magnetic fields. A changing magnetic field will induce an electric filed and a changing electric field will induce a magnetic field. An electromagnetic wave contains energy which flows in the direction of propagation. Electromagnetic waves have energy, momentum, and mass, and move through space by means of wave motion. The electromagnetic theory was developed by Maxwell who proved mathematically that electromagnetic waves could propagate through a conducting medium. He also stated that electromagnetic waves travel at the speed of light. Hertz, in 1888, experimentally proved that the velocity of electromagnetic waves was the same as the velocity of light. He also proved that electromagnetic waves could be reflected, refracted, and polarized like light and heat waves (Hertz, 1900).

## 3.2 Dielectric Materials

Materials, which have the outermost electron shell of their atoms almost completely filled, are called dielectric materials. Since the shells are completely filled, the electrons are bound and it is relatively difficult to dislodge them. Therefore dielectric materials have few electrons available for conduction and are classified as insulators. These materials usually exhibit or can be made to exhibit a dipole structure, which is the separation of two point charges of equal magnitude and opposite sign by a small distance.

The ability of a dielectric material to store a charge can be explained using a parallel plate capacitor. When the space between the plates is filled with vacuum, the capacitance, $C_o$, which is the ratio of the charge on either plate to the potential difference between the plates, is directly proportional to the area of the plates, A, and inversely proportional to the distance between the plates, d. Therefore, the relationship can be given by:

$$C_o = \varepsilon_o \left( \frac{A}{d} \right) \qquad 3.3$$

where, $\varepsilon_o$ is the permittivity of vacuum, and has a value of $8.85\times10^{-12}$ F/m. Figure 3.1 shows the charge between the plates when the space between them is filled with vacuum.

When the space between the plates is filled up with a dielectric material and an electric field applied, the dielectric material becomes polarized. While the interior of the dielectric material remains neutral, there is concentration of charges on the ends. This results in an increase in charges on the plates that is due to the polarization. Figure 3.2 shows the increased charge between the plates when the space between them is filled with the dielectric material. This increased capacitance is given by:

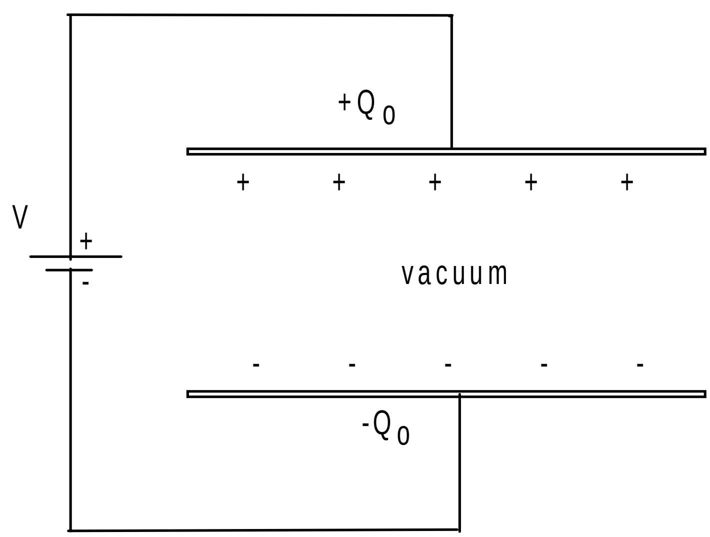


Figure 3.1. Charge on capacitor plates with vacuum between them.

$$C = \varepsilon\left(\frac{A}{d}\right) \qquad 3.4$$

Any dielectric material can polarize more than vacuum. Hence, the permittivity of the dielectric material, $\varepsilon$, is greater than the permittivity of vacuum, $\varepsilon_o$. The permittivity of a material, usually expressed relative to that of vacuum, is called the dielectric constant and is expressed as follows:

$$\varepsilon_r = \frac{\varepsilon}{\varepsilon_o} \qquad 3.5$$

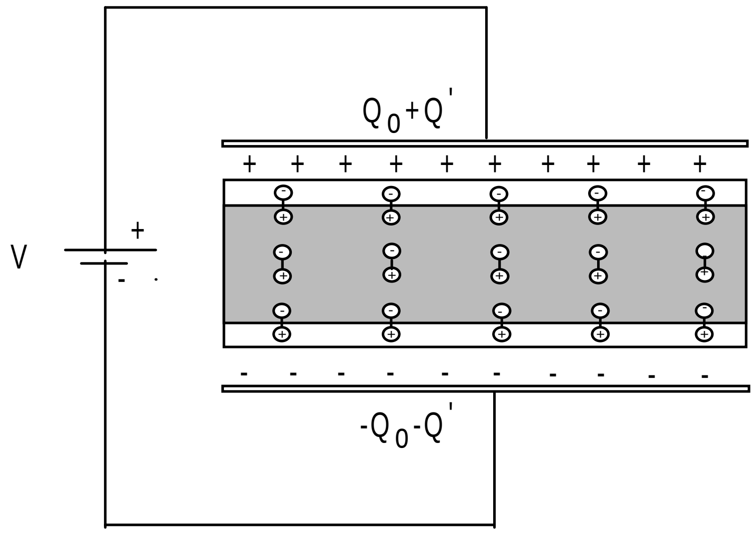


Figure 3.2. Increase in charge storing capacity due to polarization of a dielectric material between the plates.

The dielectric constant, $\varepsilon_r$, is a complex number where the real part represents the actual insulating behavior of the material and the imaginary part represents the lossy behavior of the material to an external electric field.

Any dielectric material will dissipate part of the energy from an electromagnetic wave propagating though it. The source of these losses may be investigated by considering Maxwell's equations and the two constitutive relations.

Maxwell's vector equations for steady state sinusoidal dependence are given by:

$$\nabla \times E = -j\omega B \tag{3.6}$$

$$\nabla \times H = j\omega D + J \tag{3.7}$$

$$\nabla \bullet D = \rho \tag{3.8}$$

$$\nabla \bullet B = 0 \tag{3.9}$$

where,

E = Electric field intensity vector (volts/m);

B = Magnetic flux density (webers/$m^2$);

H = Magnetic field intensity (amperes/m);

D = Electric flux density (coulombs/$m^2$);

$J = \sigma E$ = Electric current density (amperes/$m^2$);

$\rho$ = Electric charge density (coulombs/$m^2$); and

$\sigma$ = Conductivity (mhos/m).

The two constitutive relations that relate the flux densities to the field intensities for a given material are:

$$D = \varepsilon_0 E + P \qquad 3.10$$

$$B = \mu_0 (H + M) \qquad 3.11$$

where,

P = Dipole moment per unit volume;

M = Magnetic dipole polarization per unit volume;

$\varepsilon_o$ = Dielectric permittivity of free space = $8.854\times10^{-12}$ farad/m; and

$\mu_o$ = Permeability of free space = $4\pi\times 10^{-7}$ henry/m.

For an isotropic material, the relationship between E and P is linear and is given by:

$$P = \varepsilon_0 \chi_e E \qquad 3.12$$

where, $\chi_e$ is the electrical susceptibility and is given by:

$$\chi_e = \frac{\varepsilon' - j\varepsilon''}{\varepsilon_0} - 1 \qquad 3.13$$

$$D = (\varepsilon' - j\varepsilon'')E \qquad 3.14$$

For non magnetic materials, the relationship between H and M is given by:

$$M = \chi_m H \qquad 3.15$$

where, $\chi_m$ is the magnetic susceptibility and is given by:

$$\chi_m = \frac{\mu' - j\mu''}{\mu_0} - 1 \qquad 3.16$$

and,

$$B = (\mu' - j\mu'')H \qquad 3.17$$

On substituting the values in equation 3.5, it changes to:

$$\nabla \times H = (\omega\varepsilon'' + \sigma)E + j\omega\varepsilon' E \qquad 3.18$$

The loss tangent of a dielectric medium is the ratio of the loss part to the real part of equation 3.18 and is given by:

$$\tan\delta = \frac{\omega\varepsilon'' + \sigma}{\omega\varepsilon'} \qquad 3.19$$

Thus, the loss of charge in a dielectric medium is due to finite conductivity and damping effects of the dielectric material. Measurements of the loss tangent do not separate the contributions of the dielectric damping effects and conductivity. At microwave frequencies where $\omega$ is large, conductivity in poor conductors or good dielectrics is insignificant.

The molecules in a dielectric material can be characterized by dipole moment, p, which is the product of the charge, q, and the distance between the two charges, d. For a dielectric material of volume $\Delta v$, containing $n$ dipoles per unit volume, the total dipole moment, $p_{total}$, is given by the vector sum:

$$p_{total} = \sum_{i=1}^{n\Delta v} p_i \qquad 3.1$$

Polarization, P, is defined as the dipole moment per unit volume and is given by:

$$P = \lim_{\Delta v \to 0} \frac{1}{\Delta v} \sum_{i=1}^{n\Delta v} p_i \qquad 3.2$$

Polarization is also defined as the alignment of the dipoles with the electric field. Polarization results in an increase in the charge that can be stored in the material. There are four main types of polarization in the microwave range: electronic, ionic, molecular, and interfacial. Electronic polarization occurs when an electric field is applied to a material and the electrons in the atom shift away from the positively charged nucleus. Thus, the atom acts as a dipole. This polarization is only temporary and disappears when the external electric field is removed. Ionic polarization occurs when there is displacement of anions and cations in crystals relative to their normal positions. Due to the application of the electric field, the cations move towards the negative electrode and the anions move toward the positive electrode. It is also called atomic polarization. When the application of an external electric field results in the alignment of the permanent dipole in the direction of the electric field, it is called molecular polarization. The removal of the electric field does not reverse the polarization effect in this case. Mobile charge carriers are accelerated by an external electric field and on being stopped by a physical barrier, accumulate at that place. This results in interfacial polarization, which is predominant in the low frequency range of $10^{-3}$ to $10^{3}$ Hz. Figure 3.3 shows the different types of polarization.

## 3.3 Coaxial Transmission Lines

Transmission lines are used for transmission of signals and power. Two-wire lines, coaxial lines and waveguides are the different types of transmission lines in use. Coaxial lines are popular because they have low loss transmission capability. A coaxial transmission line essentially consists of two concentric, circular, nonmagnetic conductors. The space between the two conductors is usually filled with an insulator and the electromagnetic fields are confined within this space.

### 3.3.1 Electrical properties of transmission lines

The electrical properties of a coaxial transmission line depend on four parameters: distributed resistance (R), distributed inductance (L), distributed capacitance (C), and distributed conductance (G). These parameters in turn depend on the material and the dimensions of the line. They are given by:

$$R = \frac{R_S}{2\pi(b)}\left(1+\frac{b}{a}\right) \qquad 3.20$$

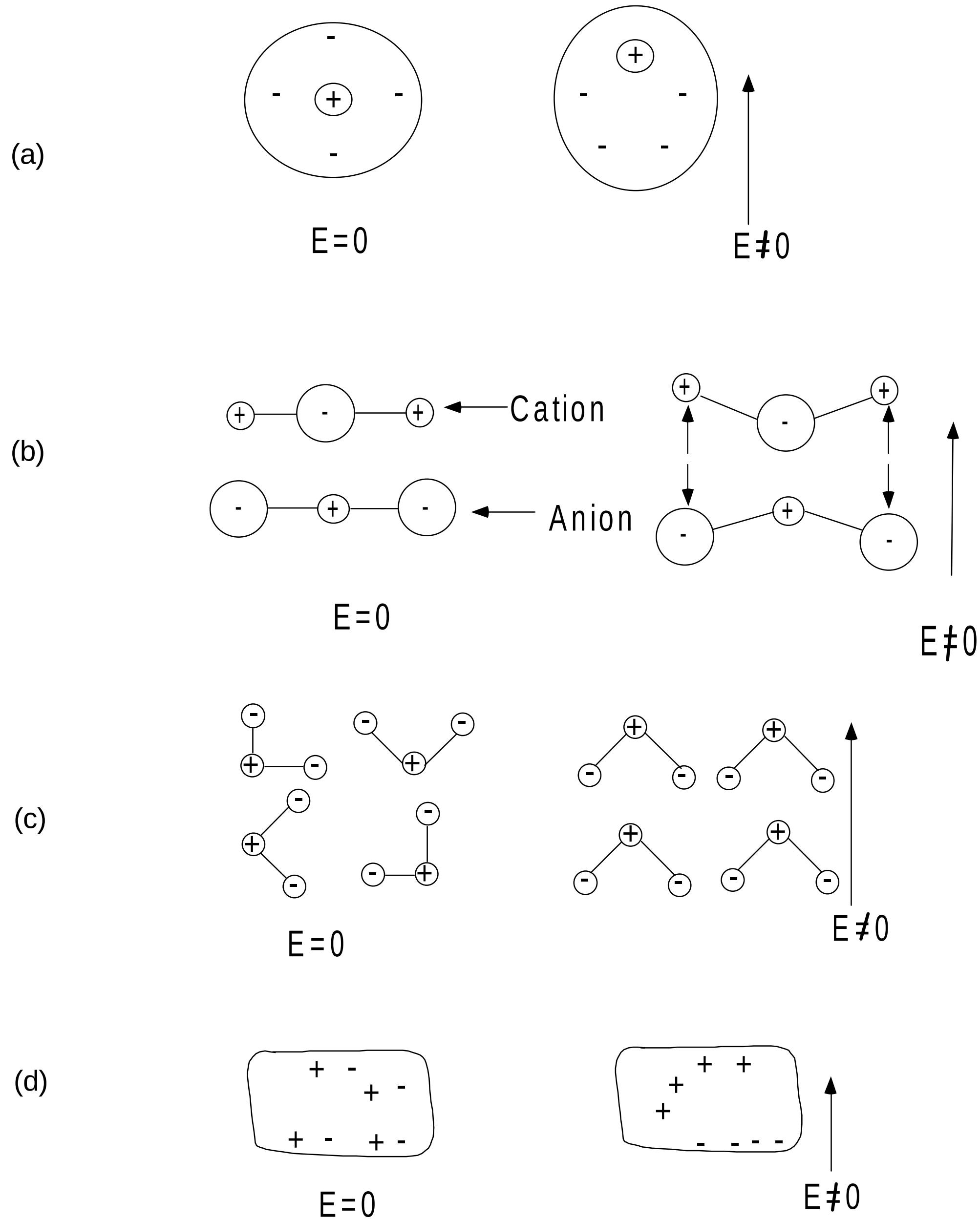


Figure 3.3. Types of Polarization: (a) Electronic, (b) Ionic, (c) Molecular, and (d) Interfacial. (After Scaffer *et al.,* 1995).

$$G = \omega \frac{\varepsilon''}{\varepsilon'} \frac{2\pi\varepsilon}{\ln(b/a)} \qquad 3.21$$

$$L = \frac{\mu}{2\pi} \ln\left(\frac{b}{a}\right) \qquad 3.22$$

$$C = \frac{2\pi\varepsilon''}{\ln(b/a)} \qquad 3.23$$

where, $R_s$ is the surface resistivity and is given by:

$$R_S = \sqrt{\frac{\omega\mu}{2\sigma}} \qquad 3.24$$

and a and b are the inner and outer diameters of the line, respectively.

The four parameters R, L, G, and C can be used for characterizing the transmission line. As shown below, properties such as characteristic impedance and propagation constant depend on these parameters.

#### *3.3.1.1 Characteristic impedance*

The characteristic impedance is the ratio of the voltage to the current on a transmission line on which there are no reflected waves. It is given by:

$$Z_o = \frac{V}{I} = \sqrt{\frac{R + j\omega L}{G + j\omega C}} \qquad 3.25$$

When the losses in the line are small, the resistance and conductance can be neglected. Therefore, equation 3.25 becomes:

$$Z_o \cong \sqrt{\frac{L}{C}} \qquad 3.26$$

$$Z_o = \frac{1}{2\pi}\sqrt{\frac{\mu}{\varepsilon}}\ln\left(\frac{b}{a}\right) \qquad 3.27$$

#### *3.3.1.2 Propagation constant*

The propagation constant, $\gamma$, is defined by:

$$\gamma = \sqrt{ZY} = \sqrt{(R + j\omega L)(G + j\varpi C)} \qquad 3.28$$

The propagation constant, $\gamma$, is a complex number and is denoted by $\alpha$+j$\beta$. $\alpha$ represents the attenuation factor of the line and $\beta$ is the phase factor and represents the phase angles of the phasor voltage and current. Its units are radians per unit length.

The attenuation factor has also been called attenuation constant, which is not true since it varies with frequency. It is a measure of decrease in intensity of the signal and its units are nepers per unit length or decibels per unit length. When the attenuation is small, it can be expressed as:

$$\alpha = \frac{R}{2Z_o} + \frac{G}{2Y_o} \qquad 3.29$$

where, $Z_o$ is the characteristic impedance of the line and $Y_o$ is the characteristic admittance.

Attenuation in coaxial transmission lines can also be expressed as the sum of the attenuation due to conductor losses and dielectric losses:

Conductor losses: Electromagnetic waves cannot penetrate metals and the current travels on the surface of the conductors. The current density is maximum at the surface and decreases exponentially with depth in the conductors. Skin depth, $\delta$, is the depth at which the current density has fallen to 1/e (e is the natural log) of its surface value. The skin depth decreases with frequency. Due to this skin depth effect, the resistance increases with frequency, thereby creating losses which are given by:

$$\alpha_c = 13.6\frac{\delta}{\lambda b}\left(1+\frac{b}{a}\right)\frac{\sqrt{\varepsilon}}{\ln\frac{b}{a}} \quad \text{dB/unit length} \qquad 3.30$$

where, $\delta$ is the skin depth and is given by:

$$\delta = \frac{1}{2\pi}\sqrt{\frac{\lambda\rho}{30\mu}} \qquad 3.31$$

$\lambda$ is the wavelength, $\rho$ is the resistivity of the conductor and $\mu$ is the permeability of the conductor.
Dielectric losses: Even a good dielectric material absorbs a part of the energy from an electromagnetic wave. These dielectric losses also lead to attenuation losses. The attenuation due to dielectric loss, $\alpha_D$, is given by:

$$\alpha_D = 27.3\frac{\sqrt{\varepsilon'}}{\lambda}\tan\delta \quad \text{dB/unit length} \qquad 3.32$$

The total attenuation in the line, $\alpha_T$ is the sum of the attenuation due to conductor losses and dielectric losses and is given by:

$$\alpha_T = \alpha_C + \alpha_D \qquad 3.33$$

### 3.3.2 Modes of propagation

The main mode of propagation in a coaxial transmission line is the transverse electromagnetic (TEM) mode. In this mode, both the electric and magnetic fields are perpendicular to the direction of propagation of the wave. However, higher modes of propagation that have components of either the electric or magnetic field in the direction of wave are sometimes generated. If the magnetic field has a component in the direction of propagation and the electric field is transverse, the waves are called transverse electric (TE) waves. Waves that have a component of the electric field in the direction of propagation and the magnetic field transverse everywhere are called transverse magnetic (TM) waves. Figure 3.4 shows the electromagnetic field pattern in a coaxial transmission line. The higher modes can propagate only when the signal frequency exceeds a certain value, which is called the cutoff frequency. These cutoff frequencies can be obtained by solving Maxwell's equations and applying the boundary conditions associated with the coaxial line. The cutoff frequencies depend on the radii of the conductors. The cutoff wavelength, $\lambda_c$, for the TE and TM waves have been determined by Ramo and Whinnery (1944) to be $\pi(a+b)$ and $2(b-a)$, respectively. The cutoff frequency, $f_c$ is then given by:

$$f_c = \frac{c}{\sqrt{\mu\varepsilon}.\lambda_c} \qquad 3.34$$

where, c is the velocity of light.

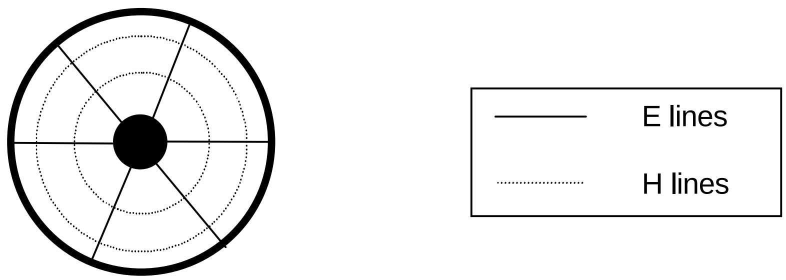


Figure 3.4. Electromagnetic field pattern in a coaxial transmission line.

While the TE and TM modes cannot propagate at frequencies below the cutoff frequencies, their field patterns can be generated by irregularities or discontinuities in the line. In such a case, the higher order modes are said to be evanescent. They are not able to propagate as waves, but diffuse a short distance from their point of origin. The evanescent modes can also be generated at the point of excitation of a TEM wave in a line. However, they attenuate exponentially with length from the point of excitation and can be considered negligible at a distance equal to the transverse dimension of the line from the point of the excitation.

Higher order modes of propagation are not desired and can be explained by the decrease in power of a signal transmitted by a coaxial line. Increasing the generator frequency decreases the power output gradually due to skin effect and dielectric loss. A further increase in the frequency leads to a sudden decrease in the power over narrow frequency bands. These losses are due to the higher order modes. Also, a part of the signal, on entering the coaxial line, is converted from the TEM to the TE mode. However, only at frequencies greater than the cutoff frequency for the TE mode, this power propagates to the output. Since the power meter can recognize only signals in the TEM mode the signal in the TE mode is reflected back to the input where it is partially re-reflected. The multiple reflections may create a resonance condition along with high losses, which would be unacceptable since a coaxial line is designed for low loss operation.

### 3.3.3 The Virginia Tech transmission line

The coaxial transmission line used in this study was developed by Al-Qadi and Riad (1996) as part of a NSF project for characterization of PCC. The dimensions of the line were chosen to characterize PCC containing aggregate with a maximum size of up to 38 mm. The line, made of brass is symmetrical and consists of the following sections: two tapered sections, two buffer sections, a specimen holder and an extra delay section.

As explained earlier, any sudden change in the cross section would lead to the generation of the higher order modes of propagation. In order to avoid this, a smooth transition has to be provided between the cable from the measuring instrument and the line. A tapered section has been used to provide a transition from the impedance of 50 Ω of the measuring instrument to the coaxial line, which has a characteristic impedance of 107.5 Ω. There is a SMA connector on one end, and the other end connects to the buffer section and is 150 mm in diameter. While the outer surface of the tapered sections is smooth, the inner conductor could not be provided with a smooth transition due to fabrication problems. Instead, the transition was done in four small steps. Figure 3.5 shows a cross sectional view of the line used for frequency domain measurements.

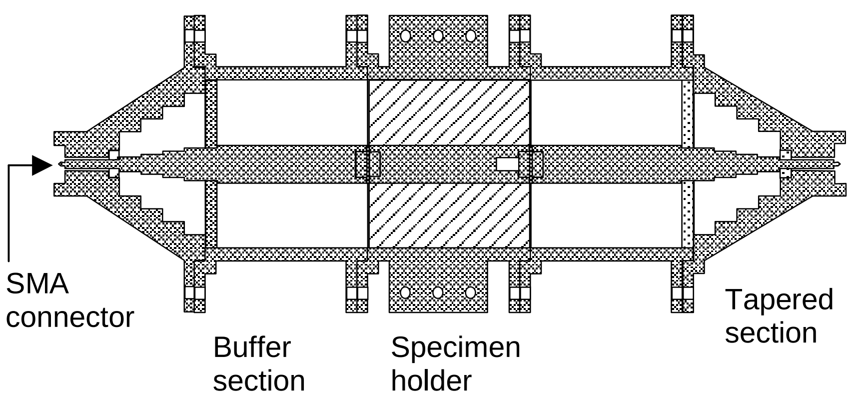


Figure 3.5. Cross sectional view of the coaxial line (After Al-Qadi and Riad, 1996).

The buffer section is 150 mm in length and diameter with a central brass conductor, 25.4 mm in diameter. This section, which is bolted to the tapered section, is the point where the actual transmission line starts. The junction of the tapered and the buffer sections contains a circular Teflon washer, 150 mm in diameter, to support the central conductor. This section's main function is to dampen any evanescent waves generated at the step discontinuities in the tapered section.

An extra-delay section, 150 mm in length and diameter, is attached to the buffer section and used when measurements were conducted in the time domain. It is similar to the buffer section and is used to provide a 1ns delay between the transmitted pulse and the reflected signal from the face of the PCC sample. If this section were not provided, the signals would overlap when measurements are taken in the time domain.

The specimen holder is 150 mm in diameter and split in two halves for easy insertion and removal of the specimens. The brass rod in the specimen acts as the central conductor. Brass connectors are used to connect the center conductors throughout the line.

Details of the coaxial transmission line measurements in the time domain and the calibration process will be presented in Chapter 4.

### 3.3.4 Electrical parameters of the Virginia Tech coaxial line

The dimensions of the line and the electrical properties of brass are:

Outer radius of inner conductor, a=12.7 mm

Inner radius of outer conductor, b=76.2 mm

Conductivity of brass, $\sigma$=1.57 $\times 10^{7}$ S/m

Permeability of brass, $\mu=4\pi \times 10^{-7}$ H/$\mu$.

Using equations 3.20 through 3.24, 3.27, 3.34, and the above values, the electrical properties of the line can be calculated. These properties are given below in Table 3.1. These parameters have been calculated assuming an air filled line.

Table 3.1. Electrical properties of the Virginia Tech coaxial line.

| **Parameter** | **Value** |
|---|---|
| Distributed Resistance, R (100 MHz) | 0.0733 Ω/m |
| Distributed Resistance, R (1000 MHz) | 0.232 Ω/m |
| Distributed Inductance, L | 0.358 μH/m |
| Distributed Capacitance, C | 31.03 pF/m |
| Distributed Conductance, G | 0 |
| Characteristic Impedance, $Z_o$ | 107.46 Ω |
| TE wave cut-off frequency | 1074 MHz |
| TM wave cut-off frequency | 2292 MHz |

### 3.3.5 Other coaxial transmission lines and probes

#### *3.3.5.1 The University of Liverpool line*

Shaw *et al.* (1993) developed a coaxial transmission line for material characterization in the 1 MHz-1.5 GHz range. The line has an outer diameter of 101 mm, and the diameter of the inner conductor is 44 mm, resulting in the characteristic impedance being 50 Ω. While this would remove any unwanted reflections due to impedance mismatch between the line and the cable connecting it to the network analyzer, it severely limits the size of the specimens. Portland cement concrete with a maximum aggregate size of only 10 mm can be used. The measurements were done in the frequency domain and converted to the time domain by an inverse FFT. Two techniques were used to obtain the dielectric constant. In the first technique, the time taken by the electromagnetic wave, t, to travel within the PCC specimen of length, L, is obtained and is substituted in equation 3.35 to obtain the dielectric constant, ε:

$$\varepsilon = \left(\frac{ct}{2L}\right)^2 \qquad 3.35$$

The line was calibrated with distilled water. The real part of the dielectric constant was found to vary from 80.4 to 79.8 at 20°C. However, discontinuities were observed in the frequency dependence of the dielectric constant which were explained by finite element modelling of the line. It was observed that the line was not responding in a pure transverse electric (TEM) mode at the junction of the conical and cylindrical sections. The electrical field at this point was not normal to the inner conductor.

This technique, however, could not be used at high frequencies, because the attenuation was too large for the response from the far end to be seen properly. Attenuation was also observed for some samples due to high conductivity. The researchers also realized that the aforementioned methods would not give the dielectric constant as a function of frequency. Also, conductivity could not be measured with these methods. They developed a numerical technique, which assumed that the dielectric constant decreases exponentially with frequency while conductivity increased linearly (Bungey *et al*., 1997). An iterative procedure was developed where the permittivities and conductivities at high and low frequencies were set and intermediate values were interpolated. The sum of the squares of the residuals between the calculated and measured S-parameters was minimized by a simplex technique that varied the end point permittivities and conductivities. The measured and calculated values of the S-parameters did not match exactly, and this has been attributed to electrical inhomogeneities in the PCC. Other changes made were the reduction of the specimen length from 500 mm to 200 mm and lowering the upper limit of the frequency range from 1.5 GHz to 1 GHz. The specimen length was shortened to introduce air gaps in the line to allow for the reduction of the distortions that were observed in the tapered sections and also to reduce the signal attenuation in the specimens.

The effect of moisture, chlorides, fly ash and ground blast furnace slag on the dielectric constant was studied. Moisture content was found to have a strong effect on the dielectric constant, which was increased with increasing water content. Specimens with high w/c ratios had higher dielectric constants and conductivity due to the high amount of free water available. Chlorides did not affect the dielectric constant and conductivity as much as expected. The addition of ground blast furnace slag and fly ash did not make any significant change to the electrical properties. A 150-mm diameter transmission line, which can measure PCC with an aggregate size upto 20 mm, was also developed (Bungey *et al*., 1997). However, results from using this line have not been published.

#### *3.3.5.2 The University of Illinois line*

A coaxial transmission line was developed by Chew *et al.* (1991) at the University of Illinois, for measuring the electrical properties of cement mortar in the 1 MHz to 3 GHz range. Since the spacing between the outer and the inner conductors was only 35 mm, this line could not be used for testing PCC. While the inner conductor was tapered at the end to match with the connector, the outer conductor was not tapered and the cross section abruptly changed to match that of the connector. This discontinuity might result in the generation of higher modes of propagation. However, the researchers assumed that placing Teflon pieces at these regions would decay the higher modes and only TEM mode would be present at the sample.

Measurements were done in the frequency domain. The scattering parameter matrix of the line was determined using three standard terminations: short, open and matched loads. Since an open termination would not behave uniformly over the entire frequency range, three different methods were used for three frequency ranges: 1-30 MHz, 30-800 MHz, and 800 MHz-3 GHz. The equations developed by Rau and Wharton (1982) were used to calculate the dielectric constant and the permeability. Calibration of the line was done using Teflon and tap water. The dielectric constant of Teflon was found to be around 2 for the entire frequency range with the permeability being around 1. The calculated dielectric constant and conductivity for water were compared with the values calculated using the Klein-Swift formula (Klein and Swift, 1977) and were found to match well. Testing was done on cement mortar specimens with a w/c ratio of 0.6 and a sand/cement ratio of 2.75. The conductivity of the mortar was shown to decrease from the time of casting to 24 hours after casting because of the decreasing amount of water in the mortar as hydration progresses. While the dielectric constant would be expected to decrease with curing time, this research shows an increase from the time of casting to 24 hours after casting. No valid explanation has been given for that phenomenon.

#### *3.3.5.3 The EPFL LMC line*

A large broad band coaxial line was developed by Robert *et al.* (1995) for measuring the complex permittivity of PCC at EPFL LMC from 50 MHz to 1 GHz. This line was modelled on the line developed at the University of Illinois, but this line is much larger and can measure PCC with a maximum aggregate size of 30 mm. The outer conductor of the line is 160 mm in diameter (b) with an inner conductor diameter (a) of 49.2 mm. These dimensions were selected based on three different criteria:

- the representative volume (EVR) criteria, according to which the minimum dimension of the sample must be four times the largest dimension of the aggregate

- a limiting value of the b/a ratio of 3.59 to avoid conductivity losses

- a limiting value of the ln(b/a) ratio of 1.18 to keep the characteristic impedance of the line at 50 Ω

The measurements were done in the frequency domain and involved calculating the scattering matrix. An iterative method to solve the complex permittivity from the scattering equations was used. Teflon was used to verify the working of the line. The real part of the dielectric was found to vary within 5% of the expected value of 2.1. The imaginary part of the dielectric constant was 0.1± 0.01. The line was used to test PCC with maximum aggregate sizes of 15 mm and 30 mm and mortar. Only the effect of curing was studied. Measurements were taken at curing periods ranging from 1 to 24 days. It was observed that the variation of the dielectric constant with the frequency was more for PCC at low curing periods. As the specimens cured, the dielectric constant became stable across the frequency range. The dielectric constant was higher for specimens with a high w/c ratio while the mortar specimens had a higher dielectric constant than both the PCC mixes.

#### ***3.3.5.4 The Voss Scientific Line***

A small diameter transmission line was developed at Voss Scientific by Courtney *et al.* (1996) for measuring the dielectric properties of various materials including cement mortar. The outer diameter of the line is 70 mm while the inner diameter is 30 mm. These dimensions were selected to make the characteristic impedance of the line 50 Ω. The spacing between the two conductors was only 19.75 mm, thereby limiting the testing to cement mortar. The line was setup for measurement both in the time and frequency domains. The measurement range in the time domain was 1 MHz-8 GHz, while it was 0.1-5 GHz in the frequency domain. In the time domain, sensors were placed at three different points along the line to record the time taken for the pulse to be reflected from the air-specimen interface and the time taken to pass through the specimen. These values were then used to obtain the scattering matrix from which the dielectric constant was extracted.

Measurements were done on PVC, Noryl (Polyphenylene oxide) and mortar. The real part of the dielectric constant for Noryl was measured as 2.7 and this was constant over the entire frequency range. The imaginary part was varied from -0.15 to 0.08. The theoretically expected values for Noryl are 2.69 and 0.0007, respectively. The relative permeability was measured to be varying about 1.0, thereby showing that Noryl was a non-magnetic material. Measurements were also conducted on mortar samples in the time domain. Both the real and imaginary parts of the dielectric constant showed a decrease with frequency. However, the results show a lot of scatter that has not been explained. Negative values were resulted for the loss part which is not physically possible.

Table 3.2 summarizes the physical and electrical properties of the five aforementioned transmission lines discussed above.

Table 3.2. Comparison of different transmission lines.

| Fixture | Inner Conductor Radius (mm) | Outer Conductor Radius (mm) | Sample Length (mm) | Characteristic Impedance (ohms) | FirstTE Mode (MHz) | First TM Mode (MHz) |
|---|---|---|---|---|---|---|
| Virginia Tech | 12.7 | 75.0 | 150 | 107.5 | 1074 | 2292 |
| University of Liverpool | 22.0 | 50.5 | 200 | 49.9 | 1317 | 5263 |
| University of Illinois | 7.7 | 25.0 | 30 | 70.7 | 2920 | 8670 |
| EPFL LMC | 24.6 | 80.0 | 120 | 70.8 | 912 | 2707 |
| Voss Scientific | 15.2 | 34.9 | 225 | 50 | 1906 | 7614 |

#### *3.3.5.5 The MIT Coaxial Probe*

Rhim and Buyukozturk (1998), at MIT, studied the variation of the dielectric constant of PCC with moisture content in the 0.1-20 GHz range. An open-ended coaxial probe connected to a network analyzer was used for the measurements in the frequency domain. The principle of the coaxial probe is similar to that of a coaxial transmission line. The procedure involved putting the probe on the PCC surface, sending an electromagnetic pulse, and recording the reflected signal. The scattering matrix was obtained from these measurements. Three equations were developed by taking measurements on three standards. The terminating load admittance was then found from the equivalent circuit and used to determine the electromagnetic properties. Four parameters, The parameters $\varepsilon_o$, $\varepsilon_{inf}$, $\tau$, and $\alpha$ were measured and substituted in equation 3.36, the Cole-Cole dielectric model (1941) to obtain the complex dielectric constant, $\varepsilon^*(f)$ expressed by:

$$\varepsilon^*(f) = \varepsilon_{inf} + \frac{(\varepsilon_o - \varepsilon_{inf})}{1 + (j2\pi f\tau)^{(1-\alpha)}} \qquad 3.36$$

The calibration of the setup was done using methanol, ethylene glycol, distilled water, and air. The researchers state that the measured values were in good agreement with other published data with an error of less than 10%. Cylindrical PCC specimens, 76.2 mm in diameter and 152.4 mm high with a w/c ratio of 0.45, were made for testing. The effect of moisture on the dielectric constant was observed by testing the specimens in four different conditions: wet specimens with water on the surface, saturated specimens with the surface dry, air dried specimens, and oven dried specimens with no moisture. For the oven-dried specimens, the dielectric constant was relatively stable over the frequency range. However, the change over the frequency range was significant for the saturated specimens. It was also observed that the dielectric constant for the saturated specimens was almost twice that of the oven dried specimens, thus showing the effect of moisture on the dielectric constant.

#### *3.3.5.6 The University of Edinburgh Cell*

At the University of Edinburgh, McCarter and Curran (1984) studied the electrical properties of cement pastes at a frequency of 1 KHz using a coaxial cell as a function of the hydration process. The coaxial cell consisted of two concentric conductors mounted on an insulated base plate. In an earlier study (Whittington *et al.,* 1981), the researchers had modelled the electrical behavior of PCC using just resistance. They later realized that capacitance also had an effect on the over-all impedance of the cement paste. Therefore, both resistance and capacitance were measured by connecting the cell to an impedance bridge. The dielectric constant of the cement paste was the ratio of the capacitance of the system with cement paste filling the cell to the capacitance of the cell with vacuum. The loss tangent was defined as the ratio of the current flowing through the resistive element to the current flowing through the capacitive element. Measurements were taken every 5 minutes after casting to gain a better understanding of the effect of hydration on the dielectric constant. The coaxial cell was calibrated with cyclohexane and butanol, which have known dielectric constants of 2.025 and 17.8, respectively.

Three cement pastes of varying w/c ratios along with two mortars having different sand/cement ratios and w/c ratios were tested. When water was first added to cement, the dielectric constant of the paste was found to be as high as $10^6$ because of the release of a large amount of $Ca^{++}$ and $OH^-$ ions into the water. The presence of these ions resulted in the paste becoming highly polarizable and conductive. As expected, the resistivity at that point of time was very small. However, as hydration progresses, the free water in the paste starts changing to adsorbed water and irrotationally bound. Due to the increasing formation of the CSH gel, the polar molecules start getting bound and unable to polarize. Calcium hydroxide, the main source of ions, starts to crystallize. For these reasons, the dielectric constant showed a rapid decrease. The decrease in conductivity was also indicated by a tremendous increase in the resistivity. At about 500 minutes after casting, there was an increase in the dielectric constant. At this point, there is a release of lime from the $C_3S$ grains due to the further hydration of the alite phase. The resulting increase of ions in the water increases the dielectric constant. After this, the PCC hardens and the polar molecules find it difficult to move, resulting in less polarization and a decrease in the dielectric constant. The dielectric constant has been observed to be higher for higher w/c ratios, as expected.

The research reported herein took into consideration the results of the aforementioned research and developed a research plan to verify the effectiveness of the Virginia Tech coaxial transmission line to measure the dielectric properties of different PCC mixes.

# CHAPTER 4. RESEARCH PROGRAM

The research program of this study involved measuring the complex dielectric constant of various PCC mixes using a time domain approach and converting the results into frequency domain. The coaxial transmission line developed at Virginia Tech was used to obtain the dielectric measurements at 100-1000 MHz. The effect of aggregate type, w/c ratio, curing time, admixtures, chlorides, and moisture on measured dielectric properties was evaluated. Testing was also conducted to determine the correlation between chloride permeability (based on conductance measurements) of the PCC mixes and measured dielectric properties.

## 4.1 Materials

Granite and limestone and Type I Portland cement were used in the PCC mixes. The aggregates were obtained from Rocky Dale Quarries, Roanoke, Virginia. The gradation of both the limestone and granite aggregate meet the ASTM C33-93 specifications. Appendix A provides the details of the gradation and the physical properties of both the limestone and granite. The shrinkage admixture was obtained from W. R. Grace & Company, Cambridge, Massachusetts. The high range water reducer and microsilica were purchased from Marshall Concrete, Christiansburg, Virginia.

## 4.2 Specimen Preparation

The absolute volume method, as specified by ACI, has been used in preparation of all the mixes. Table 4.1 gives the details of the specimens that were cast. All the specimens were cast in duplicates. Although the main reason for mixing PCC using different parameters is to measure the effect of these parameters on the dielectric properties, practical selection of parameter changes were made. Since limestone is more commonly used than granite, it was chosen for the majority of the mixes. Three w/c ratios of 0.35, 0.42, and 0.5 were selected. A w/c ratio of 0.42 is used because the cement undergoes complete hydration at this ratio as reported by Mindess and Young (1981). Water/cement ratios of 0.35 and 0.5 were selected in order to observe the effect of w/c ratios above and below the optimum w/c of 0.42. Control specimens were cast at all the three w/c ratios and for both aggregates. Microsilica was selected to be used with the higher w/c ratio mixes, since the lower w/c ratios already have low permeability and high strength. Superplasticizers were used for w/c ratios of 0.35 and 0.42, since the PCC at these ratios is not as workable as it is at higher w/c ratios. The shrinkage admixture is a relatively new admixture and not much is known about its behavior. Therefore, it has been used for all the three w/c ratios. All the specimens except for those containing chlorides are identified by three characters. The first character indicates the type of aggregate: L for limestone and G for granite. The second character indicates the w/c ratio: 3 for 0.35, 4 for 0.42, and 5 for 0.5. The third character stands for the type of admixture used: S for shrinkage, M for microsilica and H for high range water reducer. 'N' indicates that the PCC does not contain any admixtures. Specimens containing chlorides are designated by four characters with the first three being similar to the designation used for the other specimens. The fourth character stands for the amount of chlorides mixed: 2 for 2.38 $kg/m^3$ of PCC and 4 for 4.76 $kg/m^3$ of PCC.

The aggregate was oven dried at 100°C for 24 hours before mixing with cement and water. Slump, unit weight, and air content were taken at the time of casting to check for the PCC quality according to ASTM C 143-90a and C 138-92. Cylinders, 100 mm in diameter and 200 mm in height, were also cast to check for the compressive strengths at three, seven, and 28 days after casting.

The specimens for the coaxial transmission line testing are 150 mm in diameter and 150 mm in length with a center brass conductor (25 mm in diameter). Special molds, which allow the center conductor to be fixed with a screw at the bottom, were used. After the conductor had been secured with the screw, the PCC was placed in three layers with each layer being consolidated using a tamping rod and a vibrating table. The surface was made smooth using a trowel and the molds put in a curing room. After one day, the specimens were removed from their molds and left to moist cure for 90 days.

Specimens for the chloride permeability testing are 100 mm in diameter and 50 mm in height (ASTM C 1202-94). These specimens were cut from cylinders 100 mm in diameter and 200 mm long which were cast at the time of preparation of the coaxial transmission line specimens. All specimens were prepared in duplicates.

Table 4.1. Portland cement concrete mixes used in the research program.

| | w/c ratio | | | | | |
|---|---|---|---|---|---|---|
| | **0.35** | | **0.42** | | **0.5** | |
| | Limestone | Granite | Limestone | Granite | Limestone | Granite |
| Control | | | | | | |
| Micro Silica | | | | | | |
| Chloride Testing | | | | | | |
| Water Reducer | | | | | | |
| Shrinkage | | | | | | |

*Shaded area indicates mix considered in study.

## 4.3 Specimen Conditioning

The effect of chlorides and moisture content on the dielectric properties of PCC was observed. Chlorides were introduced into the PCC by adding NaCl to the mixing water. The NaCl addition rate was 1.65 kg/m$^3$ of PCC when a chloride level of 1 kg/m$^3$ of PCC was desired. Portland cement concrete specimens were cast at two levels of chlorides, 2.38 and 4.76 kg/m$^3$ of PCC, using both granite and limestone at a w/c of 0.42. Specimens were also cast with limestone at a w/c ratio of 0.35 with a chloride concentration of 4.76 kg/m$^3$ of PCC. The level of chlorides in the cast PCC was determined using the water-soluble chloride test in accordance with ASTM C 1218-92b after 90 days of curing. After casting, the specimens were put in a moist curing room. Prior to taking measurements with the coaxial transmission line, the specimens were taken out of the curing room and air dried for an hour.

The effect of moisture content on the dielectric properties of PCC has also been studied. This involved submerging the specimens in a water bath until they were completely saturated. Saturation was determined by checking their weights at regular intervals. Any change in weight would indicate that the PCC was not yet totally saturated. Measurements were taken after the specimens were completely saturated. The specimens were then heated in an oven at 100° C and measurements were taken at regular intervals after the specimen was cooled to room temperature by air drying. Measurements were also taken after the specimen had completely dried and no further reduction in weight was observed for two days after being in an oven at 100° C. The amount of moisture was expressed as a percentage volume of the dry PCC.

For the chloride permeability test, the sides of the specimens were first coated with an EP 308 rapid setting epoxy that was then allowed to cure for about three hours. Next the specimens were placed in a vacuum desiccator and pressure was reduced to less than 1 mm Hg for three hours. At this point, distilled water was added till the PCC specimen was submerged and the pump run for one more hour before being shut down. The specimens were allowed to soak for eighteen hours in order to become fully saturated prior to the permeability measurements.

## 4.4 Measurements

### 4.4.1 Coaxial line measurements

The coaxial transmission line can be setup for measurements in either the time domain or the frequency domain. However, in this study, all measurements were conducted in the time domain because a network analyzer in the 0-1000 MHz range was not available. Time domain measurements by themselves are not useful since the objective of material characterization is to observe the effect of parameters over frequency. Therefore, Fourier Transform is used to interpret the time domain measurements as a function of frequency. Time domain spectroscopy, which deals with quantitative analysis, as opposed to time domain reflectometer, which deals with qualitative analysis, was used. This involves generating an impulse and propagating it through the transmission line. Depending on the load impedance and the characteristic impedance of the line, there will be a reflection of the impulse. The incident and reflected waves can be then analyzed to yield the permittivity and permeability of the load.

A one port measurement technique was used. This technique assumes an infinitely long specimen. If the specimen is infinitely long, the only reflection observed will be the one from the air-specimen interface. Time domain gating techniques were used to simulate an infinitely long specimen (Al-Qadi and Riad, 1996). The waveforms were gated so that the tails become horizontal. Figure 4.1 shows a representation of this technique.

The measurement setup used in this study includes the coaxial transmission line, a Tektronix 11801 oscilloscope, and a computer with a National Instruments IEEE 488.2 GPIB card. The coaxial transmission line was modified for the measurement. Only one half of the line and the extra-delay section were used. The oscilloscope is equipped with a pulse generator, which acts as a source of excitation for the line. The function of the oscilloscope is to display and record the waveforms. The GPIB card in the computer acts as an interface between the computer and the oscilloscope. A software package, WAVESTAR, developed by TEKTRONIX, was used for acquiring the waveforms and converting them into data points. Figure 4.2 shows the measurement setup.

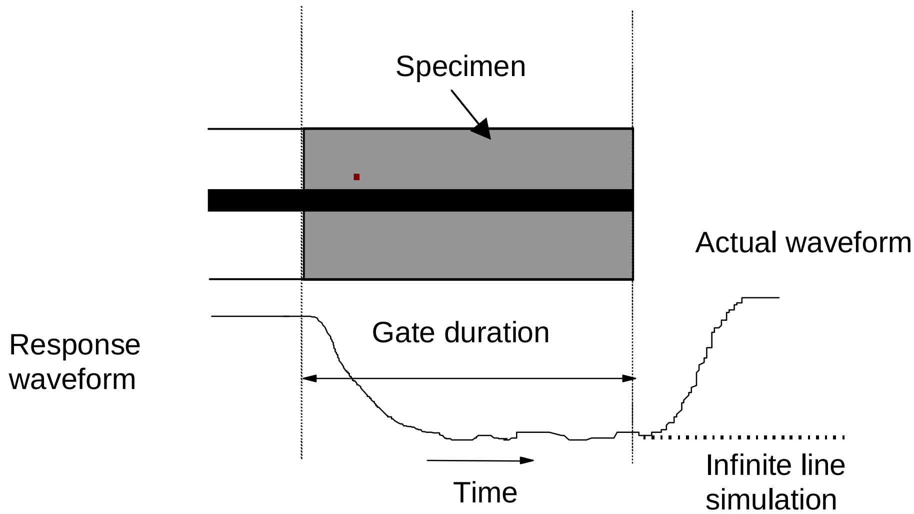


Figure 4.1. Gating technique (After Mostafa, 1995).

Two waveforms, the incident and the reflected waveform from the specimen are needed to obtain the dielectric constant of the specimen (Mostafa, 1995). The incident waveform is obtained by connecting a circular brass plate, which acts as a short, at the end of the extra delay section. The waveform thus obtained is highly reflected since it is assumed that the short results in a reflection coefficient of -1. This waveform is flipped to give the incident waveform. Figure 4.3 shows the setup of the coaxial transmission line for this measurement.

The reflected waveform is obtained by attaching the specimen holder to the delay section and putting the specimen in it. This waveform is denoted by $v_r$. Figure 4.4 shows the setup of the coaxial transmission line for this measurement.

Measurements were taken to observe the effect of curing on the dielectric properties of PCC. Measurements were taken at one, three, seven, 14, 21, 28, 50, 75, and 90 days of moist curing. After the measurement of the dielectric properties of the specimens to observe the effect of curing were completed, measurements were taken at five different levels of moisture content to determine the effect of moisture on the dielectric properties.

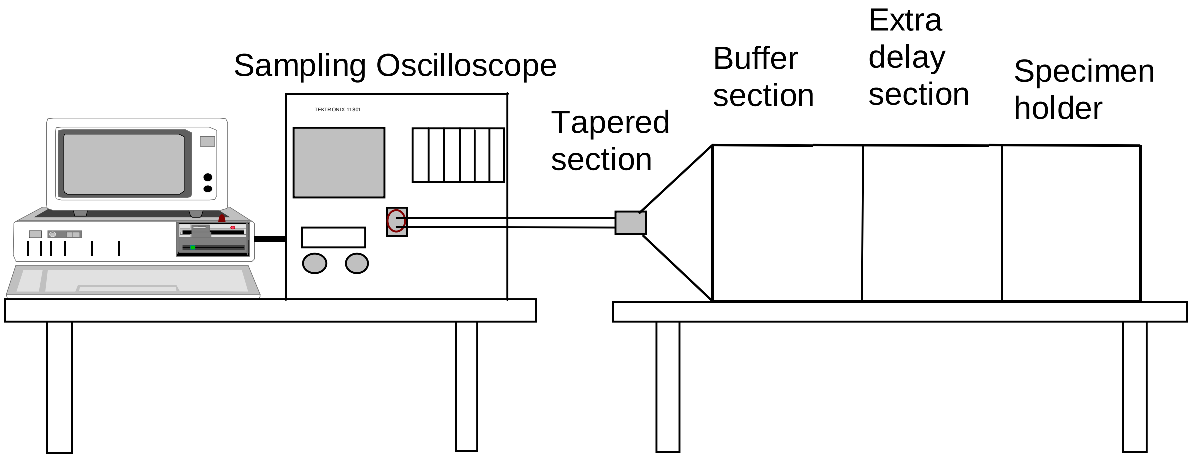


Figure 4.2. Measurement setup in the time domain.

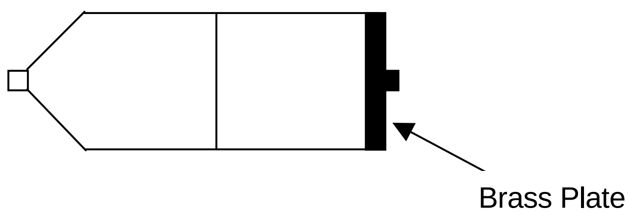


Figure 4.3. Coaxial transmission line setup for acquisition of incident waveform.

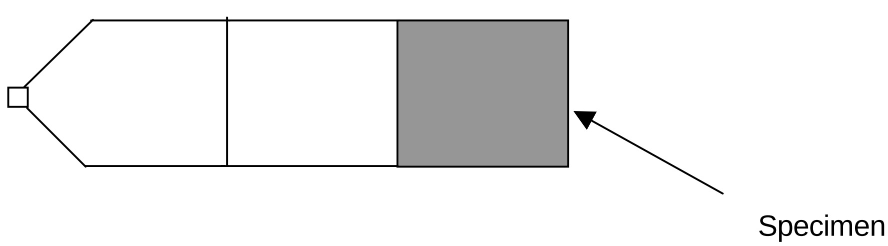


Figure 4.4. Coaxial transmission line setup for acquisition of reflected waveform.

### 4.4.2 Chloride permeability measurements

The chloride permeability of PCC was measured in accordance with ASTM C 1202-94. This test measures the electrical conductance of PCC, which can be correlated to the chloride ion permeability. Since the permeability of the PCC depends on the pore structure, which in turn depends on hydration, the test was conducted after 75 days of curing so that the PCC was well cured. A rapid chloride permeability test apparatus manufactured by Germann Instruments Inc. was used for the testing. This device was available at a late time during the research, therefore, a limited number of samples were evaluated.

The specimens were put in the testing cells after being conditioned and epoxy coated. One end is in 0.3M sodium hydroxide solution while the other end is in a 3% sodium chloride solution. The test measures the amount of electrical current passing through the PCC during a six-hour period when a potential difference of 60 V DC exists between the two ends of the specimen. The cells are connected to a computer which runs a software that computes the total charge.

# CHAPTER 5. DATA ANALYSIS AND RESULTS

All measured waveforms were obtained in the time domain. They were then converted into frequency domain and the complex dielectric constant was calculated. The effect of frequency, aggregate type, curing time, w/c ratio, chloride content, admixture type, and water content on the dielectric constant was studied. The results from the permeability test are also discussed in this chapter.

## 5.1 Analysis Procedure

All dielectric measurements were performed in the time domain. Two waveforms, $v_I$ , and $v_r$, were taken. Fast Fourier Transform (FFT) was used to obtain these waveforms in the frequency domain, $V_I$, and $V_r$.

The $S_{11}$ parameter is equivalent to the reflection coefficient and is given by

$$S_{11} = \frac{V_r}{V_i} \qquad 5.1$$

In terms of impedance, the reflection coefficient is given by

$$\Gamma = \frac{Z - Z_0}{Z + Z_0} \qquad 5.2$$

where Z is the impedance of the specimen and $Z_0$ is the characteristic impedance of the transmission line with no specimen.

Z can be expressed in terms of the relative permeability and permittivity constant of the specimen and $Z_0$ :

$$Z = Z_0\sqrt{\frac{\mu_r}{\varepsilon_r}} \qquad 5.3$$

Therefore, equation 5.2 can be rewritten as:

$$\Gamma = \frac{\sqrt{\frac{\mu_r}{\varepsilon_r}} - 1}{\sqrt{\frac{\mu_r}{\varepsilon_r}} + 1} \qquad 5.4$$

$$\Gamma = \frac{\sqrt{\mu_r} - \sqrt{\varepsilon_r}}{\sqrt{\mu_r} + \sqrt{\varepsilon_r}} \qquad 5.5$$

But $S_{11} = \Gamma$, therefore

$$S_{11} = \frac{\sqrt{\mu_r} - \sqrt{\varepsilon_r}}{\sqrt{\mu_r} + \sqrt{\varepsilon_r}} \qquad 5.6$$

Since the permeability of the specimen is assumed to be 1,

$$S_{11} = \frac{1 - \sqrt{\varepsilon_r}}{1 + \sqrt{\varepsilon_r}} \qquad 5.7$$

$$\varepsilon_r = \left( \frac{1 - S_{11}}{1 + S_{11}} \right)^2 \qquad 5.8$$

$S_{11}$ is a complex number. Solving the above equation would also give a complex number, which represents the real and loss parts of the dielectric constant. The above computations were performed using a computer program written in MATLAB.

## 5.2 Time Window

Initially, measurements were performed using a 3 ns window. However, it was observed that the real part of the dielectric constant showed an increase after 700 MHz. On observing the frequency spectrum, it was seen that the amplitude dropped down to almost zero at 333 and 667 MHz. After 700 MHz, the energy available is low. This might be responsible for the increase in the real part of the dielectric constant. Figure 5.1 shows the frequency spectrum for the 3 ns window. Figure 5.2 shows the frequency spectrum for the 1 ns window. The frequency spectrum for these measurements did not drop down to zero at any point in the frequency range of 100-1000 MHz as exhibited by measurements performed using a 3 ns window. By observing the trend of the frequency spectrum for both the 1 and the 3 ns windows, it can be seen that on selecting a window smaller than 1 ns, the power output would not attain a value of zero within the desired frequency range. However, based on measurements conducted to define the smallest window, the 1 ns window was the smallest possible window that could show the first reflection from the PCC specimen. The loss part of the dielectric constant showed an increase in the 100 to 250 MHz frequency range, because only the first reflection from the air-specimen interface was used. The exclusion of the secondary reflections from the specimen results in an alteration of the low frequency behavior which manifests in the form of the increasing behavior of the loss part of the dielectric constant. Measurements with the 1 ns window were started late in the curing process and only a few were taken. However, all the measurements for studying the effect of water content were taken in both the 1 and the 3 ns windows.

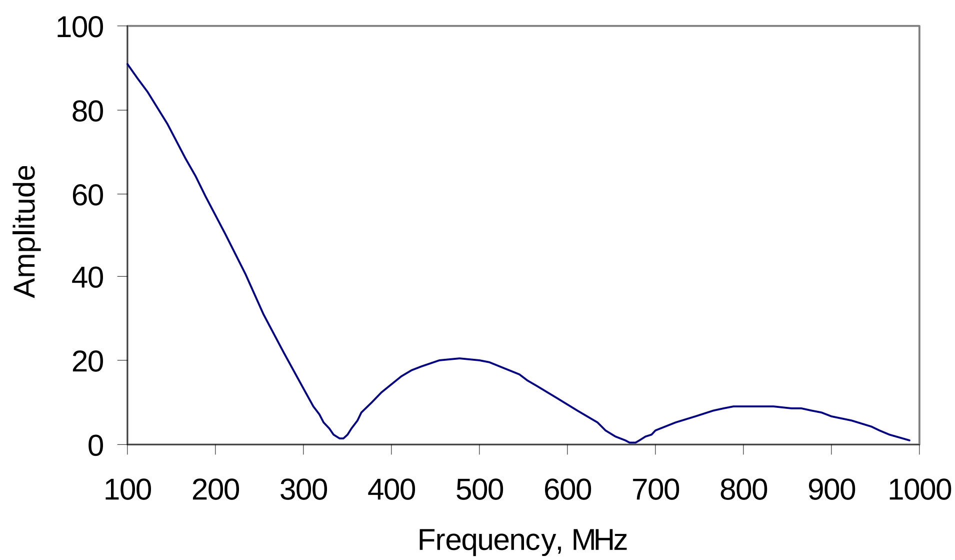


Figure 5.1. Frequency spectrum for measurement taken in 3 ns window.

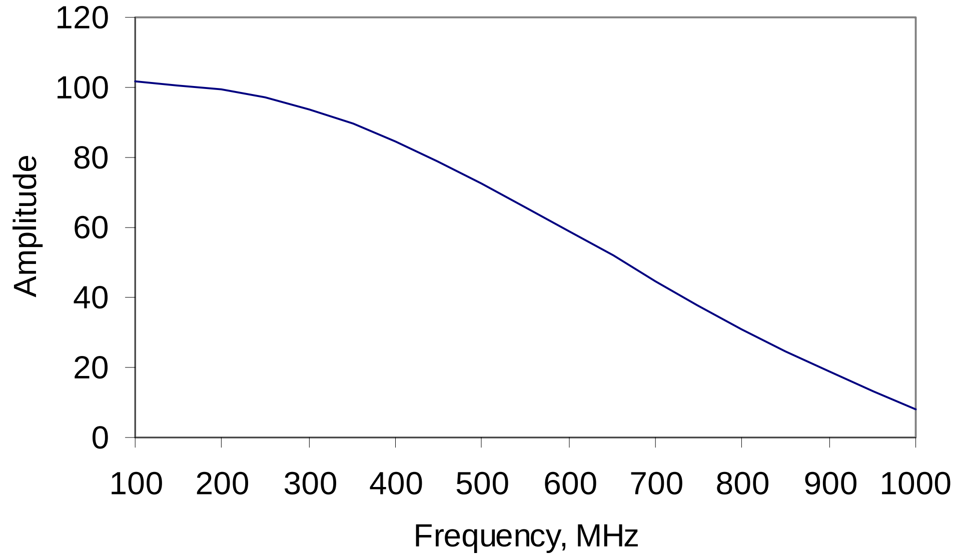


Figure 5.2. Frequency spectrum for measurement in 1 ns window.

## 5.3 Parameters Affecting Measured Dielectric Properties

The effect of frequency, aggregate type, curing time, w/c ratio, admixture, chloride content, water content, and results from the permeability test, on the measured dielectric constant were studied.

### 5.3.1 Frequency

For measurements taken with a 3 ns window, the loss part of the dielectric constant exhibits an increase from 100 MHz to about 250 MHz after which it gradually decreases. This anomalous behavior is due to the exclusion of the secondary reflections from the specimen. In order to rectify this, an attempt was made to introduce a correction factor based on the calculated and theoretical values of the $S_{11}$ parameter for Teflon and apply this factor for measurements with the PCC specimens. However, this correction factor made a significant change in the real part of the dielectric constant for the PCC specimen and was, therefore, not considered. As was explained earlier, the real part of the dielectric constant showed an increase after 700 MHz. Therefore, a decision was made to consider data only in the range of 250 to 700 MHz. Figure 5.3 shows the real and loss parts of the dielectric constant for specimen G4C21 at 50 days of curing. Since the effect of polarization reduces with increasing frequency, the real part of the dielectric constant decreases with frequency. In PCC, conductivity, is more responsible for the lossy behavior than the damping effects (Rhim and Buyukozturk, 1998). Since conductivity ($\delta$)

increases with frequency ($\omega$), the loss part ($\varepsilon''$) which is given by $\delta/\omega$ decreases with frequency; the increase of $\delta$, however, is much smaller than the increase in $\omega$. Figure 5.4 presents the real and loss parts of the dielectric constant for specimen G4C41 at 50 days of curing for measurements with a 1 ns window. The real part of the dielectric constant decreases gradually over the range of 100 to 1000 MHz. However, this decrease is not as steep as that observed for measurements with a 3 ns window. The loss part of the dielectric constant for measurements with the 1 ns window shows an increase with frequency which was not expected. Values of the real part of the dielectric constant for measurements with the 1 ns window, are less than those taken with a 3 ns window. However, measurements on a Teflon specimen with the 1 ns window show less variation from the theoretical dielectric constant values of 2.0 and 0 than with those taken with a 3 ns window. Appendix C presents the change in the dielectric constant for all the mixes at different curing periods.

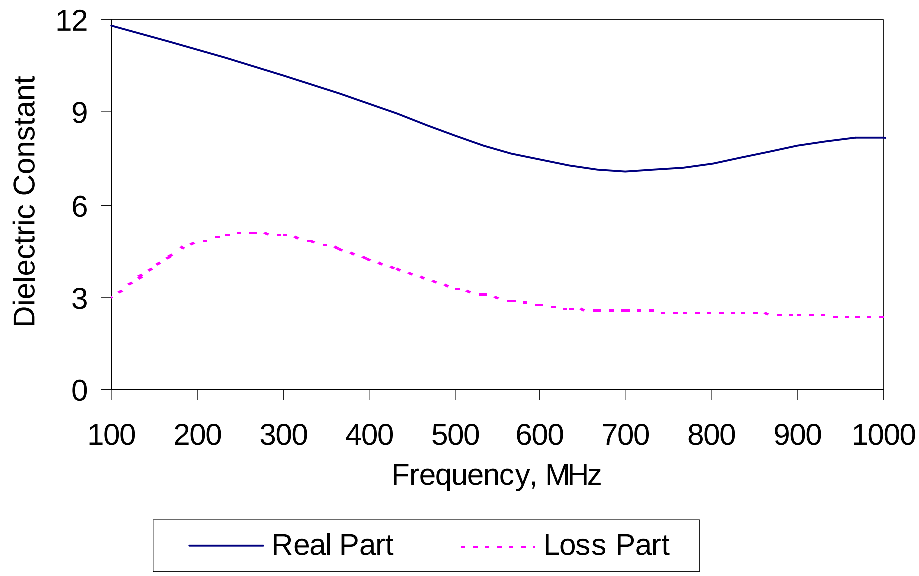


Figure 5.3. Effect of frequency on the dielectric constant for specimen G4C41 at 50 days of curing for measurements with a 3 ns window.

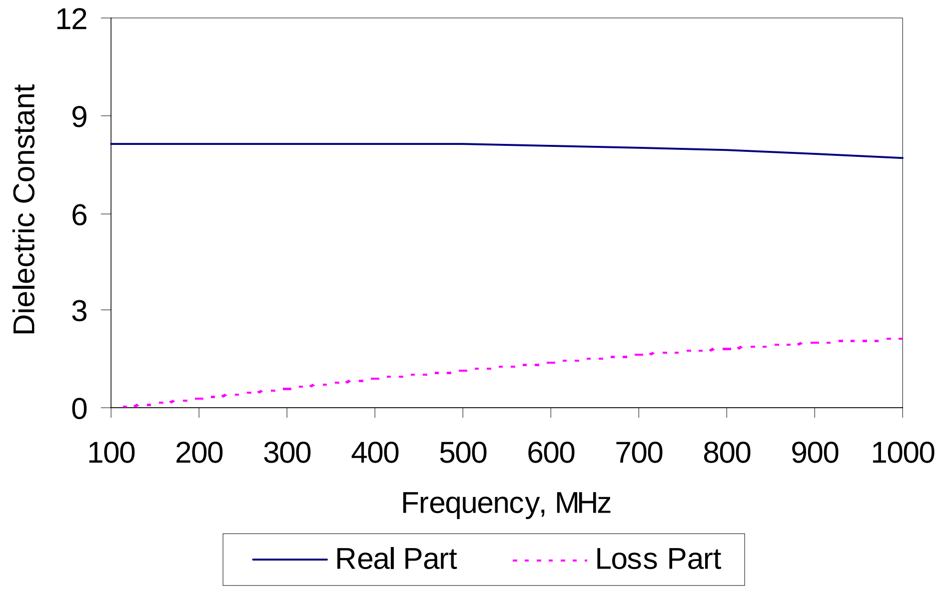


Figure 5.4. Effect of frequency on the dielectric constant for specimen G4C21 at 50 days of curing for measurements with a 1 ns window.

### 5.3.2 Aggregate type

From the research conducted at Virginia Tech earlier, it is known that limestone has a dielectric constant of 8 compared to 4 for granite (Al-Qadi and Riad, 1996). Since aggregates occupy up to 60% of the volume of PCC, the aggregate is expected to have a significant effect on the dielectric properties of the PCC. Figures 5.5 and 5.6 show the real and loss parts of the dielectric constant for G3N and L3N mixes at 28 days of curing, respectively. As would be expected, the real part of the dielectric constant for L3N is significantly higher than G3N over the entire frequency range. The loss part of the dielectric constant for the L3N is also significantly higher than G3N over the entire frequency range. Also, the real part of the dielectric constant of mixes containing limestone aggregate has been found to be more sensitive to the frequency range than mixes containing granite aggregate.

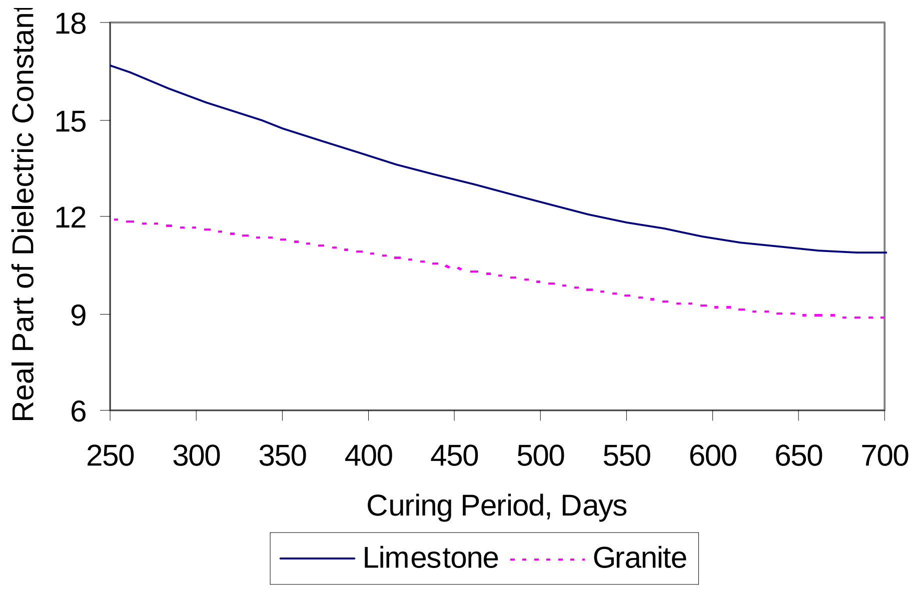


Figure 5.5. Effect of aggregate type on the real part of the dielectric constant at 28 days for concrete at a w/c ratio of 0.35.

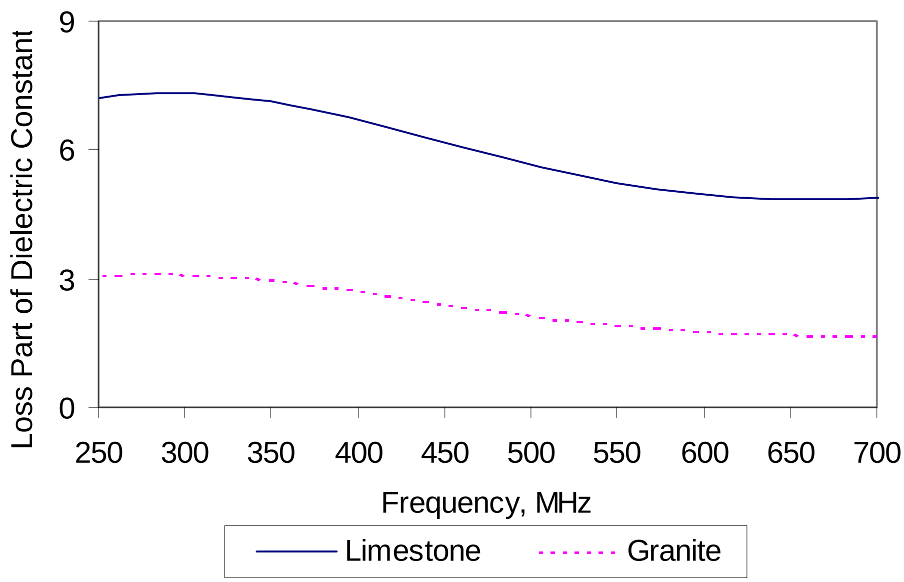


Figure 5.6. Effect of aggregate type on the loss part of the dielectric constant at 28 days for concrete at a w/c ratio of 0.35.

### 5.3.3 Curing time

As the curing time increases, the amount of free water in the PCC decreases due to the cement hydration. The water changes from a free to an adsorbed state, which reduces ionic polarization and also conductivity due to decrease in ion production. Also, the pore structure changes with curing time. The pore sizes become very small, thus making it difficult for the movement of the free ionized water remaining in the PCC. Therefore, the dielectric constant would decrease with curing time. Figures 5.7 and 5.8 show the effect of curing time on the dielectric constant for L4N1 at a frequency of 300 MHz. Appendix D shows the effect of curing time on the dielectric constant for all the mixes.

A statistical analysis using least significant difference (LSD) test was conducted to evaluate the significance of the curing time on the dielectric constant. The analyses were done for one, seven, 28, and 90 days of curing at frequencies of 305 and 505 MHz. These frequencies were selected to represent the lower and mean frequencies in the range of 250-700 MHz. A frequency higher than 505 MHz was not selected since the dielectric constant showed little variation with frequency after 505 MHz. Table 5.1 presents the results of the LSD test. There is a significant difference in the real part of the dielectric constant between one and seven days of curing at a frequency of 305 MHz. However, there is no significant difference between seven and 28 days, indicating that the real part is sensitive during the initial curing period. At 90 days of curing, the real part is different from one, seven, and 28 days. The same level of difference is not

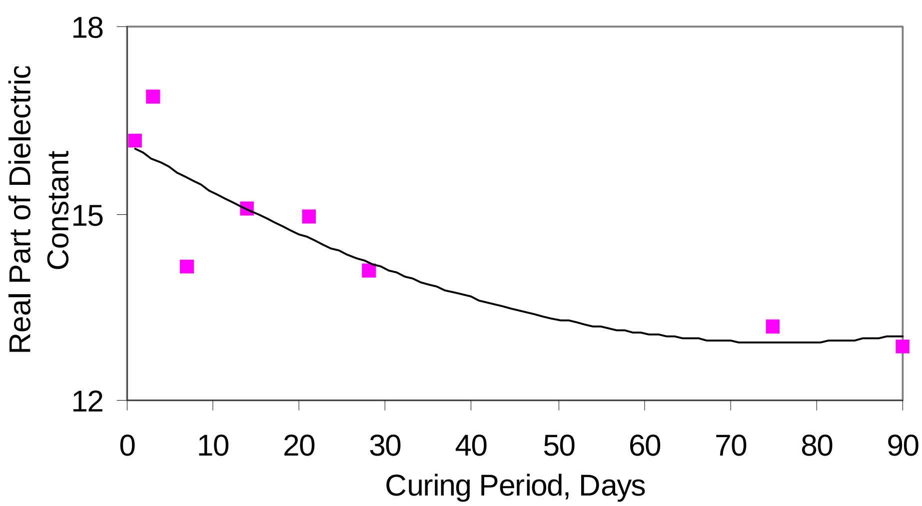


Figure 5.7. Effect of curing period on the real part of the dielectric constant for PCC at a w/c ratio of 0.35.

shown at a frequency of 505 MHz. There was a significant difference in the loss part of the dielectric constant over the entire curing cycle at 305 MHz.

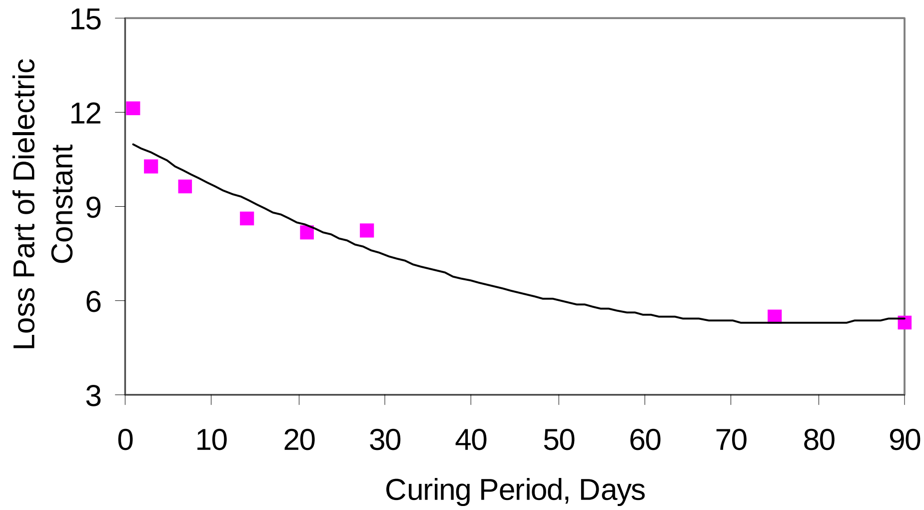


Figure 5.8. Effect of curing period on the loss part of the dielectric constant for PCC at a w/c ratio of 0.35.

Table 5.1. Least significant difference (LSD) test results for the effect of curing period on the dielectric constant.

| **Curing Period (Days)** | **ε'** | | **ε"** | |
|---|---|---|---|---|
| | **305 MHz** | **505 MHz** | **305 MHz** | **505 MHz** |
| 1 | 15.885 A* | 11.975 A | 11.935 A | 6.36 A |
| 7 | 14.41 B | 10.34 B | 9.69 B | 4.32 A |
| 28 | 14.255 B | 10.56 B | 8.24 C | 5.495 AB |
| 90 | 12.695 C | 9.78 C | 5.275 D | 3.43 B |

* Same letter indicates no significant differences among the groups.

### 5.3.4 Water/cement ratio

Portland cement concrete with a higher w/c ratio would be expected to have a higher dielectric constant due to a higher pore water content. Figures 5.9 and 5.10 show the variation of the real and loss parts of the dielectric constant for mixes G3N and G4N, one day after casting.

Both the real and the loss parts are greater for G4N and G3N. According to Mindess and Young (1981), PCC having a w/c ratio of 0.42 would hydrate completely. Therefore, at 28 days of curing, there might not be a large difference in the amount of free water available in mixes G3N and G4N. Figures 5.11 and 5.12 show the effect of the w/c ratios for the same mixes at 28 days. The difference in the real part of the dielectric constant for both mixes is negligible. However, the loss part for G4N is greater than G3N. Even a small amount of free water significantly affects the loss part of the dielectric constant due to an increase in conductivity. Therefore, it appears that G4N has a slightly greater amount of free water than G3N at 28 days of curing. This difference is large enough to affect the loss part of the dielectric constant, but not the real part.

Table 5.2 gives the results of the LSD test performed to evaluate the effect of w/c ratio on mixes containing granite. A significant difference was found in the real part of the dielectric constant at one day of curing between G3N and G4N at 261 MHz. However, there was no difference in the loss part. At 28 days, the real part was essentially the same for G3N and G4N, while the difference in the loss part was significant.

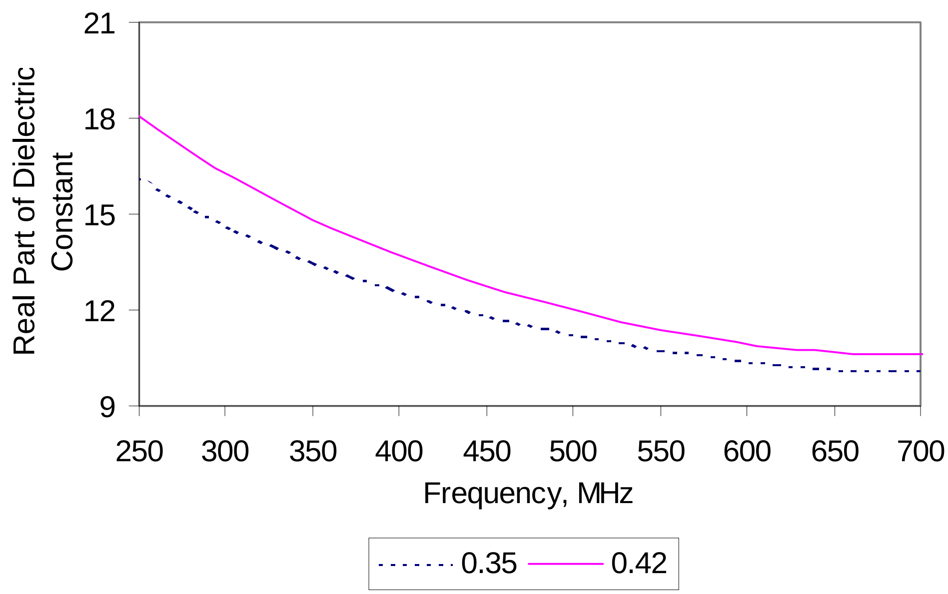


Figure 5.9. Effect of w/c ratio on the real part of the dielectric constant at one day for PCC containing granite aggregate.

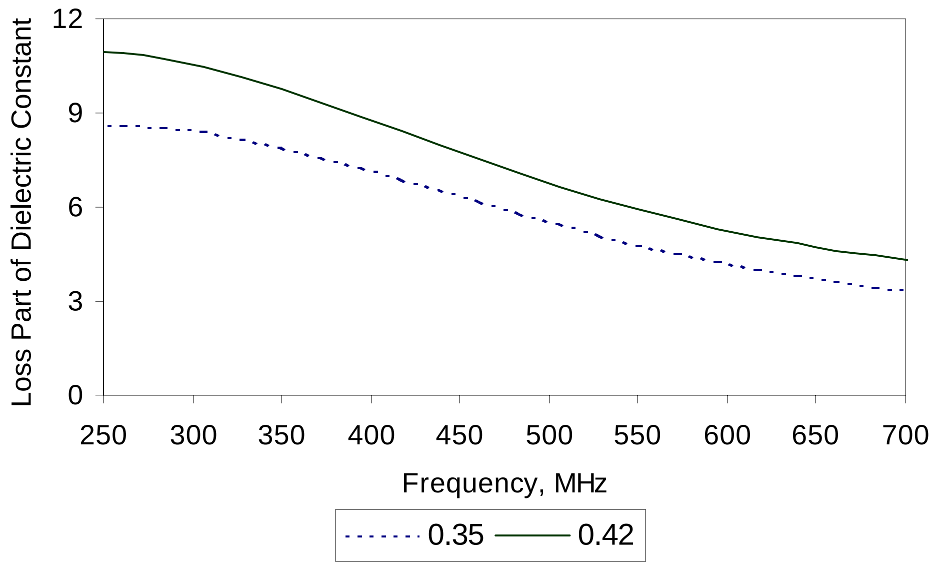


Figure 5.10. Effect of w/c ratio on the loss part of the dielectric constant at one day for PCC containing granite aggregate.

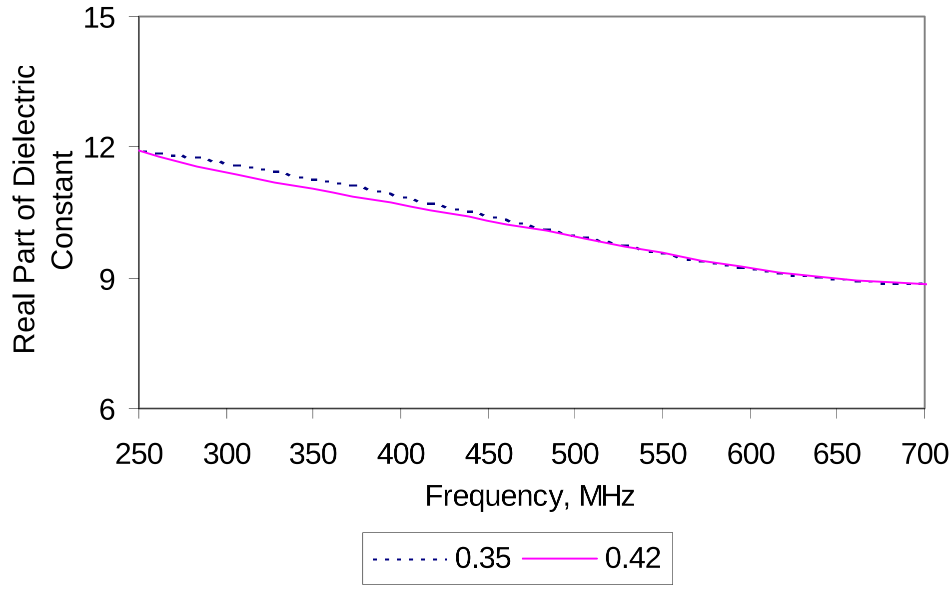


Figure 5.11. Effect of w/c ratio on the real part of the dielectric constant at 28 days for PCC containing granite aggregate.

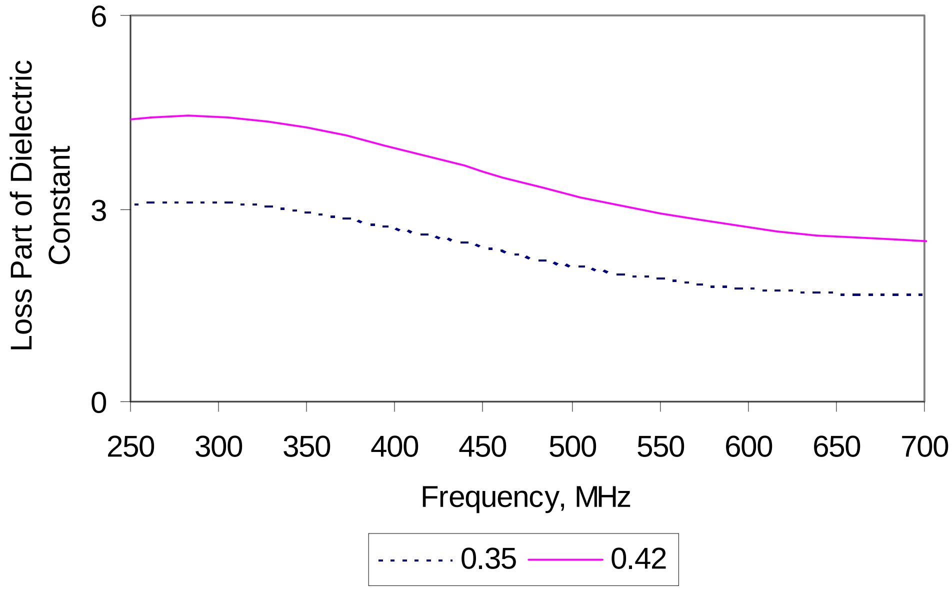


Figure 5.12. Effect of w/c ratio on the loss part of the dielectric constant at 28 days for PCC containing granite aggregate.

Table 5.2. Least significant difference (LSD) test results for the effect of w/c ratio on the dielectric constant.

| w/c ratio | ε' | | ε" | |
|---|---|---|---|---|
| | **1 day** | **28 days** | **1 day** | **28 days** |
| 0.35 | 15.785 A* | 11.9 A | 8.63 A | 3.09 A |
| 0.42 | 17.655 B | 11.8 A | 10.93 A | 4.41 B |

* Same letter indicates no significant differences among the groups.

### 5.3.5 Admixtures

The admixtures used in this research include microsilica, shrinkage admixture and super plasticizer. The only w/c ratio at which all the mixes have been made is 0.42 and those that contain limestone. Therefore, mixes L4N, L4S, L4H, and L4M have been compared at both one and 28 days of curing as shown in Figures 5.13 through 5.16. At one day of curing, there is no significant difference between L4N, L4H, and L4S. However, the real part of the dielectric constant for L4M is slightly lower than the other three, because the microsilica particles have a larger surface area and have early reaction with water. There is not much difference in the loss parts of the dielectric constant for the four mixes at one day. At 28 days, the effect of microsilica can be seen on the loss part. Microsilica fills up the transition zone and makes the PCC less permeable. This makes it difficult for the conduction of the ions loss part. There is also a reduction in polarization, thereby decreasing the real part of the dielectric constant.

Superplasticizers are long chained hydrocarbons with a large number of polar groups in the hydrocarbon chain. But the polar chain is adsorbed on the cement particle, thus making it difficult to polarize. Therefore, mixes containing super plasticizers do not show an increase in the real part of the dielectric constant as evident in Figures 5.13 and 5.15. While there is no appreciable effect on the loss part at one day, the loss part is lower than the control mix at 28 days. It has been reported that the colloidal size of the long-chain particles of the superplasticizer obstruct the bleed-water flow channels in the PCC (Mehta, 1986). This might be responsible for the decrease in the loss part of the dielectric constant. Mix L4S which contains shrinkage admixture does not show any difference in the real part of the dielectric constant from the control mix at one day. However at 28 days, it is higher than the control mix. Since the shrinkage admixture reduces the water tension, it will allow water polarization easier than in the control mixes after 28 days. Therefore, a higher real dielectric constant would be expected for mixes with shrinkage admixture. However conductivity is reduced, thereby resulting in a decrease in the loss part of the dielectric constant.

The significance of the effect of admixtures on the dielectric constant was evaluated using LSD analysis. Table 5.3 gives the results. The results showed no significant difference for both the real and loss parts at one day of curing at frequencies of 305 and 505 MHz. Significant differences were observed in both the real and loss parts at 28 days between the control mix and mixes containing admixtures.

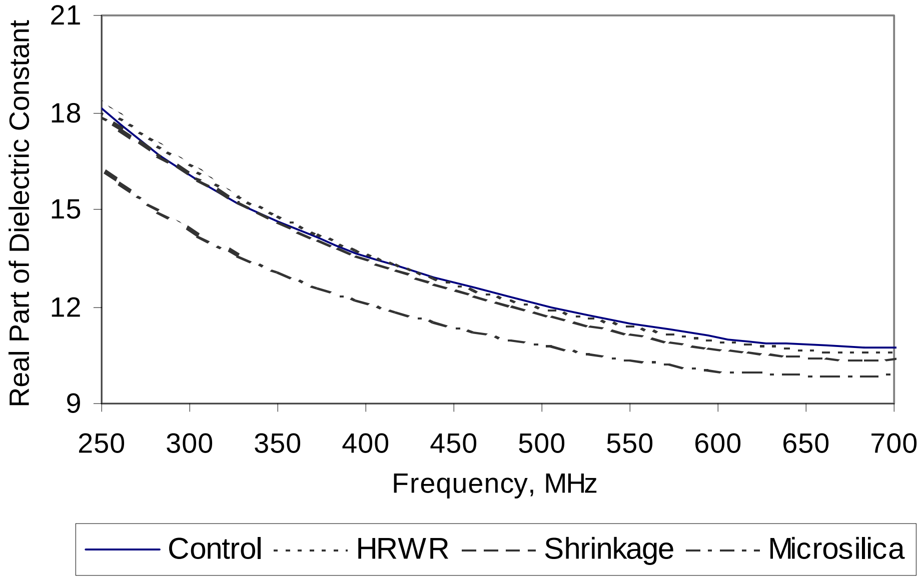


Figure 5.13. Effect of admixtures on the real part of the dielectric constant at one day for mixes containing limestone at a w/c ratio of 0.42.

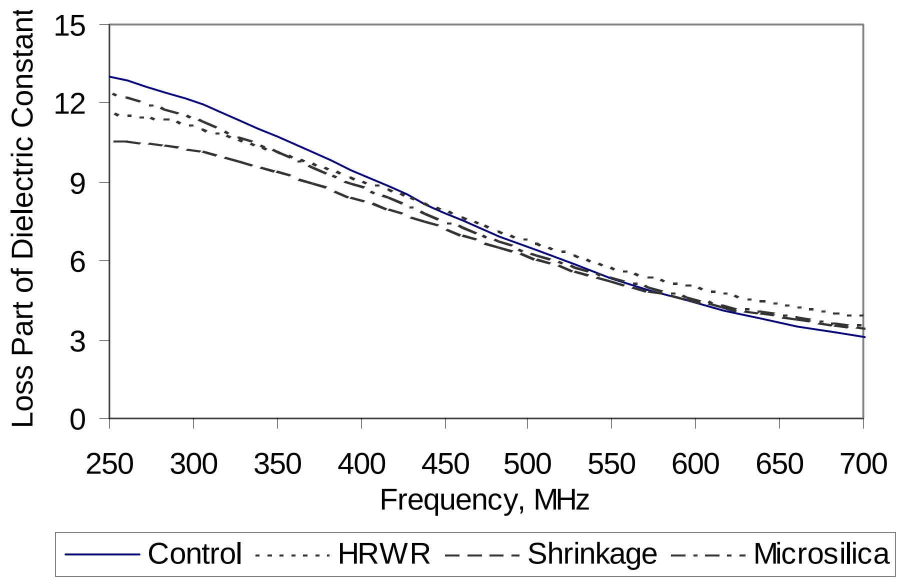


Figure 5.14. Effect of admixtures on the loss part of the dielectric constant at one day for mixes containing limestone at a w/c ratio of 0.42.

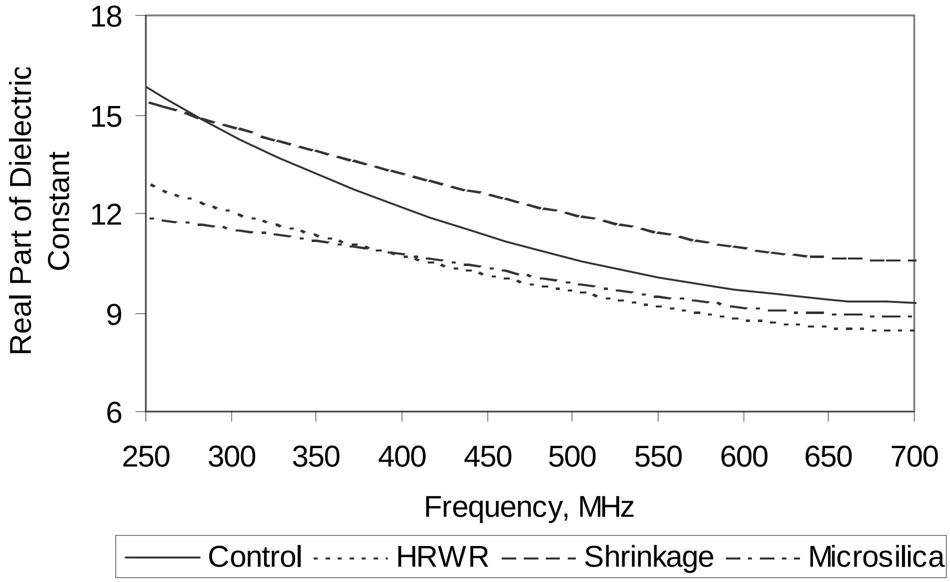


Figure 5.15. Effect of admixtures on the real part of the dielectric constant at 28 days for mixes containing limestone at a w/c ratio of 0.42.

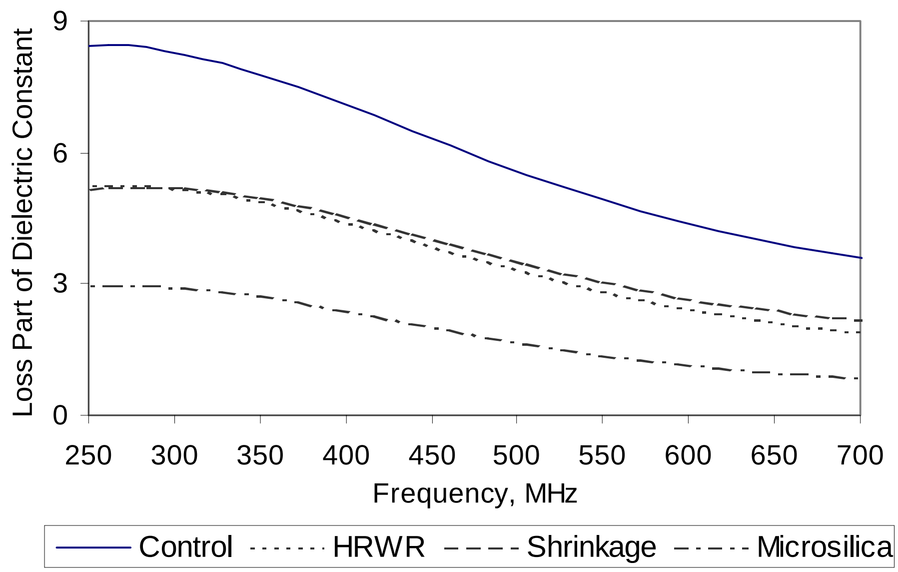


Figure 5.16. Effect of admixtures on the loss part of the dielectric constant at 28 days for mixes containing limestone at a w/c ratio of 0.42.

Table 5.3. Least significant difference (LSD) test results for the effect of admixtures on the dielectric constant.

| Curing Time (Days) | Mix | ε' | | ε" | |
|---|---|---|---|---|---|
| | | 305 MHz | 505 MHz | 305 MHz | 505 MHz |
| 1 | L4N | 15.885 A* | 11.975 A | 11.935 A | 6.36 A |
| | L4S | 15.915 A | 11.705 A | 10.165 A | 6.09 A |
| | L4H | 16.165 A | 11.905 A | 11.07 A | 6.695 A |
| | L4M | 14.22 A | 10.77 A | 11.32 A | 6.275 A |
| 28 | L4N | 14.255 A | 10.56 B | 8.24 A | 5.495 A |
| | L4S | 14.585 A | 11.92 A | 5.19 B | 3.455 B |
| | L4H | 12.025 B | 9.61 C | 5.17 B | 3.275 B |
| | L4M | 11.535 B | 9.89 BC | 2.915 C | 1.645 C |

* Same letter indicates no significant differences among the groups.

### 5.3.6 Chlorides

Figures 5.17 and 5.18 show the effect of chlorides on the real and loss parts of the dielectric constant at one day of curing. The mixes being compared are G4N, G4C2, and G4C4. Both the real and the loss parts of the dielectric constant showed a dependence on the amount of chlorides in the PCC, with higher values for mixes containing chlorides. At one day of curing, there is a lot of free water in the mix along with the large number of chloride ions from the sodium chloride and calcium and hydroxyl ions from the hydration. This results in high ionic polarization and conductivity leading to higher values of the dielectric constant. However the increase in the dielectric constant is not significant. This insignificant increase is in direct proportion to the concentration of chlorides. An earlier study by Al-Qadi and Riad (1996) also showed insignificant changes in the both the real and the loss part of the dielectric constant with different amounts of chlorides at 28 days of curing. Figures 5.19 and 5.20 show the effect of chlorides for the same specimens at 90 days of curing, when the concrete is well hydrated. Due to the formation of the CSH gel, the amount of free water in the PCC is greatly reduced. The reduction in the permeability of the PCC would make it difficult for the chloride ions to move through the pores. The locking up of the polar molecules would result in a decrease in both polarization and conductivity. However, the results at 90 days of curing do not reflect a decrease in the real part of the dielectric constant. The real part is still higher than the control mix for both G4C2 and G4C4. However, the real part of the dielectric constant for mix G4C4 is lower than mix G4C2. The higher amount of chlorides in G4C4 might have led to crystallization. This would lead to a decrease in ionic polarization and thus the dielectric constant. Also, the reduction in conductivity might be more for G4C2 and G4C4 than G4N due to possible crystallization in the former two mixes which may result in a lower value for the loss part.

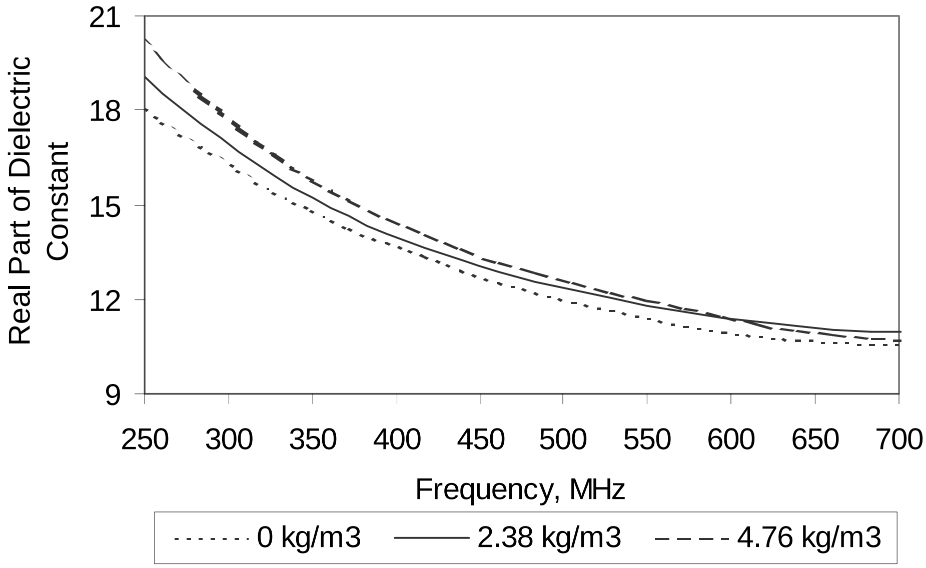


Figure 5.17. Effect of chlorides on the real part of the dielectric constant at one day for mixes containing granite at a w/c ratio of 0.42.

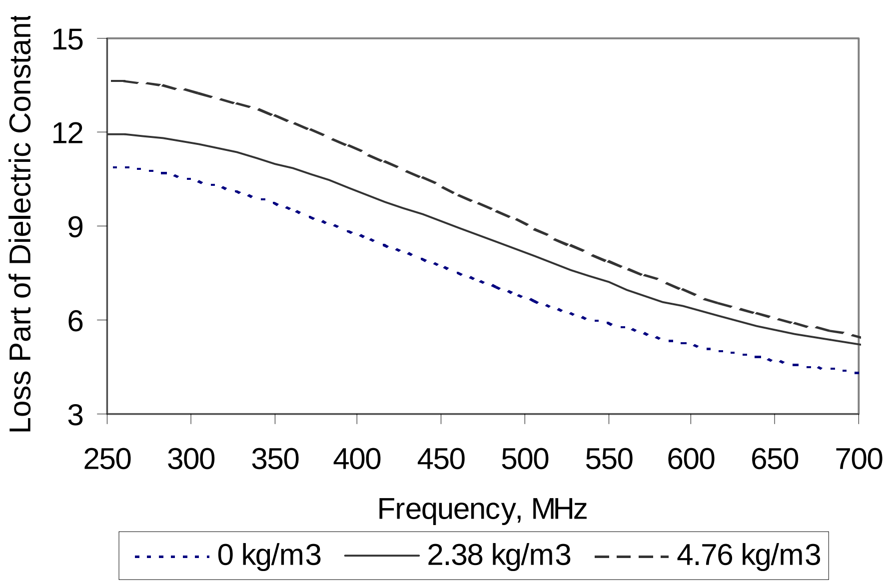


Figure 5.18. Effect of chlorides on the real part of the dielectric constant at one day for mixes containing granite at a w/c ratio of 0.42.

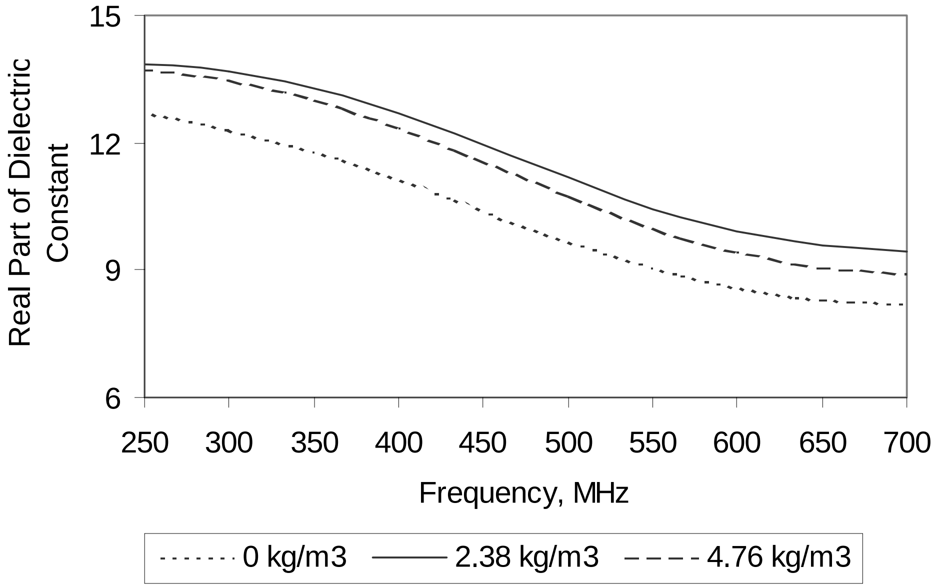


Figure 5.19. Effect of chlorides on the real part of the dielectric constant at 90 days for mixes containing granite at a w/c ratio of 0.42.

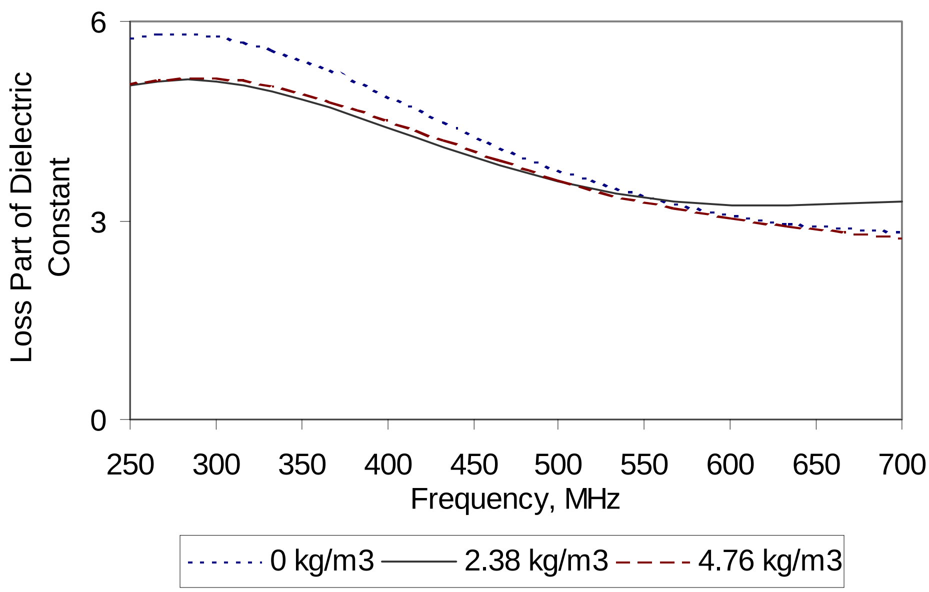


Figure 5.20. Effect of chlorides on the loss part of the dielectric constant at 90 days for mixes containing granite at a w/c ratio of 0.42.

Table 5.4 gives the results of the LSD analysis performed to evaluate the significance of the addition of chlorides on the real and loss parts of the dielectric constant at one day of curing. No significant difference in the real part of the dielectric constant at 261 and 505 MHz for mixes G4N, G4C2, and G4C4 was observed. The loss part at 261 MHz for G4C4 is significantly higher than G4N and G4C2. At 505 MHz, the loss part is significantly different for all three mixes.

Table 5.4. Least significant difference (LSD) test results for the effect of chloride content on the dielectric constant.

| **Added chloride level (kg/m$^3$ of PCC)** | **Measured chloride level (kg/m$^3$ of PCC)*** | **ε'** | | **ε"** | |
|---|---|---|---|---|---|
| | | **261 MHz** | **505 MHz** | **261 MHz** | **505 MHz** |
| 0 | 0.22 | 17.655 A | 11.935 A | 10.93 A | 6.67 A |
| 2.38 | 2.24 | 18.545 A | 12.285 A | 11.915 A | 8.02 B |
| 4.76 | 4.39 | 19.605 A | 12.545 A | 13.65 B | 8.94 C |

* Chloride content is measured using water soluble chloride test in accordance with ASTM C 1218-92b after 90 days of moist curing.

### 5.3.7 Water content

The water content of the PCC by weight, $W_W$, in terms of percentage can be calculated by:

$$W_w = \frac{M_w - M_d}{M_d} \times 100 \qquad 5.9$$

where, $M_w$ is the weight of PCC with water, and $M_d$ is the weight of concrete in an oven-dry state.

The water content of PCC by volume, $W_v$, can be calculated by:

$$W_v = \frac{\rho_d}{\rho_w} \times W_w \qquad 5.10$$

where, $\rho_d$ is the density of concrete in the oven-dry state, and $\rho_w$ is the density of water.

Measurements for studying the effect of water content on the dielectric constant were performed in both the 1 ns and the 3 ns windows. Figure 5.21 and 5.22 show the variation of the real and loss parts of the dielectric constant for G4M2 at different levels of moisture and the dry state, with the frequency for measurements at a 3 ns window. The amount of free water in PCC is expected to play a significant role in the dielectric constant of PCC since it has a dielectric constant of 81, which is far greater than that of PCC (4-17, from present study). After all the specimens were moist cured for 90 days, they were submerged in a water bath to be saturated till they showed no further increase in weight. The dielectric constant at this level of moisture was found to be lower than that at a lower moisture level. This behavior was observed for all the mixes. Subsequent measurements at lower levels of moisture did not show this behavior. Since the specimens were allowed to dry for about an hour after taking them out of the water, it might be possible that a thin film of water might have formed on the surface. This might be responsible for the low value of the dielectric constant while compared to the dielectric constant at lower moisture contents.

As expected, both the real and the loss parts of the dielectric constant show a decrease with the decreasing water content, except for a water content of 16.54% which is the water content at saturation. Both the real and the loss parts of the dielectric constant show a decrease over the frequency range when there is water in the PCC. When there is no water present in the PCC (0%), both the real and the loss parts show stable behavior over the entire frequency range. There is a significant reduction in the loss part when the water content drops from 3.62% to 0% thereby proving that water is mainly responsible for the lossy behavior.

The real part at 0% water is constant over the entire frequency range. Since there is no water, and hence no polarization of the water, the real part of the dielectric constant is due only to the aggregate and the cement paste. The polarization depends on the frequency of oscillation of the polar molecules. The absence of any polar molecules at 0% water content would therefore lead to a stable value of the dielectric constant over the entire frequency range. The very small value for the loss part of the dielectric constant at 0% would indicate that the lossy behavior of the PCC is dominated by conductivity and the dielectric loss does not contribute much. It can also be interpreted to show that the bound water does not have much of an effect on the loss part. Since the specimens have varying adsorption rates and hence varying water contents, it is not possible to compare them statistically. However, it can be seen that water content, has a greater effect on the dielectric constant than the type of mix or w/c ratio. Appendix E presents the results from measurements at a 3 ns window while Appendix F provides the results for measurements at a 1 ns window.

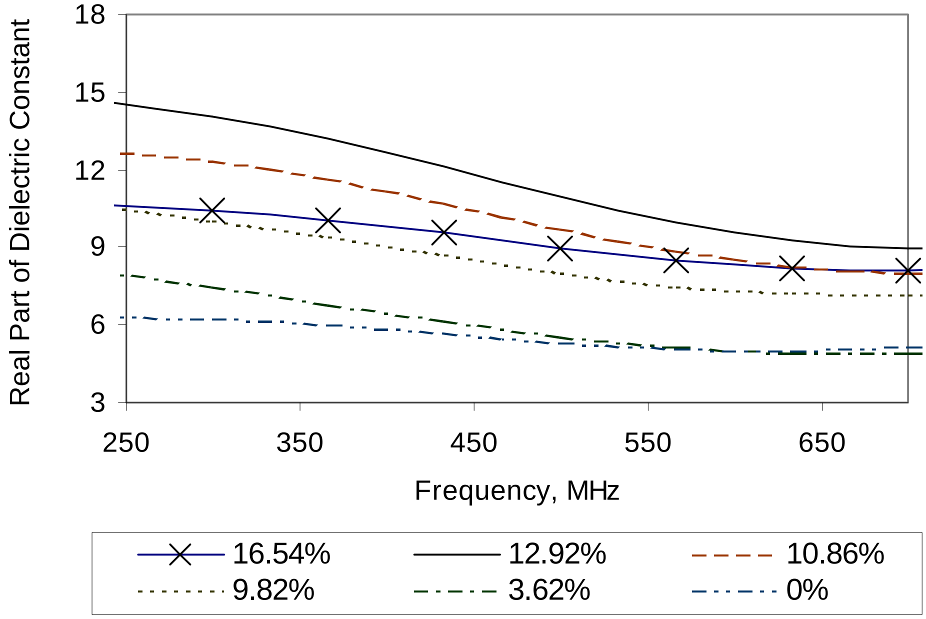


Figure 5.21. Effect of water content on the real part of the dielectric constant for G4M2, for measurements taken at a 3 ns time window.

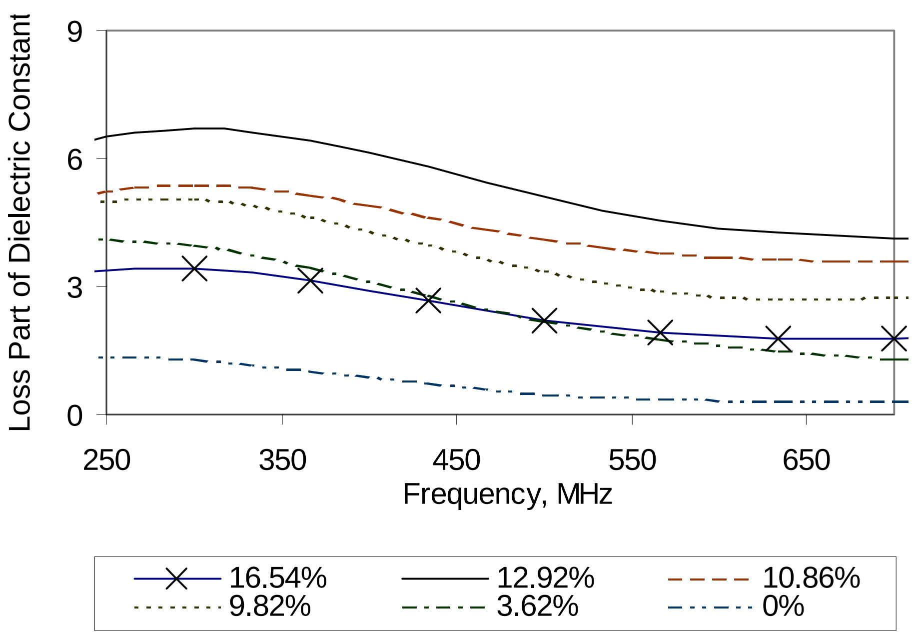


Figure 5.22. Effect of water content on the loss part of the dielectric constant for G4M2, for measurements taken at a 3 ns time window.

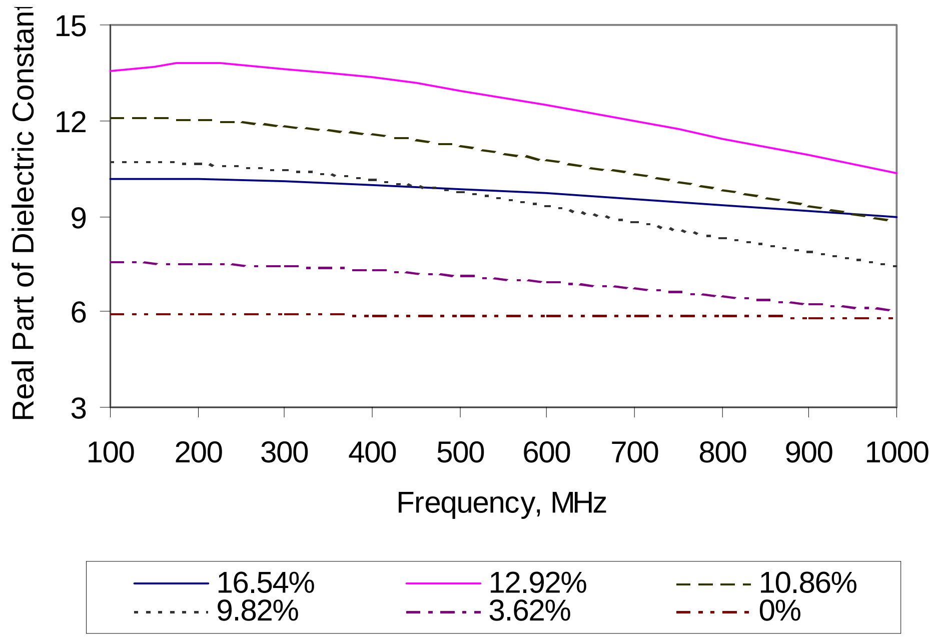


Figure 5.23. Effect of water content on the real part of the dielectric constant for G4M2, for measurements taken at a 1 ns time window.

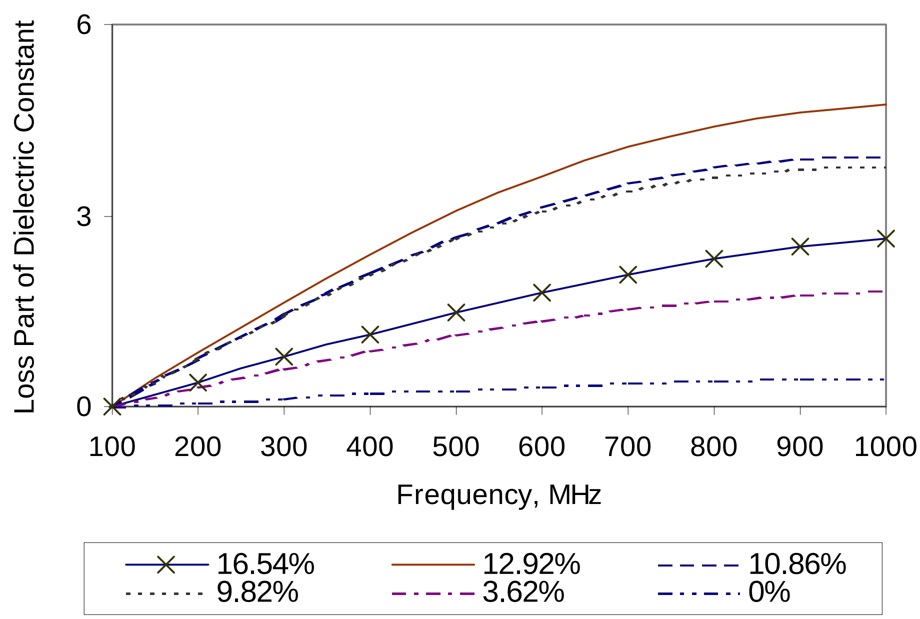


Figure 5.24. Effect of water content on the loss part of the dielectric constant for G4M2, for measurements taken at a 1 ns time window.

## 5.4 Results from Permeability Testing

Table 5.5 lists the coulomb values of the different mixes tested at 75 days of curing. Specimens were cast in duplicates and the average value of the two measurements is presented. Mixes with low w/c ratios, which have much less permeability, exhibited low coulomb values. Mixes with microsilica have a low permeability due to the improvement in the microstructure of the transition zone and the subsequent reduction in porosity of the PCC. Mixes L4M and L5M exhibited low coulomb values of 952 and 1056, respectively, thus showing that the use of microsilica had a more dominant effect than the w/c ratio unlike the other mixes. Since the permeability test measures the current passing through the PCC specimen, concrete containing chlorides would have a higher coulomb value because of their high conductivity. Mix G4C4, which has a chloride level of 4.76 kg/$m^3$ of PCC, had a coulomb value of 5853 compared to 4509 for control mix G4N. Similarly mixes L4C2 and L4C4 which have chloride levels of 2.38 kg/$m^3$ of PCC and 4.76 kg/$m^3$ of PCC, respectively, had high coulomb values of 4918 and 5629, respectively. Compared to L4C4 which has a coulomb value of 5629, mix L3C4 has a relatively low coulomb value of 2750 since the PCC has a low w/c ratio. Therefore, the microstructure of the concrete is more important than the presence of chlorides.

## 5.5 Correlation between the Permeability and Measured Dielectric Properties

The permeability of PCC depends on the pore structure, which in turn depends on how long the PCC has cured. The dielectric constant also depends on the amount of curing. Therefore, it might be possible to establish a relationship between the permeability and dielectric constant of PCC. Table 5.5 also lists the real and loss parts of the dielectric constant at 75 days. Since the dielectric constant is sensitive to change at the lower frequencies, the comparison was made at 300 MHz. Since the loss part of the dielectric constant depends on the conductivity, mixes exhibiting lossy behavior should have a high coulomb value. Figures 5.25, 5.26, and 5.27 show the linear regression between the coulomb value and the real, loss, and magnitude of the dielectric constant, respectively. The correlation coefficient, r, between the loss part and the coulomb value for the twelve mixes tested is 0.79, while it is 0.75 between the real part and the coulomb value. This indicates that the coulomb value is dependent on both the real and the loss parts. On comparing the magnitude of the complex dielectric constant with the coulomb value, the correlation coefficient, r, is 0.81, thus indicating that there is a strong correlation of the coulomb value with both parts of the complex dielectric constant. The root mean square error (RMSE) is also lower for the model between the coulomb value and magnitude of the dielectric constant.

Table 5.5. Coulomb values and dielectric constant at 75 days.

| Mix | Coulombs | Dielectric Constant (300 MHz) | |
|---|---|---|---|
| | | **Real** | **Loss** |
| L3H | 1552 | 12.47 | 4.94 |
| L4H | 3416 | 11.36 | 5.15 |
| L3S | 1999 | 14.23 | 2.11 |
| L4M | 952 | 11.73 | 3.41 |
| L5M | 1056 | 11.94 | 4.4 |
| L3C8 | 2750 | 14.05 | 5.82 |
| L4C4 | 4918 | 16.1 | 7.08 |
| L4C8 | 5629 | 16.21 | 7.72 |
| G3N | 3540 | 12.6 | 4.15 |
| G4N | 4509 | 14.67 | 6.02 |
| G4C8 | 5853 | 14.26 | 6.25 |
| G4M | 1236 | 10.52 | 3.8 |

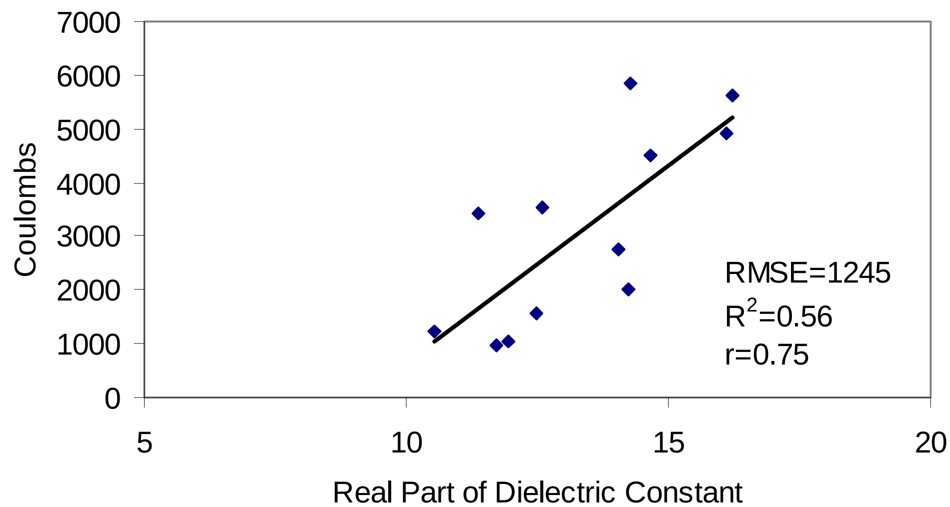


Figure 5.25. Linear regression between Coulomb value and real part of the dielectric constant.

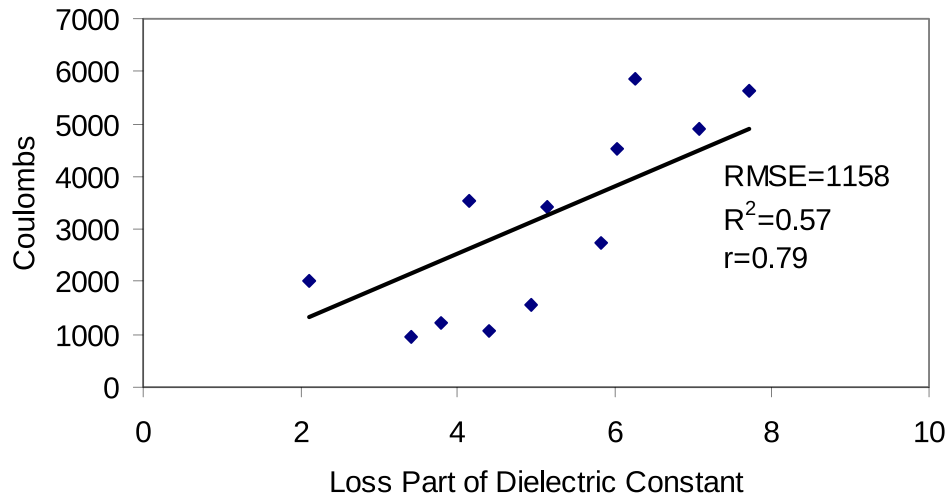


Figure 5.26. Linear regression between Coulomb value and loss part of the dielectric constant.

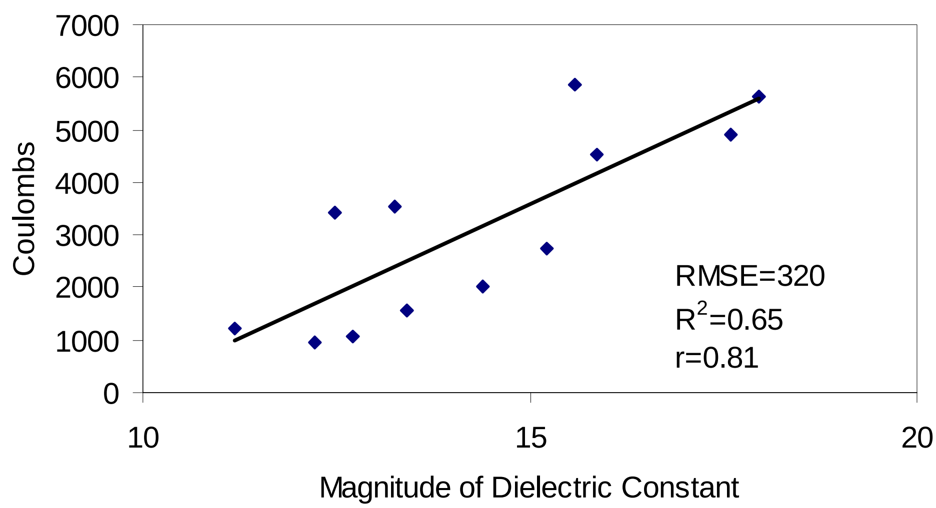


Figure 5.27. Linear regression between Coulomb value and magnitude of the complex dielectric constant.

# CHAPTER 6. SUMMARY, FINDINGS, AND CONCLUSIONS

This study was conducted to characterize PCC electrically in the 100 to 1000 MHz range using a coaxial transmission line developed earlier at Virginia Tech. All measurements were obtained in the time domain and converted to the frequency domain using Fast Fourier Transform. The effect of water content, aggregate type, w/c ratio, curing period, and admixtures on measured dielectric properties was studied. The relationship between the chloride permeability (based on conductance measurements) and the dielectric constant at 75 days of moist curing was also investigated.

## 6.1 Findings

Based on this study, the following findings were made:

- Measurements taken with a 3 ns window showed an increase in the real part of the dielectric constant after 700 MHz and an increase in the loss part between 100 and 250 MHz. Measurements taken with a 1 ns window showed a continuous decrease for the real part of the dielectric constant from 100 to 1000 MHz. The loss part unexpectedly increased from 100 to 1000 MHz.

- Mixes containing limestone aggregate have a greater dielectric constant than mixes containing granite aggregate because of the higher dielectric constant of limestone compared to granite.

- Mixes containing granite at a w/c ratio of 0.42, showed no significant difference in the real part of the dielectric constant from mixes at a w/c ratio of 0.35 after 28 days of moist curing.

- Both the real and loss parts of the dielectric constant showed a decrease with increasing curing time.

- The presence of chlorides in PCC increased both the real and the loss parts of the dielectric constant, particularly at one day of moist curing.

- Admixtures did not have any significant effect on the dielectric constant at one day of curing.

- The dielectric constant increased with increasing the amount of free water in PCC. However, in an oven dry condition, the dielectric constant of oven-dried PCC maintained a constant value over the frequency range of 250-700 MHz.

- Concrete containing chlorides exhibited a high coulomb value (using permeability test).

## 5.2 Conclusions

The following conclusions can be drawn from this study:

- The dielectric constant behavior of PCC depends on the selected time window for measurements.

- Difference in the dielectric constant for different mixes is more apparent at low microwave frequencies.

- Aggregate type affects the measured dielectric constant of PCC.

- The dielectric constant depends on the amount of free water available in the PCC and the degree of hydration. When there is no free water available in the PCC, there is a large reduction in the polarization and conductivity and thus measured dielectric constant of PCC is mainly due to its composition (aggregate and the cement paste).

- Chlorides have a more significant influence on the loss part of the dielectric constant than the real part.

- There is a correlation between the permeability test (based on conductance measurements) of PCC and the measured complex dielectric constant; both values are related to the conductivity of PCC.

## REFERENCES

Al-Qadi, I. L., and Riad, S. M., Characterization of Portland Cement Concrete: Electromagnetic and Ultrasonic Measurement Techniques, Report Submitted to the National Science Foundation, Washington, DC, 1996.

Al-Qadi, I. L., Riad, S. M., Mostafa, R., and Su, W., "Design and Evaluation of a Coaxial Transmission Line Fixture to Characterize Portland Cement Concrete," Proceeding of the 6th International Conference on Structural Faults and Repairs, Edinburgh, UK, 1995, pp. 337-347.

Al-Qadi, I. L., Su, W., Riad, S. M., Mostafa, R., and Hazim, O. A., "Coaxial Fixture Development to Characterize Portland Cement Concrete," Proceedings of the Symposium and Workshop on Time Domain Reflectometry in Environment, Infrastructure and Mining Applications, Evanston, Il, 1994, pp. 443-452.

Annual Book of ASTM Standards, Concrete and Aggregate, Section 4, Vol. 4.02, ASTM, Philadelphia, PA, 1995.

Bungey, J. H., Shaw, M. R., Millard, S. G., Soutsos, M. N., and Austin, B. A., "The Influence of Concrete Composition upon Radar Test Results," Conference Proceedings of The British Institute of Non-Destructive Testing, International Conference NDT in Civil Engineering, England, 1997, pp 474-481.

Cement and Concrete Association Publication 45.030, Superplasticizing Admixtures in Concrete, Cement and Concrete Association, England, 1976.

Chew, W. C., Olp, K. J. and Otto, G. P., “Design and Calibration of a Large Broadband Dielectric Measurment Cell,” IEEE Transactions on Geoscience and Remote Sensing, Vol. 29, No. 1, January 1991, pp. 42-47.

Chipman, R. A., *Theory and Problems of Transmission Lines*, Schaum's Outline Series, McGraw Hill Book Company, New York, NY, 1968.

Cole, K. S., and R. H. Cole., “Dispersion and Absorption in Dielectrics; I. Alternating Current Characteristics,” Journal of Chemical Physics, Vol. 9, 1941, pp. 341-351.

Courtney, C., Lehr, J., Mason, D., Motil, B., and Lovesee, A., Measurement and Characterization of the Electromagnetic Properties of Materials, Voss Scientific Technical Report No. VS-603, Albuquerque, August 1996.

Hertz, H. R., *Electric Waves,* Macmillan and Co., Ltd., London, 1900.

Klein, L. A., and Swift, C. T., "An Improved Model for the Dielectric Constant of Sea Water at Microwave Frequencies," IEEE Trans. Antennas Propagation, Vol. AP-25, January 1977, pp. 104-111.

Kreigger, P. C., Admixtures, Proceedings of International Congress on Admixtures, The Construction Press, New York, NY, 1980.

Lea, F. M., *The Chemistry of Cement and Concrete*, Chemical Publishing Company, Inc., New York, NY, 1971.

McCarter, W. J., and Curran, P. N., “The Electrical Response Characteristics of Setting Cement Paste,” Magazine of Concrete Research, Vol. 36, No. 126, March 1984, pp. 42-49.

Mehta, P. K., *Concrete: Structure, Properties and Materials*, Prentice Hall, Englewood Cliffs, NJ, 1986.

Mindess, S., and Young, J. F., *Concrete*, Prentice-Hall, Inc., New Jersey, NJ, 1981.

Mostafa, R., Wideband Electromagnetic Characterization of Portland Cement Concrete, Masters Thesis, The Bradley Department of Electrical Engineering, Virginia Tech, Blacksburg, VA, 1995.

Ozyildirim, C., and Halstead, W., “Improved Concrete Quality with Combinations of Fly Ash and Silica fume,” ACI Materials Journal, Vol. 91, No. 6, November-December 1994.

Powers, T. C., "Structure and Physical Properties of Hardened Portland Cement Paste," Journal of American Ceramic Society, Vol. 61, No. 1, 1958, pp. 1-5.

Product information brochure, "Shrinkage Reducing Admixture from Grace Construction Products," W. R. Grace & Co., Cambridge, Massachusetts, 1997.

Ramachandran, V. S., *Concrete Admixtures Handbook*, Noyes Publication, Canada, 1995.

Ramo, S., and Whinnery, J. R., *Fields and Waves in Modern Radio,* John Wiley and Sons, Inc., New York, NY, 1944.

Rau, R. N., and Wharton, R. P., "Measurement of Core Electrical Parameters at Ultrahigh and Microwave Frequencies," Journal of Petroleum Technology, November 1982, pp. 2689-2700.

Rhim, H. C., and Buyukozturk, O., “Electromagnetic Properties of Concrete at Microwave Frequency Range,” ACI Materials Journal, Vol. 95, No. 3, May-June 1998, pp. 262-271.

Robert, A., Baillon, L., and Huet, C., "Design and Calibration of a Dielectric Measurement Cell for Concrete with Large Grain Heterogeneities,” International Symposium Non-Destructive Testing in Civil Engineering, Berlin, 1995, pp. 1053-1061.

Scaffer, J. P., Saxena, A., Antolovich, S. D., Sanders, T. H., and Warner, S. B., *The Science and Design of Engineering Materials*, Richard D. Irwin, Inc., New York, NY, 1995.

Shaw, M. R., Millard, S. G., Houlde, M. A., Austin, B. A., and Bungey, J. H., “A Large Diameter Transmission Line for the Measurement of the Relative Permittivity of Construction Materials,” British Journal of NDT, Vol. 35, No. 12, December 1993, pp. 696-704.

Weyers, R. E., Prowell, B. D., Sprinkel, M. M., and Vorster, M., Concrete Bridge Protection, Repair, and Rehabilitation Relative to Reinforcement Corrosion: A Methods Application Manual, SHRP-S-360, Strategic Highway Research Program, National Research Council, 1993.

Whittington, H. W., McCarter, W. J., and Forde, M. C., "The Conduction of Electricity Through Concrete," Magazine of Concrete Research, Vol. 33, No. 114, March 1981, pp. 48-60.

# APPENDIX A

## PROPERTIES OF AGGREGATES , MIX DESIGN, AND QUALITY CONTROL MEASUREMENTS

Table A.1. Physical properties of aggregates.

| Physical Propery | Granite | | Limestone | |
|---|---|---|---|---|
| | CA | FA | CA | FA |
| Bulk Specific Gravity | 2.86 | 2.45 | 2.8 | 2.53 |
| Absorption (%) | 0.72 | 1.39 | 0.7 | 3.31 |
| Fineness Modulus | | 2.92 | | 3.2 |
| Unit Weight (kg/m3) | 100.5 | | 93.2 | |

CA: Coarse aggregate
FA: Fine aggregate

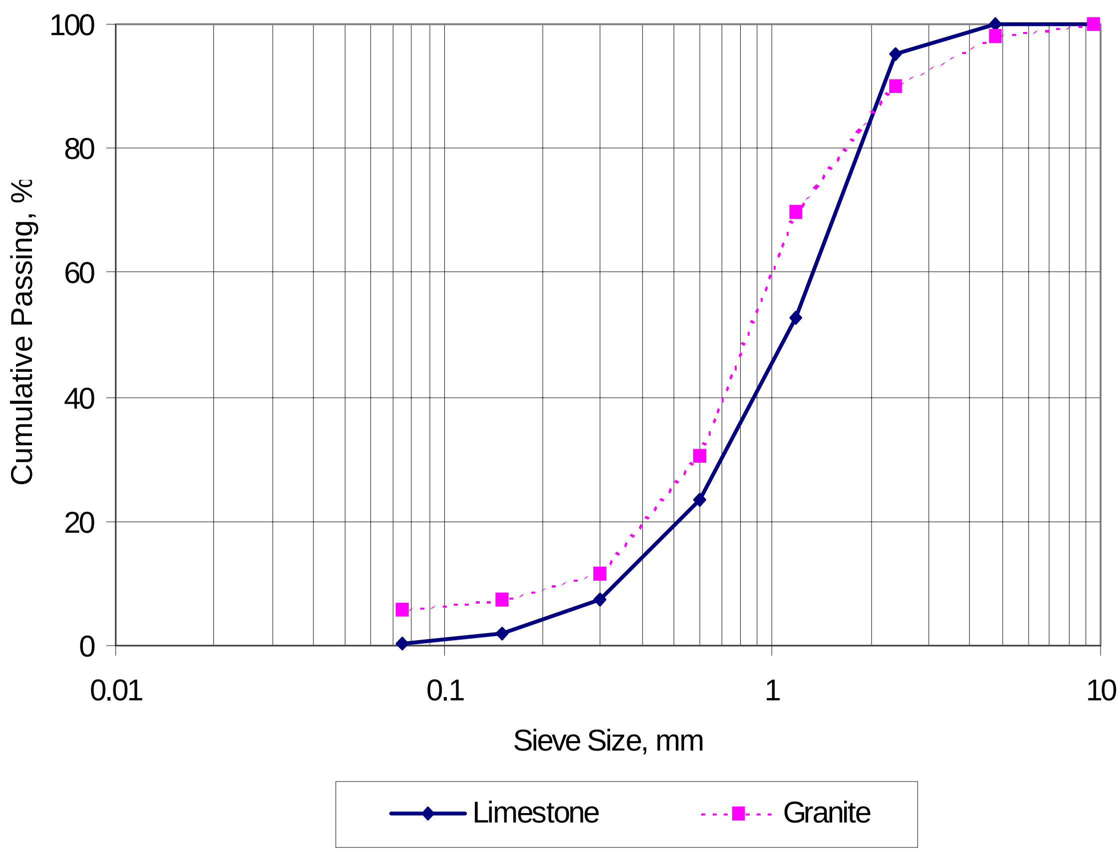


Figure A.1. Gradation of fine aggregate.

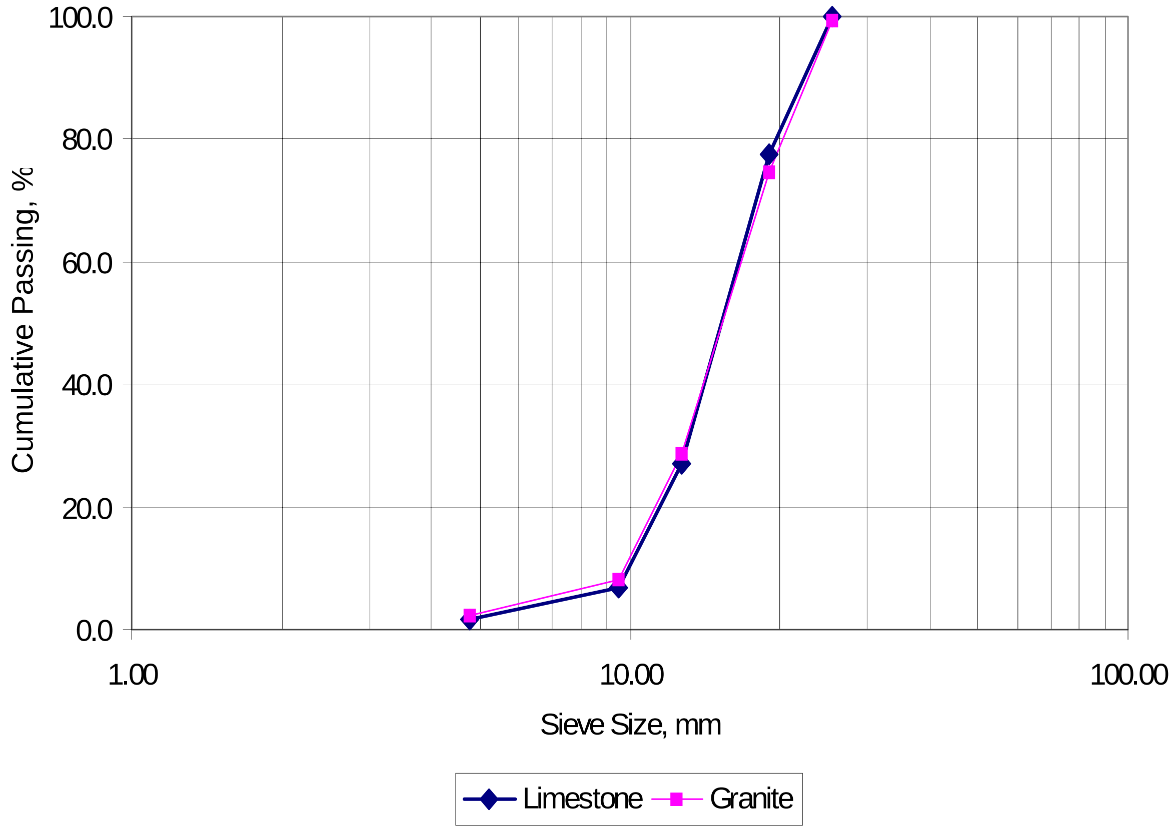


Figure A.2. Gradation of coarse aggregate.

Table A.2. Design of mixes.

| Mix | Water | FA | CA | Cement |
|---|---|---|---|---|
| | kg | kg | kg | kg |
| L3N | 4.10 | 12.60 | 17.88 | 10.15 |
| L4N | 4.14 | 13.96 | 17.88 | 8.46 |
| L5N | 4.18 | 15.05 | 17.88 | 7.11 |
| L4M | 4.13 | 14.39 | 17.88 | 7.86 |
| L5M | 4.16 | 15.53 | 17.88 | 6.61 |
| L3H | 4.09 | 11.78 | 19.18 | 7.11 |
| L4H | 4.09 | 13.18 | 19.18 | 8.46 |
| L3S | 4.10 | 12.60 | 17.88 | 10.15 |
| L4S | 3.81 | 13.30 | 16.53 | 7.81 |
| L5S | 3.59 | 13.85 | 15.95 | 6.34 |
| L3C8 | 4.71 | 15.00 | 20.63 | 11.71 |
| L4C4 | 4.09 | 13.18 | 19.18 | 8.46 |
| L4C8 | 4.09 | 13.18 | 19.18 | 8.46 |
| G3N | 3.77 | 11.76 | 19.45 | 10.15 |
| G4N | 3.79 | 13.17 | 19.45 | 8.46 |
| G4M | 3.79 | 13.17 | 19.45 | 7.87 |
| G4C4 | 4.08 | 14.44 | 20.66 | 9.11 |
| G4C8 | 3.79 | 13.17 | 19.45 | 8.46 |

Table A.3. Quality control measurements for different mixes.

| Mix | Slump | Unit weight | Air content | 28 day compressive |
|---|---|---|---|---|
| | mm | $kg/m^3$ | % | strength, MPa |
| L3N | 25 | 2474.5 | 1.5 | 53 |
| L4N | 102 | 2470.7 | 1.4 | 42 |
| L5N | 140 | 2478.4 | 2.1 | 35 |
| L4M | 38 | 2474.5 | 1.2 | 51 |
| L5M | 76 | 2432.2 | 1.8 | 44 |
| L3H | 114 | 2446.3 | 1.6 | 54 |
| L4H | 140 | 2470.7 | 1.5 | 52 |
| L3S | 51 | 2473.3 | 1.8 | 44 |
| L4S | 102 | 2474.5 | 1.6 | 40 |
| L5S | 140 | 2484.8 | 1.5 | 31 |
| L3C8 | 51 | 2446.3 | 1.6 | 50 |
| L4C4 | 102 | 2446.3 | 1.7 | 44 |
| L4C8 | 102 | 2443.8 | 1.7 | 42 |
| G3N | 64 | 2443.8 | 1.7 | 66 |
| G4N | 127 | 2443.8 | 1.5 | 55 |
| G4M | 38 | 2474.5 | 2 | 54 |
| G4C4 | 140 | 2489.9 | 1.6 | 55 |
| G4C8 | 127 | 2443.8 | 1.5 | 46 |

# APPENDIX B

# MATLAB PROGRAMS

### B.1. Program for measurements in 3 ns window

```
clear

load ll5m23

N=35;
iii=4:2:N;
F1=(1e3/(30))*(iii-1);
ref1=-(refa-refa(1));
res1=resa-resa(1);

for k1=1:512;
ref1(512+k1)=ref1(512)-ref1(k1);
res1(512+k1)=res1(512)-res1(k1);
end

N_zero1=1024*4;
ref2=[ref1' zeros(1,N_zero1)];
res2=[res1' zeros(1,N_zero1)];
RF=fft(ref2);
RS=fft(res2);
s11a=RS(iii)./RF(iii);
epsln1=((1-s11a)./(1+s11a)).^2;
end

figure(1)
clf
plot(F1,real(epsln1),'k',F1,-imag(epsln1),'k')
grid
xlabel('Frequency, MHz')
ylabel('Dielectric Constant')
axis([100 1000 -1 25])
```

```
disp('Saving File')
yy=[F1;real(epsln1);-imag(epsln1)];
fid=fopen('ll5m23.txt','a+');
fprintf(fid,'%10.4f\t %10.4f\t %10.4f\n',yy);
fclose(fid);
```

### B.2. Program for measurements in 1 ns window

```
clear

load teflon1

N=10;
iii=1:1:N;
F1=(1e3/(10))*(iii);
ref1=-(refa-refa(1));
res1=resa-resa(1);

for k1=1:512;
ref1(512+k1)=ref1(512)-ref1(k1);
res1(512+k1)=res1(512)-res1(k1);
end

N_zero1=1024*4;
ref2=[ref1' zeros(1,N_zero1)];
res2=[res1' zeros(1,N_zero1)];
RF=fft(ref2);
RS=fft(res2);
s11a=RS(iii)./RF(iii);
epsln1=((1-s11a)./(1+s11a)).^2;
end

figure(1)
clf
plot(F1,real(epsln1),'k',F1,-imag(epsln1),'k')
grid
xlabel('Frequency, MHz')
ylabel('Dielectric Constant')
axis([100 1000 -1 25])
```

```
disp('Saving File')
yy=[F1;real(epsln1);-imag(epsln1)];
fid=fopen('teflon1.txt','a+');
fprintf(fid,'%10.4f\t %10.4f\t %10.4f\n',yy);
fclose(fid);
```

# APPENDIX C

## EFFECT OF FREQUENCY ON THE DIELECTRIC CONSTANT OVER DIFFERENT CURING TIMES (3 ns WINDOW)

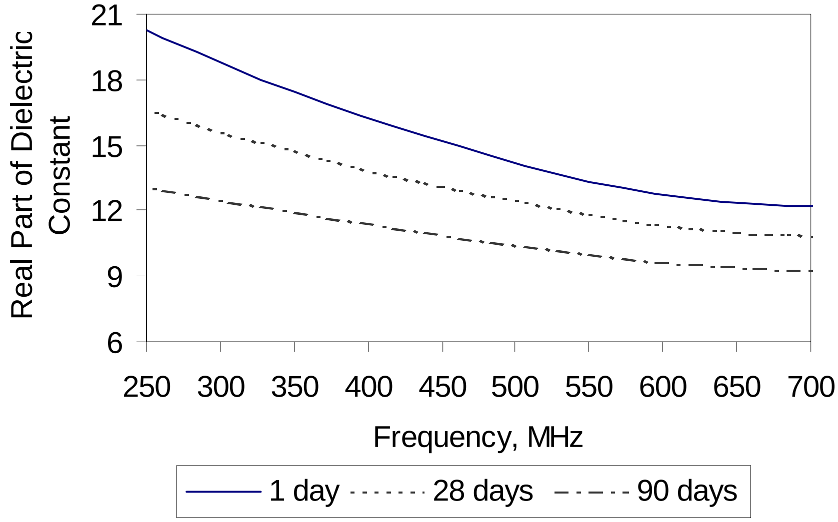


Figure C.1. Effect of frequency on the real part of the dielectric constant for L3N over different curing times.

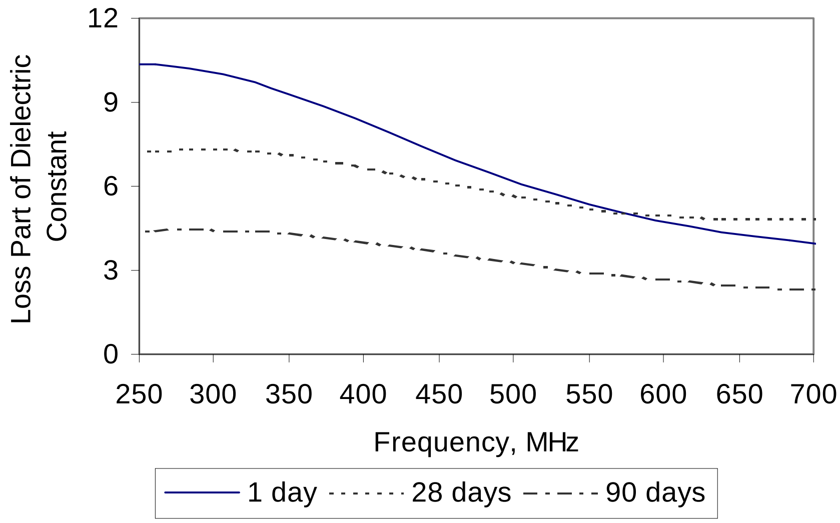


Figure C.2. Effect of frequency on the loss part of the dielectric constant for L3N over different curing times.

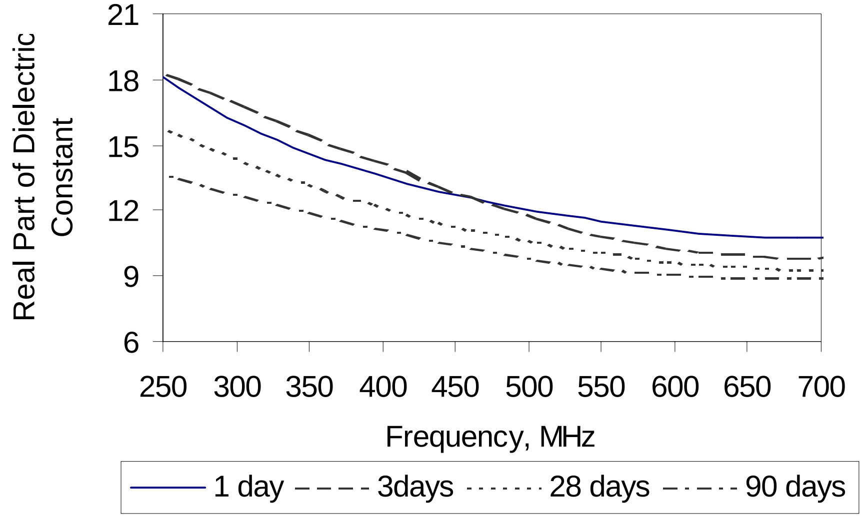


Figure C.3. Effect of frequency on the real part of the dielectric constant for L4N over different curing times.

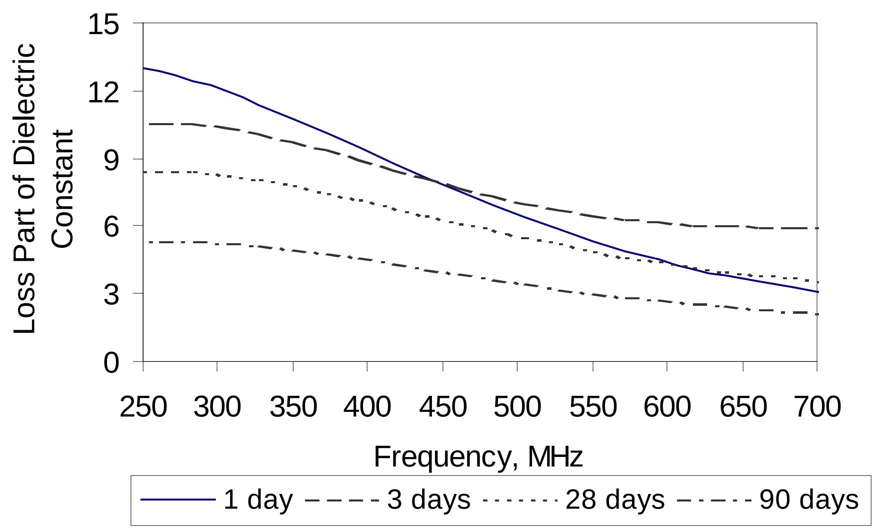


Figure C.4. Effect of frequency on the loss part of the dielectric constant for L4N over different curing times.

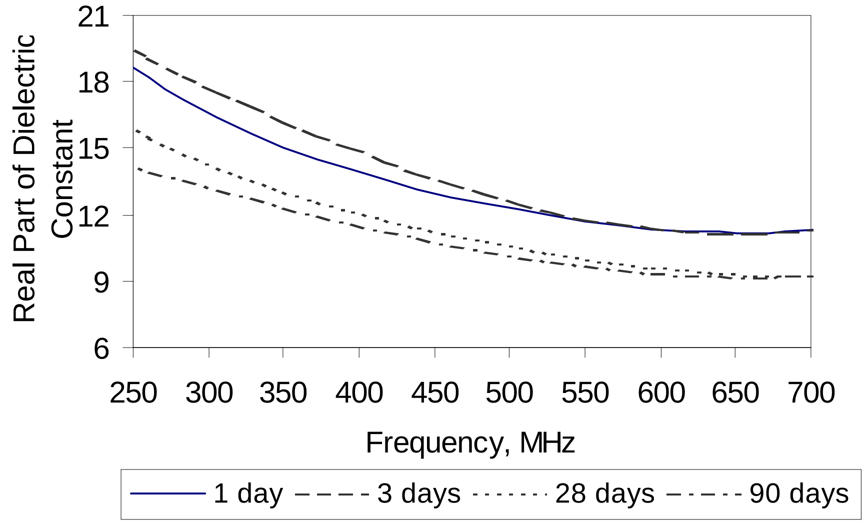


Figure C.5. Effect of frequency on the real part of the dielectric constant for L5N over different curing times.

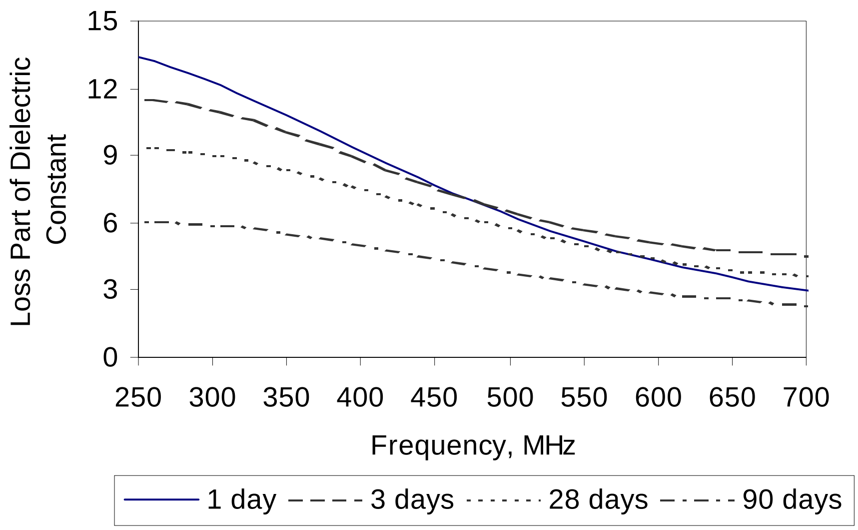


Figure C.6. Effect of frequency on the loss part of the dielectric constant for L5N over different curing times.

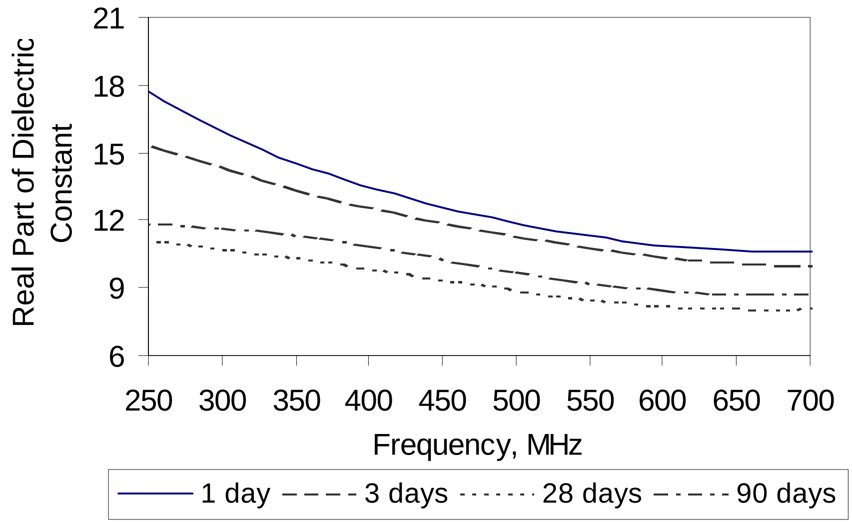


Figure C.7. Effect of frequency on the real part of the dielectric constant for L3S over different curing times.

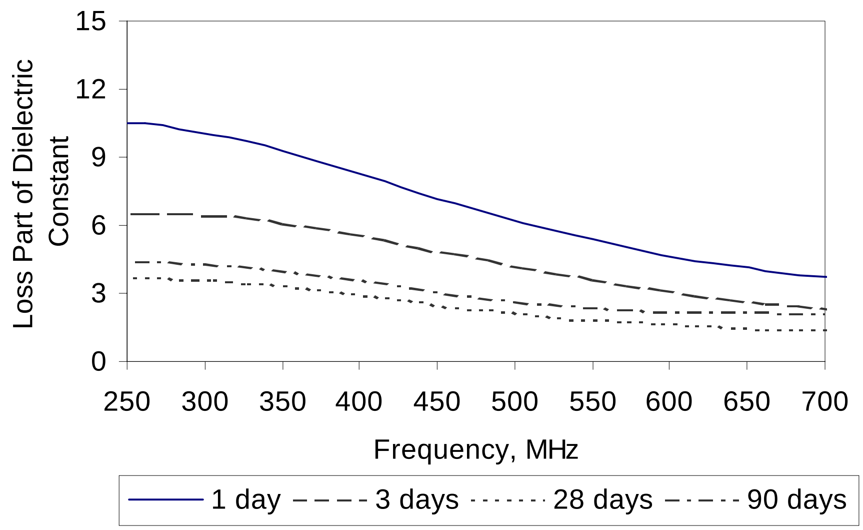


Figure C.8. Effect of frequency on the loss part of the dielectric constant for L3S over different curing times.

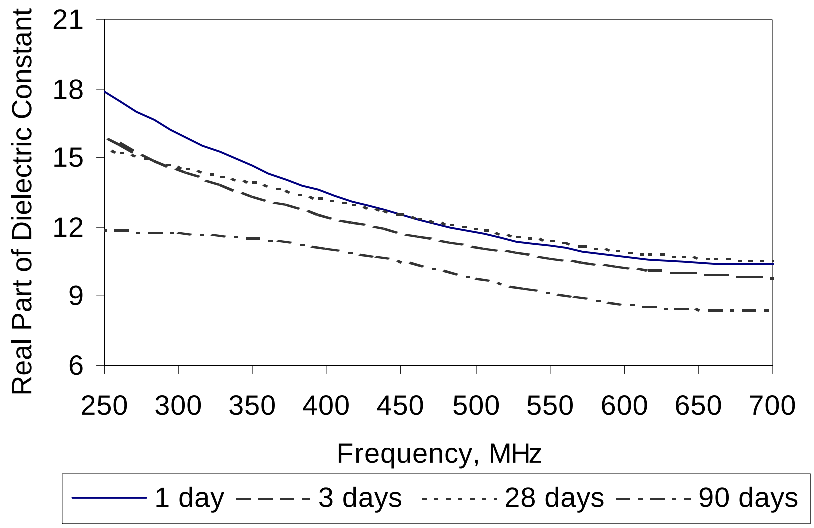


Figure C.9. Effect of frequency on the real part of the dielectric constant for L4S over different curing times.

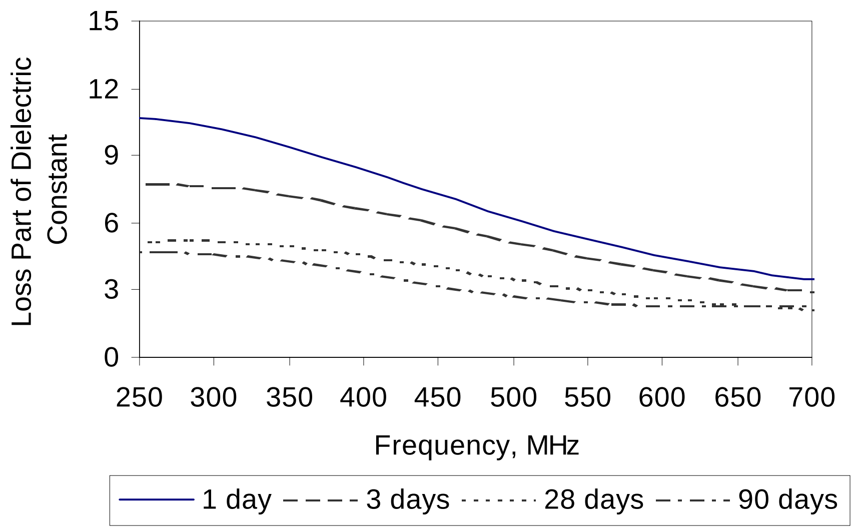


Figure C.10. Effect of frequency on the loss part of the dielectric constant for L4S over different curing times.

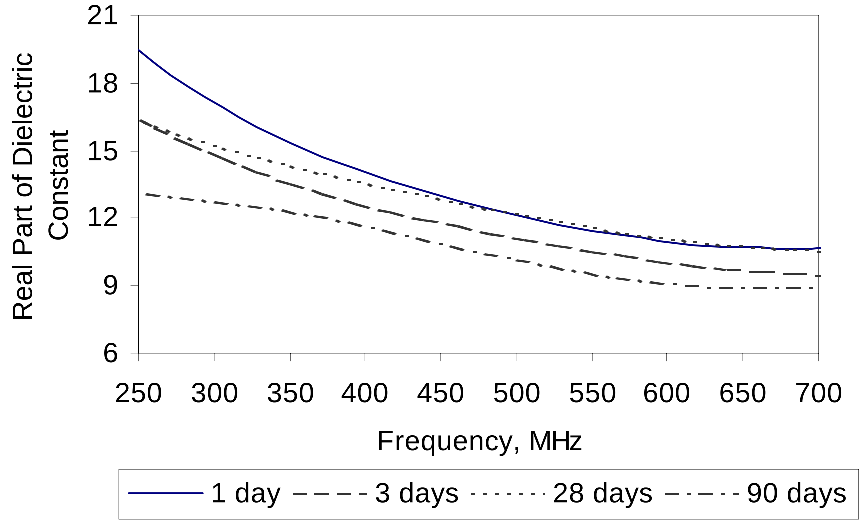


Figure C.11. Effect of frequency on the real part of the dielectric constant for L5S over different curing times.

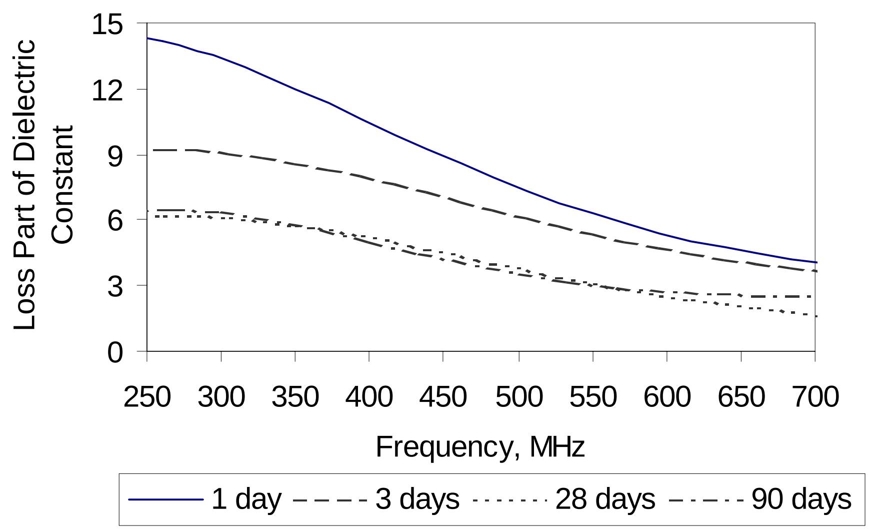


Figure C.12. Effect of frequency on the loss part of the dielectric constant for L5S over different curing times.

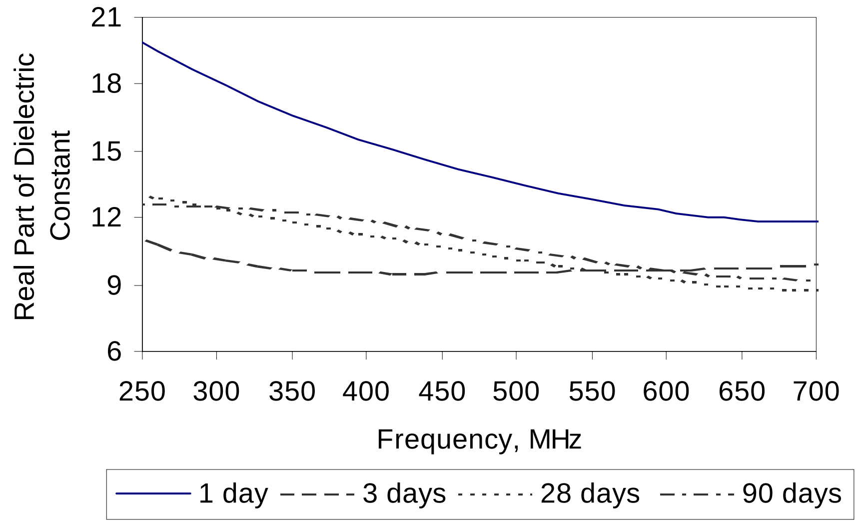


Figure C.13. Effect of frequency on the real part of the dielectric constant for L3H over different curing times.

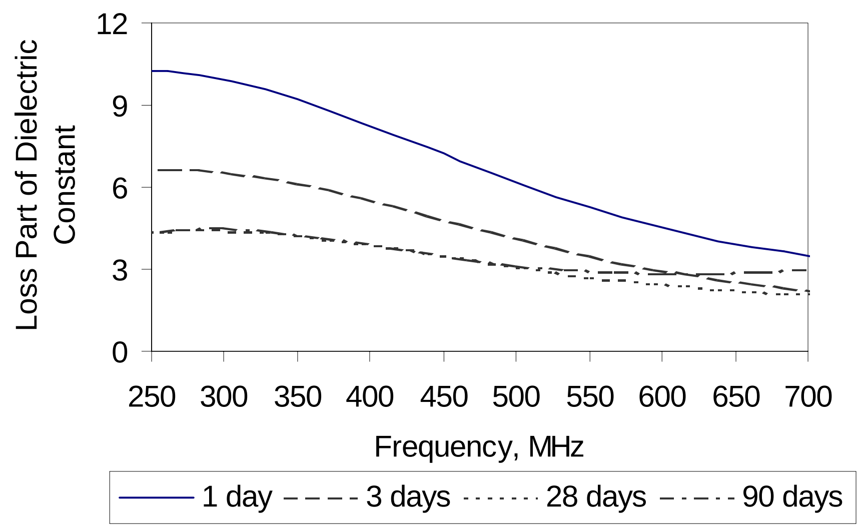


Figure C.14. Effect of frequency on the loss part of the dielectric constant for L3H over different curing times.

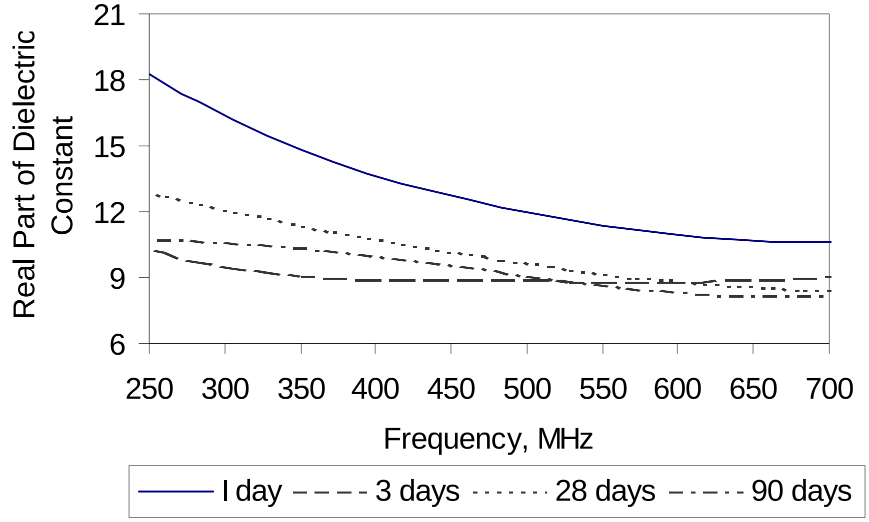


Figure C.15. Effect of frequency on the real part of the dielectric constant for L4H over different curing times.

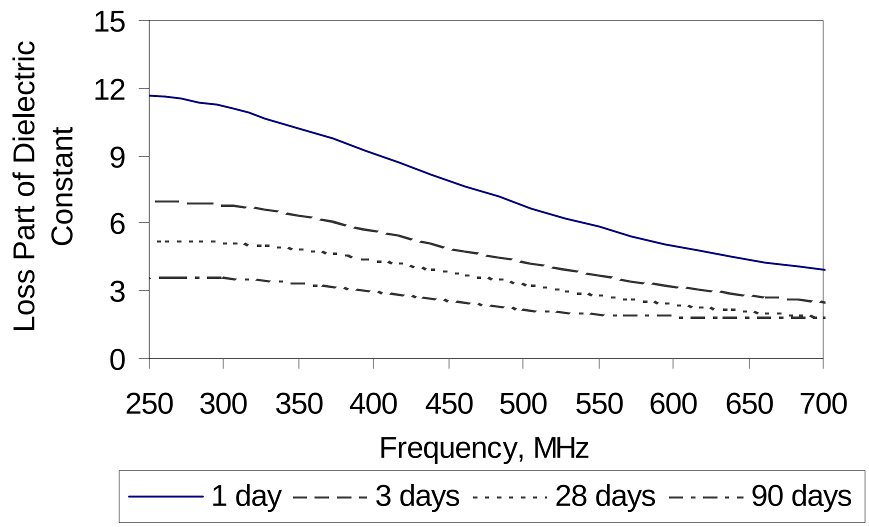


Figure C.16. Effect of frequency on the loss part of the dielectric constant for L4H over different curing times.

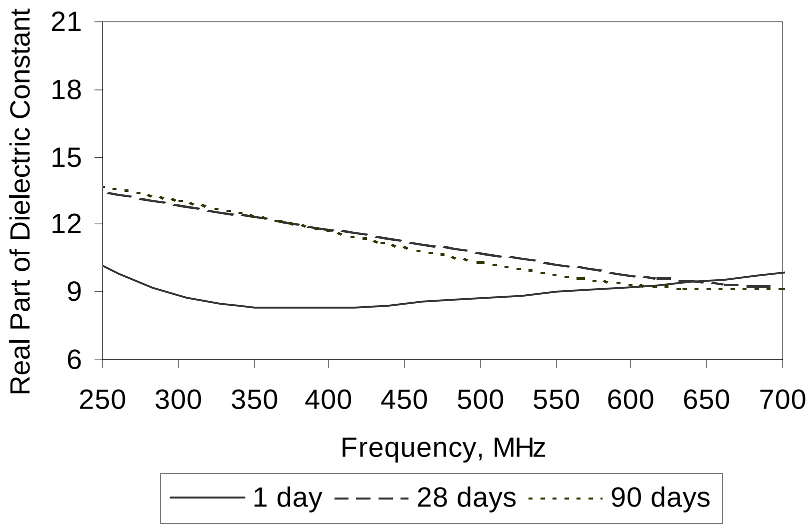


Figure C.17. Effect of frequency on the real part of the dielectric constant for L4C2 over different curing times.

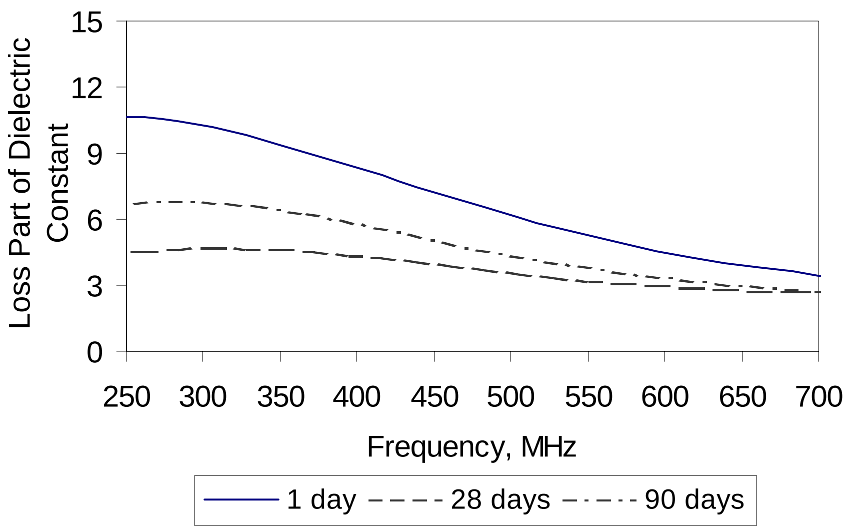


Figure C.18. Effect of frequency on the loss part of the dielectric constant for L4C2 over different curing times.

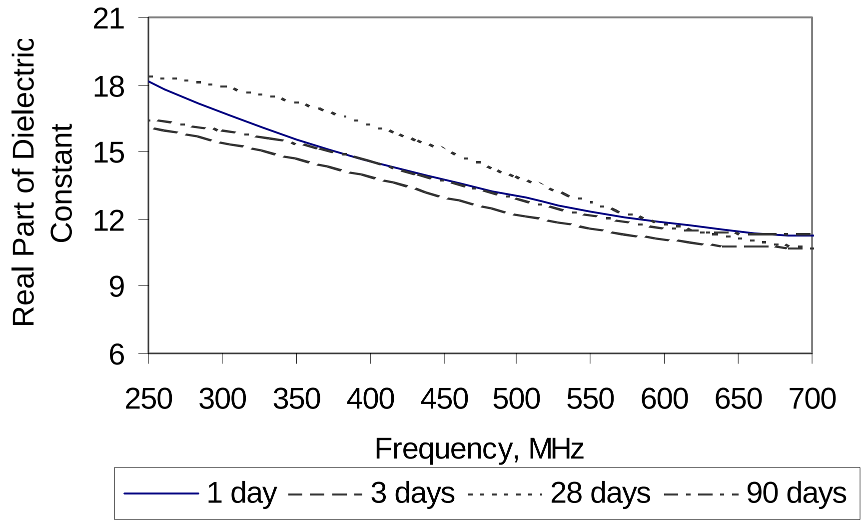


Figure C.19. Effect of frequency on the real part of the dielectric constant for L3C4 over different curing times.

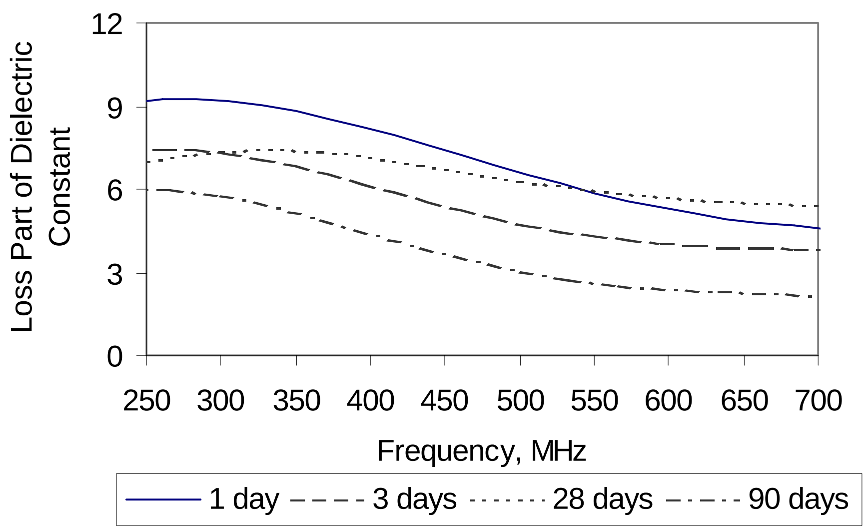


Figure C.20. Effect of frequency on the loss part of the dielectric constant for L3C4 over different curing times.

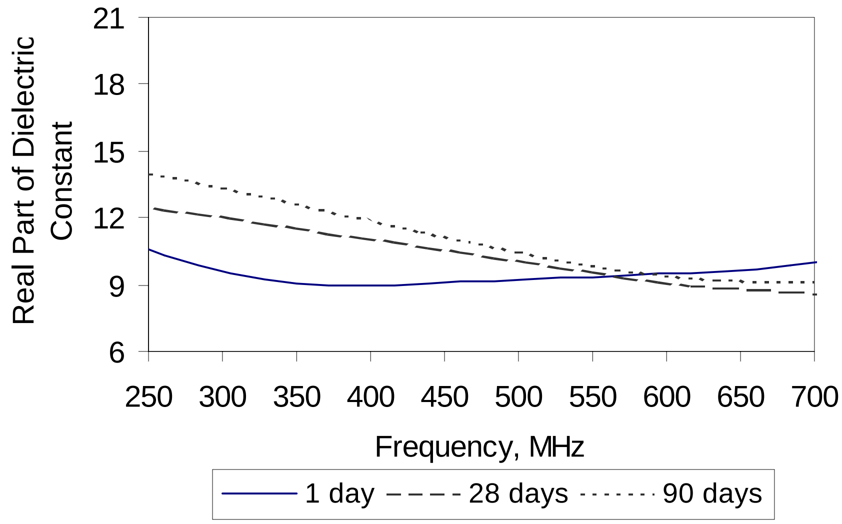


Figure C.21. Effect of frequency on the real part of the dielectric constant for L4C4 over different curing times.

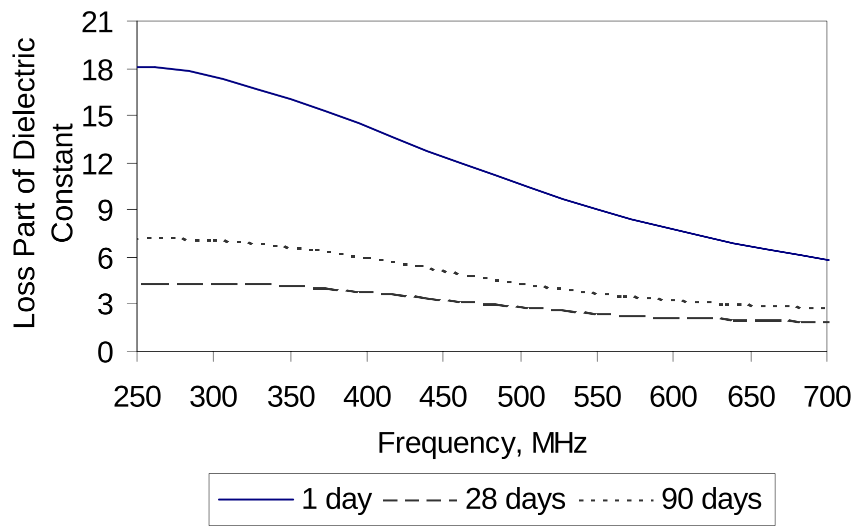


Figure C.22. Effect of frequency on the loss part of the dielectric constant for L4C4 over different curing times.

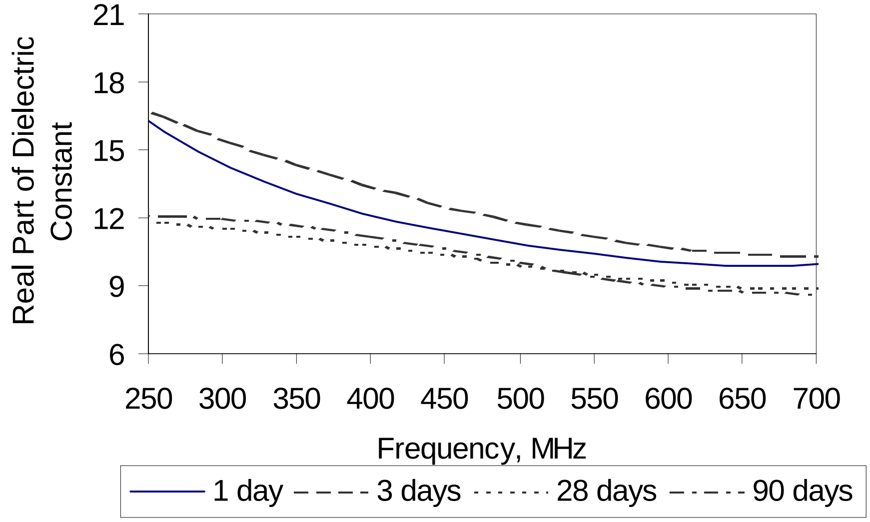


Figure C.23. Effect of frequency on the real part of the dielectric constant for L4M over different curing times.

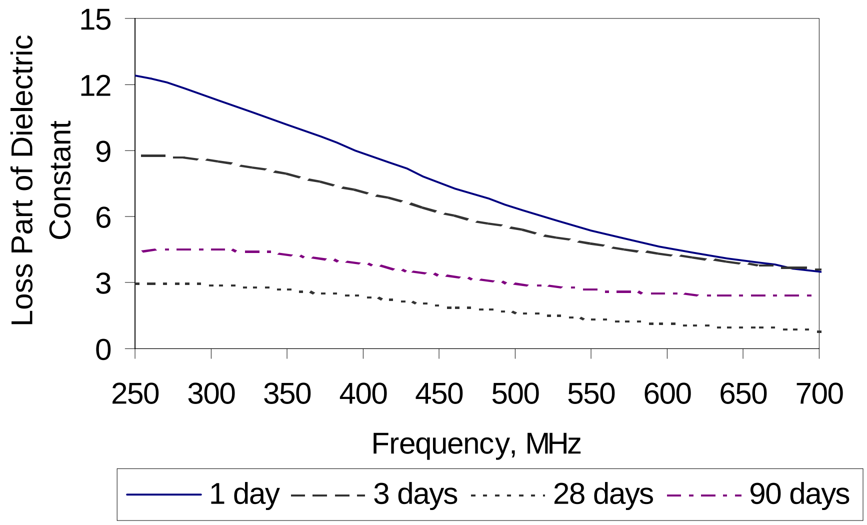


Figure C.24. Effect of frequency on the loss part of the dielectric constant for L4M over different curing times.

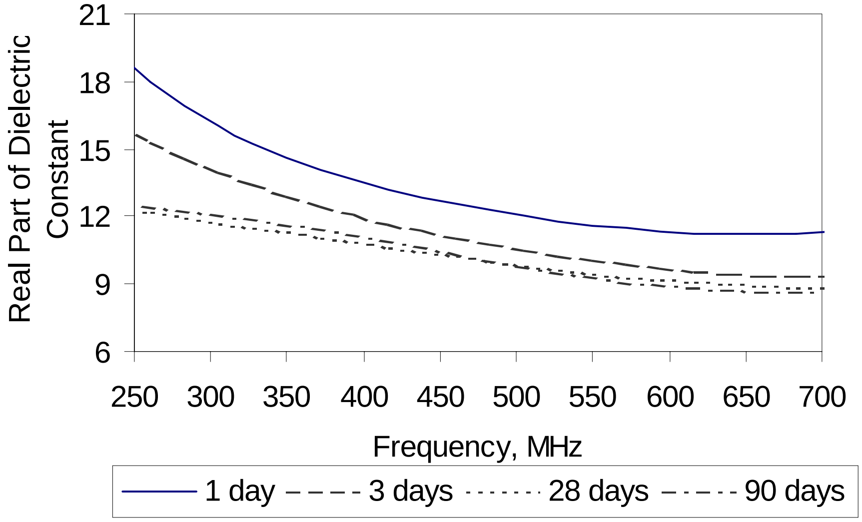


Figure C.25. Effect of frequency on the real part of the dielectric constant for L5M over different curing times.

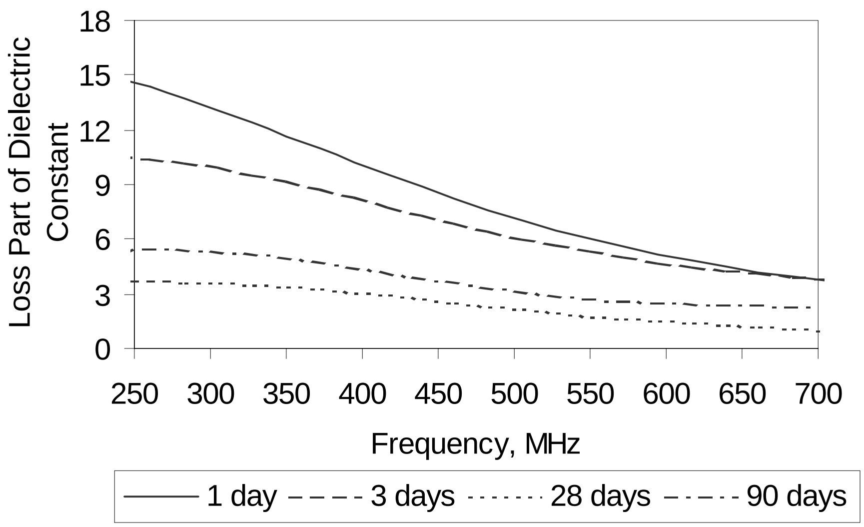


Figure C.26. Effect of frequency on the loss part of the dielectric constant for L5M over different curing times.

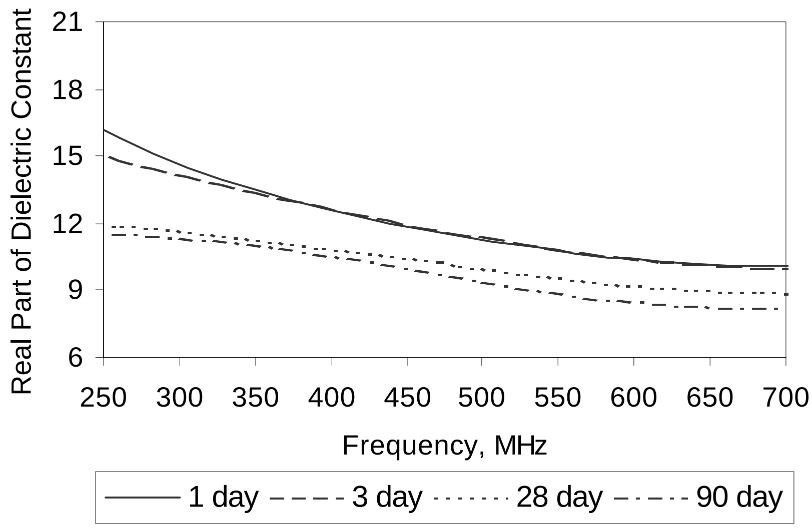


Figure C.27. Effect of frequency on the real part of the dielectric constant for G3N over different curing times.

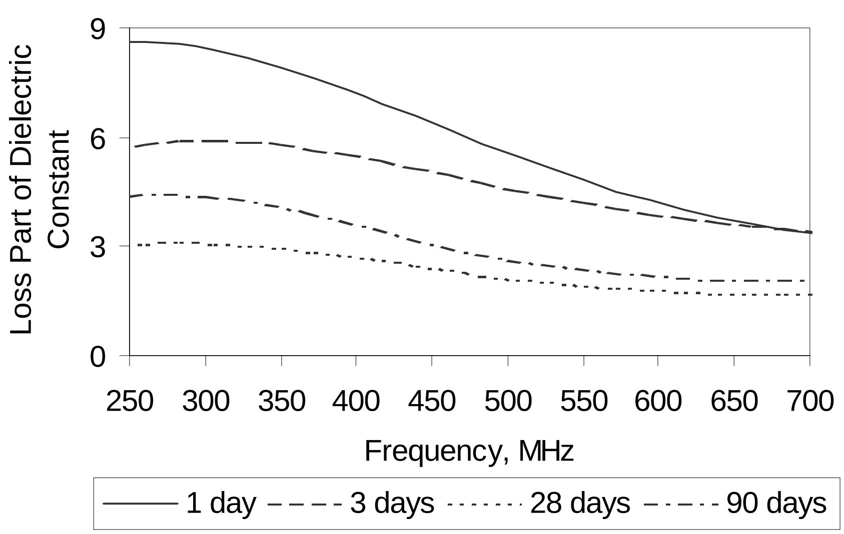


Figure C.28. Effect of frequency on the loss part of the dielectric constant for G3N over different curing times.

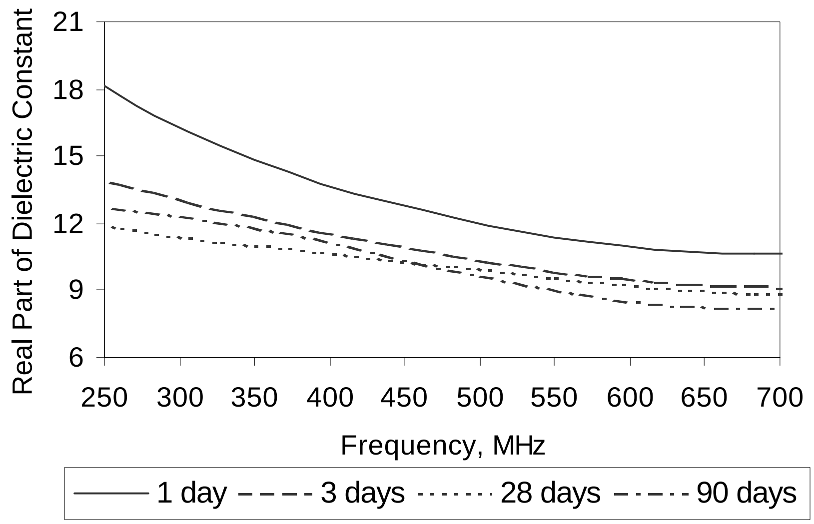


Figure C.29. Effect of frequency on the real part of the dielectric constant for G4N over different curing times.

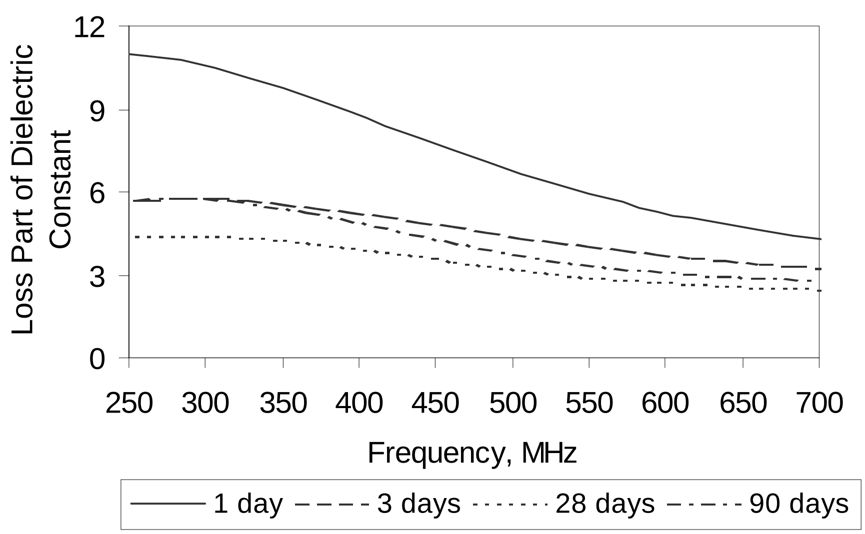


Figure C.30. Effect of frequency on the loss part of the dielectric constant for G4N over different curing times.

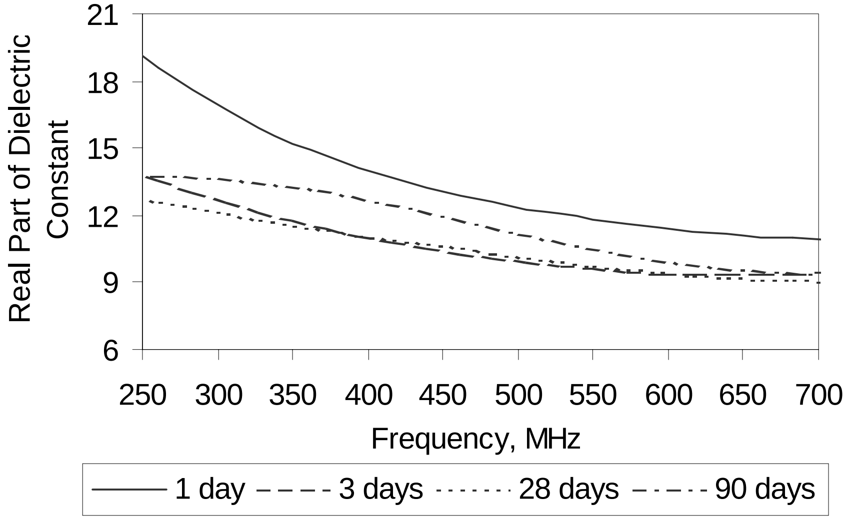


Figure C.31. Effect of frequency on the real part of the dielectric constant for G4C2 over different curing times.

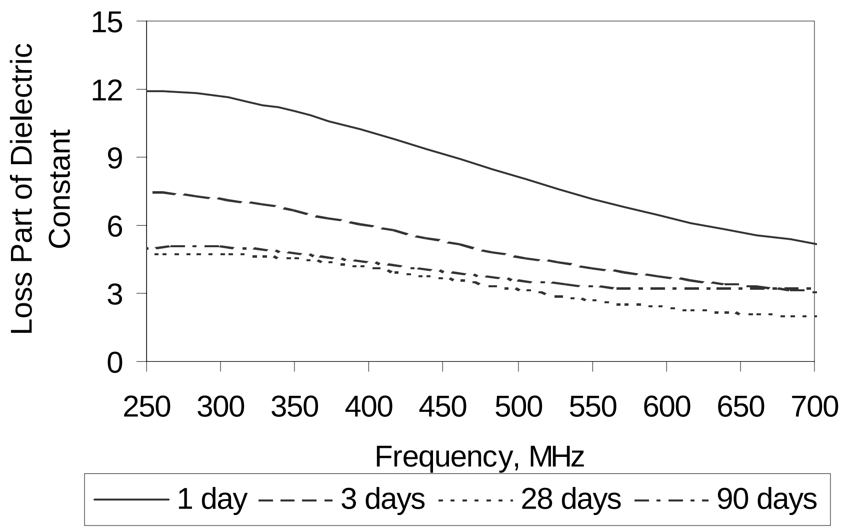


Figure C.32. Effect of frequency on the loss part of the dielectric constant for G4C2 over different curing times.

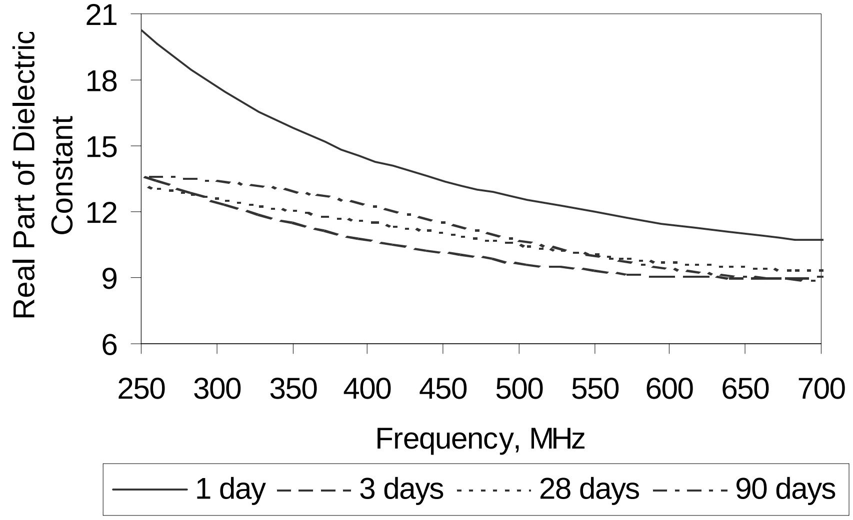


Figure C.33. Effect of frequency on the real part of the dielectric constant for G4C4 over different curing times.

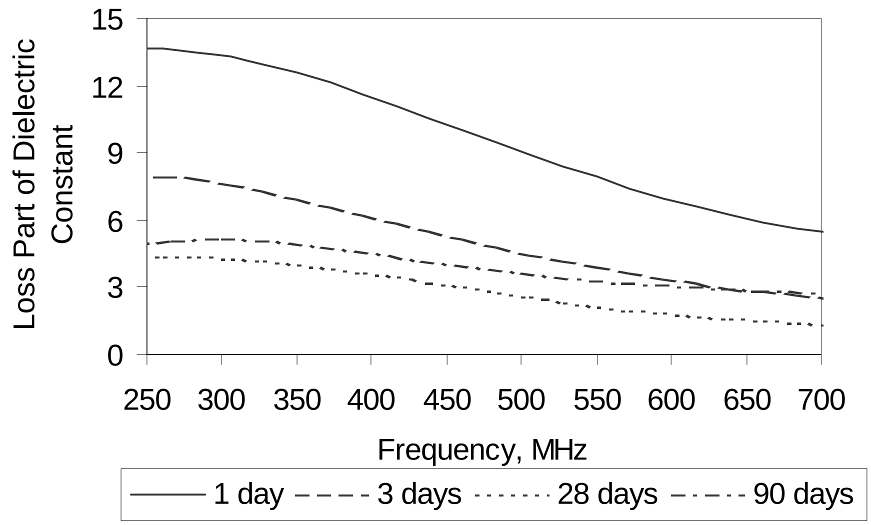


Figure C.34. Effect of frequency on the loss part of the dielectric constant for G4C4 over different curing times.

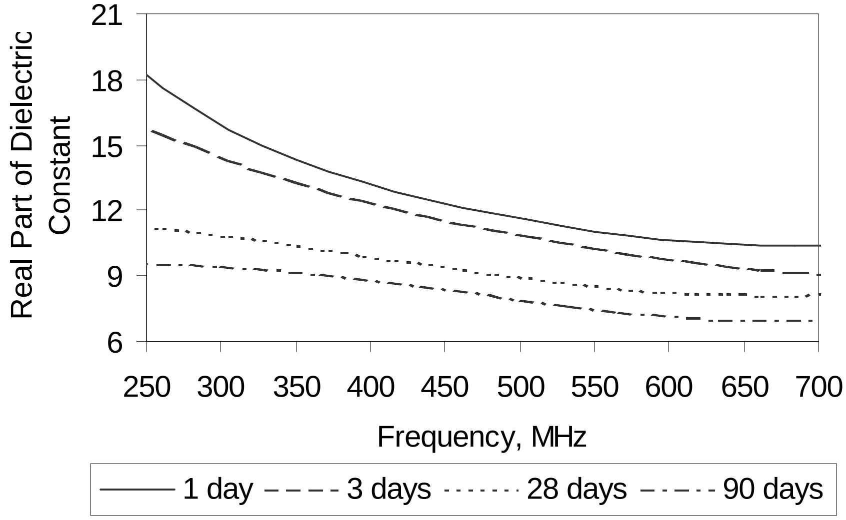


Figure C.35. Effect of curing time on the real part of the dielectric constant for G4M over different curing times.

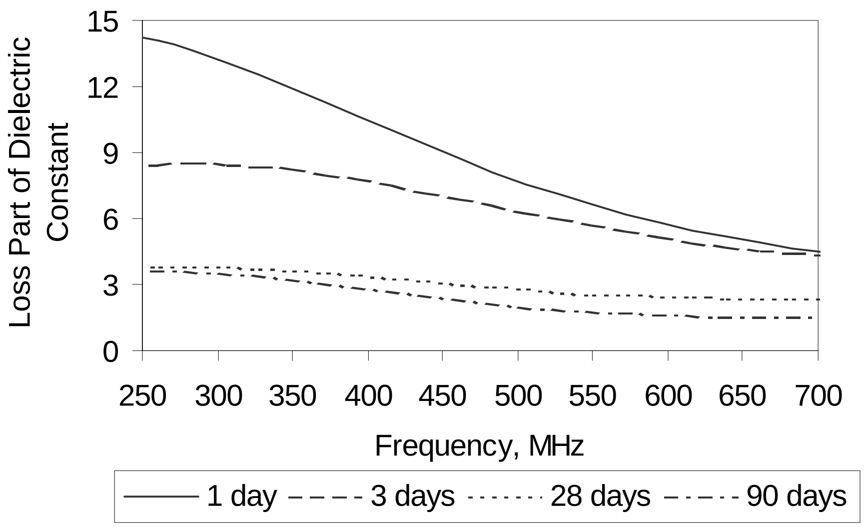


Figure C.36. Effect of curing time on the loss part of the dielectric constant for G4M over different curing times.

# APPENDIX D

# EFFECT OF CURING TIME ON THE DIELECTRIC CONSTANT OVER DIFFERENT FREQUENCIES (3 ns WINDOW)

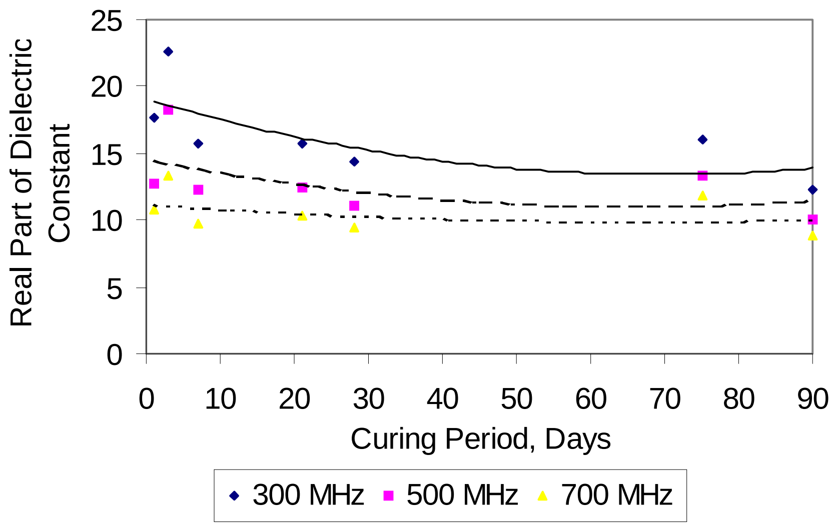


Figure D.1. Effect of curing time on the real part of the dielectric constant for L3N over three different frequencies.

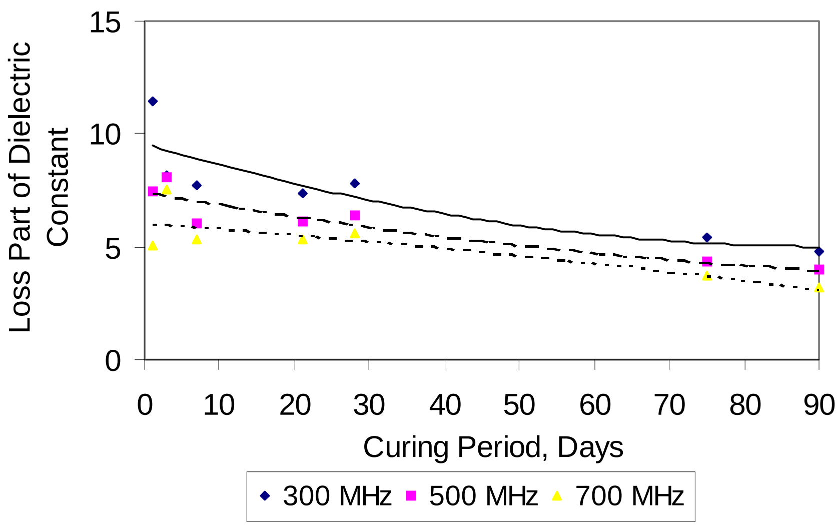


Figure D.2. Effect of curing time on the loss part of the dielectric constant for L3N over three different frequencies.

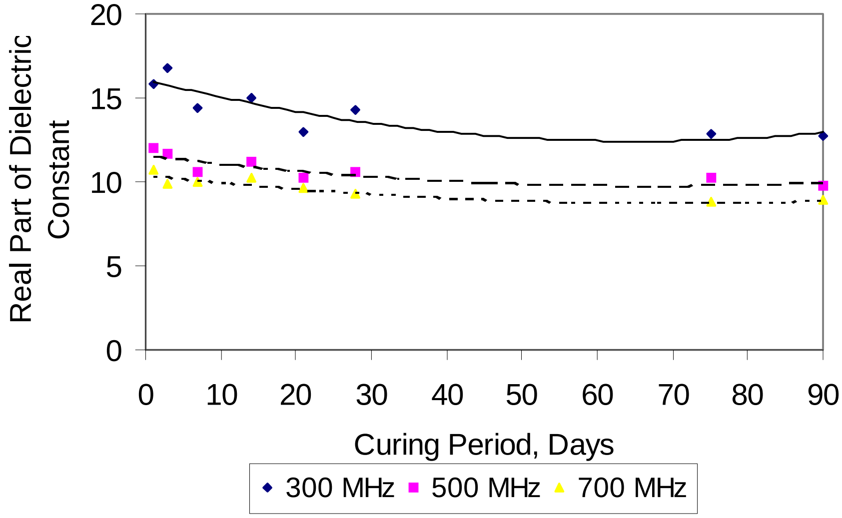


Figure D.3. Effect of curing time on the real part of the dielectric constant for L4N over three different frequencies.

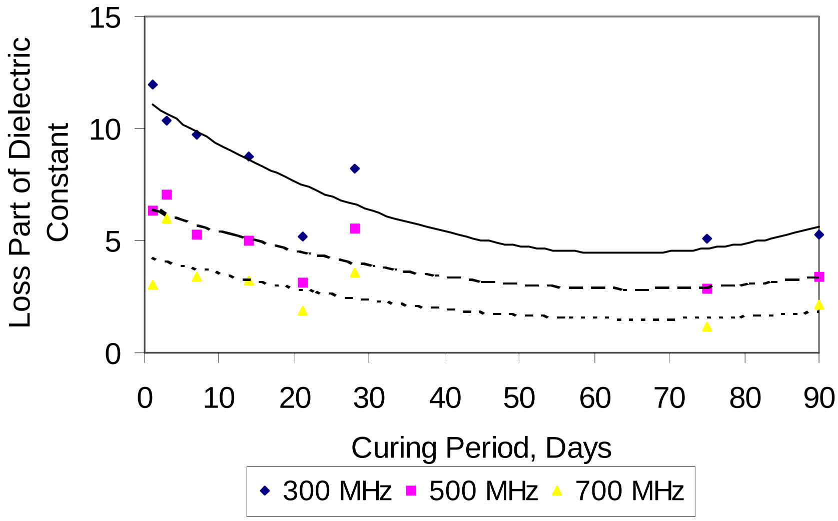


Figure D.4. Effect of curing time on the loss part of the dielectric constant for L4N over three different frequencies.

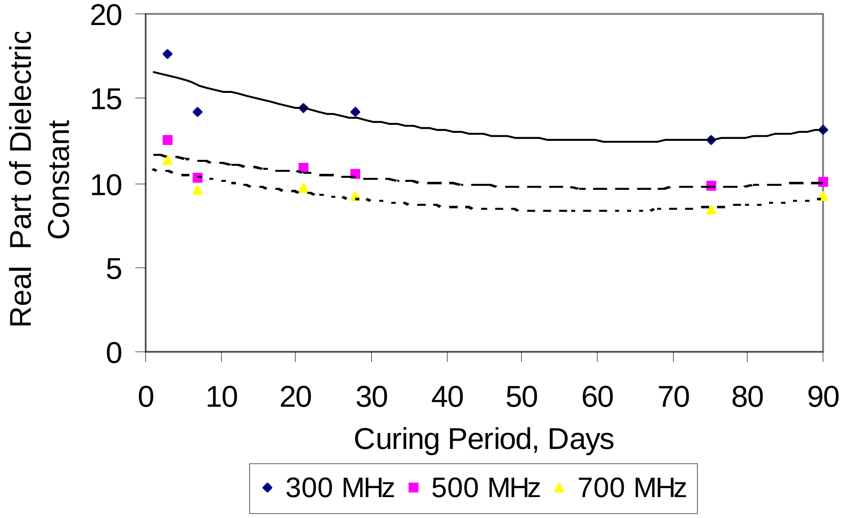


Figure D.5. Effect of curing time on the real part of the dielectric constant for L5N over three different frequencies.

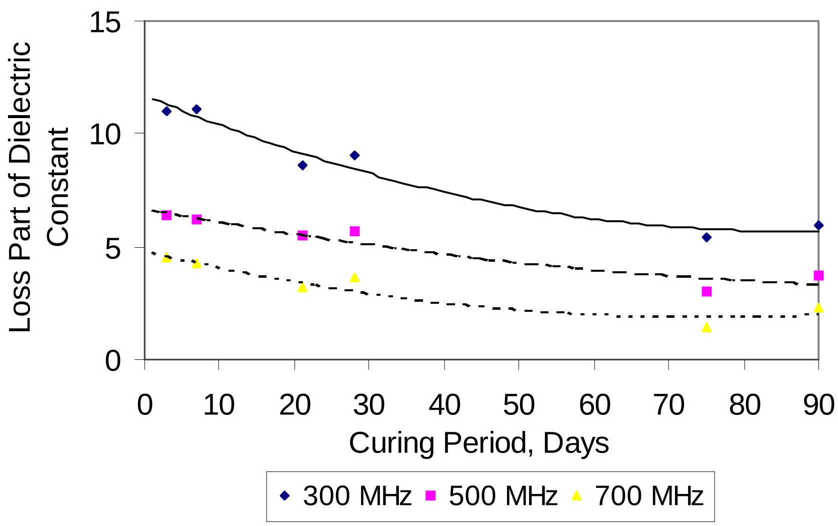


Figure D.6. Effect of curing time on the loss part of the dielectric constant for L5N over three different frequencies.

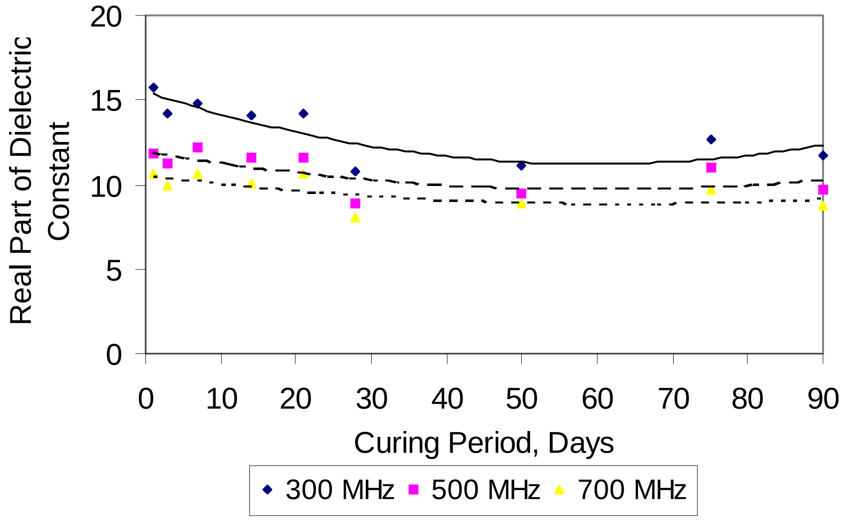


Figure D.7. Effect of curing time on the real part of the dielectric constant for L3S over three different frequencies.

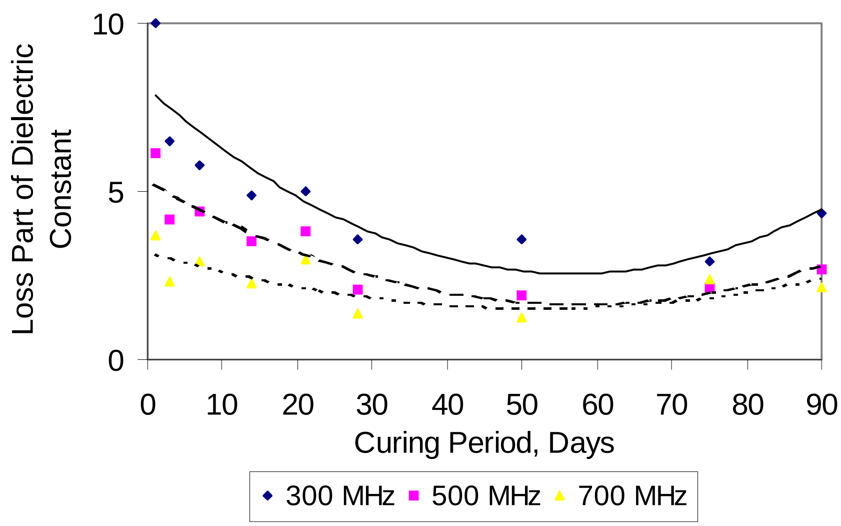


Figure D.8. Effect of curing time on the loss part of the dielectric constant for L3S over three different frequencies.

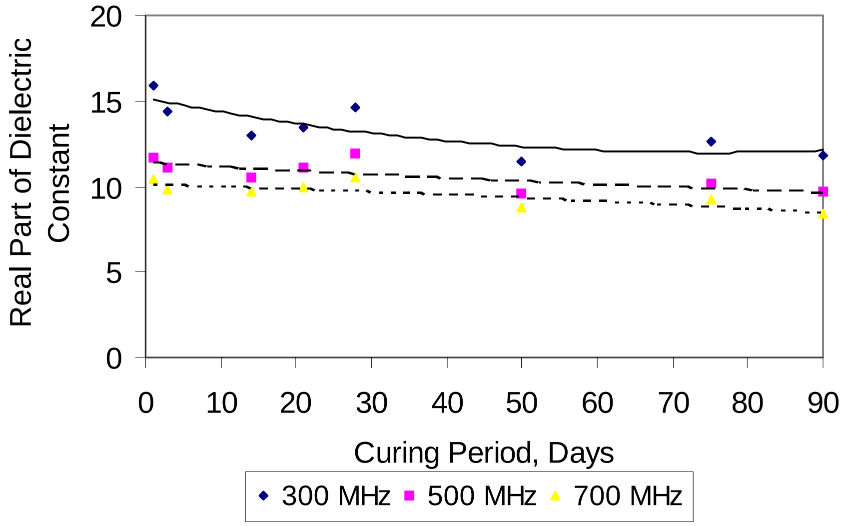


Figure D.9. Effect of curing time on the real part of the dielectric constant for L4S over three different frequencies.

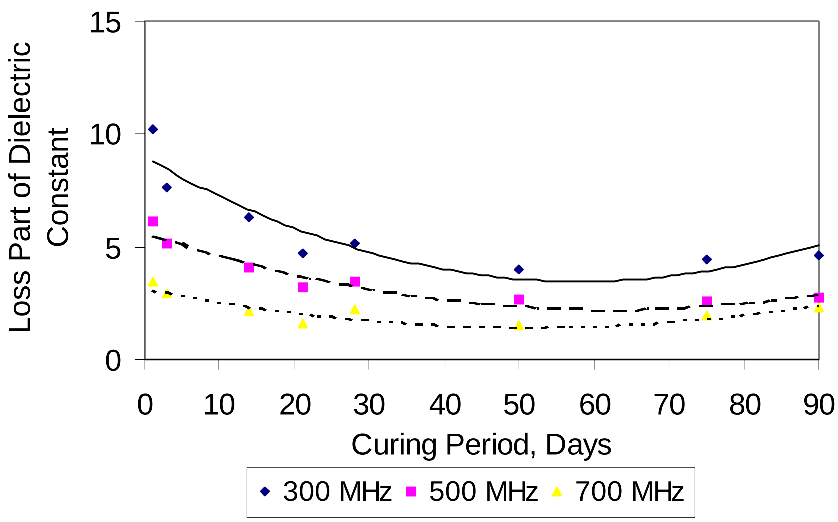


Figure D.10. Effect of curing time on the loss part of the dielectric constant for L4S over three different frequencies.

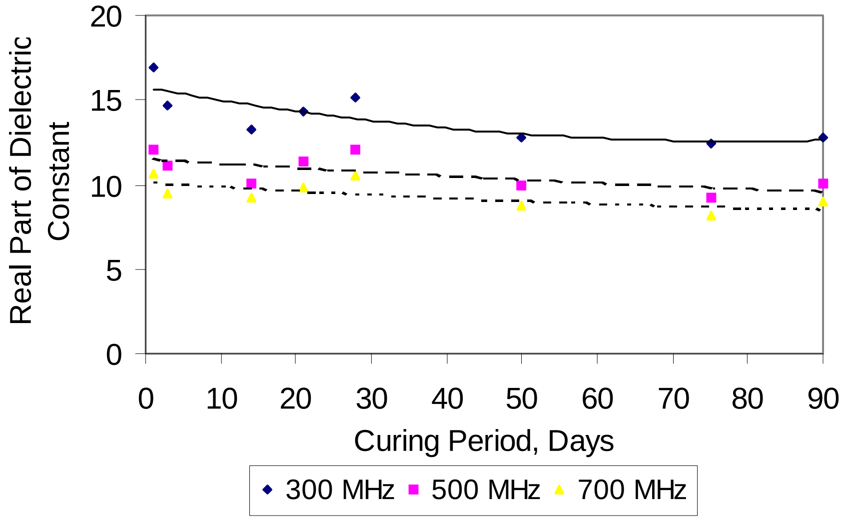


Figure D.11. Effect of curing time on the real part of the dielectric constant for L5S over three different frequencies.

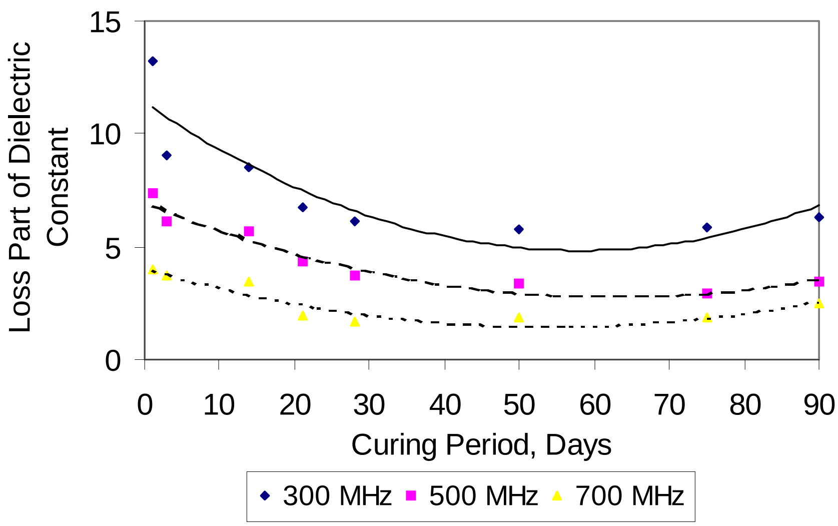


Figure D.12. Effect of curing time on the loss part of the dielectric constant for L5S over three different frequencies.

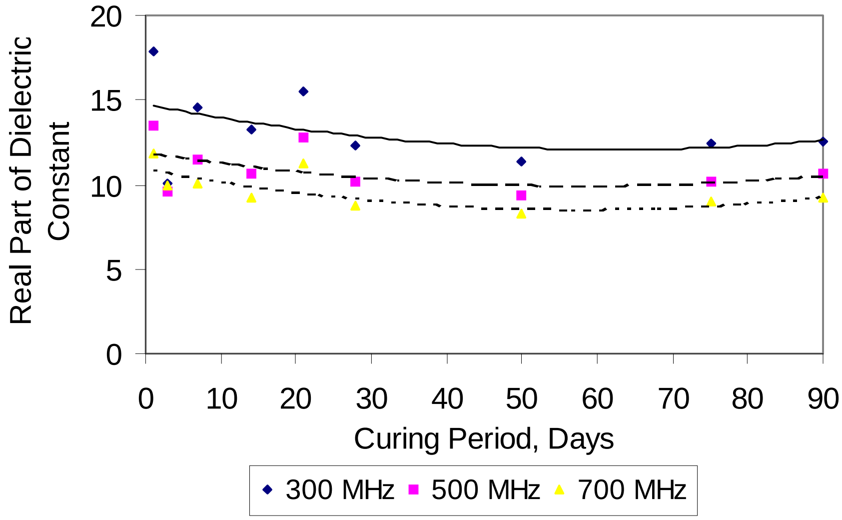


Figure D.13. Effect of curing time on the real part of the dielectric constant for L3H over three different frequencies.

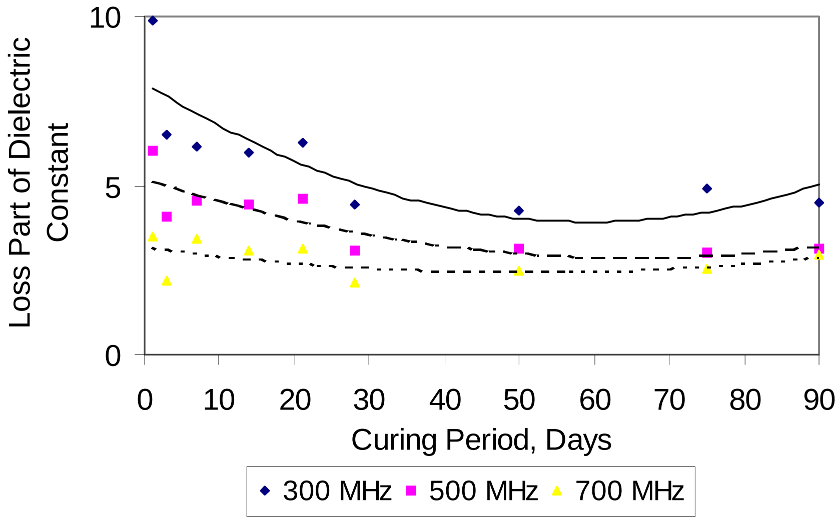


Figure D.14. Effect of curing time on the loss part of the dielectric constant for L3H over three different frequencies.

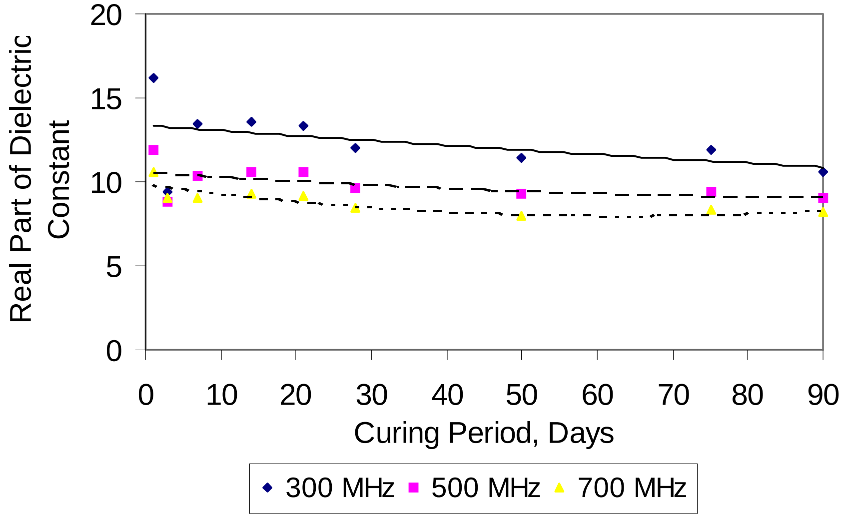


Figure D.15. Effect of curing time on the real part of the dielectric constant for L4H over three different frequencies.

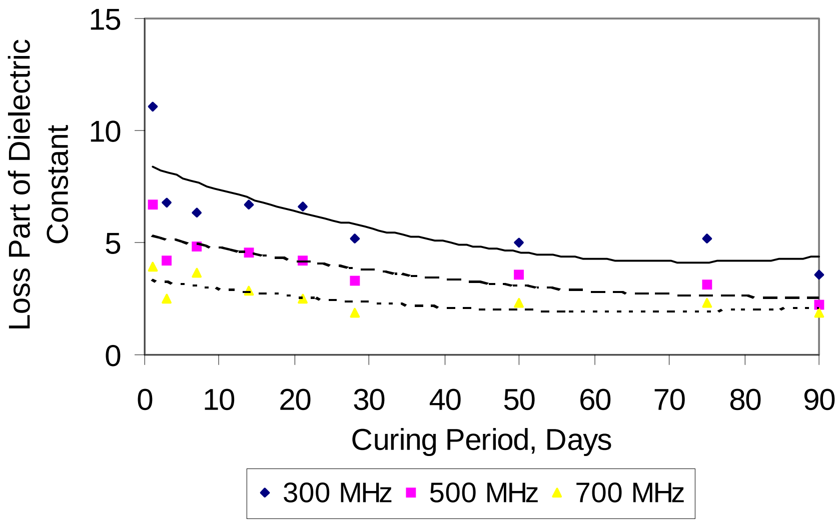


Figure D.16. Effect of curing time on the loss part of the dielectric constant for L4H over three different frequencies.

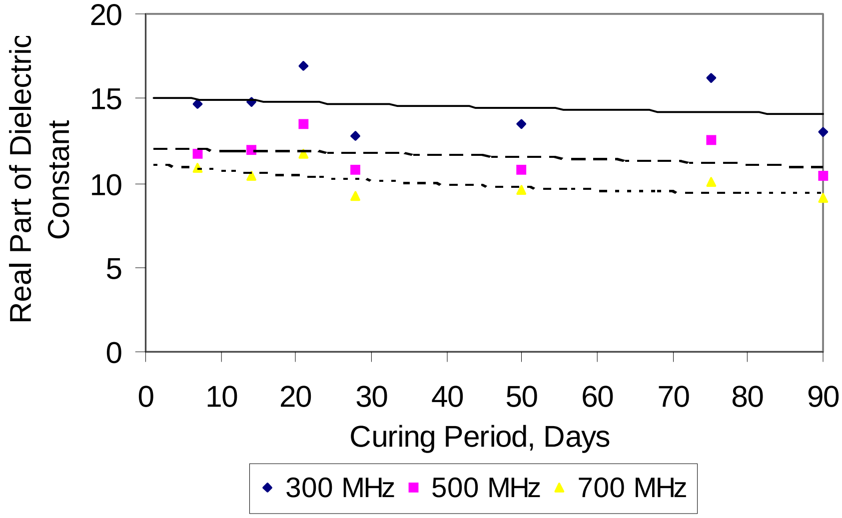


Figure D.17. Effect of curing time on the real part of the dielectric constant for L4C2 over three different frequencies.

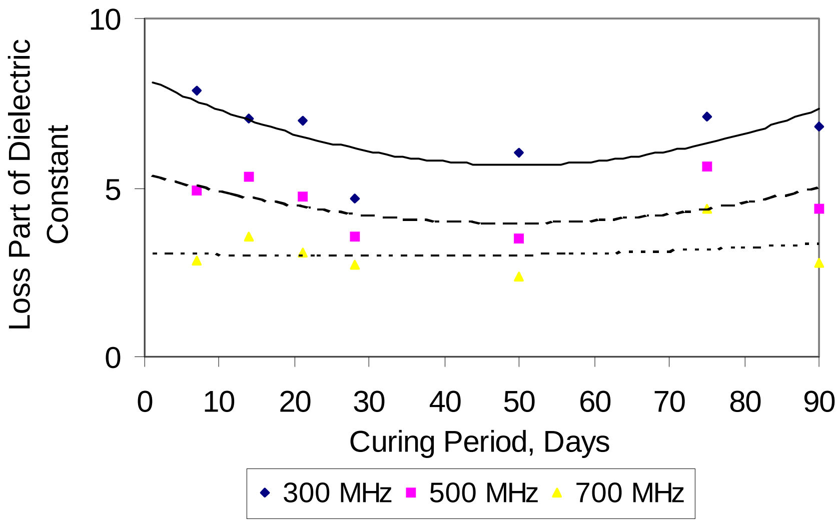


Figure D.18. Effect of curing time on the loss part of the dielectric constant for L4C2 over three different frequencies.

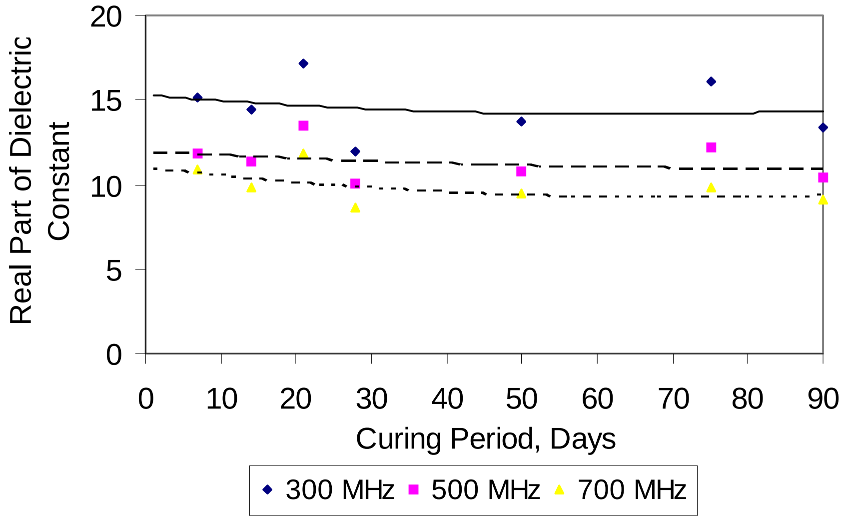


Figure D.19. Effect of curing time on the real part of the dielectric constant for L4C4 over three different frequencies.

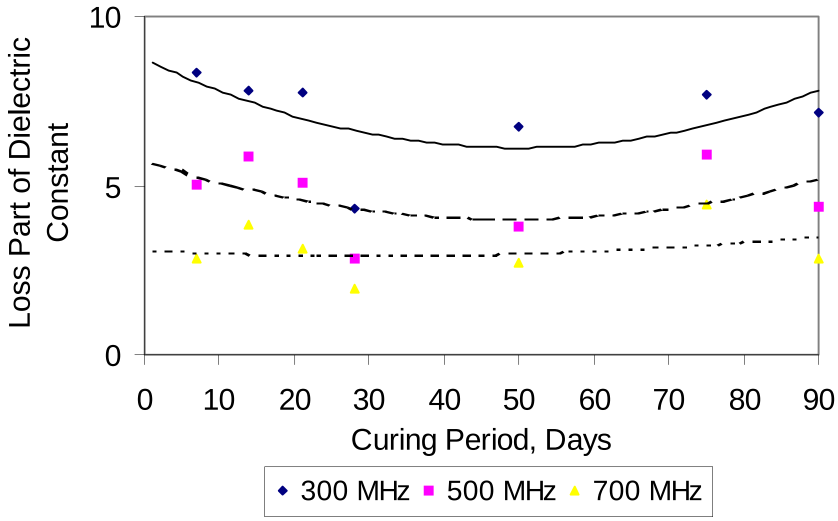


Figure D.20. Effect of curing time on the loss part of the dielectric constant for L4C4 over three different frequencies.

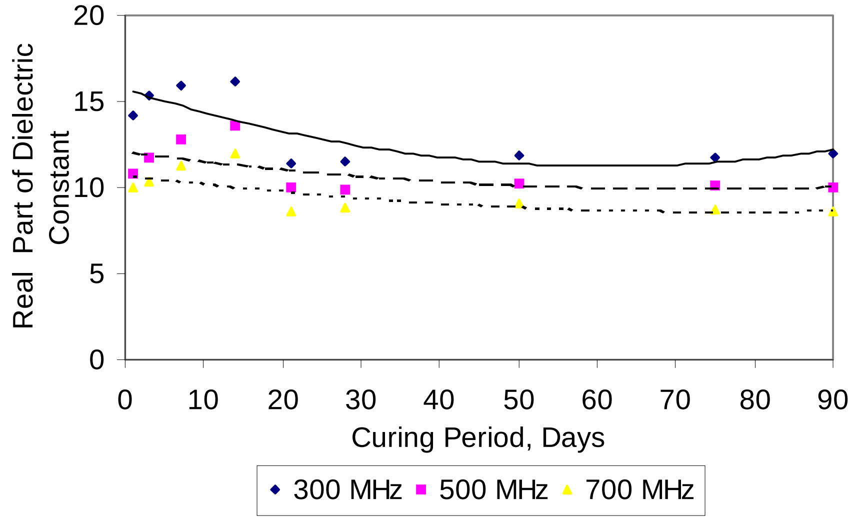


Figure D.21. Effect of curing time on the real part of the dielectric constant for L4M over three different frequencies.

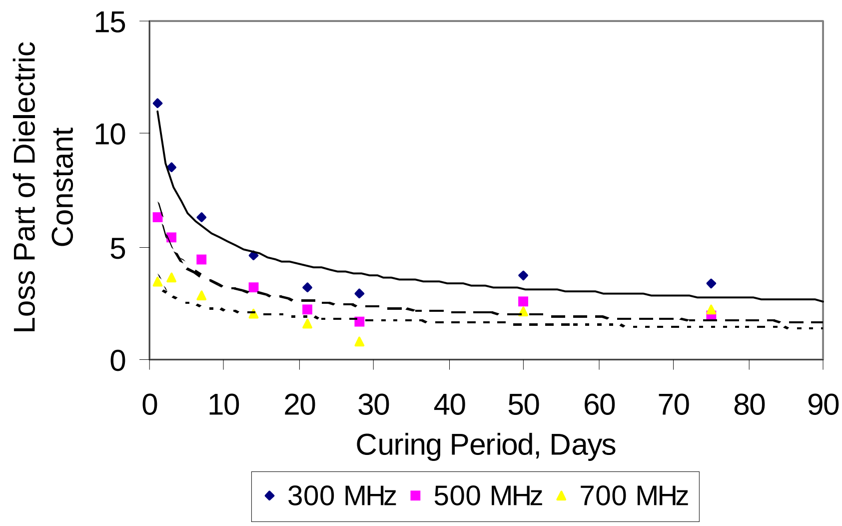


Figure D.22. Effect of curing time on the loss part of the dielectric constant for L4M over three different frequencies.

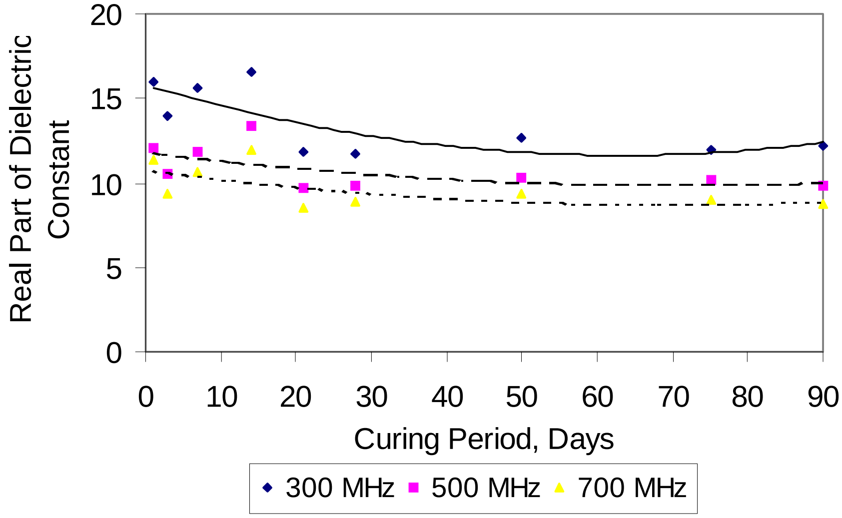


Figure D.23. Effect of curing time on the real part of the dielectric constant for L5M over three different frequencies.

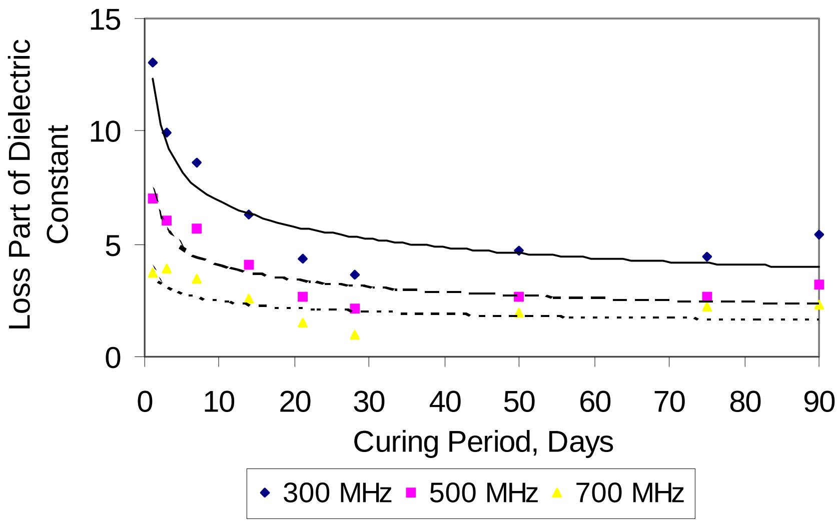


Figure D.24. Effect of curing time on the loss part of the dielectric constant for L5M over three different frequencies.

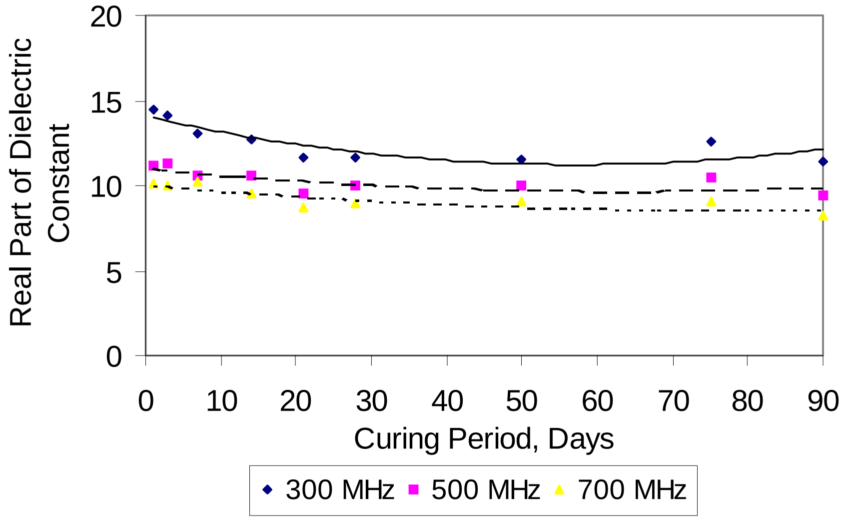


Figure D.25. Effect of curing time on the real part of the dielectric constant for G3N over three different frequencies.

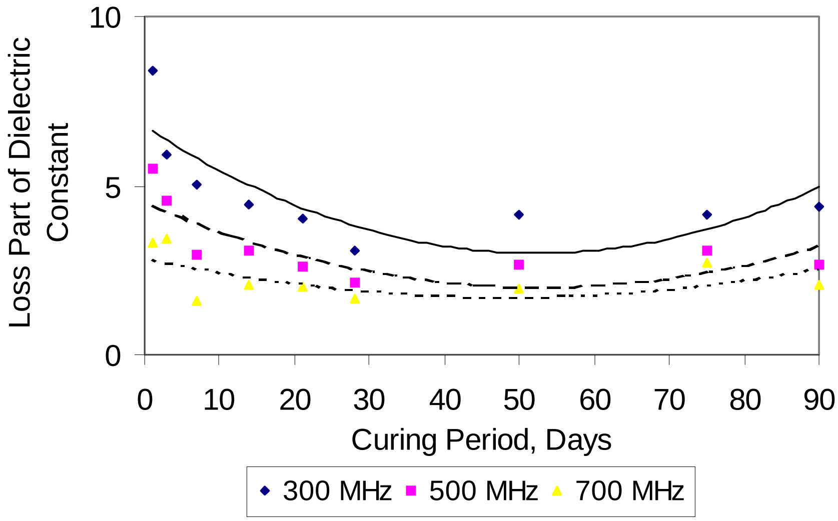


Figure D.26. Effect of curing time on the loss part of the dielectric constant for G3N over three different frequencies.

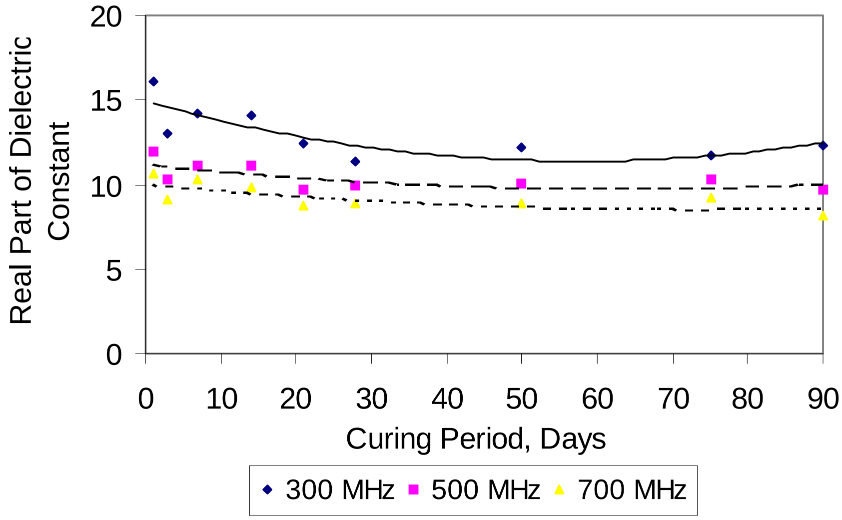


Figure D.27. Effect of curing time on the real part of the dielectric constant for G4N over three different frequencies.

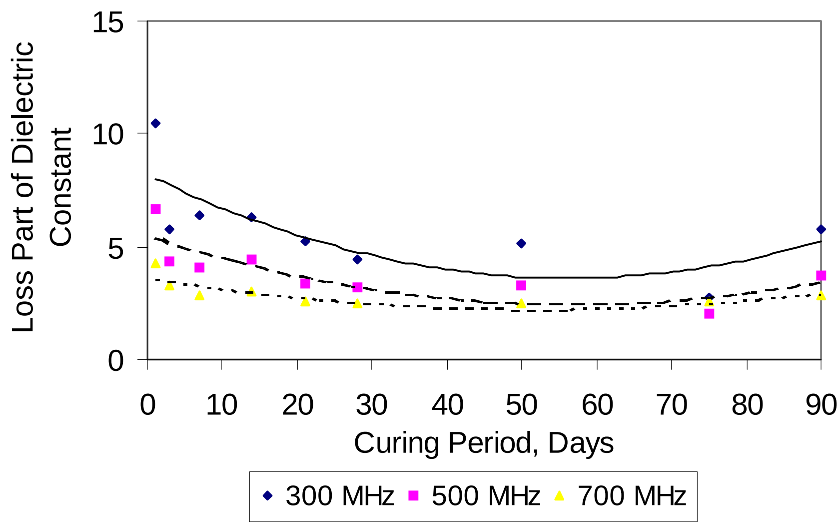


Figure D.28. Effect of curing time on the loss part of the dielectric constant for G4N over three different frequencies.

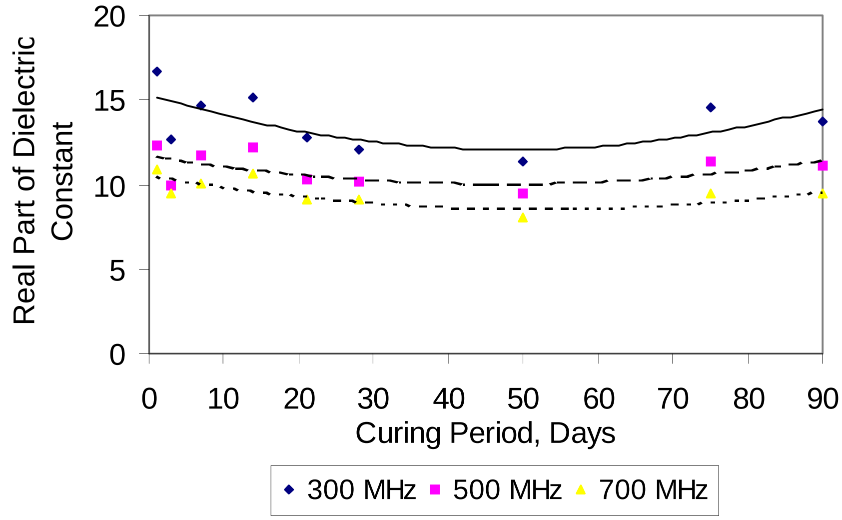


Figure D.29. Effect of curing time on the real part of the dielectric constant for G4C2 over three different frequencies.

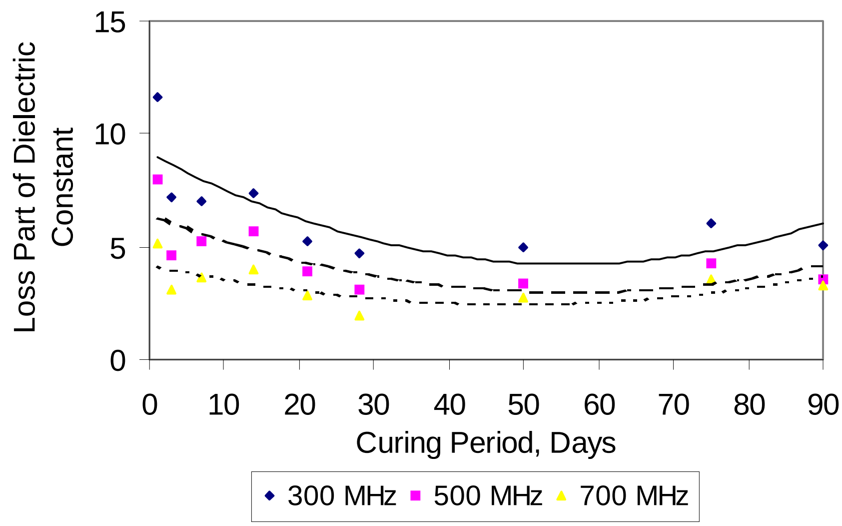


Figure D.30. Effect of curing time on the loss part of the dielectric constant for G4C2 over three different frequencies.

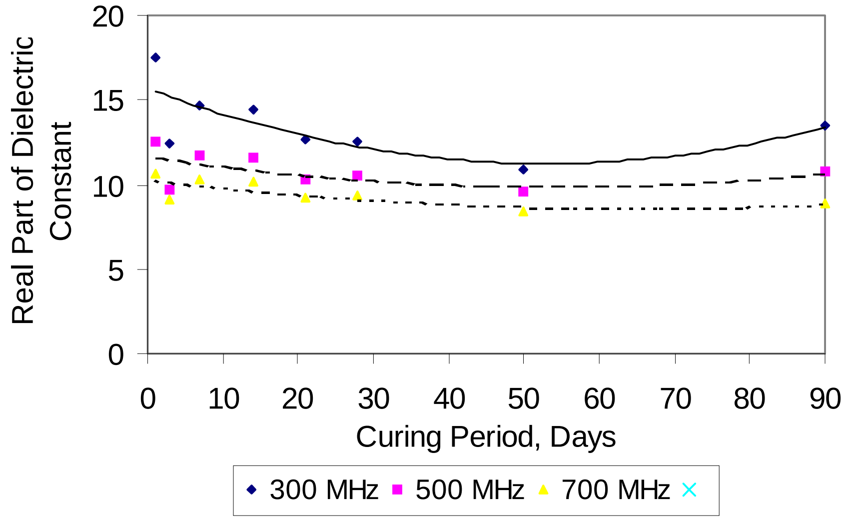


Figure D.31. Effect of curing time on the real part of the dielectric constant for G4C4 over three different frequencies.

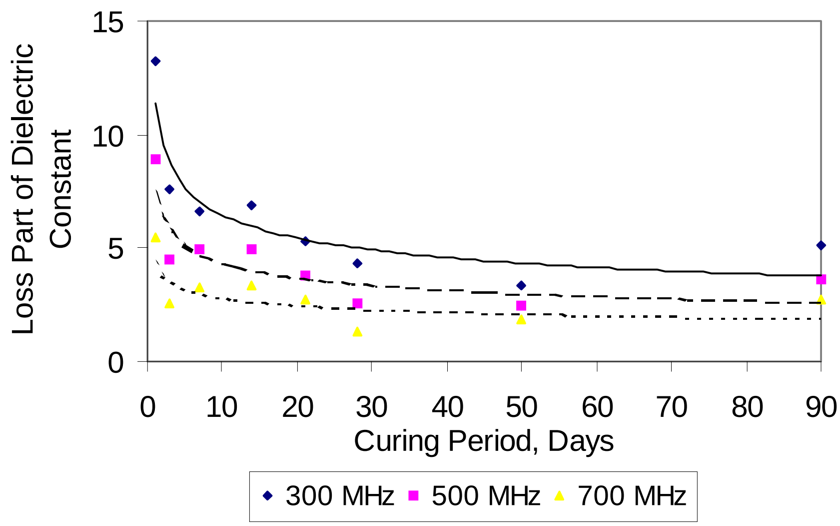


Figure D.32. Effect of curing time on the loss part of the dielectric constant for G4C4 over three different frequencies.

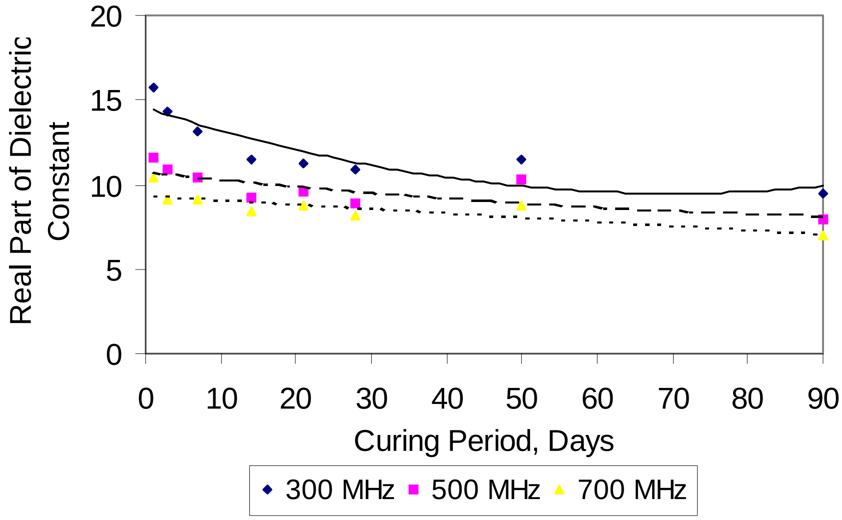


Figure D.33. Effect of curing time on the real part of the dielectric constant for G4M over three different frequencies.

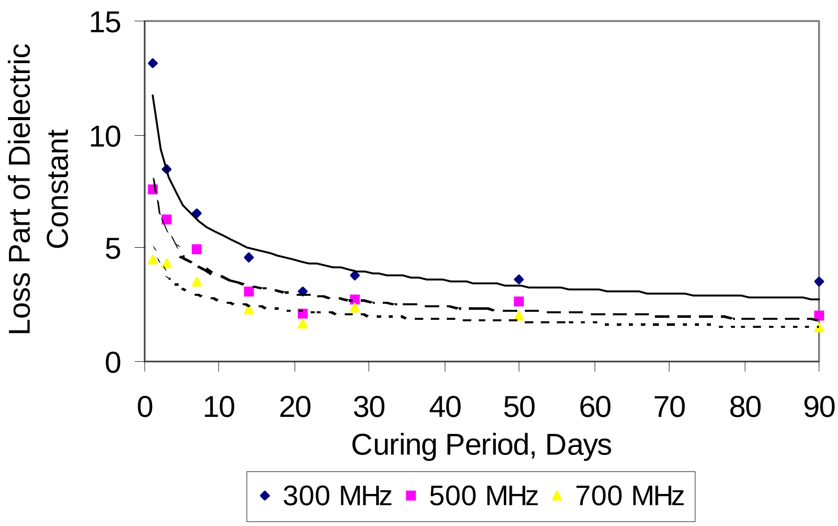


Figure D.34. Effect of curing time on the loss part of the dielectric constant for G4M over three different frequencies.

# APPENDIX E

## EFFECT OF FREQUENCY ON THE DIELECTRIC CONSTANT FOR DIFFERENT LEVELS OF MOISTURE CONTENT (3 ns WINDOW)

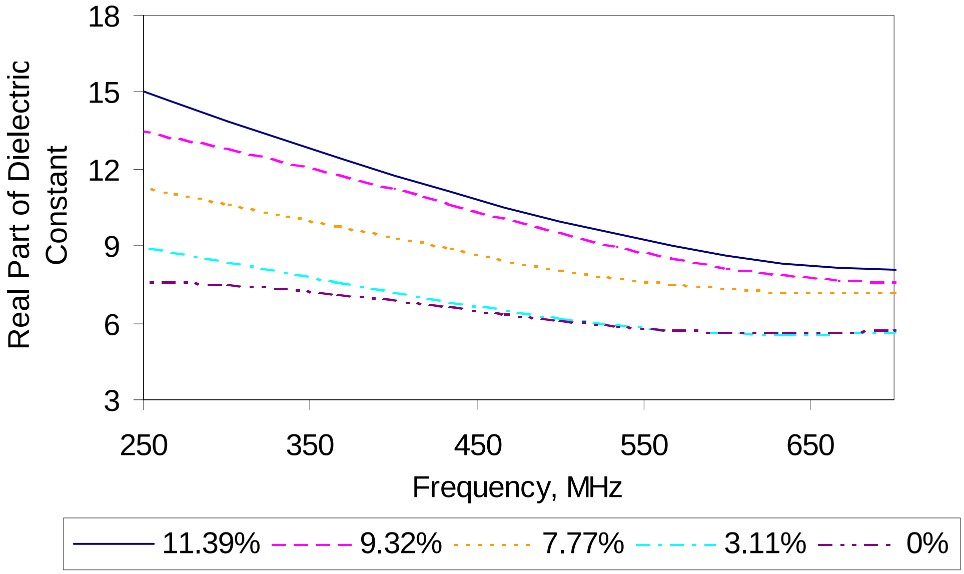


Figure E.1. Effect of frequency on the real part of the dielectric constant for L3N1 for five levels of volumetric moisture content (3 ns gating).

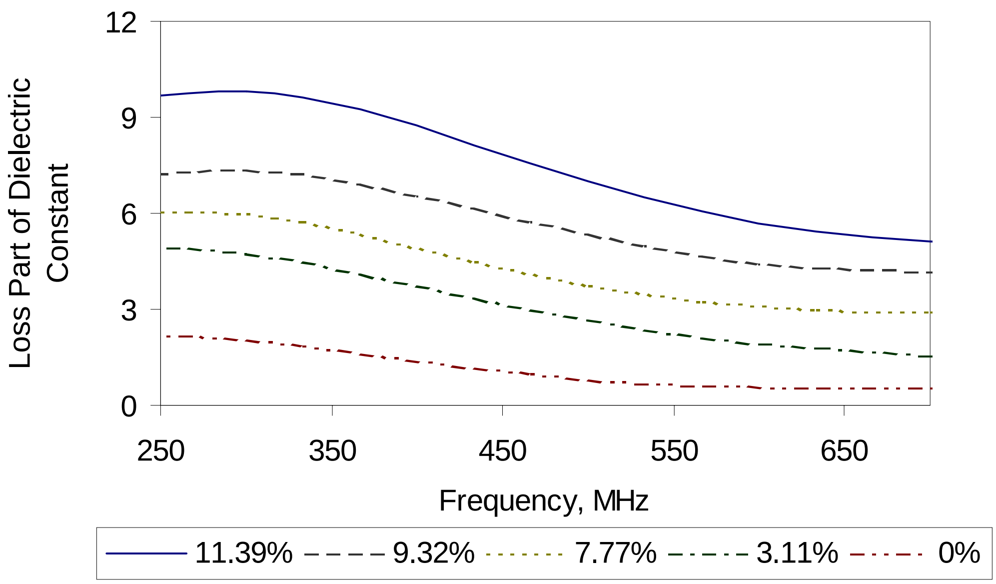


Figure E.2. Effect of frequency on the loss part of the dielectric constant for L3N1 for five levels of volumetric moisture content (3 ns gating).

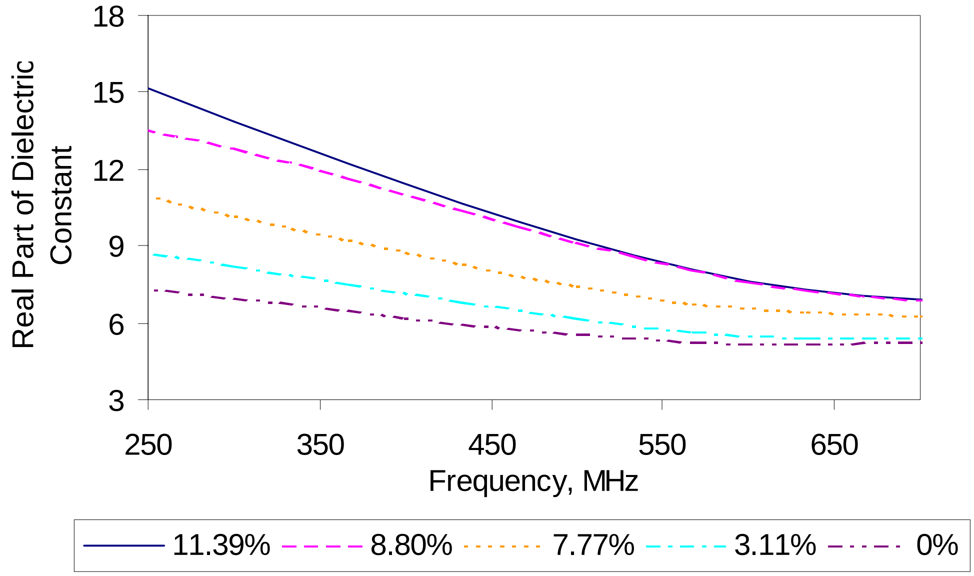


Figure E.3. Effect of frequency on the real part of the dielectric constant for L3N2 for five levels of volumetric moisture content (3 ns gating).

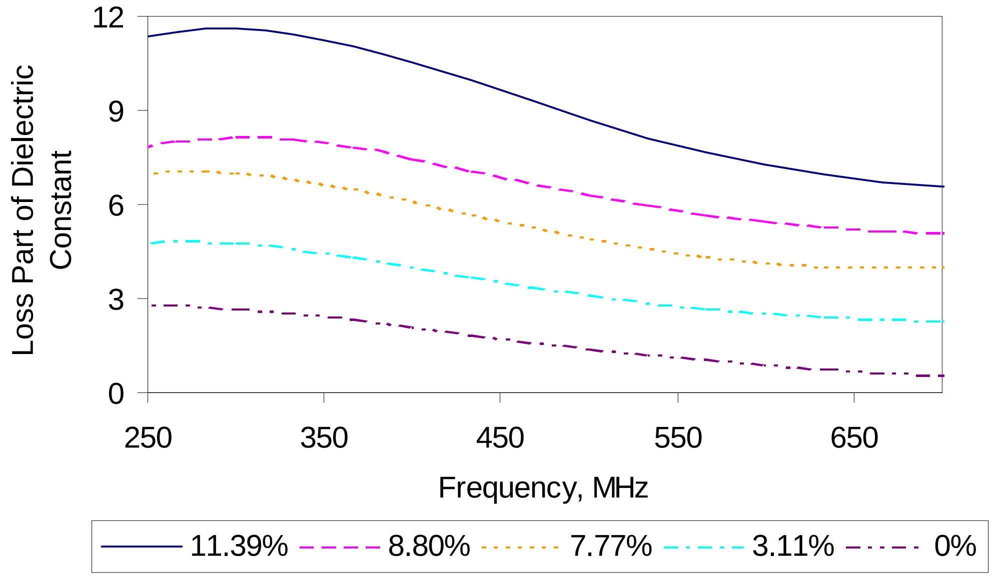


Figure E.4. Effect of frequency on the loss part of the dielectric constant for L3N2 for five levels of volumetric moisture content (3 ns gating).

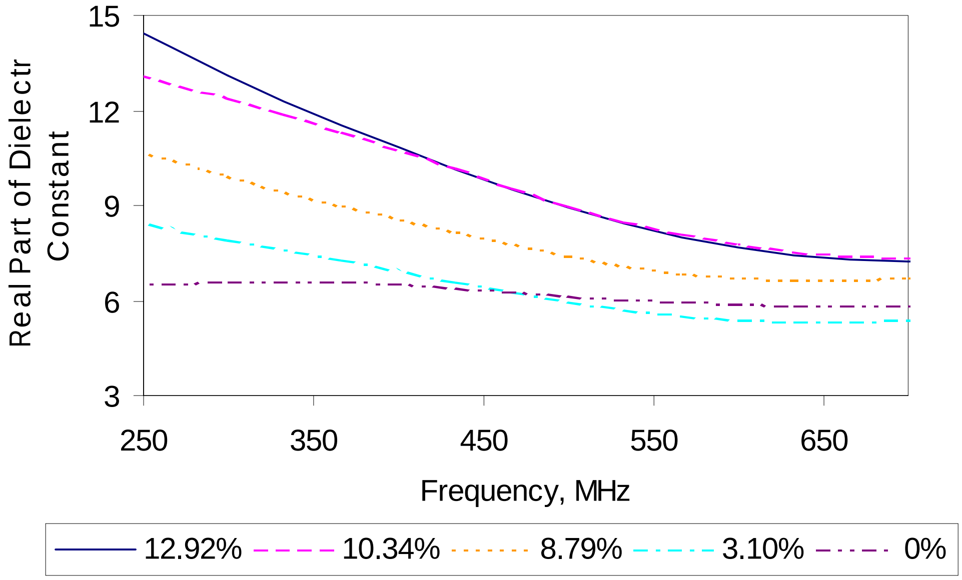


Figure E.5. Effect of frequency on the real part of the dielectric constant for L4N1 for five levels of volumetric moisture content (3 ns gating).

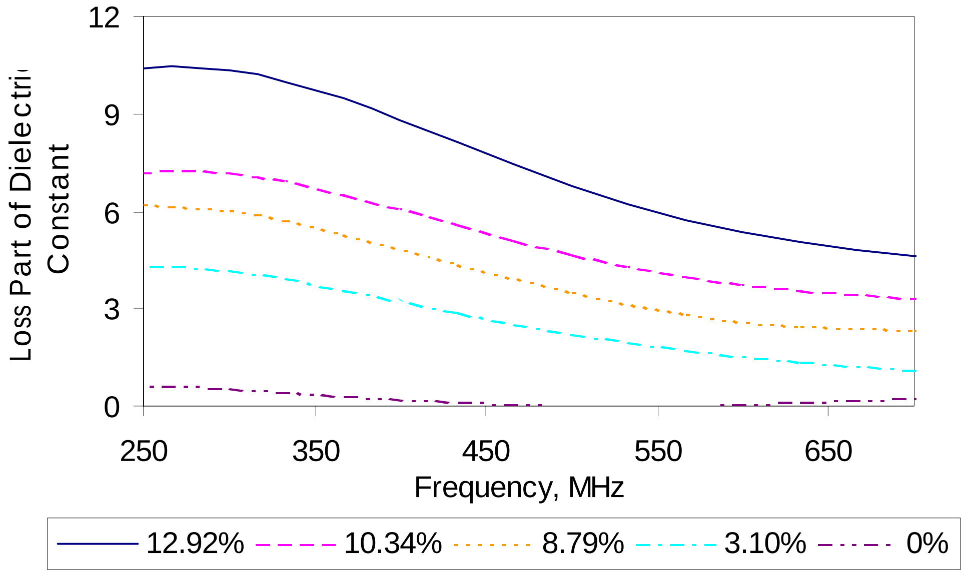


Figure E.6. Effect of frequency on the loss part of the dielectric constant for L4N1 for five levels of volumetric moisture content (3 ns gating).

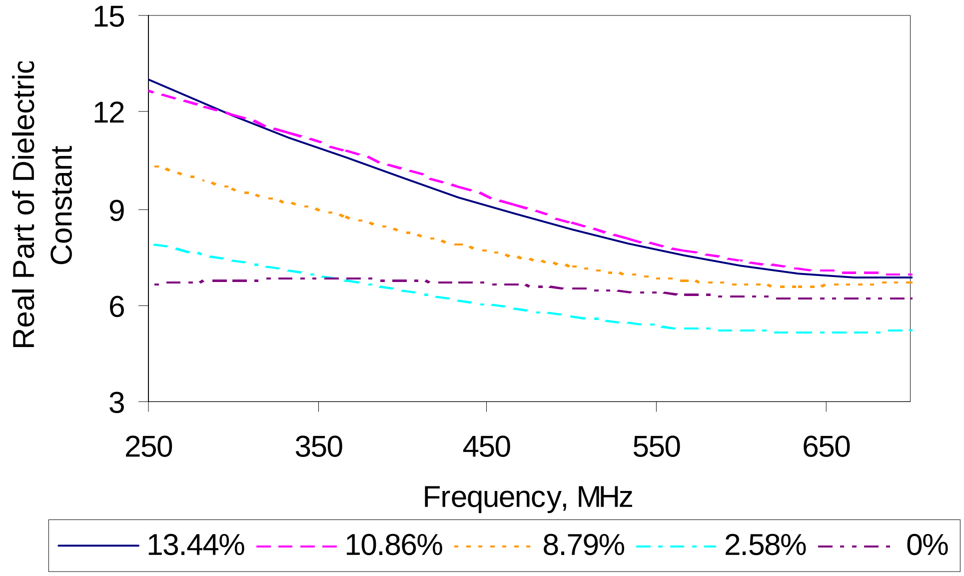


Figure E.7. Effect of frequency on the real part of the dielectric constant for L4N2 for five levels of volumetric moisture content (3 ns gating).

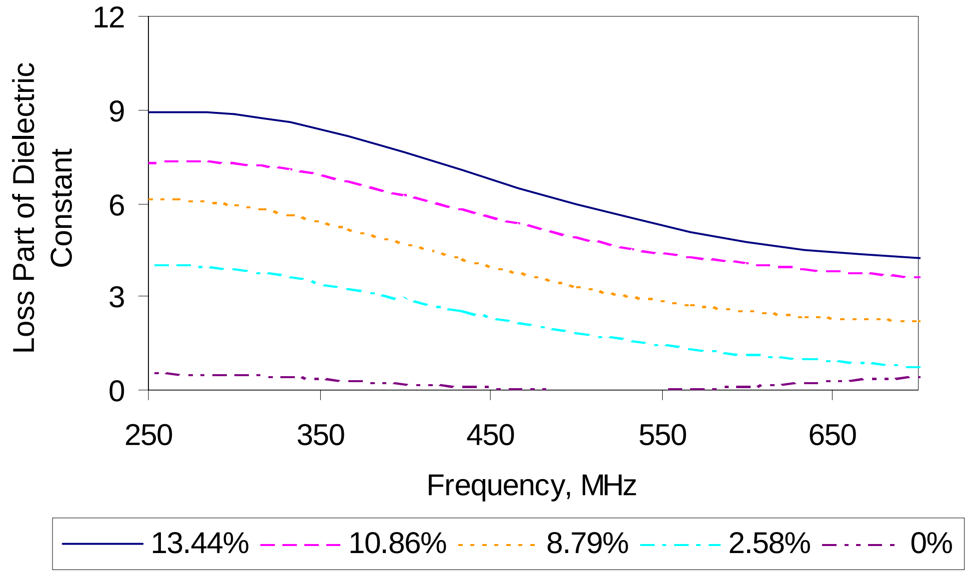


Figure E.8. Effect of frequency on the loss part of the dielectric constant for L4N2 for five levels of volumetric moisture content (3 ns gating).

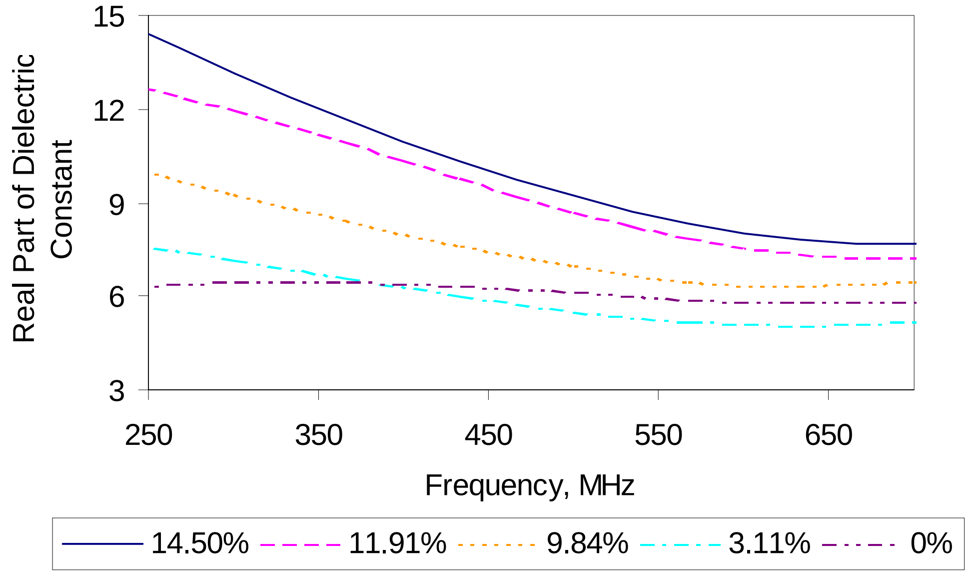


Figure E.9. Effect of frequency on the real part of the dielectric constant for L5N1 for five levels of volumetric moisture content (3 ns gating).

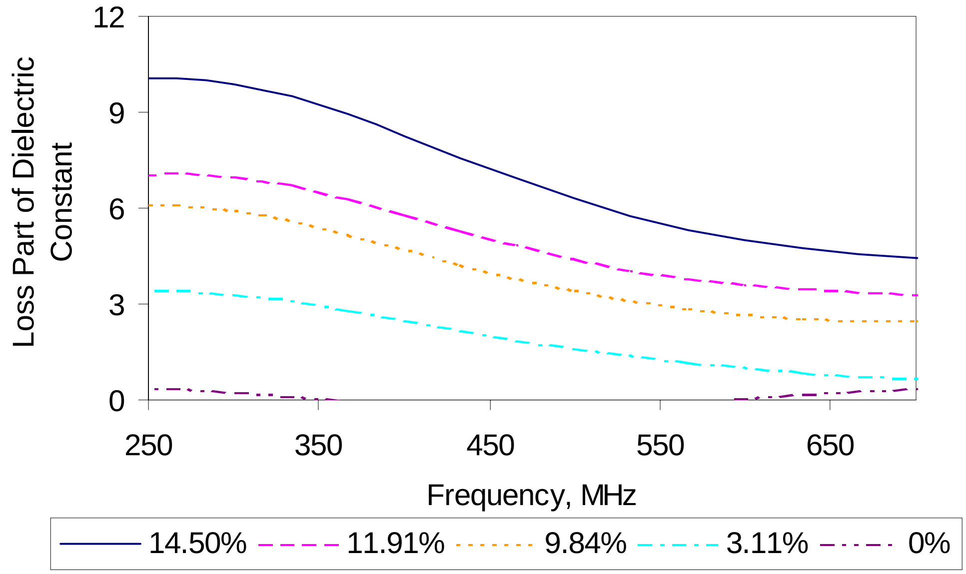


Figure E.10. Effect of frequency on the loss part of the dielectric constant for L5N1 for five levels of volumetric moisture content (3 ns gating).

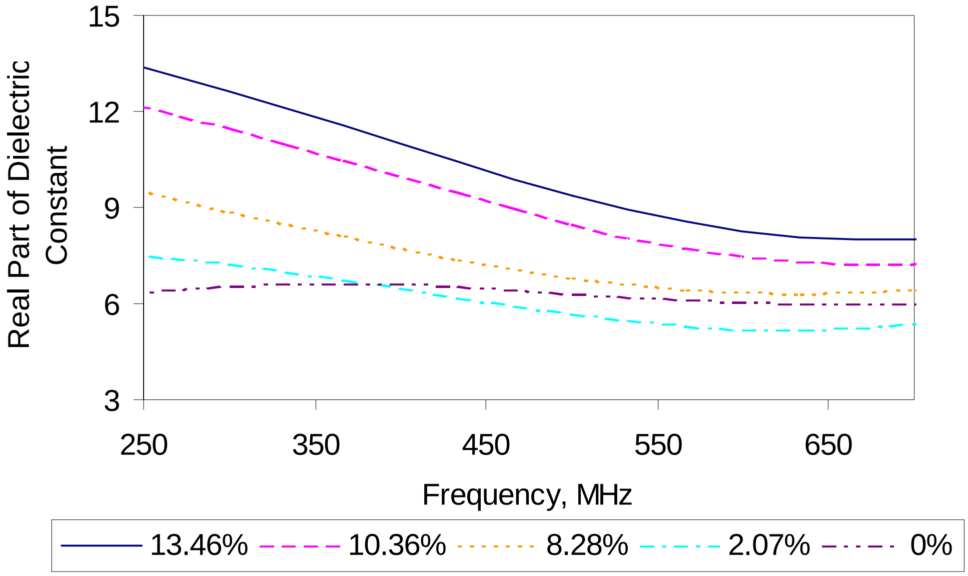


Figure E.11. Effect of frequency on the real part of the dielectric constant for L5N2 for five levels of volumetric moisture content (3 ns gating).

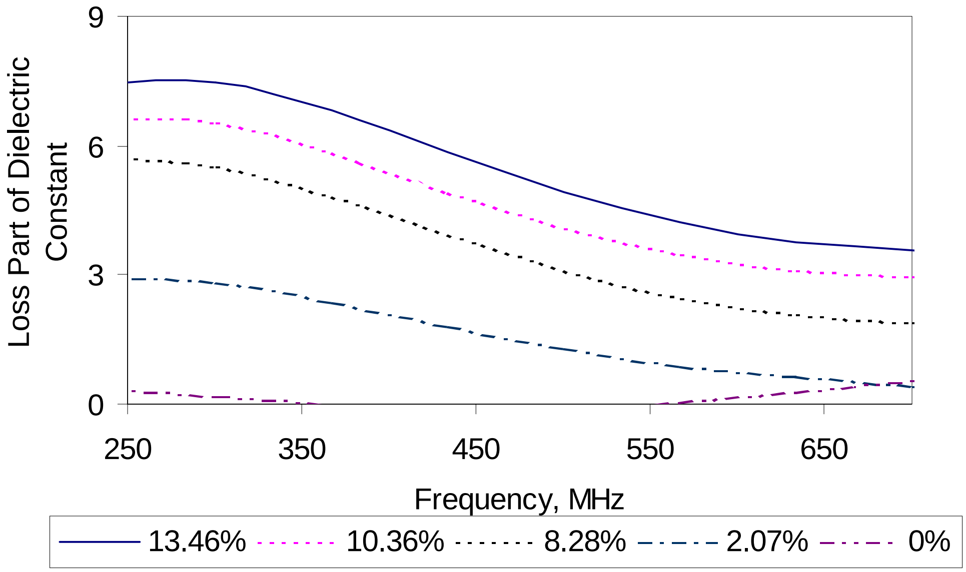


Figure E.12. Effect of frequency on the loss part of the dielectric constant for L5N2 for five levels of volumetric moisture content (3 ns gating).

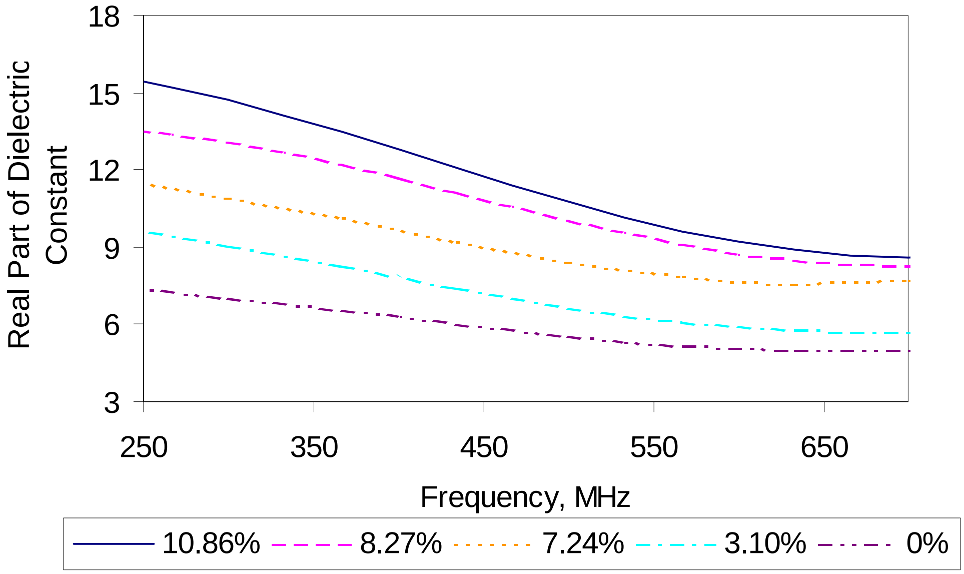


Figure E.13. Effect of frequency on the real part of the dielectric constant for L3S1 for five levels of volumetric moisture content (3 ns gating).

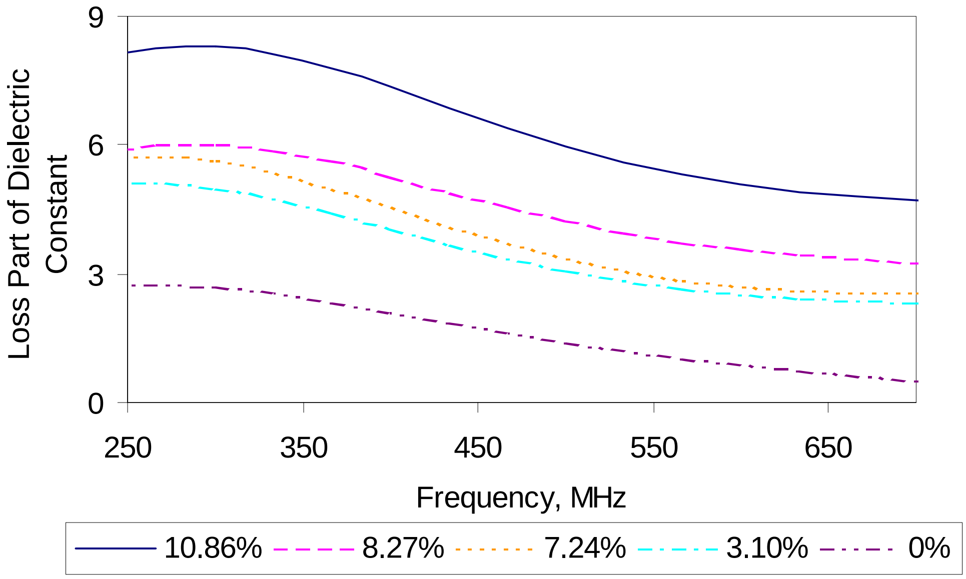


Figure E.14. Effect of frequency on the loss part of the dielectric constant for L3S1 for five levels of volumetric moisture content (3 ns gating).

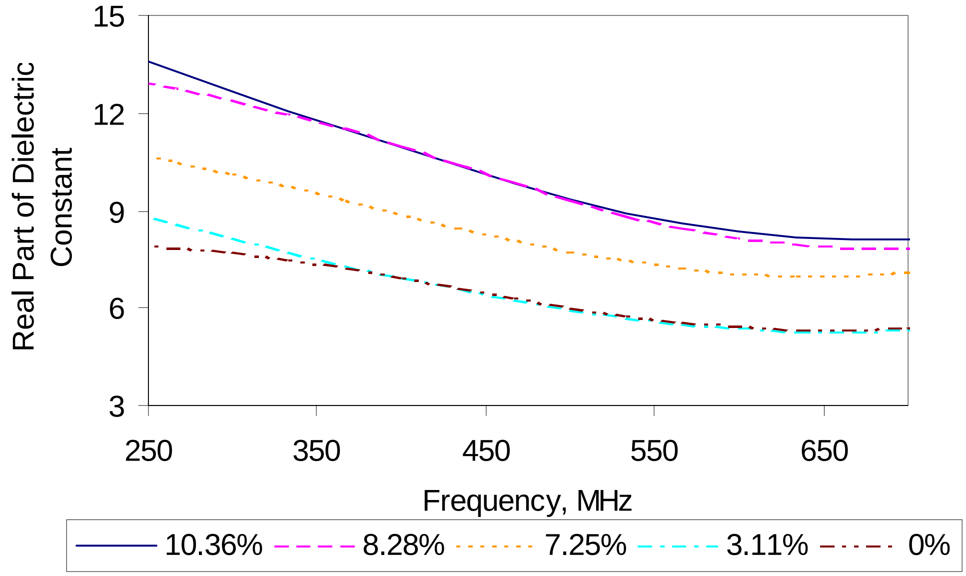


Figure E.15. Effect of frequency on the real part of the dielectric constant for L3S2 for five levels of volumetric moisture content (3 ns gating).

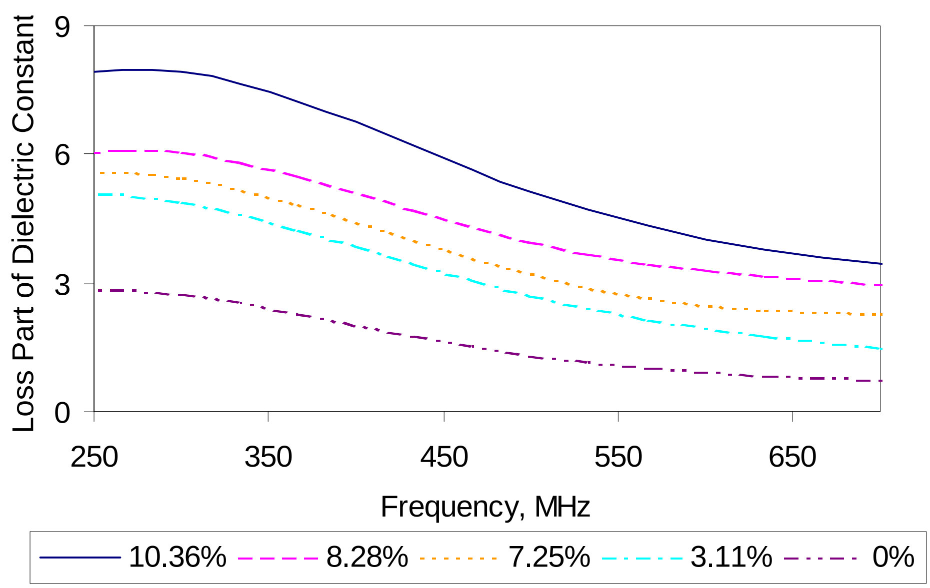


Figure E.16. Effect of frequency on the loss part of the dielectric constant for L3S2 for five levels of volumetric moisture content (3 ns gating).

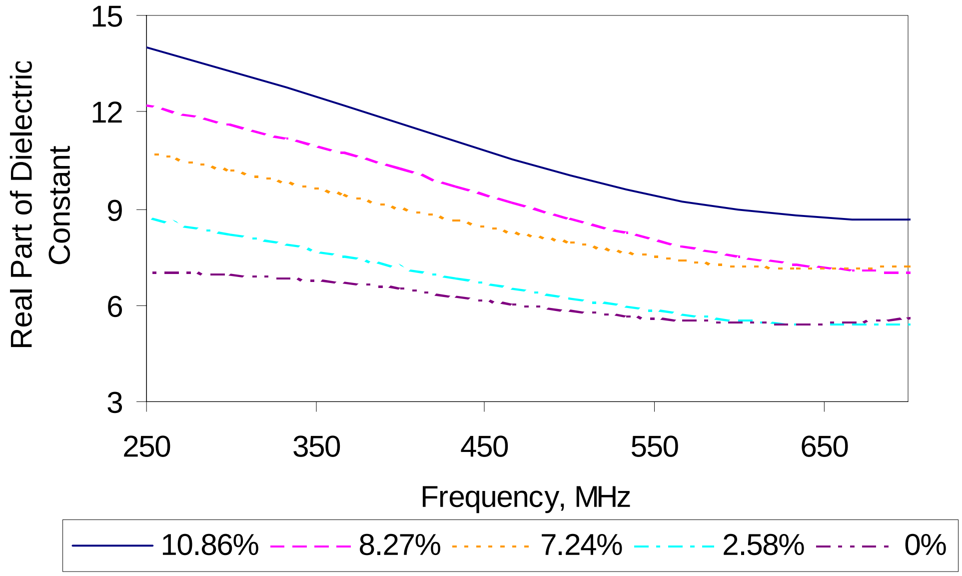


Figure E.17. Effect of frequency on the real part of the dielectric constant for L4S1 for five levels of volumetric moisture content (3 ns gating).

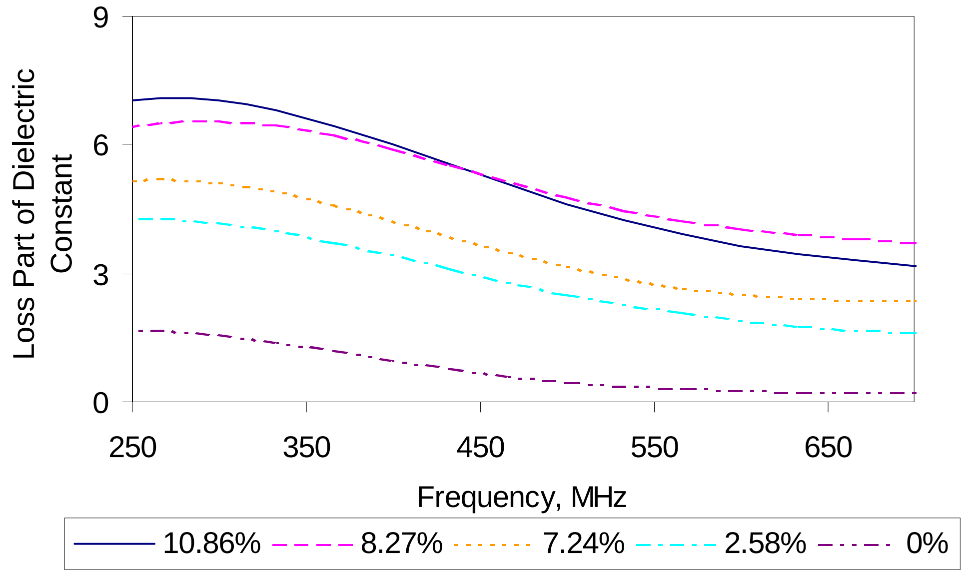


Figure E.18. Effect of frequency on the loss part of the dielectric constant for L4S1 for five levels of volumetric moisture content (3 ns gating).

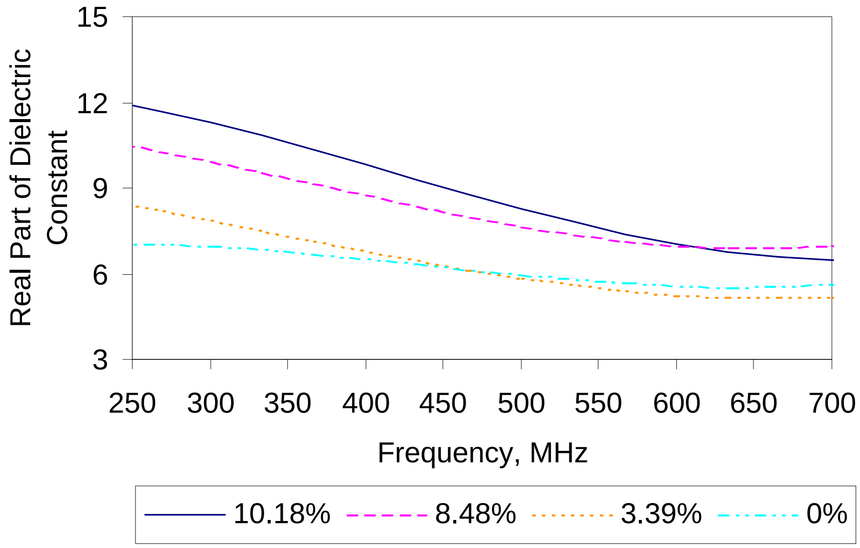


Figure E.19. Effect of frequency on the real part of the dielectric constant for L4S2 for five levels of volumetric moisture content (3 ns gating).

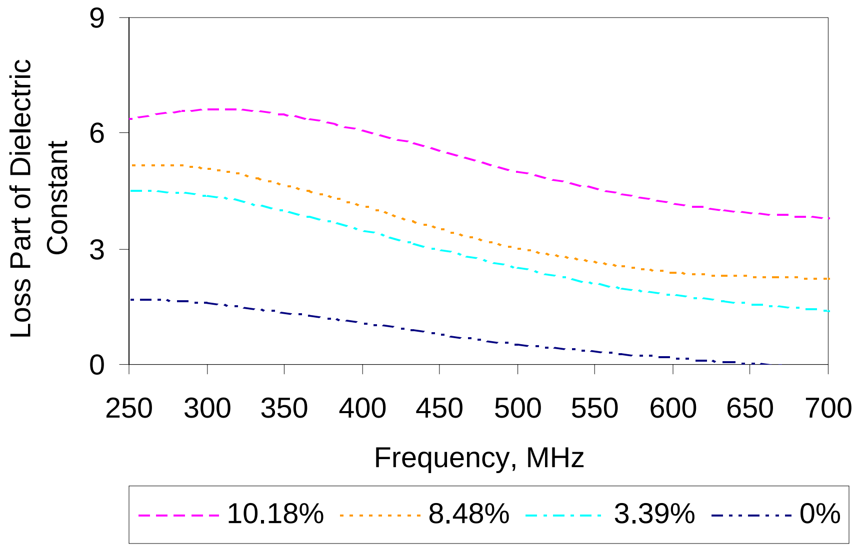


Figure E.20. Effect of frequency on the loss part of the dielectric constant for L4S2 for five levels of volumetric moisture content (3 ns gating).

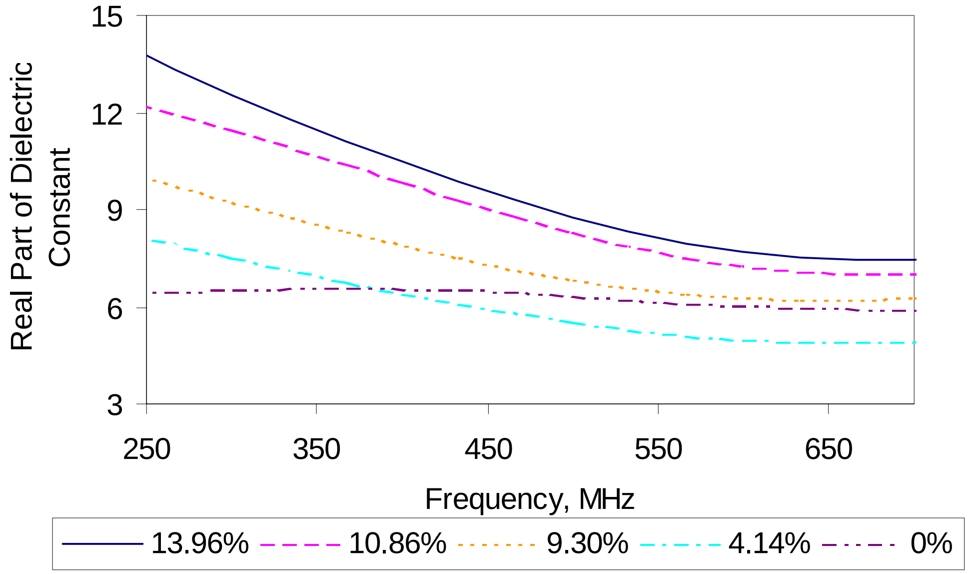


Figure E.21. Effect of frequency on the real part of the dielectric constant for L5S1 for five levels of volumetric moisture content (3 ns gating).

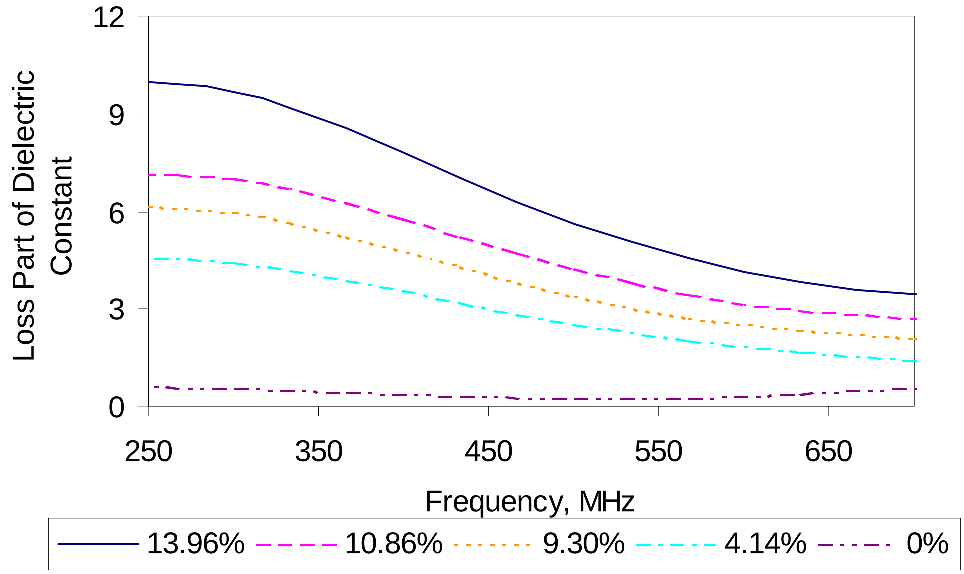


Figure E.22. Effect of frequency on the loss part of the dielectric constant for L5S1 for five levels of volumetric moisture content (3 ns gating).

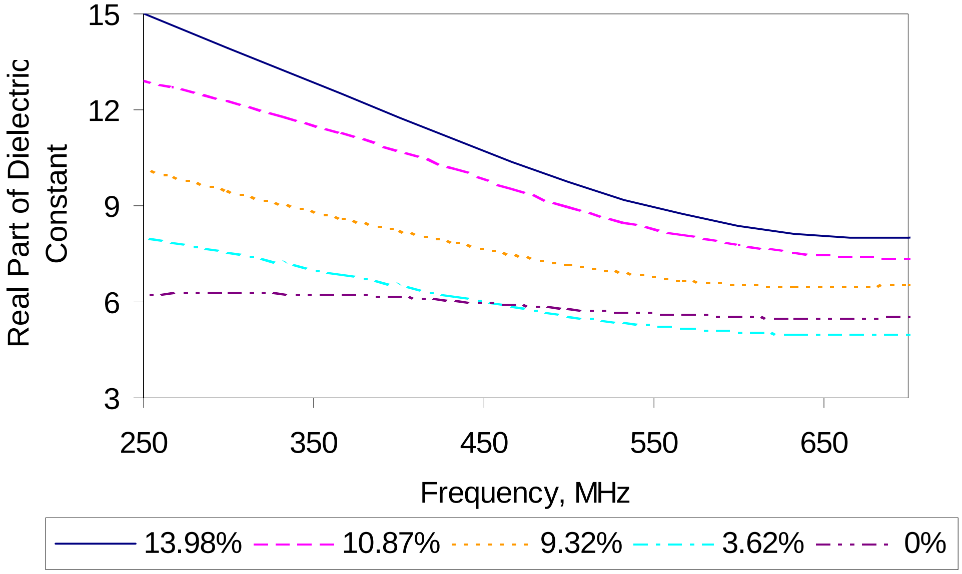


Figure E.23. Effect of frequency on the real part of the dielectric constant for L5S2 for five levels of volumetric moisture content (3 ns gating).

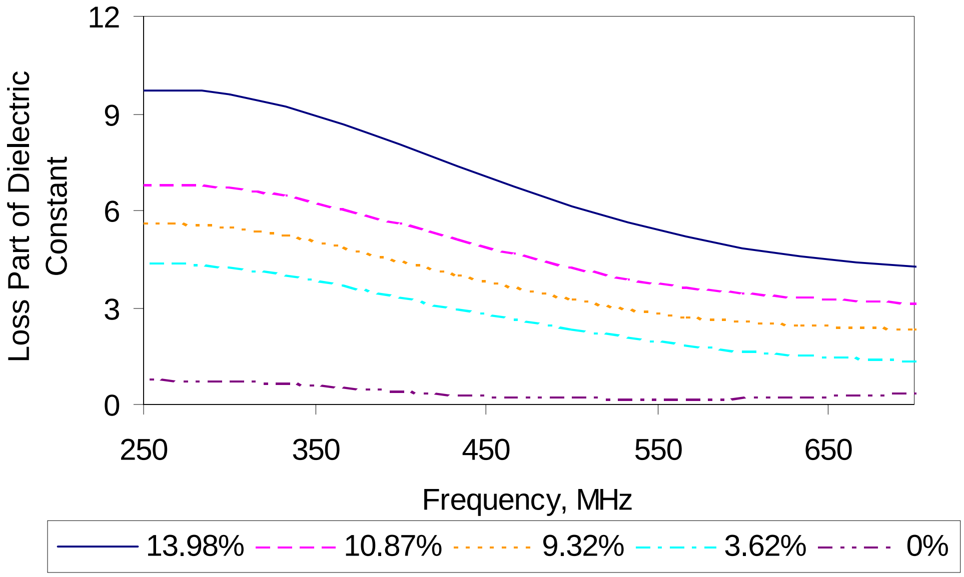


Figure E.24. Effect of frequency on the loss part of the dielectric constant for L5S2 for five levels of volumetric moisture content (3 ns gating).

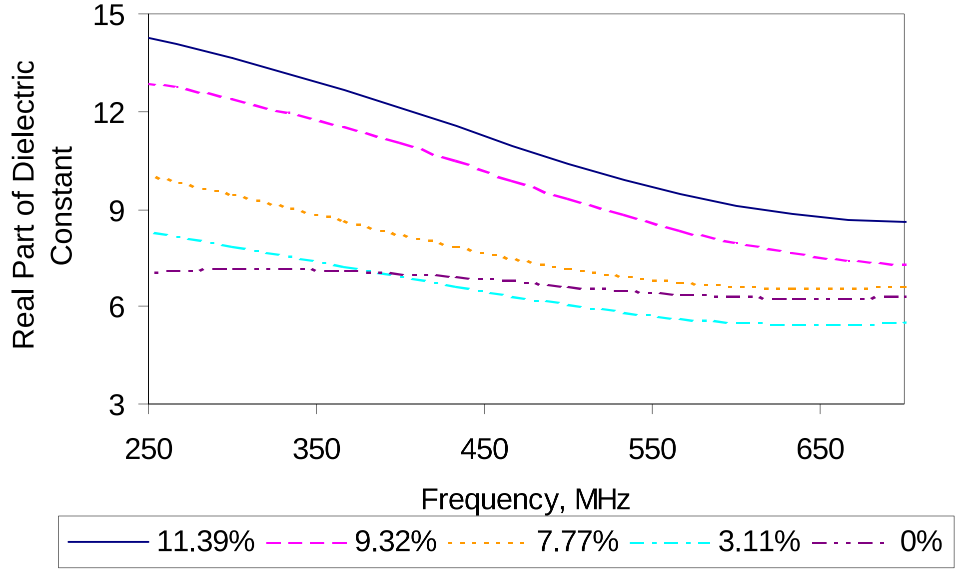


Figure E.25. Effect of frequency on the real part of the dielectric constant for L3H1 for five levels of volumetric moisture content (3 ns gating).

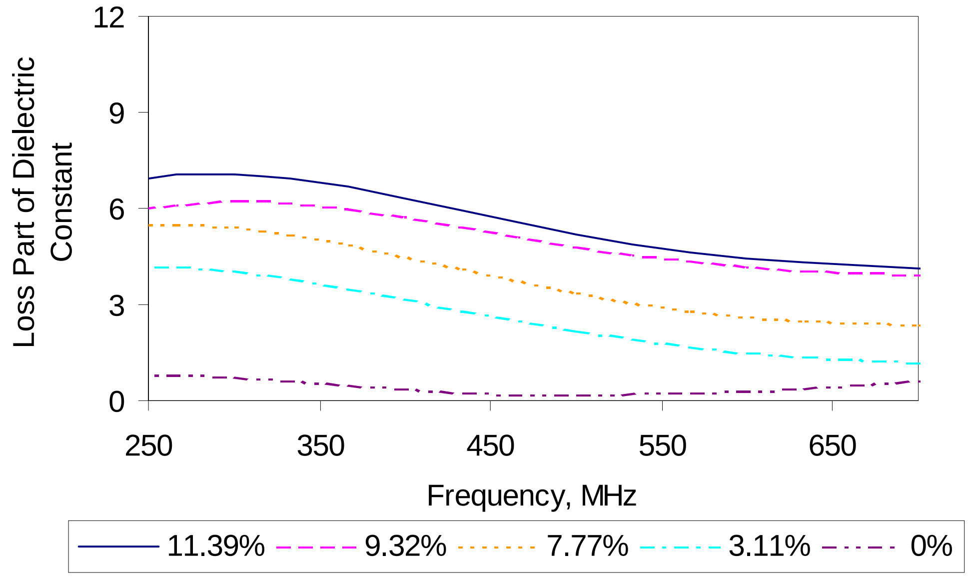


Figure E.26. Effect of frequency on the loss part of the dielectric constant for L3H1 for five levels of volumetric moisture content (3 ns gating).

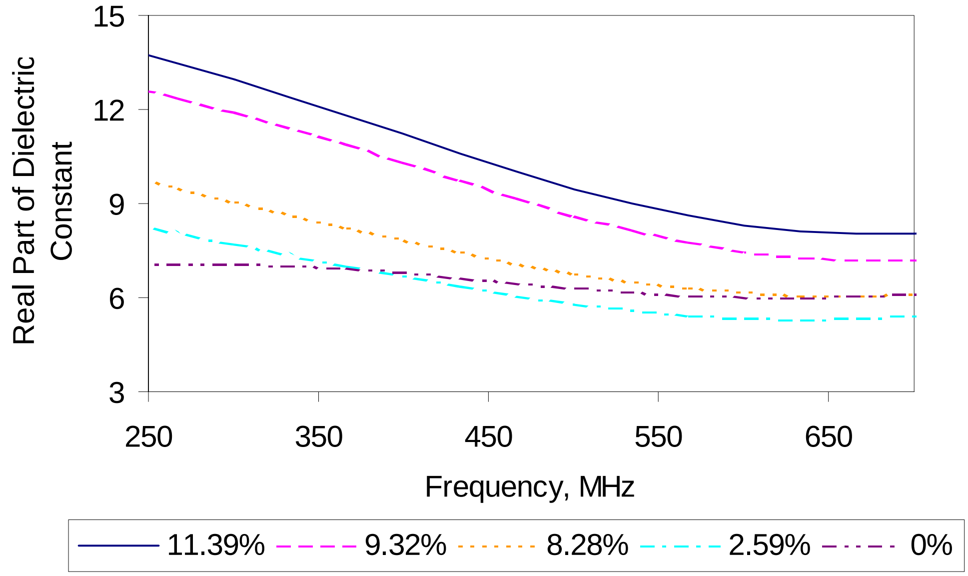


Figure E.27. Effect of frequency on the real part of the dielectric constant for L3H2 for five levels of volumetric moisture content (3 ns gating).

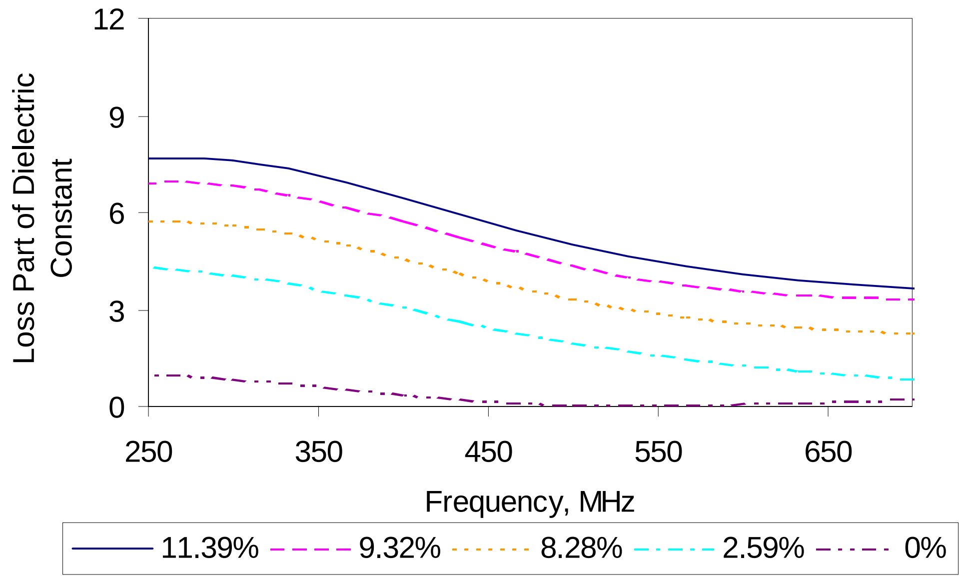


Figure E.28. Effect of frequency on the loss part of the dielectric constant for L3H2 for five levels of volumetric moisture content (3 ns gating).

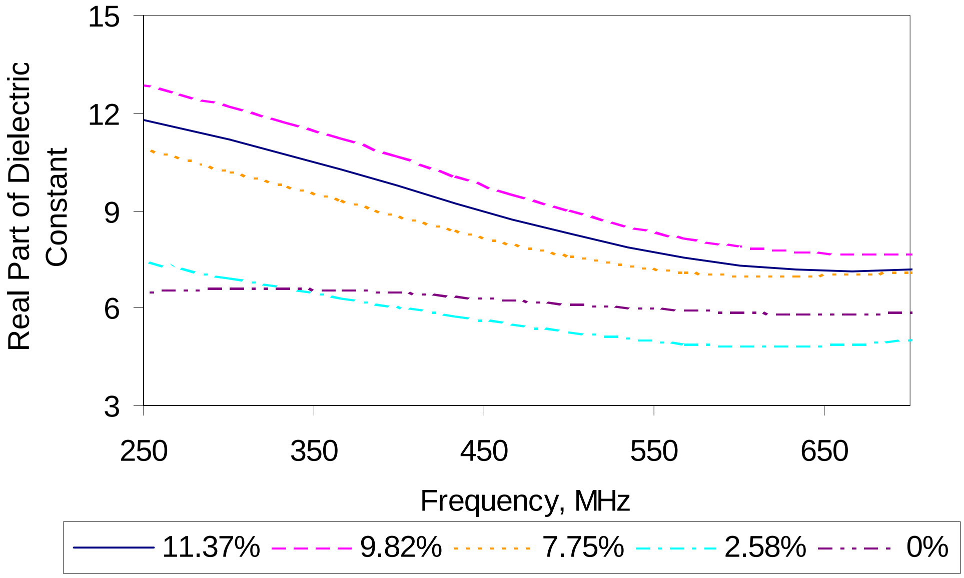


Figure E.29. Effect of frequency on the real part of the dielectric constant for L4H1 for five levels of volumetric moisture content (3 ns gating).

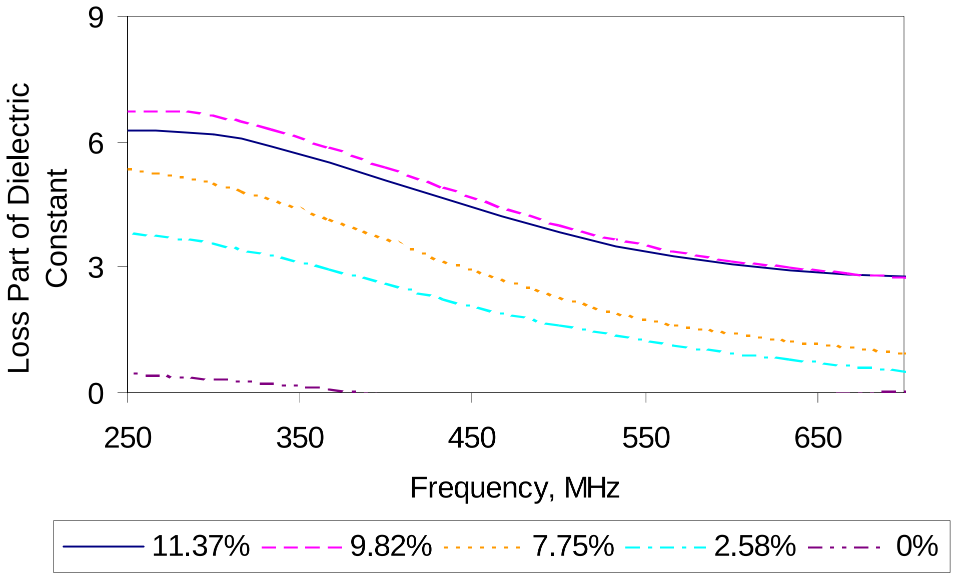


Figure E.30. Effect of frequency on the loss part of the dielectric constant for L4H1 for five levels of volumetric moisture content (3 ns gating).

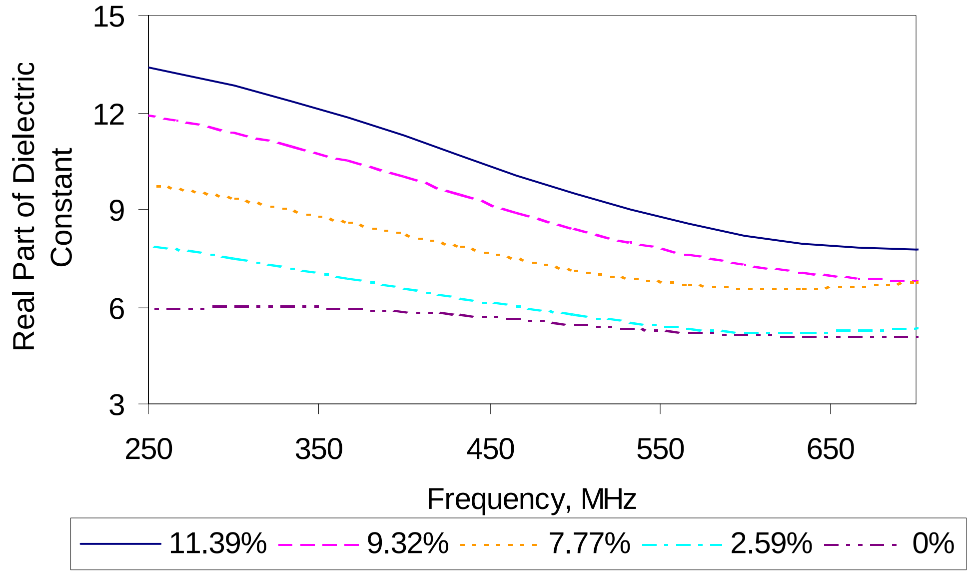


Figure E.31. Effect of frequency on the real part of the dielectric constant for L4H2 for five levels of volumetric moisture content (3 ns gating).

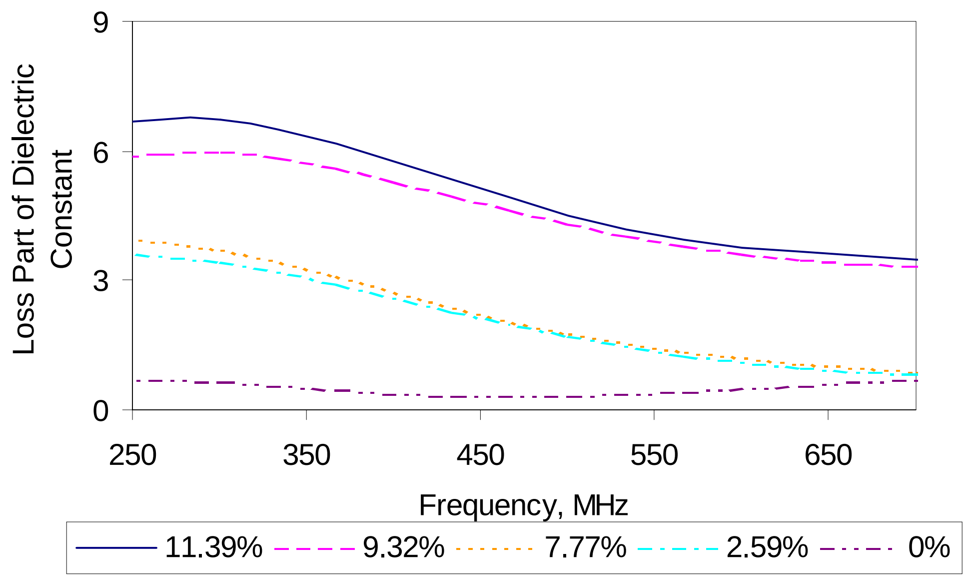


Figure E.32. Effect of frequency on the loss part of the dielectric constant for L4H2 for five levels of volumetric moisture content (3 ns gating).

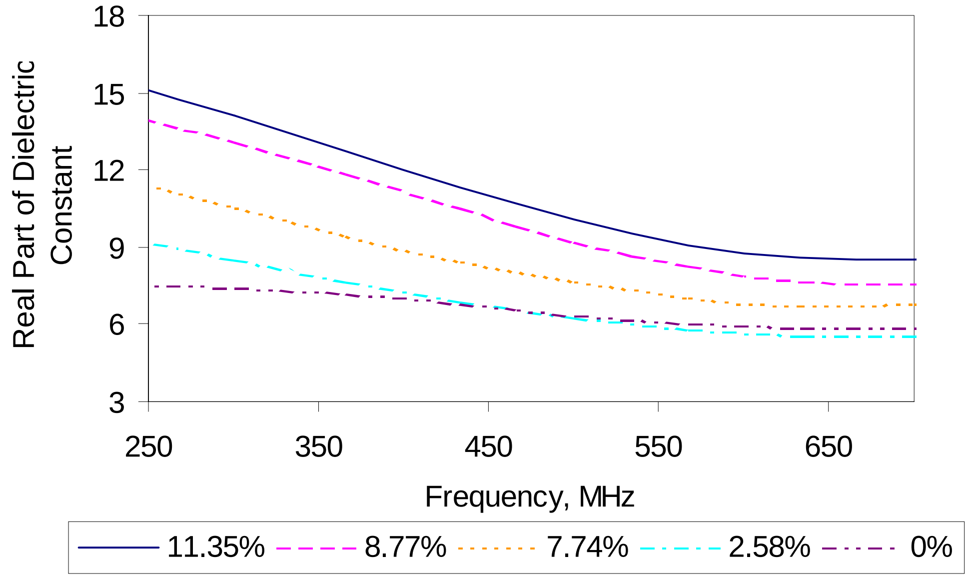


Figure E.33. Effect of frequency on the real part of the dielectric constant for L4C41 for five levels of volumetric moisture content (3 ns gating).

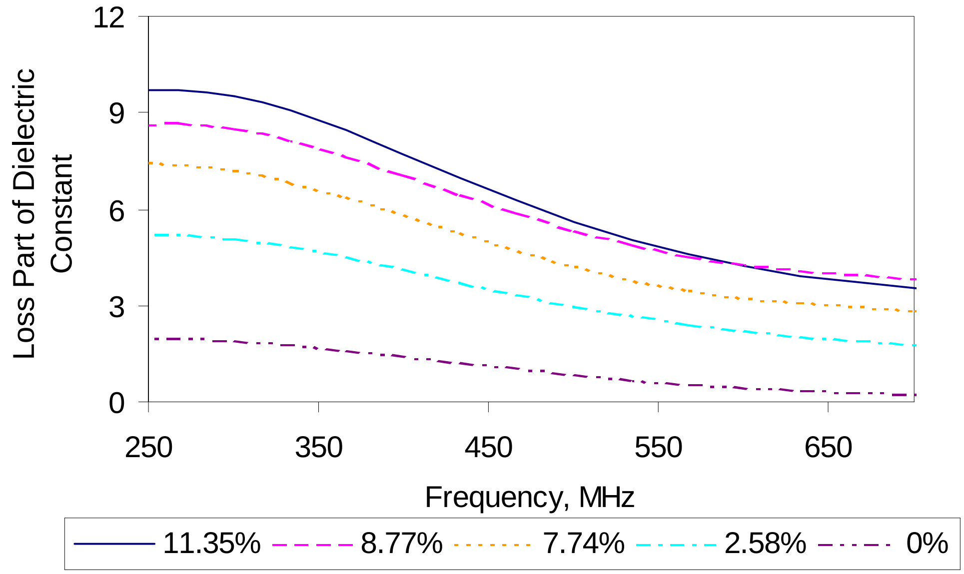


Figure E.34. Effect of frequency on the loss part of the dielectric constant for L4C41 for five levels of volumetric moisture content (3 ns gating).

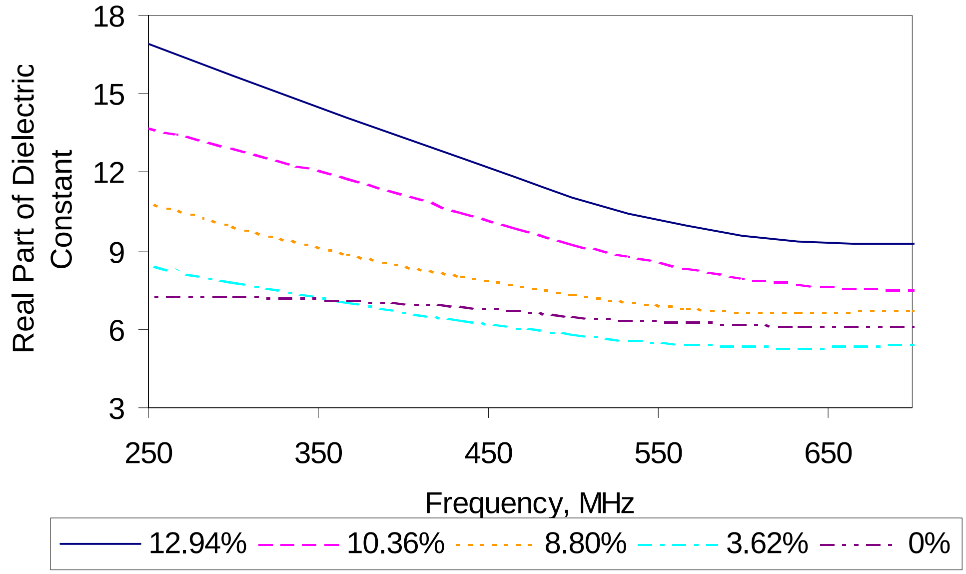


Figure E.35. Effect of frequency on the real part of the dielectric constant for L4C42 for five levels of volumetric moisture content (3 ns gating).

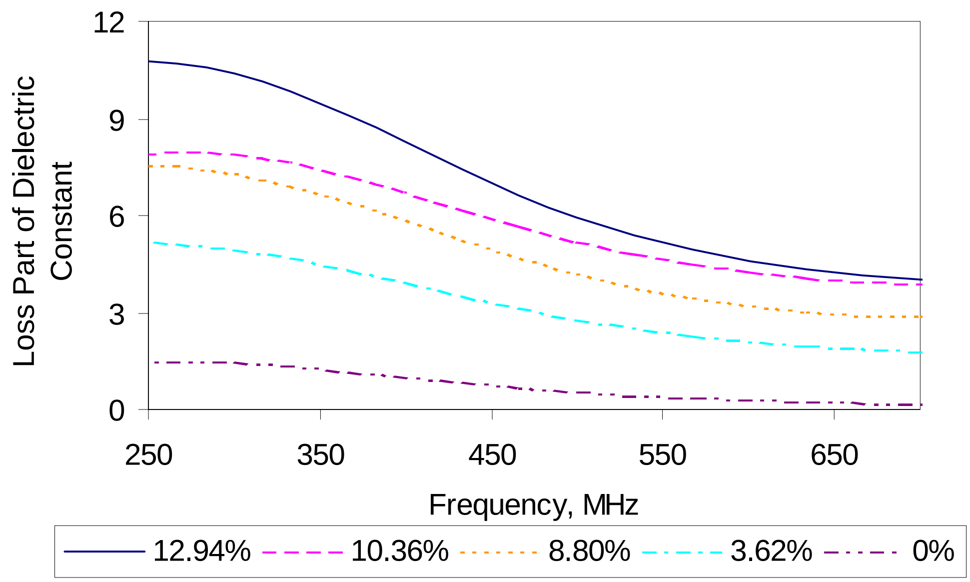


Figure E.36. Effect of frequency on the loss part of the dielectric constant for L4C42 for five levels of volumetric moisture content (3 ns gating).

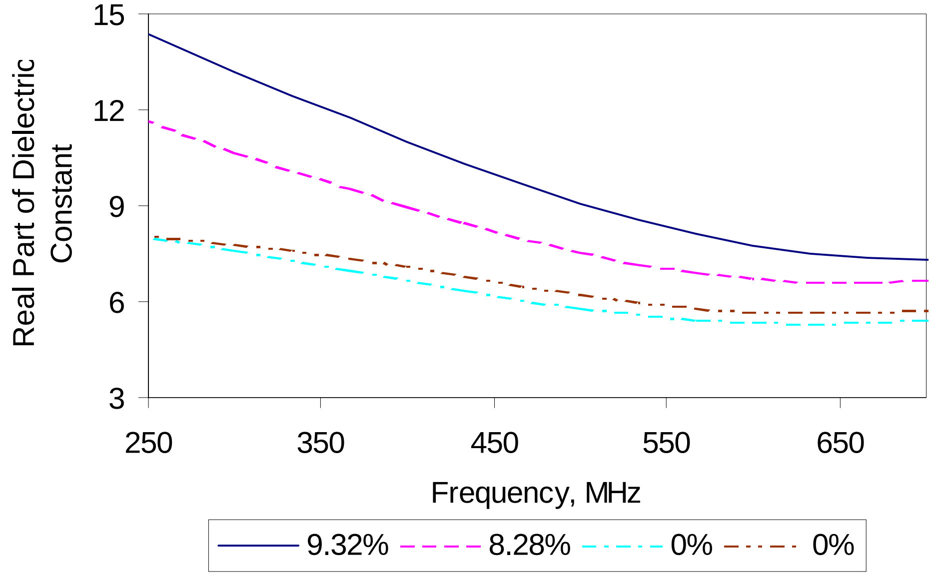


Figure E.37. Effect of frequency on the real part of the dielectric constant for L4C81 for five levels of volumetric moisture content (3 ns gating).

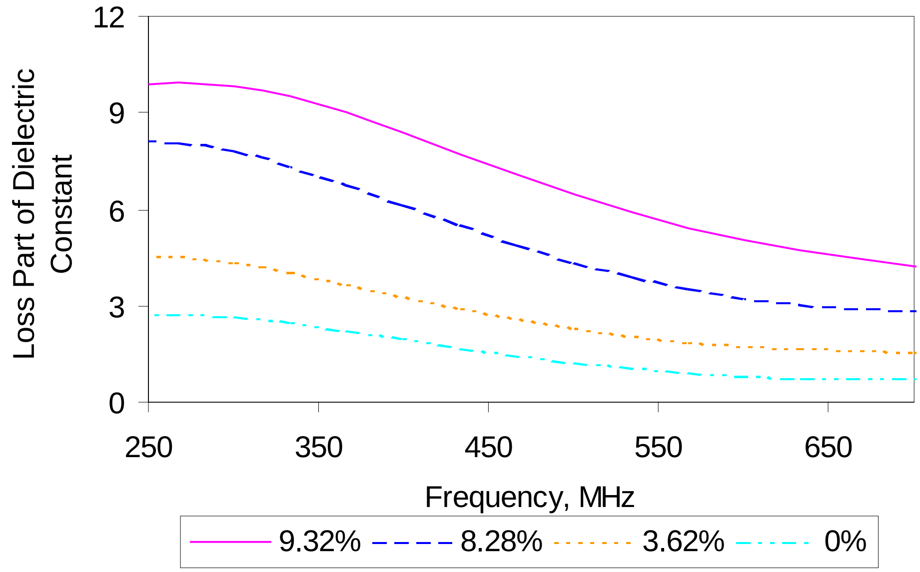


Figure E.38. Effect of frequency on the loss part of the dielectric constant for L4C81 for five levels of volumetric moisture content (3 ns gating).

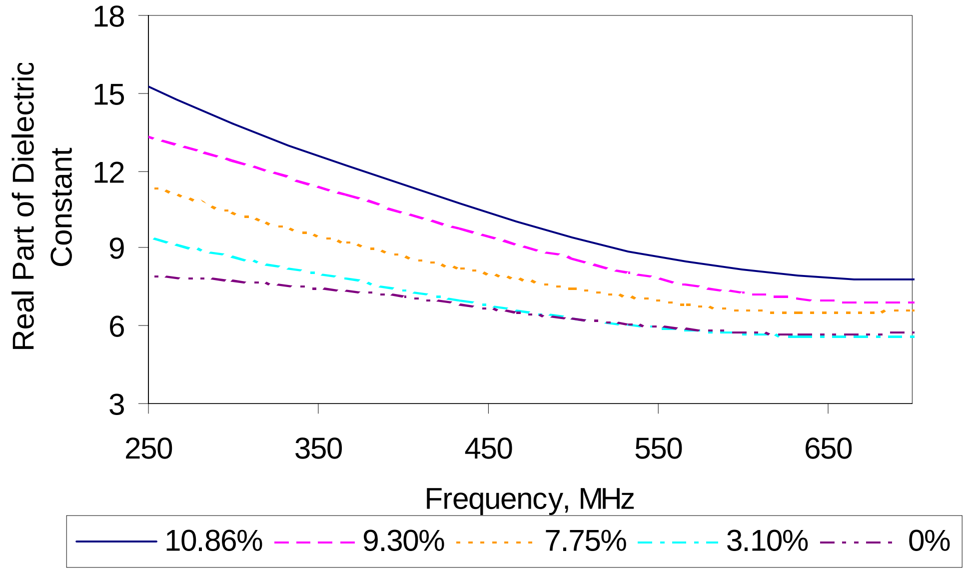


Figure E.39. Effect of frequency on the real part of the dielectric constant for L4C82 for five levels of volumetric moisture content (3 ns gating).

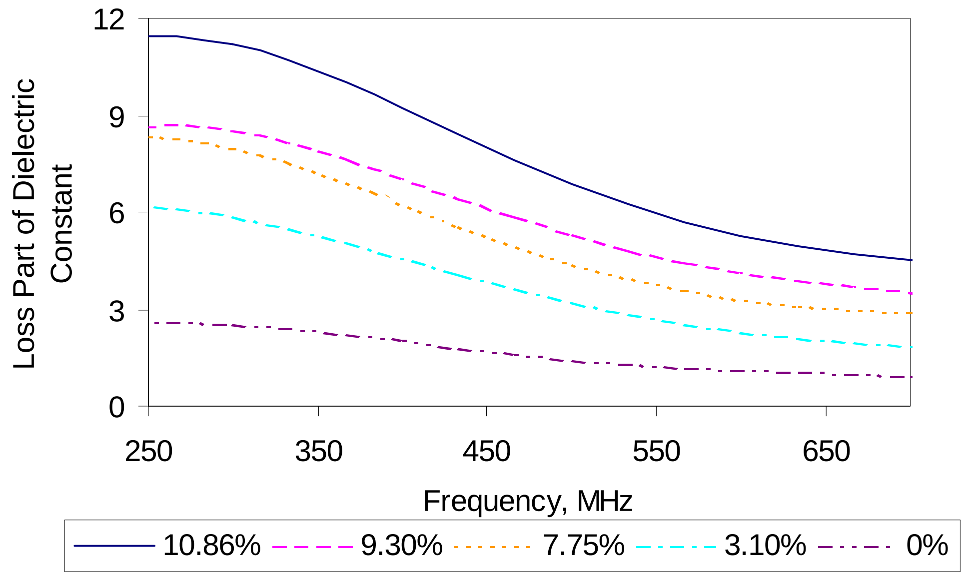


Figure E.40. Effect of frequency on the loss part of the dielectric constant for L4C82 for five levels of volumetric moisture content (3 ns gating).

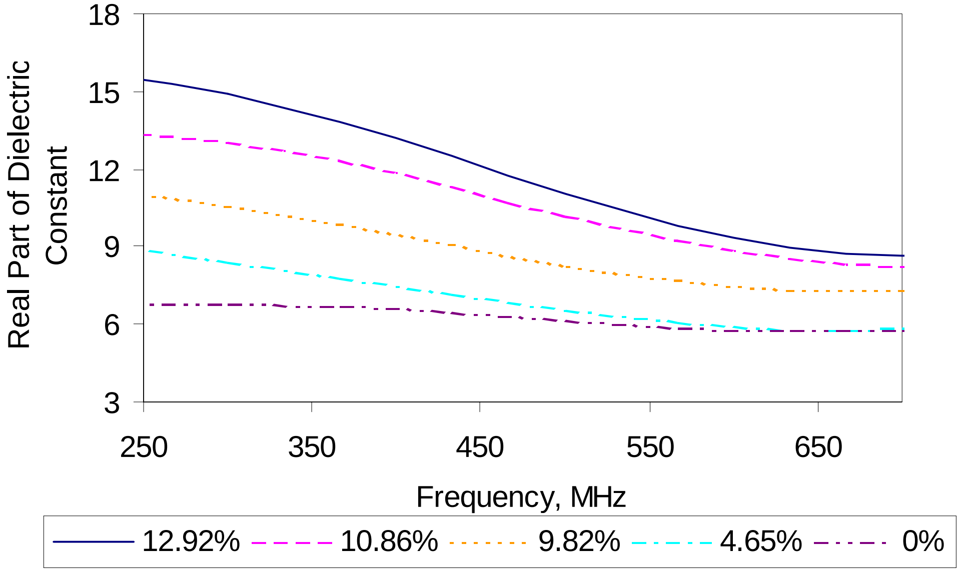


Figure E.41. Effect of frequency on the real part of the dielectric constant for L4M1 for five levels of volumetric moisture content (3 ns gating).

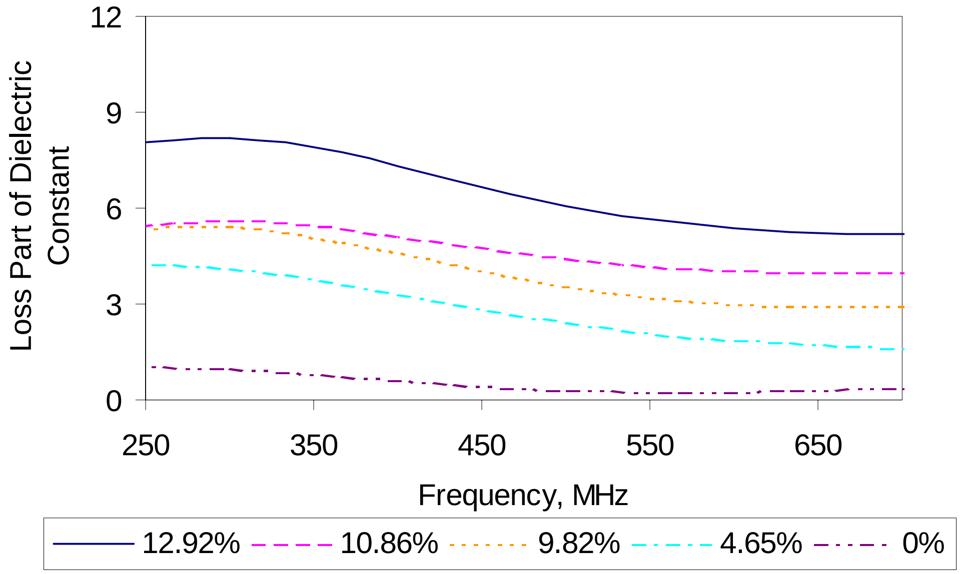


Figure E.41. Effect of frequency on the loss part of the dielectric constant for L4M1 for five levels of volumetric moisture content (3 ns gating).

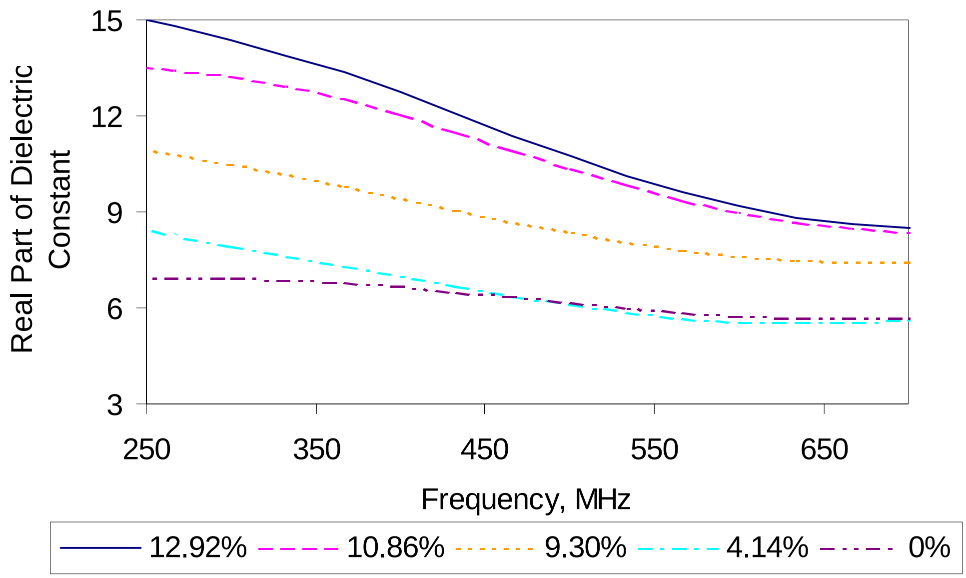


Figure E.43. Effect of frequency on the real part of the dielectric constant for L4M2 for five levels of volumetric moisture content (3 ns gating).

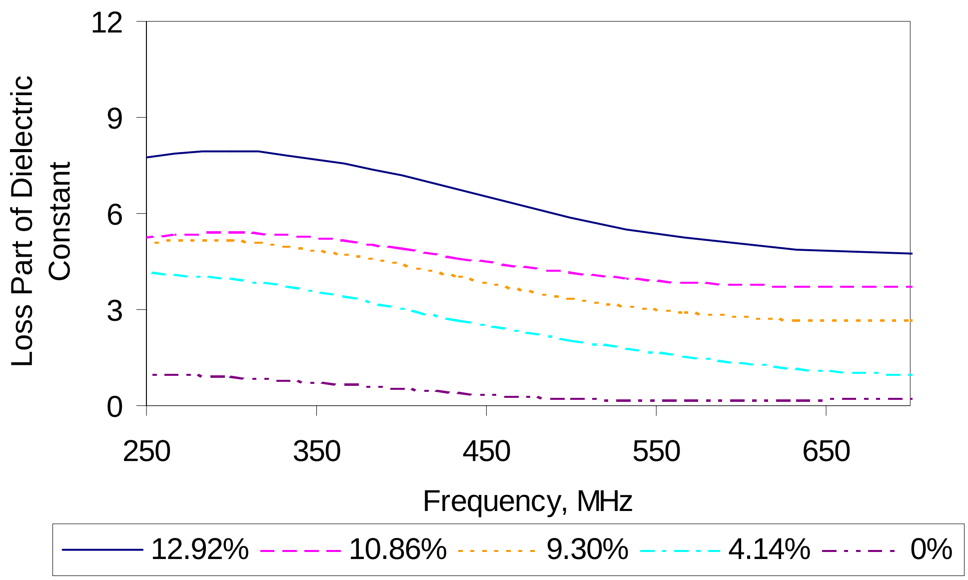


Figure E.44. Effect of frequency on the loss part of the dielectric constant for L4M2 for five levels of volumetric moisture content (3 ns gating).

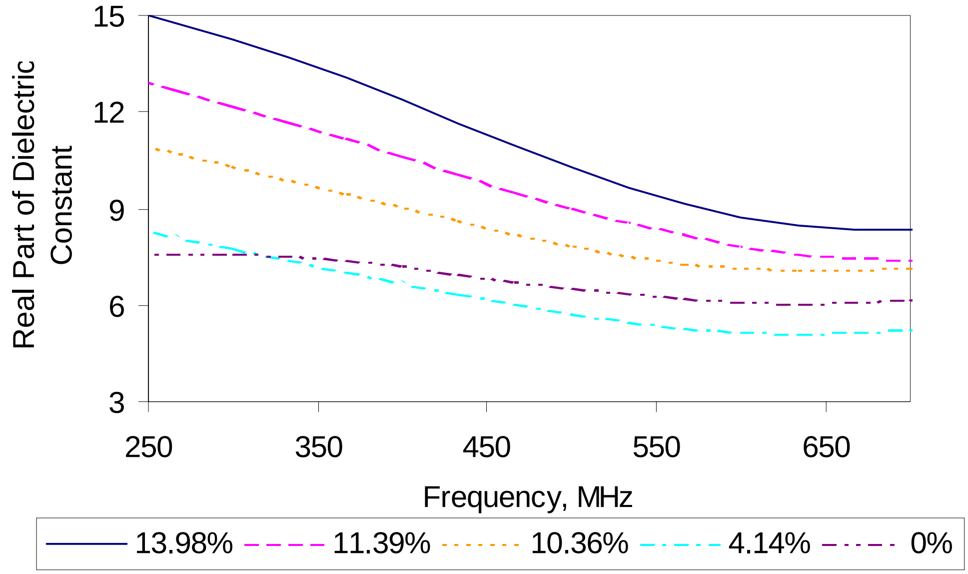


Figure E.45. Effect of frequency on the real part of the dielectric constant for L5M1 for five levels of volumetric moisture content (3 ns gating).

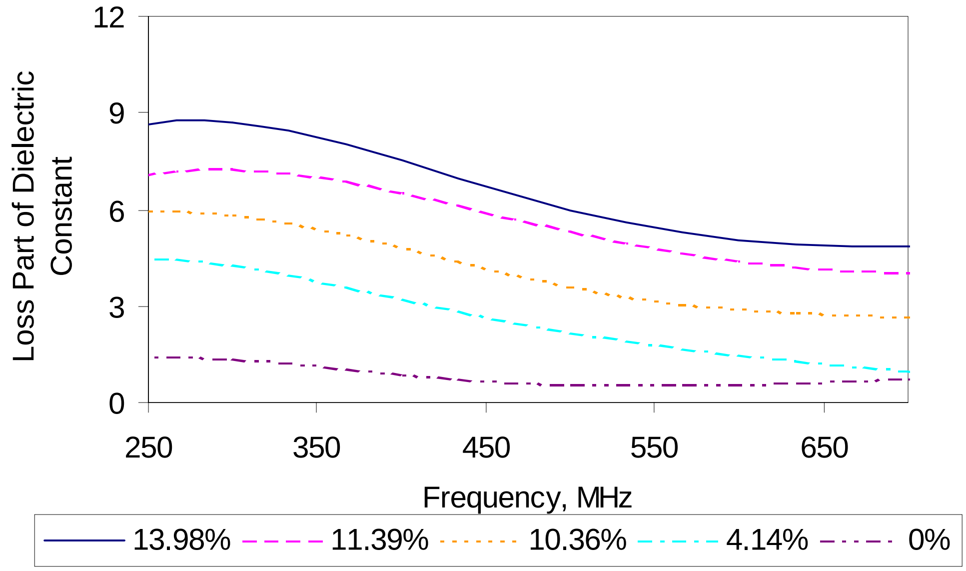


Figure E.46. Effect of frequency on the loss part of the dielectric constant for L5M1 for five levels of volumetric moisture content (3 ns gating).

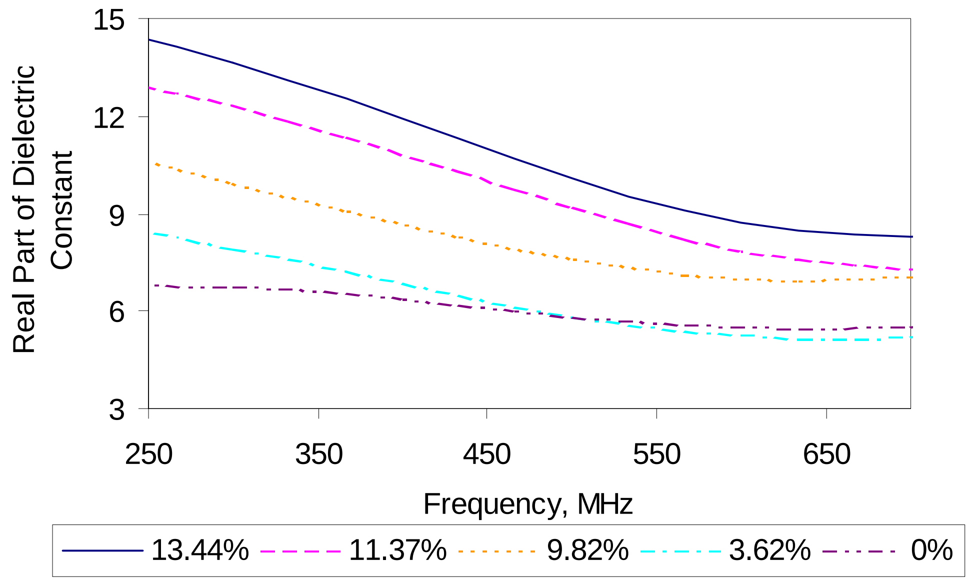


Figure E.47. Effect of frequency on the real part of the dielectric constant for L5M2 for five levels of volumetric moisture content (3 ns gating).

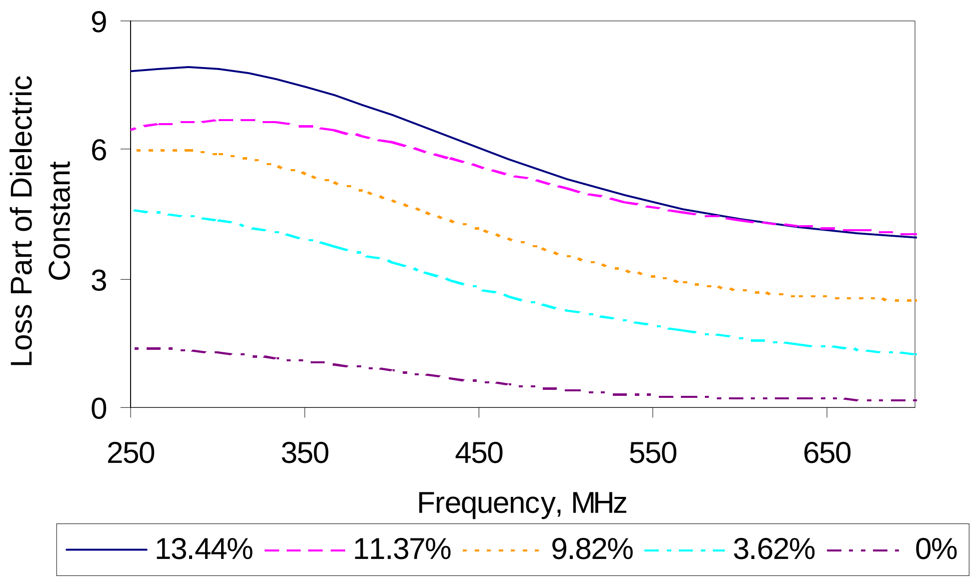


Figure E.48. Effect of frequency on the loss part of the dielectric constant for L5M2 for five levels of volumetric moisture content (3 ns gating).

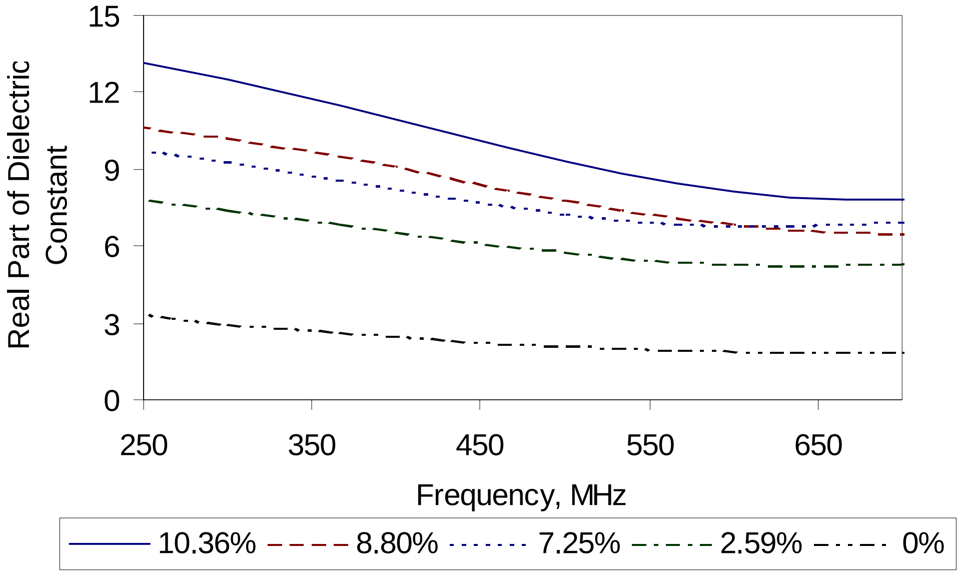


Figure E.49. Effect of frequency on the real part of the dielectric constant for G3N1 for five levels of volumetric moisture content (3 ns gating).

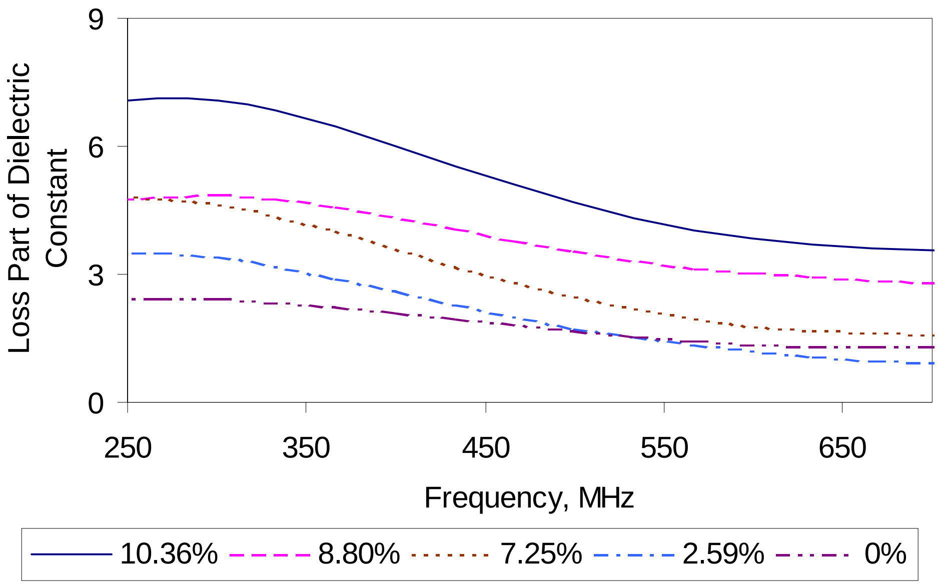


Figure E.50. Effect of frequency on the loss part of the dielectric constant for G3N1 for five levels of volumetric moisture content (3 ns gating).

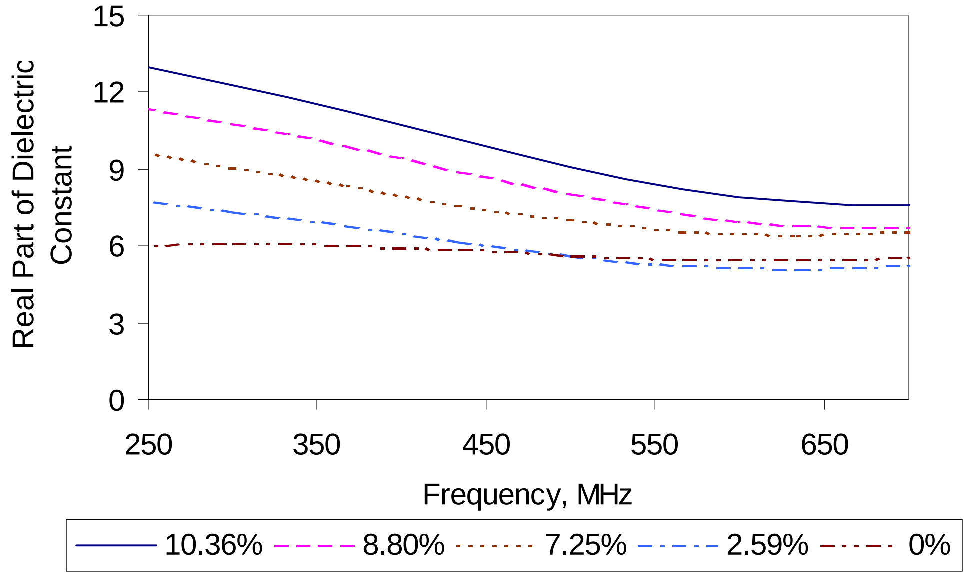


Figure E.51. Effect of frequency on the real part of the dielectric constant for G3N2 for five levels of volumetric moisture content (3 ns gating).

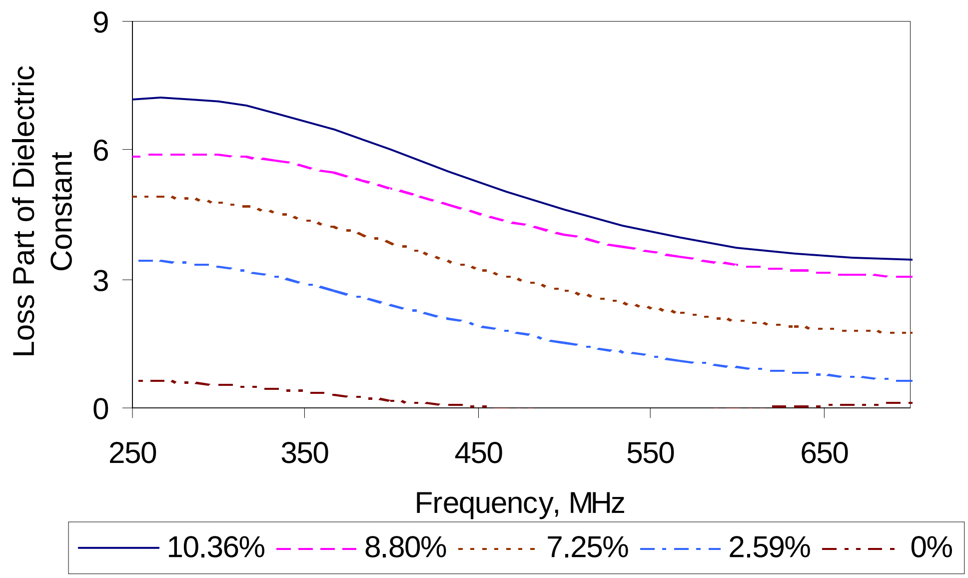


Figure E.52. Effect of frequency on the loss part of the dielectric constant for G3N2 for five levels of volumetric moisture content (3 ns gating).

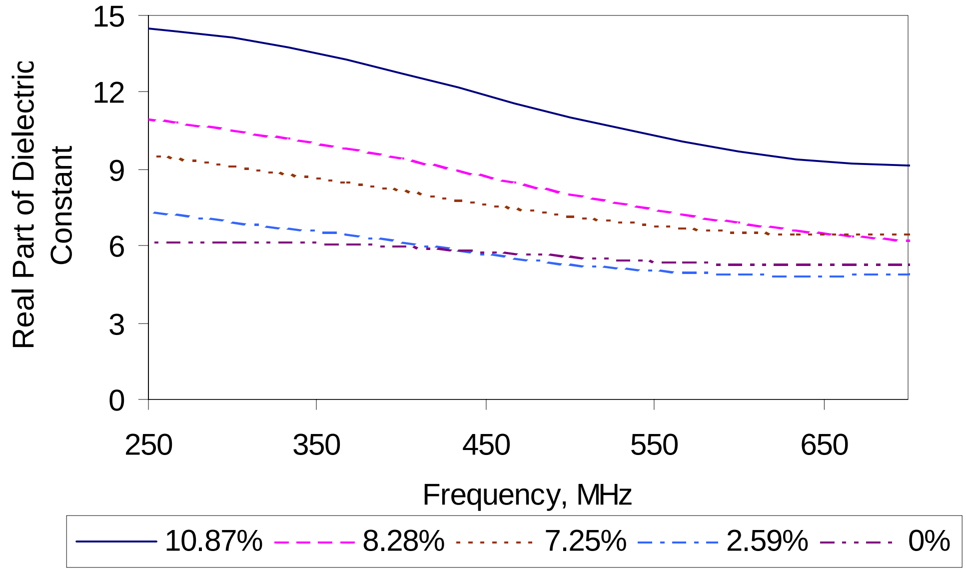


Figure E.53. Effect of frequency on the real part of the dielectric constant for G4N1 for five levels of volumetric moisture content (3 ns gating).

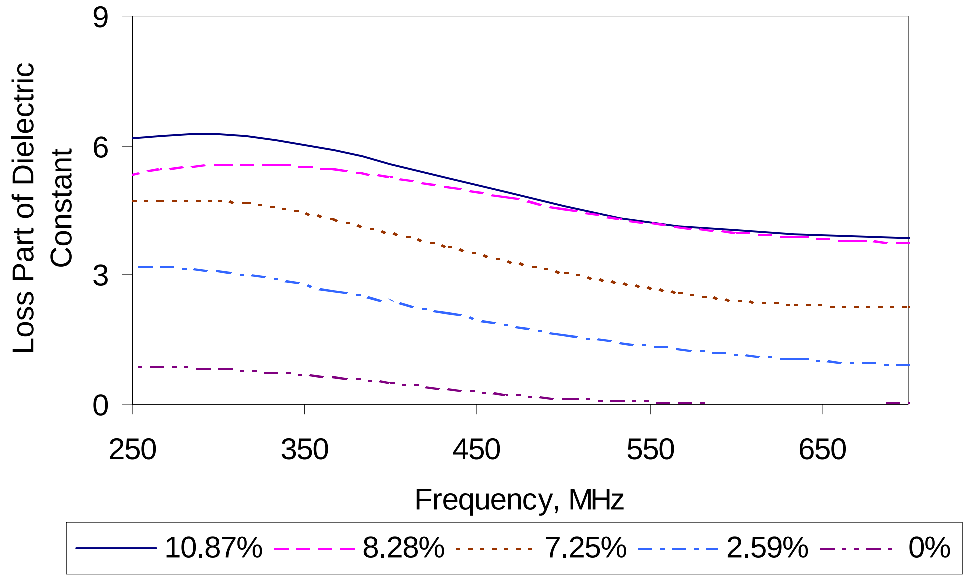


Figure E.54. Effect of frequency on the loss part of the dielectric constant for G4N1 for five levels of volumetric moisture content (3 ns gating).

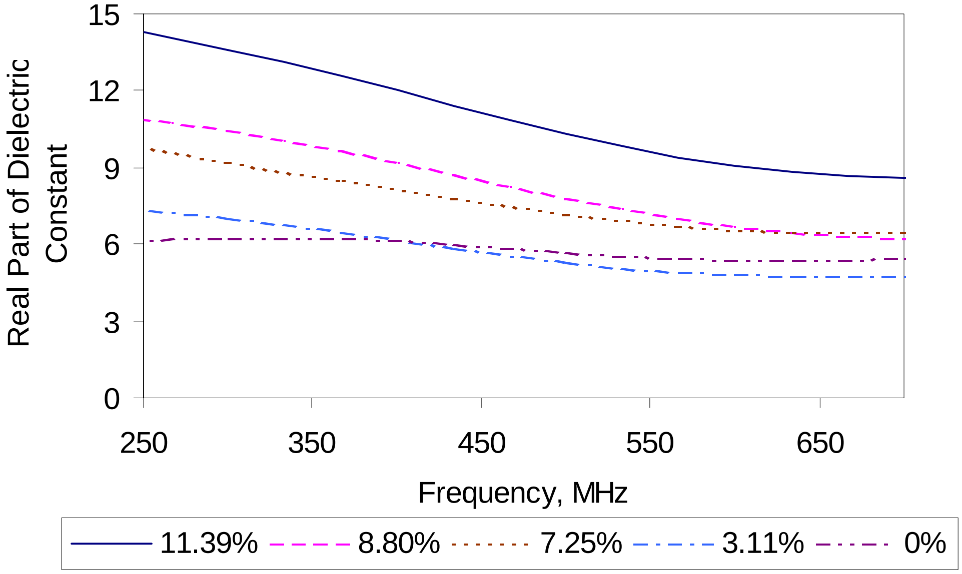


Figure E.55. Effect of frequency on the real part of the dielectric constant for G4N2 for five levels of volumetric moisture content (3 ns gating).

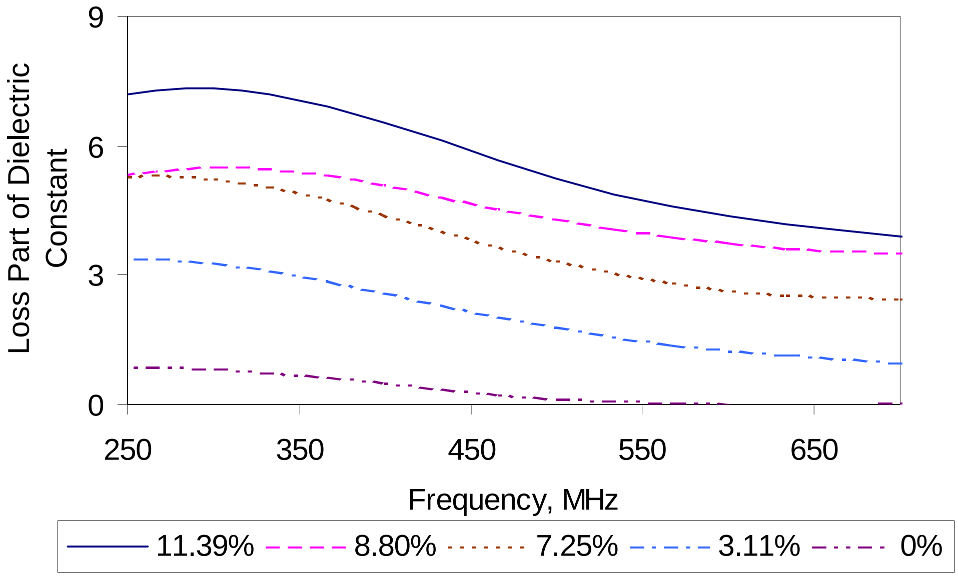


Figure E.56. Effect of frequency on the loss part of the dielectric constant for G4N2 for five levels of volumetric moisture content (3 ns gating).

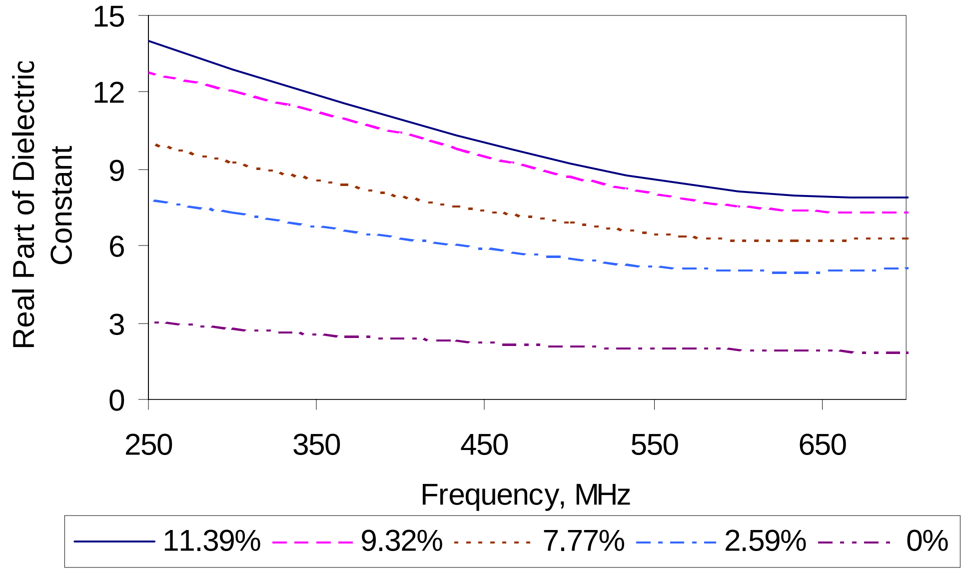


Figure E.57. Effect of frequency on the real part of the dielectric constant for G4C21 for five levels of volumetric moisture content (3 ns gating).

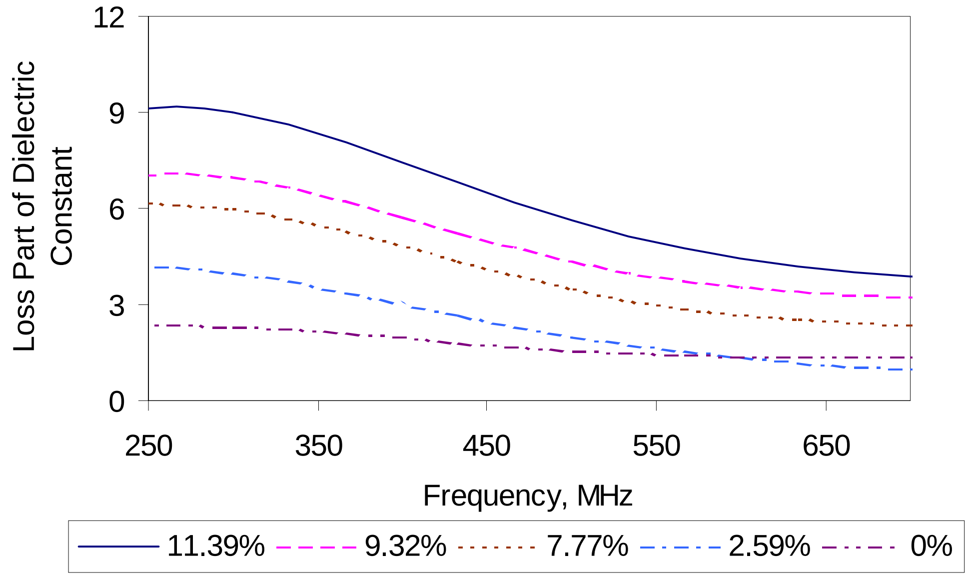


Figure E.58. Effect of frequency on the loss part of the dielectric constant for G4C21 for five levels of volumetric moisture content (3 ns gating).

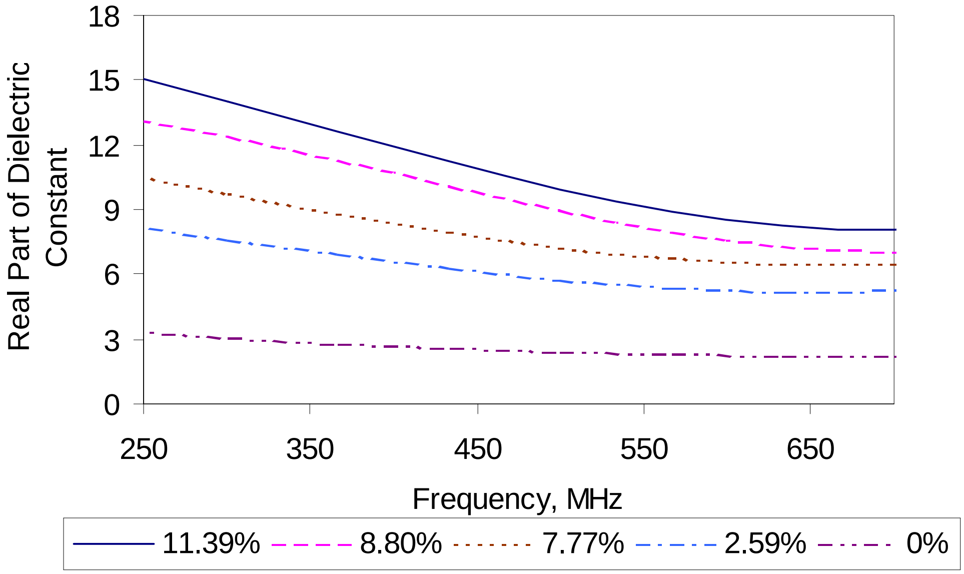


Figure E.59. Effect of frequency on the real part of the dielectric constant for G4C22 for five levels of volumetric moisture content (3 ns gating).

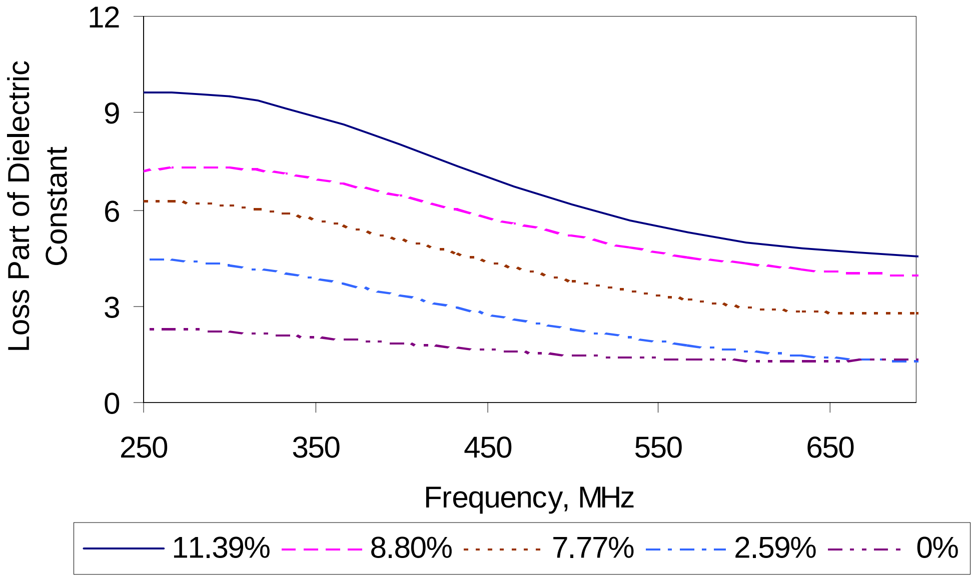


Figure E.60. Effect of frequency on the loss part of the dielectric constant for G4C22 for five levels of volumetric moisture content (3 ns gating).

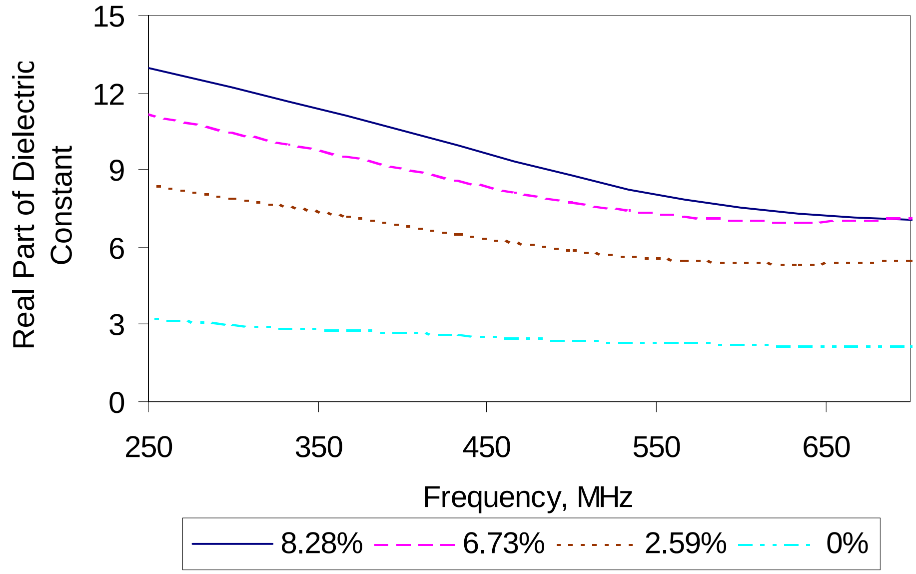


Figure E.61. Effect of frequency on the real part of the dielectric constant for G4C41 for five levels of volumetric moisture content (3 ns gating).

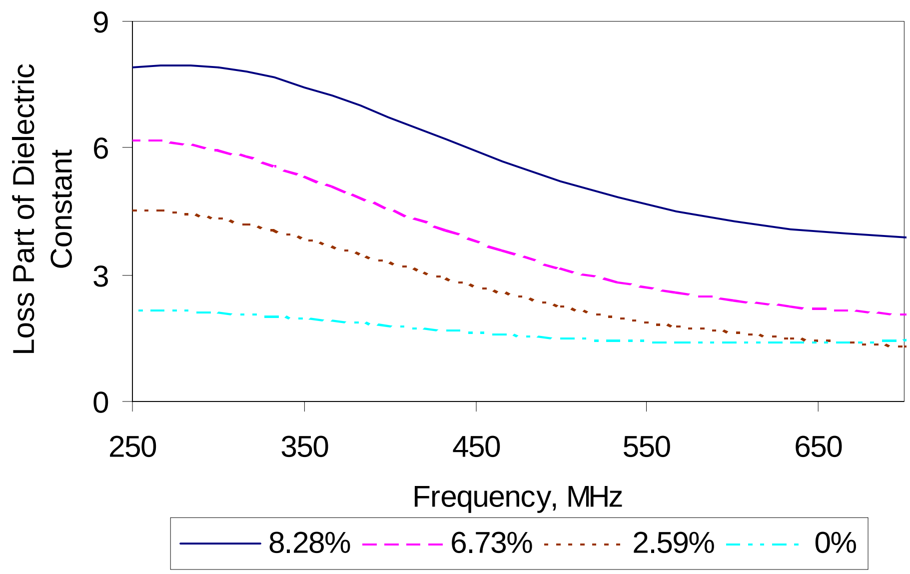


Figure E.62. Effect of frequency on the loss part of the dielectric constant for G4C41 for five levels of volumetric moisture content (3 ns gating).

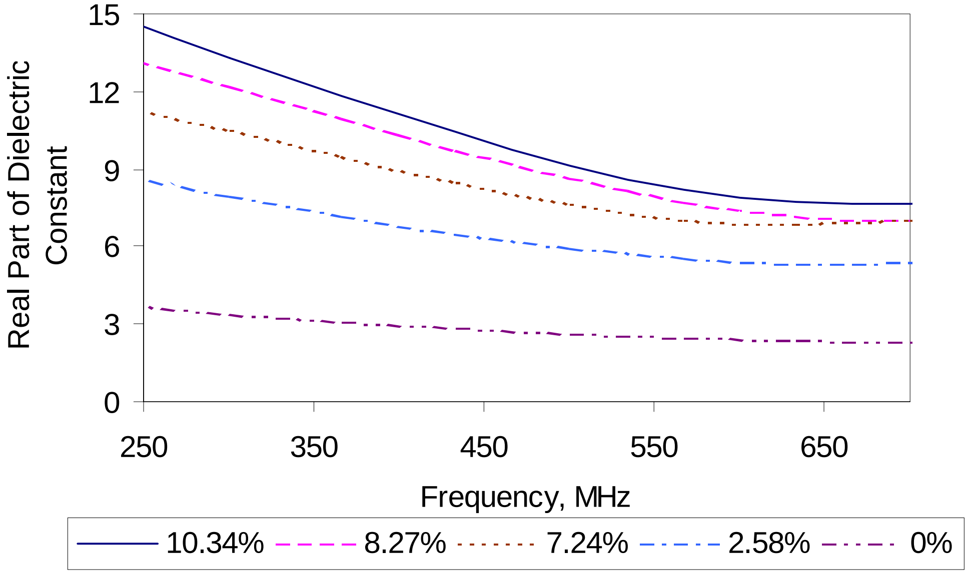


Figure E.63. Effect of frequency on the real part of the dielectric constant for G4C42 for five levels of volumetric moisture content (3 ns gating).

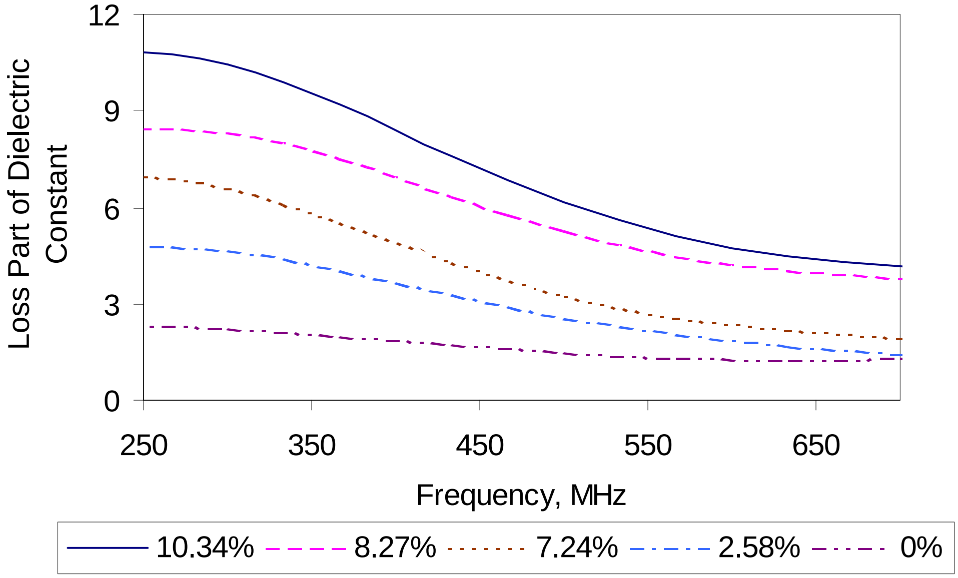


Figure E.64. Effect of frequency on the loss part of the dielectric constant for G4C42 for five levels of volumetric moisture content (3 ns gating).

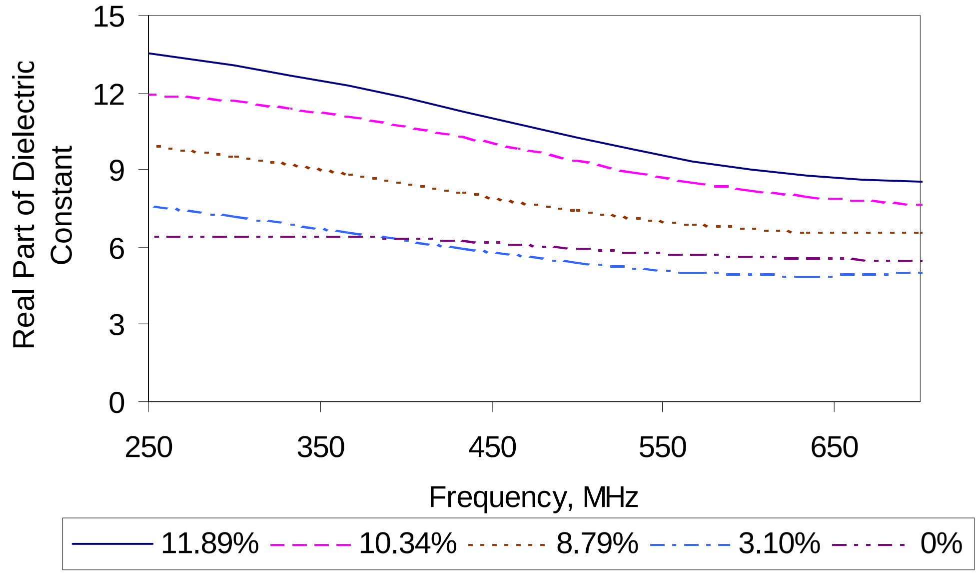


Figure E.65. Effect of frequency on the real part of the dielectric constant for G4M1 for five levels of volumetric moisture content (3 ns gating).

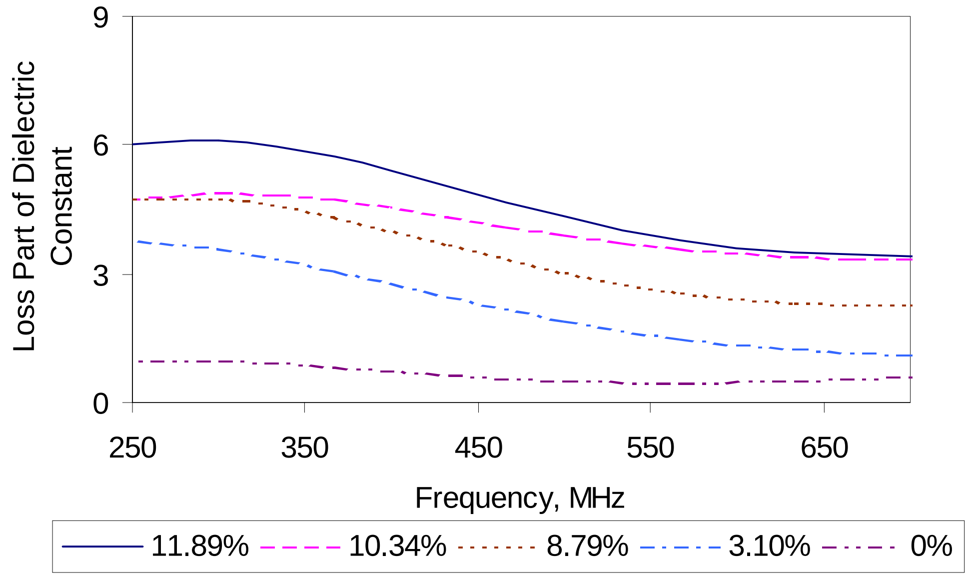


Figure E.66. Effect of frequency on the loss part of the dielectric constant for G4M1 for five levels of volumetric moisture content (3 ns gating).

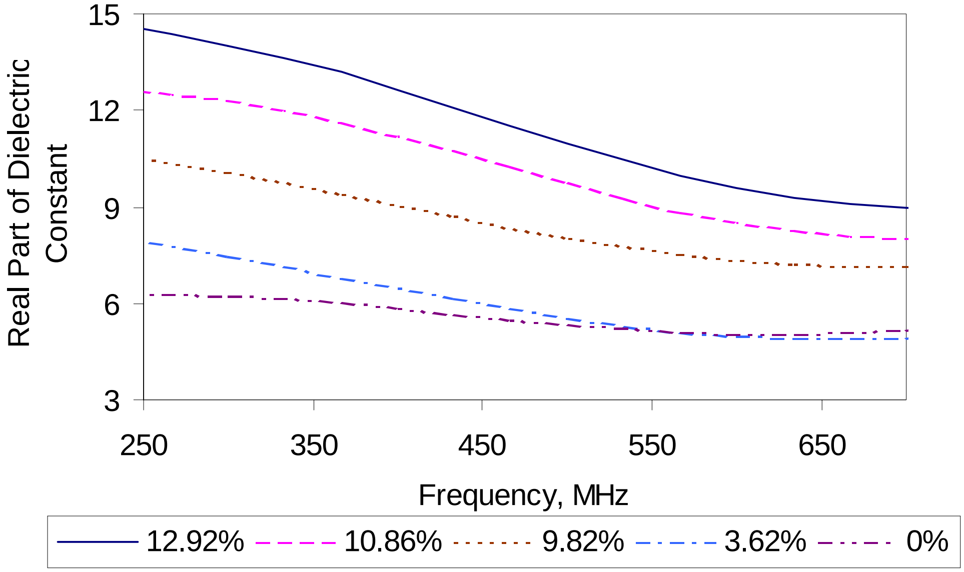


Figure E.67. Effect of frequency on the real part of the dielectric constant for G4M2 for five levels of volumetric moisture content (3 ns gating).

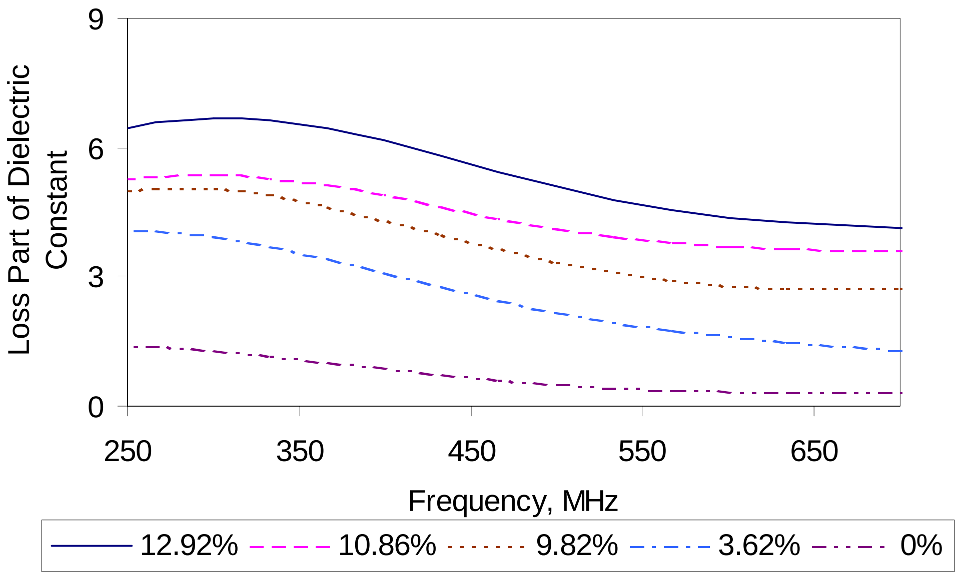


Figure E.68. Effect of frequency on the loss part of the dielectric constant for G4M2 for five levels of volumetric moisture content (3 ns gating).

# APPENDIX F

## EFFECT OF FREQUENCY ON THE DIELECTRIC CONSTANT FOR DIFFERENT LEVELS OF MOISTURE CONTENT (1 ns WINDOW)

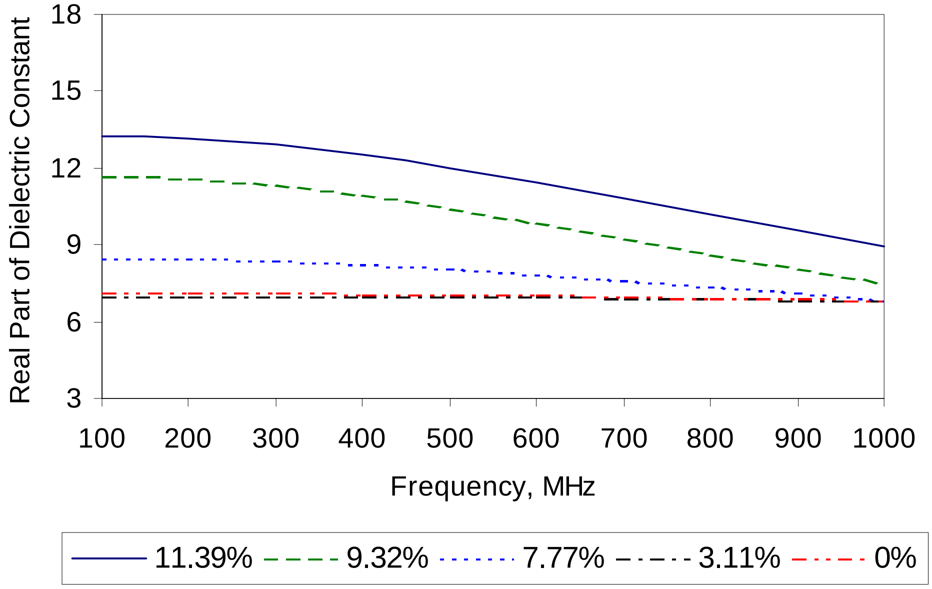


Figure F.1. Effect of frequency on the real part of the dielectric constant for L3N1 for five levels of volumetric moisture content (1 ns gating).

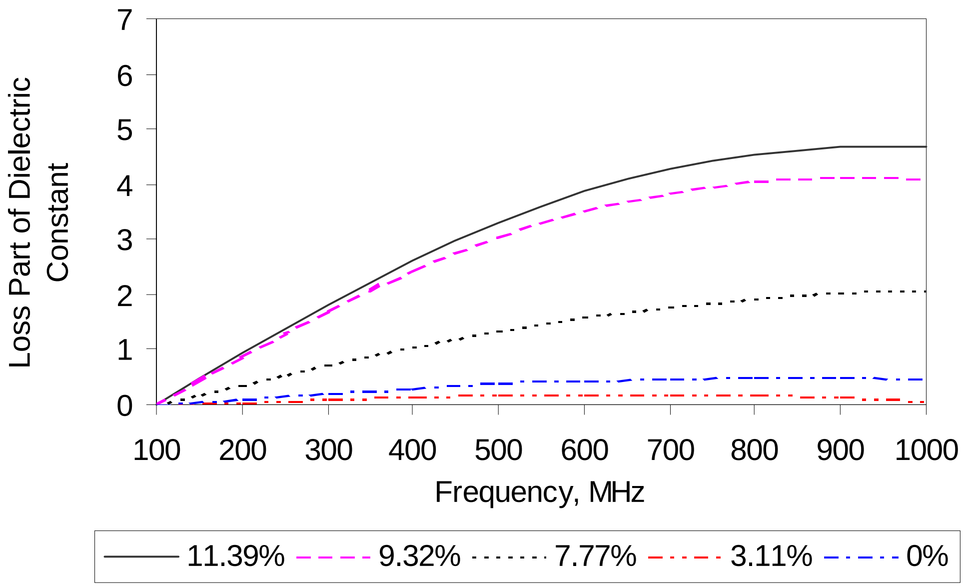


Figure F.2. Effect of frequency on the loss part of the dielectric constant for L3N1 for five levels of volumetric moisture content (1 ns gating).

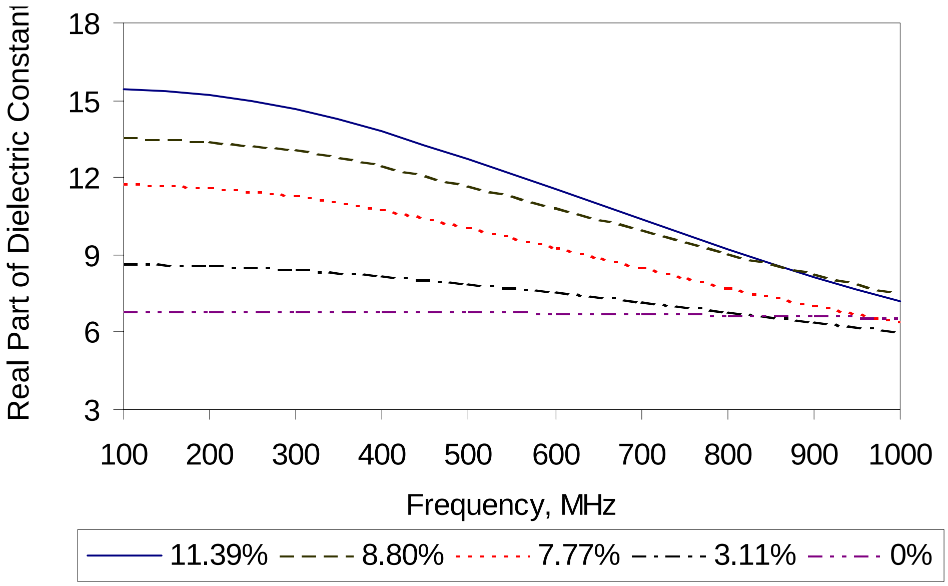


Figure F.3. Effect of frequency on the real part of the dielectric constant for L3N2 for five levels of volumetric moisture content (1 ns gating).

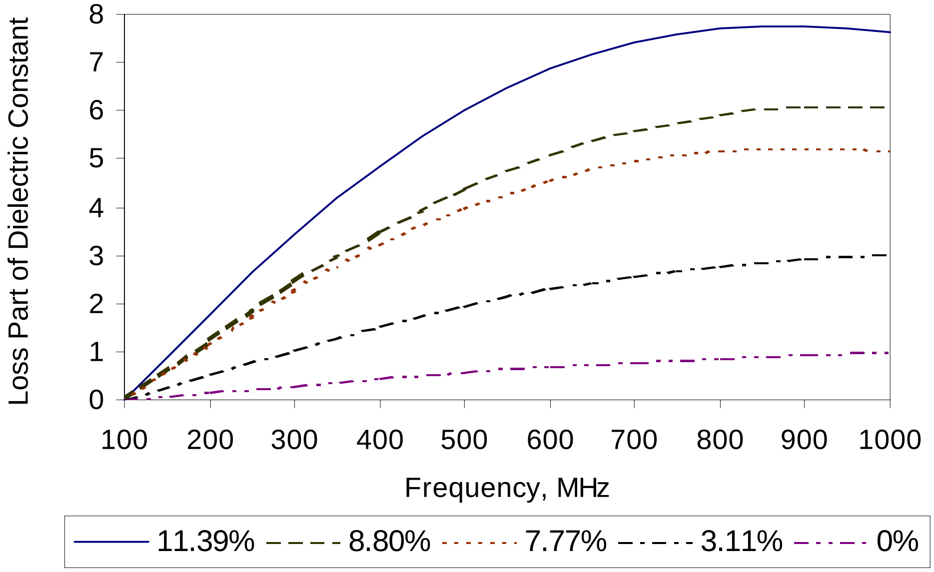


Figure F.4. Effect of frequency on the loss part of the dielectric constant for L3N2 for five levels of volumetric moisture content (1 ns gating).

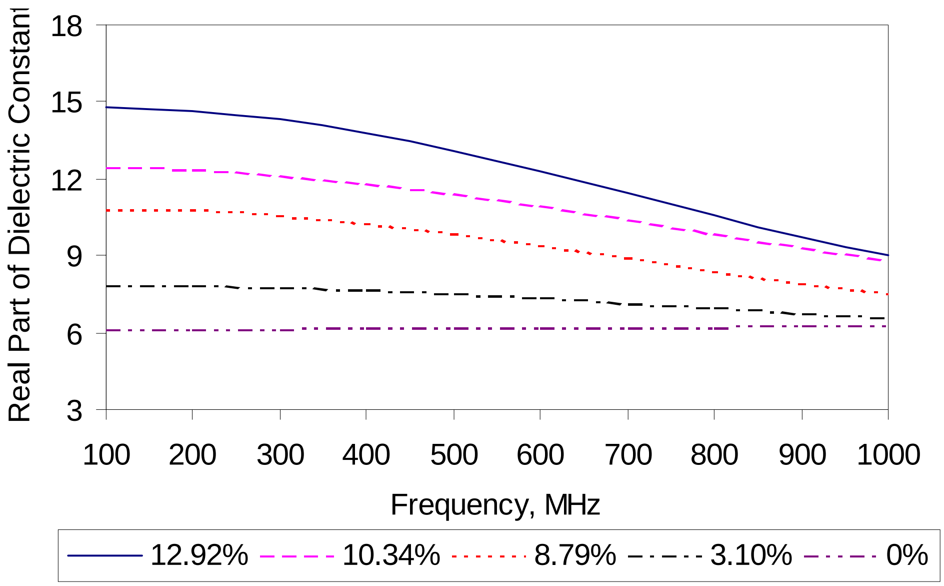


Figure F.5. Effect of frequency on the real part of the dielectric constant for L4N1 for five levels of volumetric moisture content (1 ns gating).

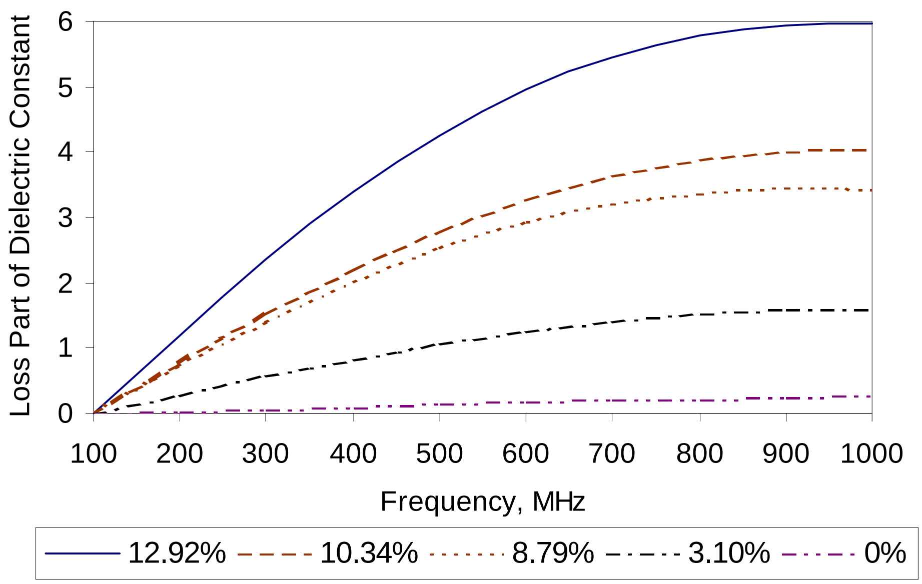


Figure F.6. Effect of frequency on the loss part of the dielectric constant for L4N1 for five levels of volumetric moisture content (1 ns gating).

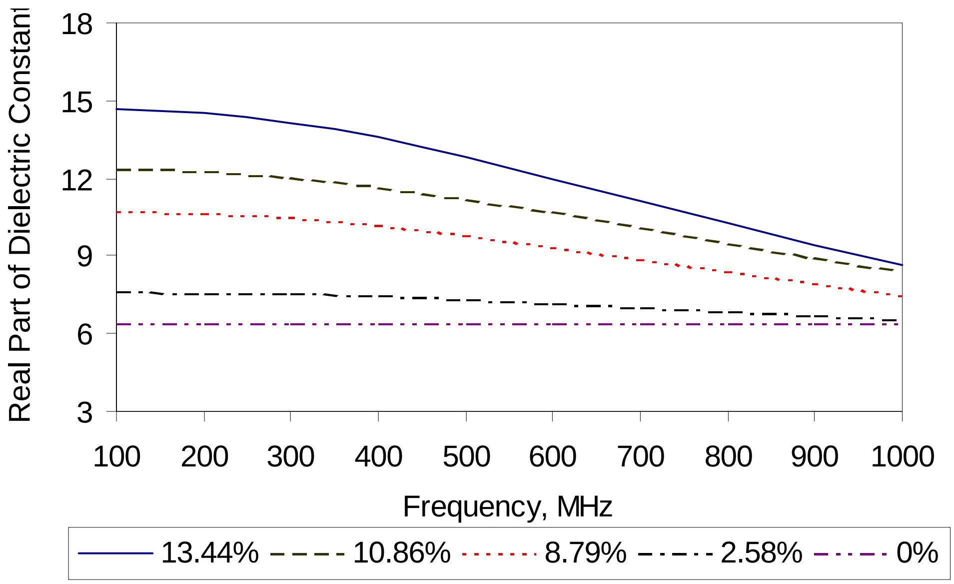


Figure F.7. Effect of frequency on the real part of the dielectric constant for L4N2 for five levels of volumetric moisture content (1 ns gating).

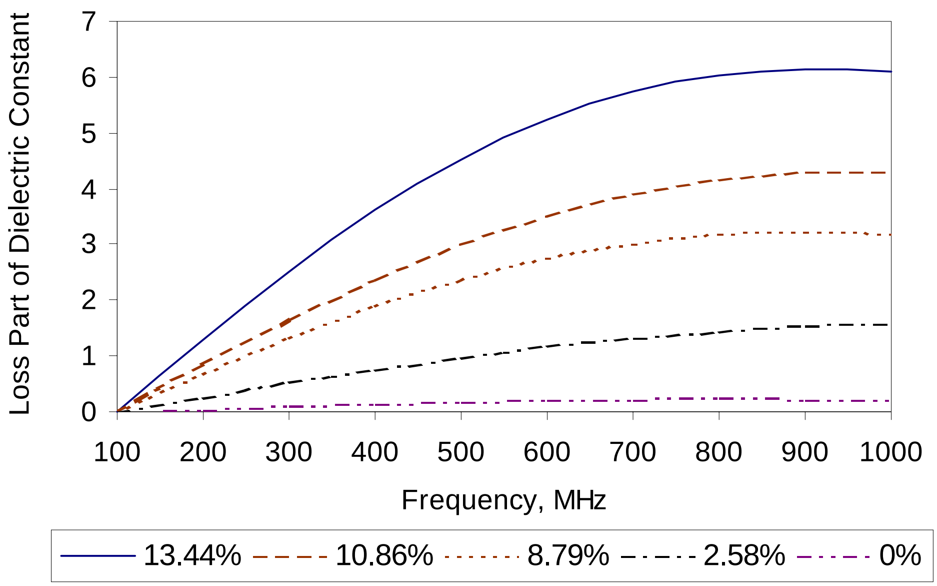


Figure F.8. Effect of frequency on the loss part of the dielectric constant for L4N2 for five levels of volumetric moisture content (1 ns gating).

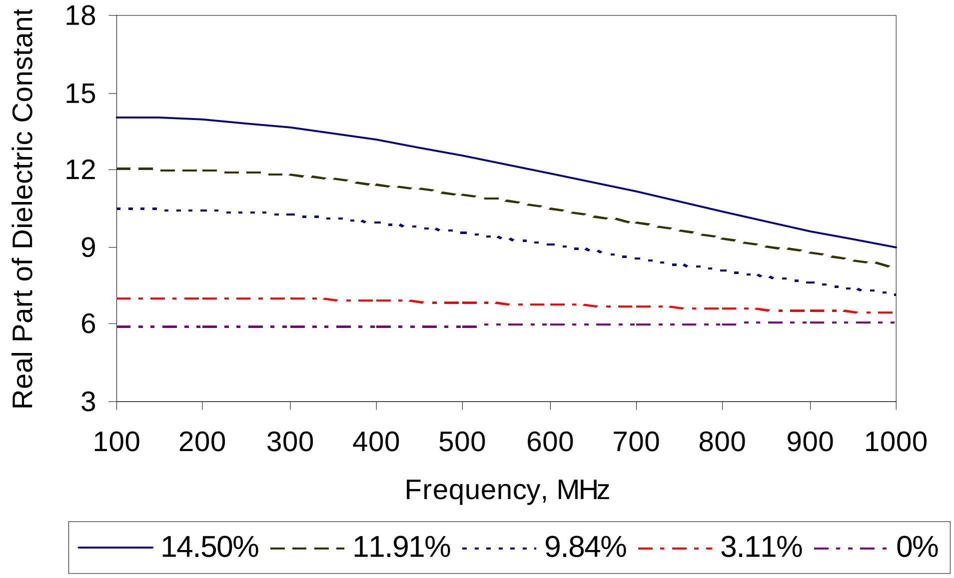


Figure F.9. Effect of frequency on the real part of the dielectric constant for L5N1 for five levels of volumetric moisture content (1 ns gating).

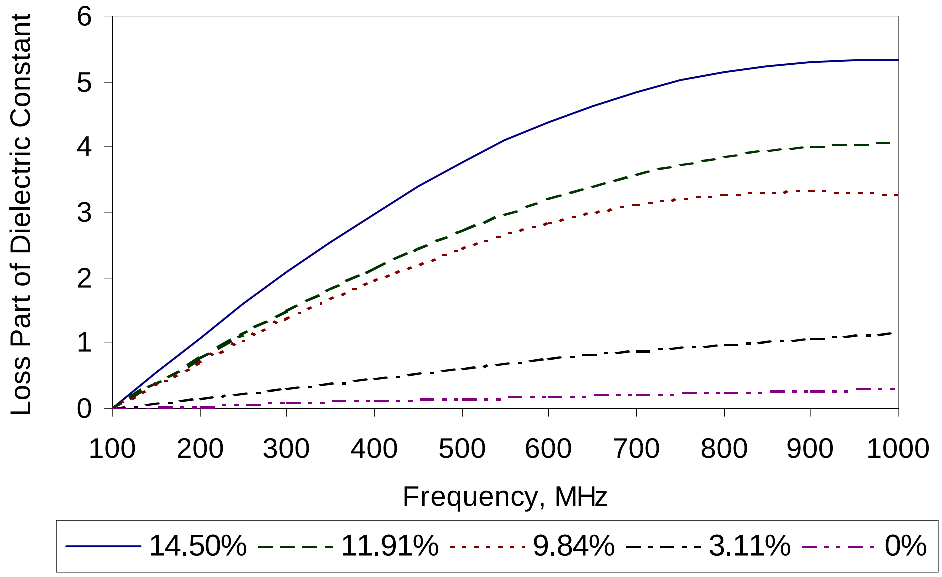


Figure F.10. Effect of frequency on the loss part of the dielectric constant for L5N1 for five levels of volumetric moisture content (1 ns gating).

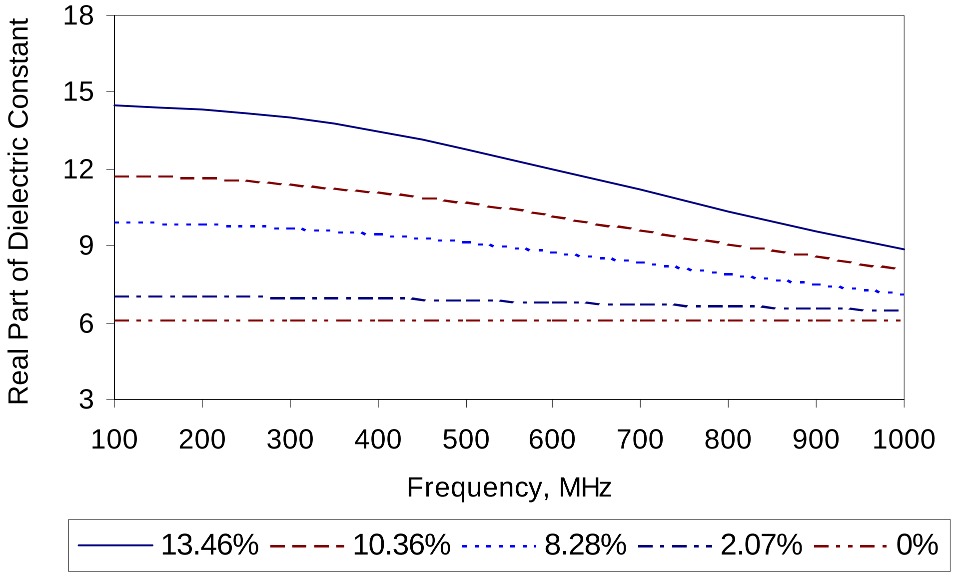


Figure F.11. Effect of frequency on the real part of the dielectric constant for L5N2 for five levels of volumetric moisture content (1 ns gating).

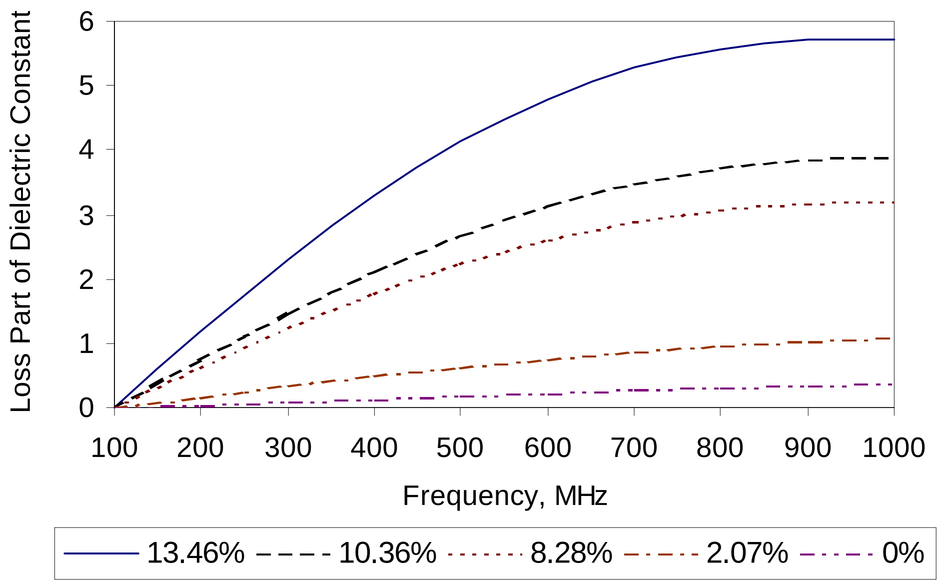


Figure F.12. Effect of frequency on the loss part of the dielectric constant for L5N2 for five levels of volumetric moisture content (1 ns gating).

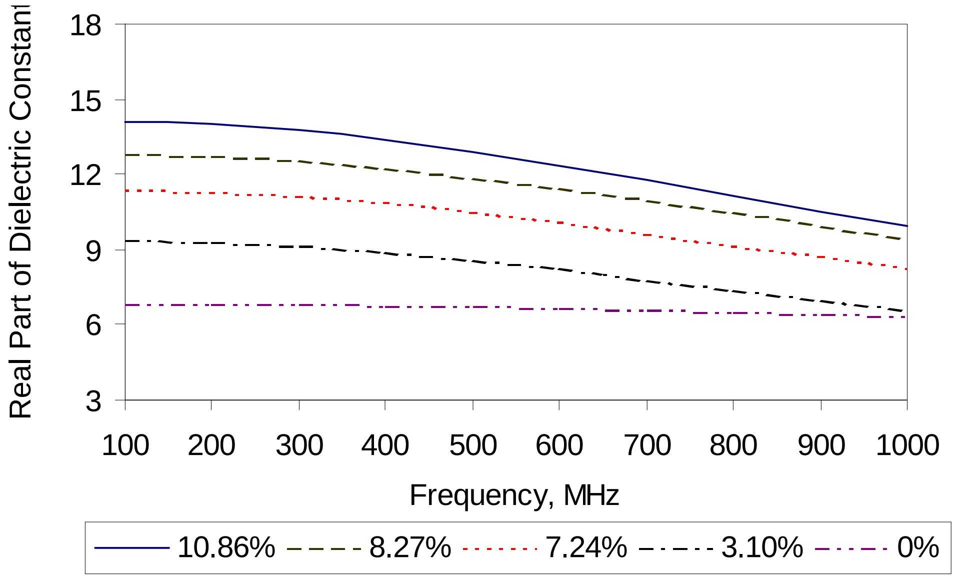


Figure F.13. Effect of frequency on the real part of the dielectric constant for L3S1 for five levels of volumetric moisture content (1 ns gating).

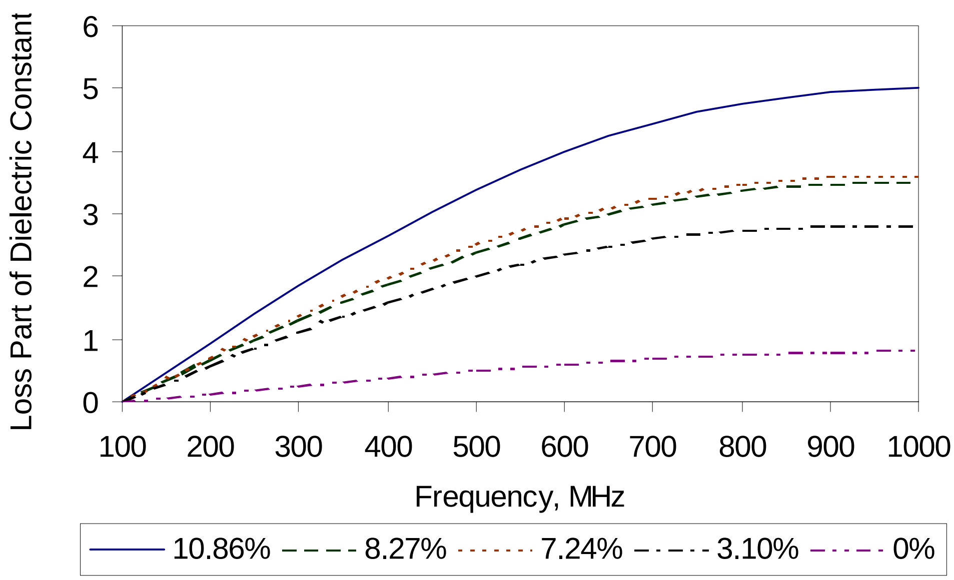


Figure F.14. Effect of frequency on the loss part of the dielectric constant for L3S1 for five levels of volumetric moisture content (1 ns gating).

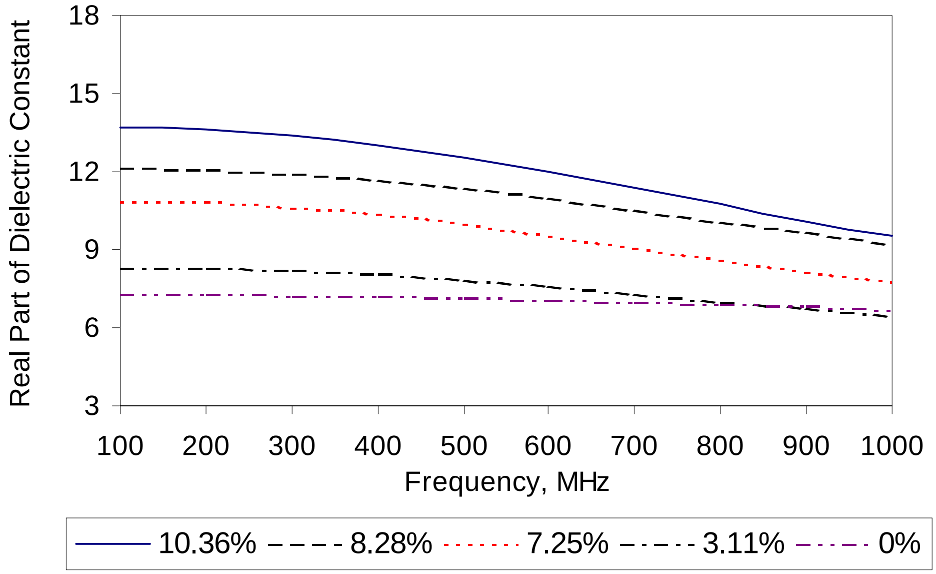


Figure F.15. Effect of frequency on the real part of the dielectric constant for L3S2 for five levels of volumetric moisture content (1 ns gating).

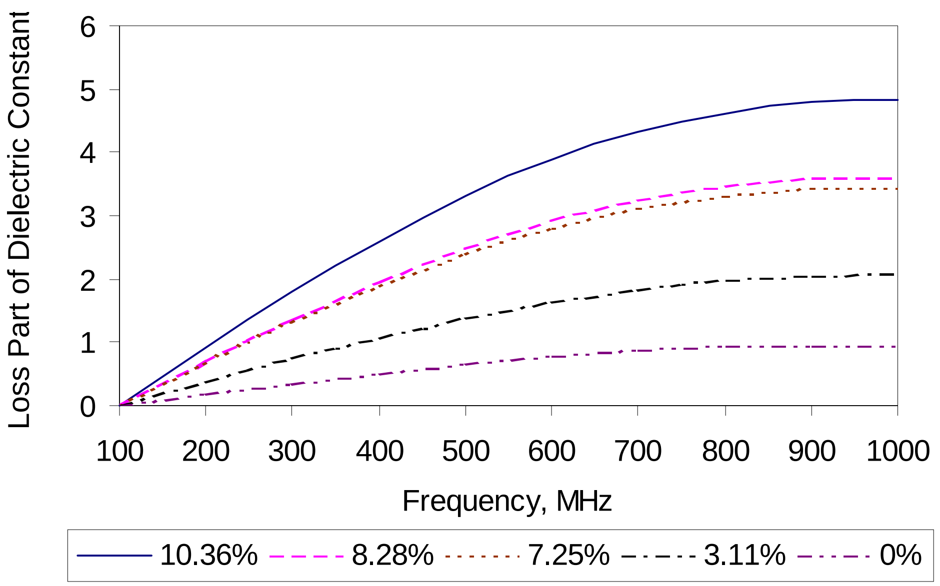


Figure F.16. Effect of frequency on the loss part of the dielectric constant for L3S2 for five levels of volumetric moisture content (1 ns gating).

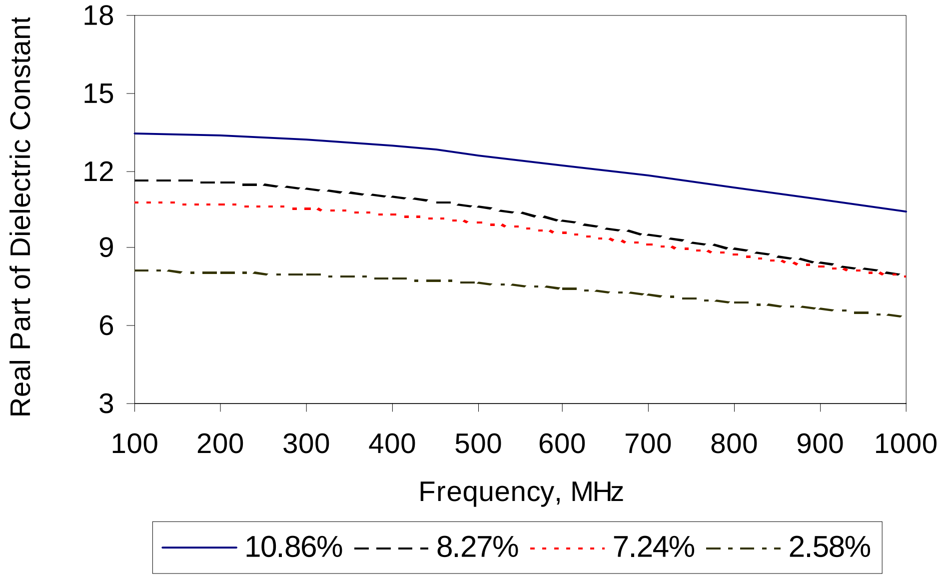


Figure F.17. Effect of frequency on the real part of the dielectric constant for L4S1 for five levels of volumetric moisture content (1 ns gating).

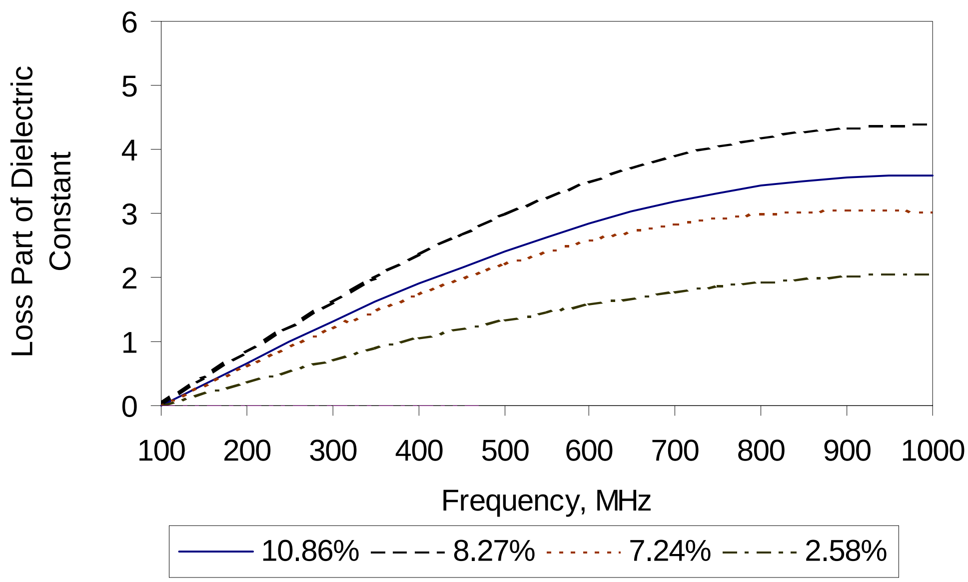


Figure F.18. Effect of frequency on the loss part of the dielectric constant for L4S1 for five levels of volumetric moisture content (1 ns gating).

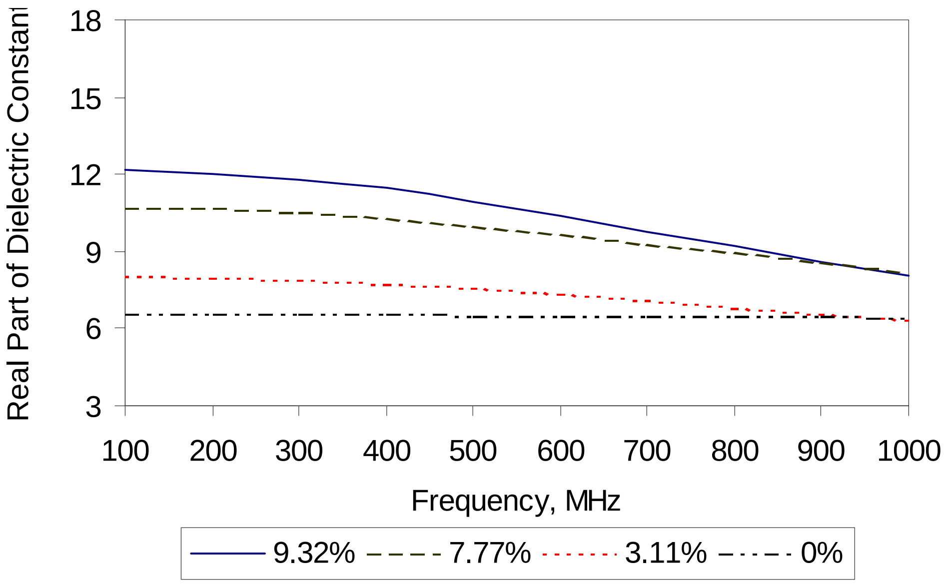


Figure F.19. Effect of frequency on the real part of the dielectric constant for L4S2 for five levels of volumetric moisture content (1 ns gating).

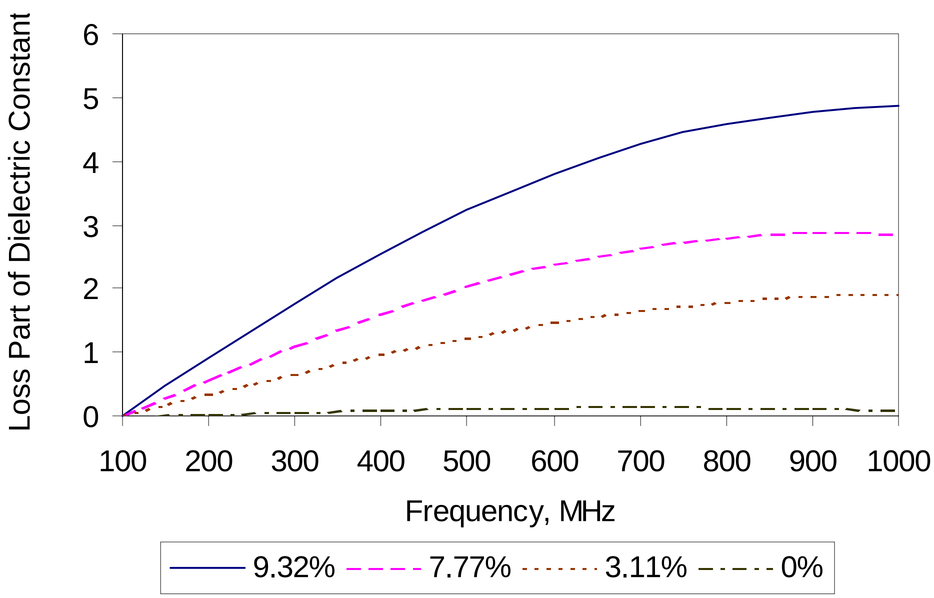


Figure F.20. Effect of frequency on the loss part of the dielectric constant for L4S2 for five levels of volumetric moisture content (1 ns gating).

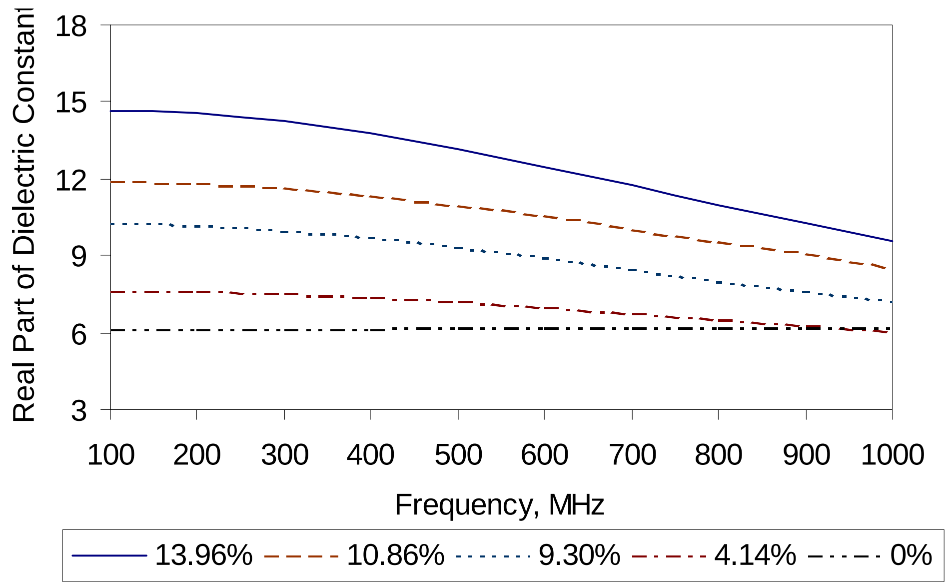


Figure F.21. Effect of frequency on the real part of the dielectric constant for L5S1 for five levels of volumetric moisture content (1 ns gating).

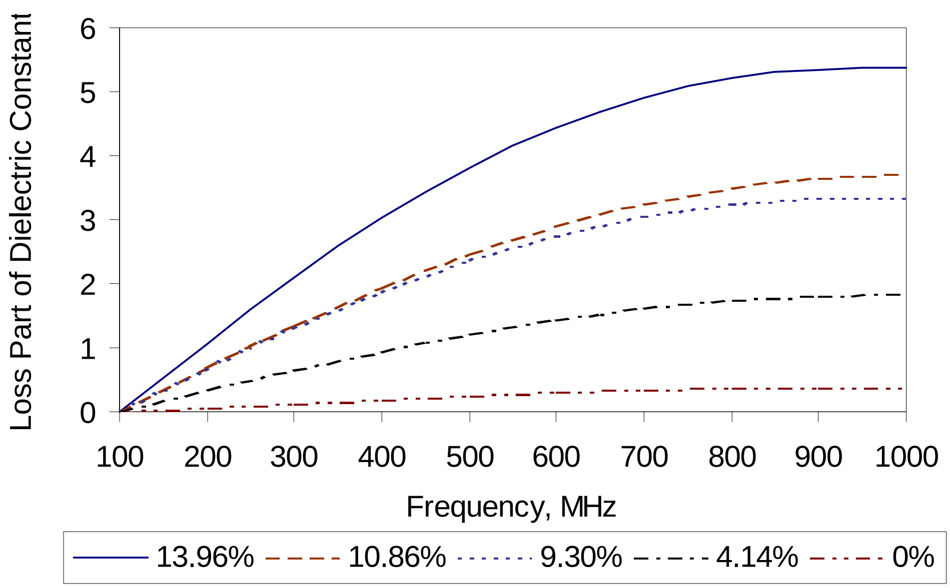


Figure F.22. Effect of frequency on the loss part of the dielectric constant for L5S1 for five levels of volumetric moisture content (1 ns gating).

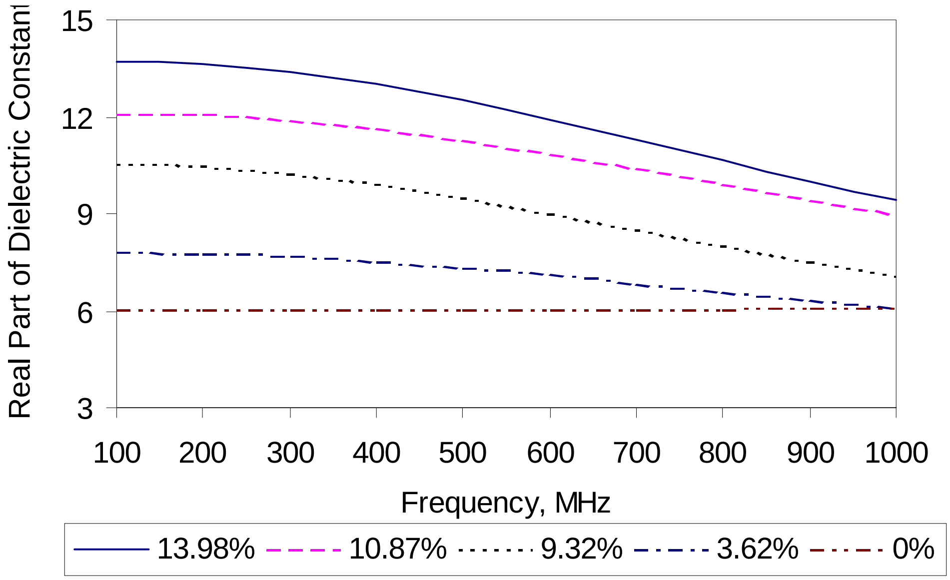


Figure F.23. Effect of frequency on the real part of the dielectric constant for L5S2 for five levels of volumetric moisture content (1 ns gating).

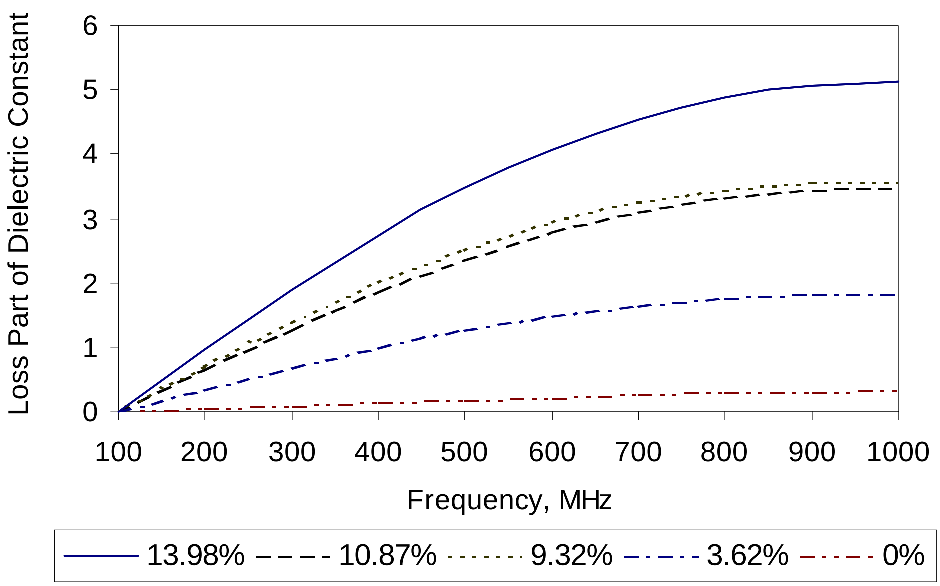


Figure F.24. Effect of frequency on the loss part of the dielectric constant for L5S2 for five levels of volumetric moisture content (1 ns gating).

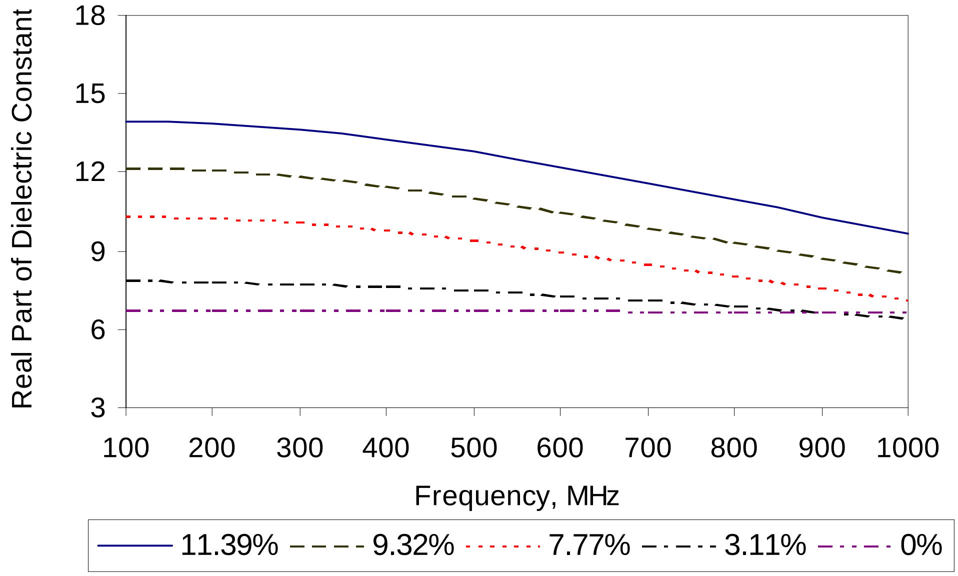


Figure F.25. Effect of frequency on the real part of the dielectric constant for L3H1 for five levels of volumetric moisture content (1 ns gating).

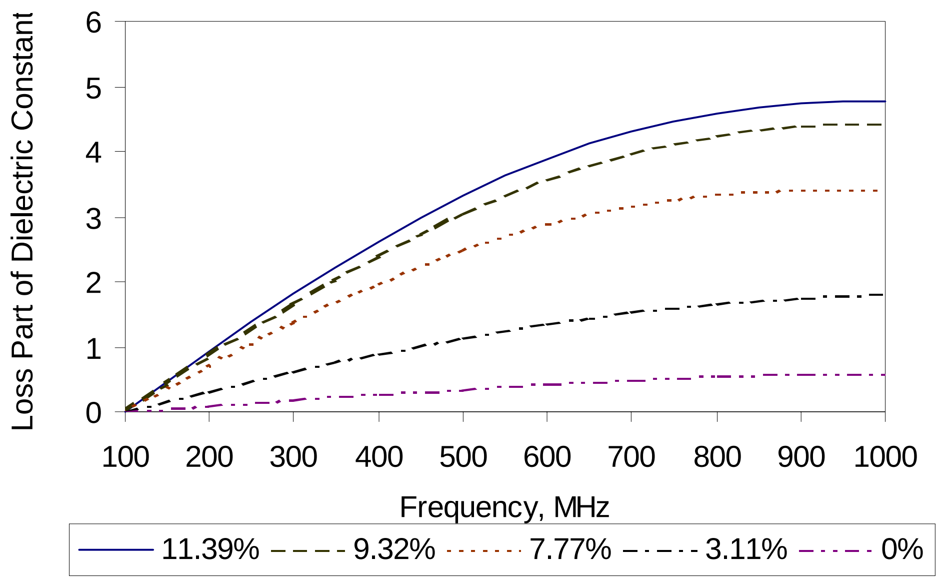


Figure F.26. Effect of frequency on the loss part of the dielectric constant for L3H1 for five levels of volumetric moisture content (1 ns gating).

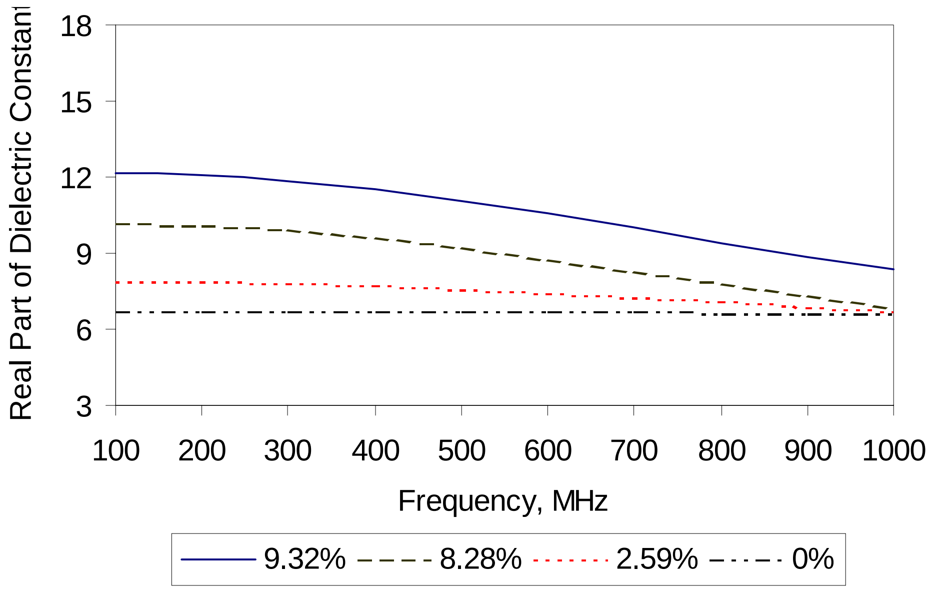


Figure F.27. Effect of frequency on the real part of the dielectric constant for L3H2 for five levels of volumetric moisture content (1 ns gating).

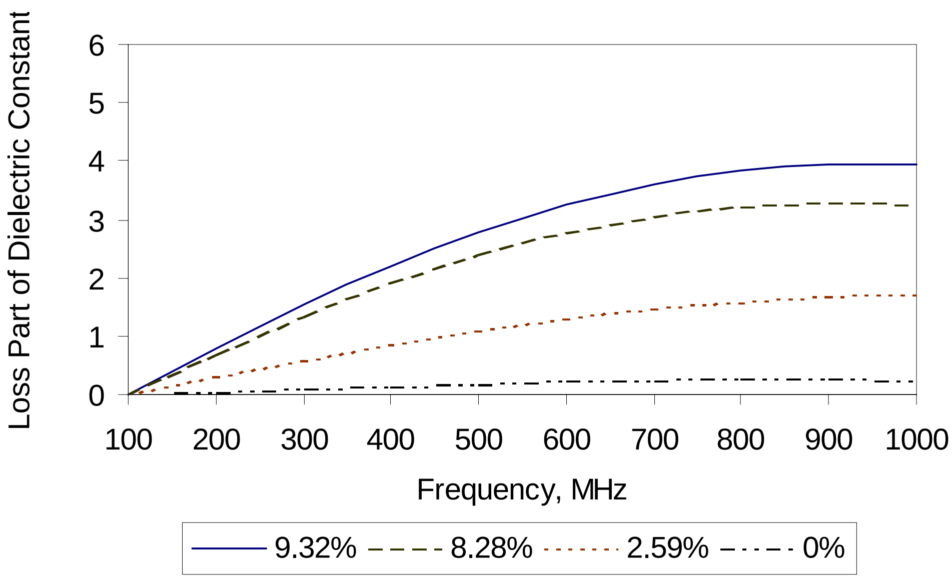


Figure F.28. Effect of frequency on the loss part of the dielectric constant for L3H2 for five levels of volumetric moisture content (1 ns gating).

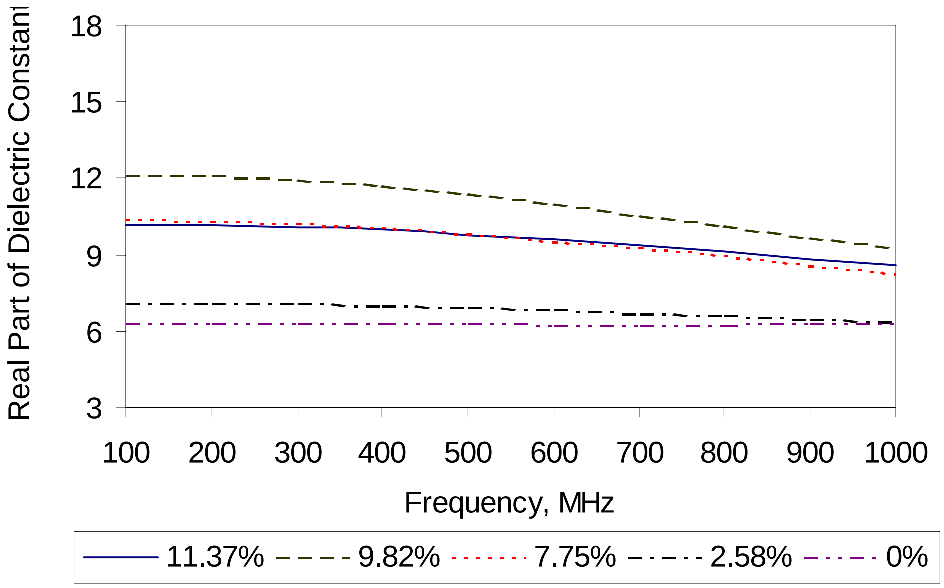


Figure F.29. Effect of frequency on the real part of the dielectric constant for L4H1 for five levels of volumetric moisture content (1 ns gating).

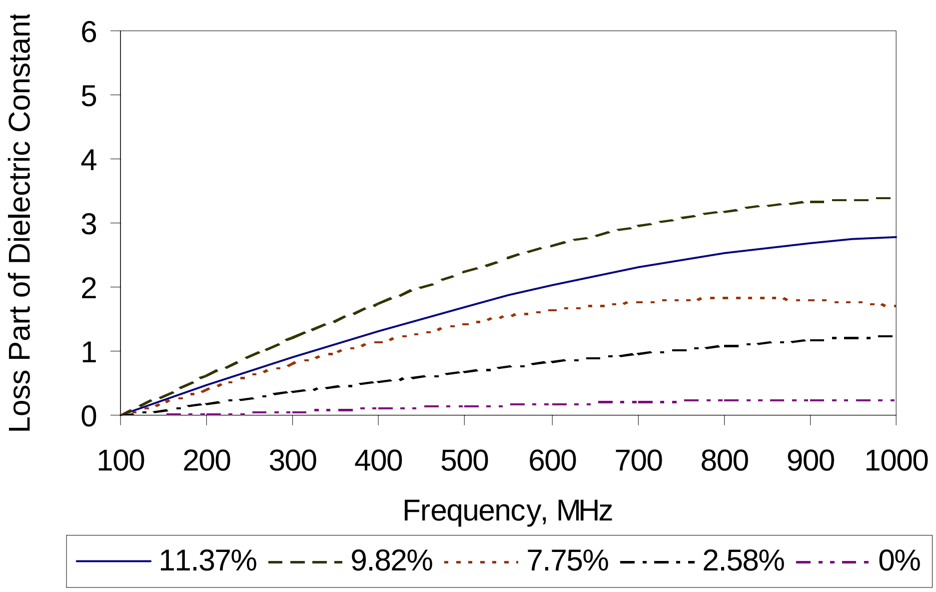


Figure F.30. Effect of frequency on the loss part of the dielectric constant for L4H1 for five levels of volumetric moisture content (1 ns gating).

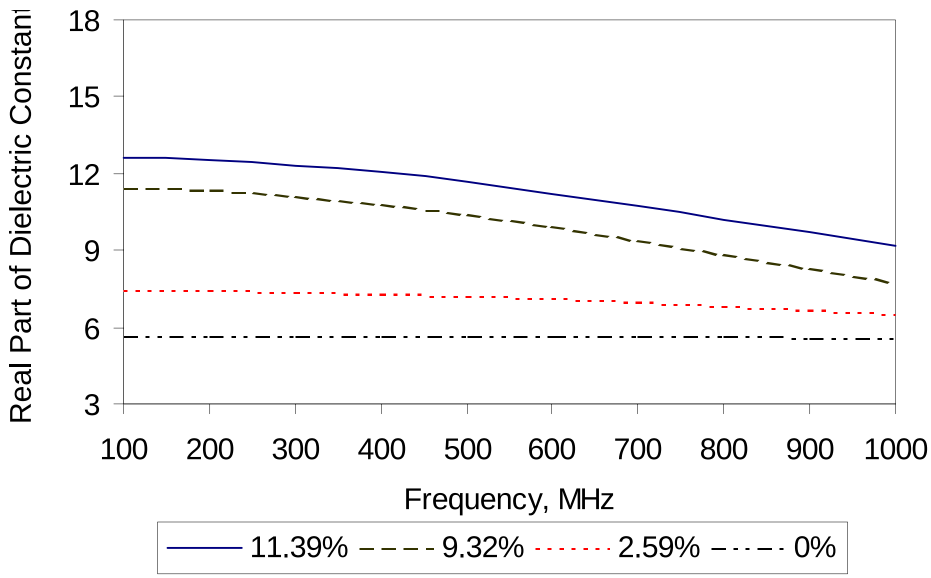


Figure F.31. Effect of frequency on the real part of the dielectric constant for L4H2 for five levels of volumetric moisture content (1 ns gating).

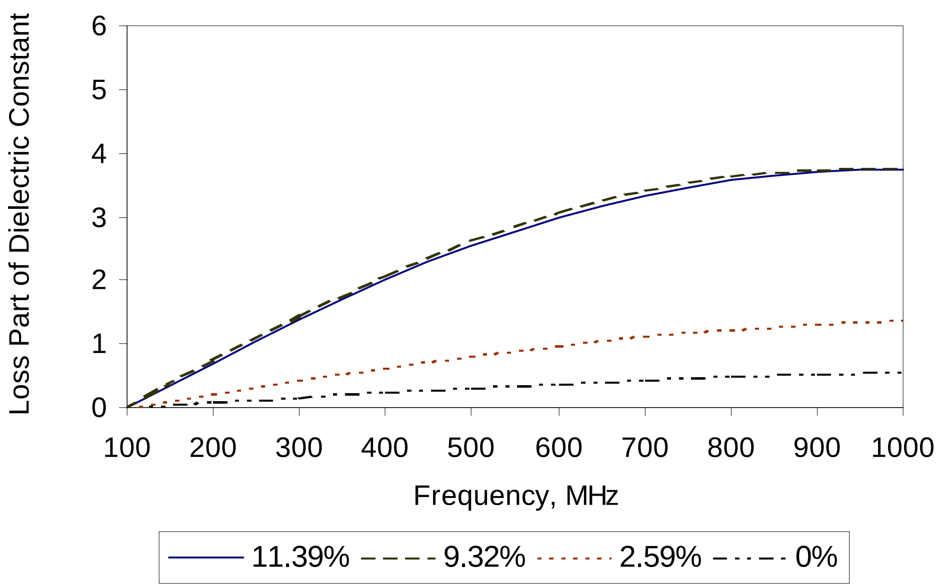


Figure F.32. Effect of frequency on the loss part of the dielectric constant for L4H2 for five levels of volumetric moisture content (1 ns gating).

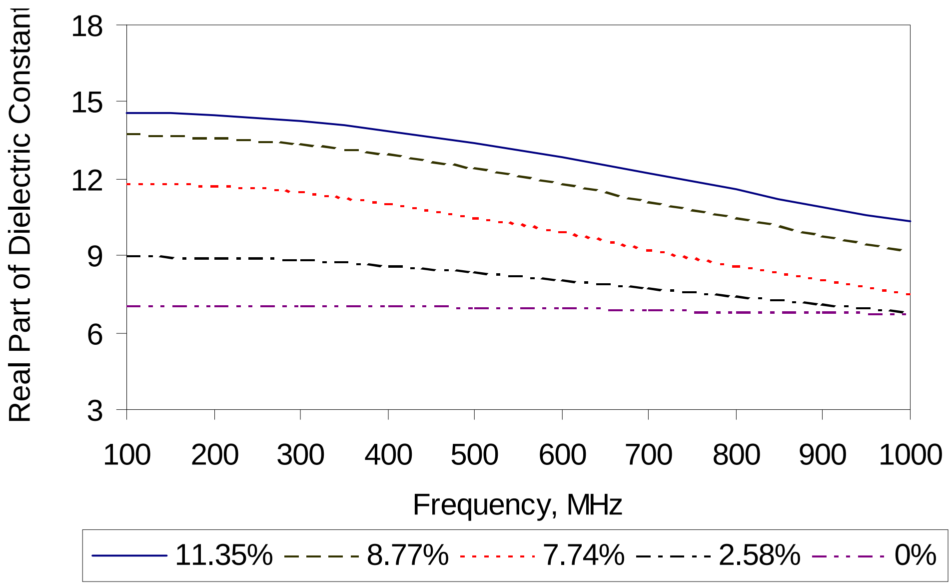


Figure F.33. Effect of frequency on the real part of the dielectric constant for L4C41 for five levels of volumetric moisture content (1 ns gating).

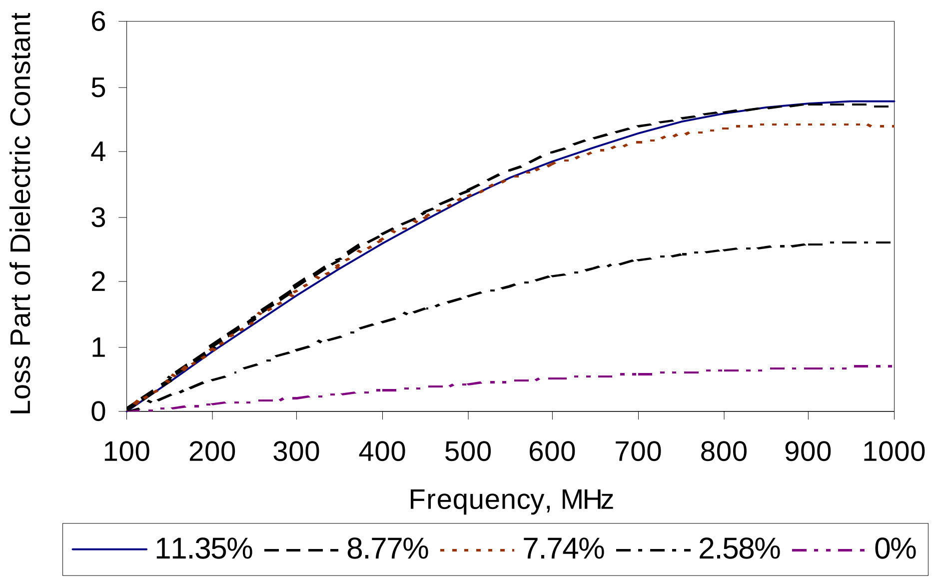


Figure F.34. Effect of frequency on the loss part of the dielectric constant for L4C41 for five levels of volumetric moisture content (1 ns gating).

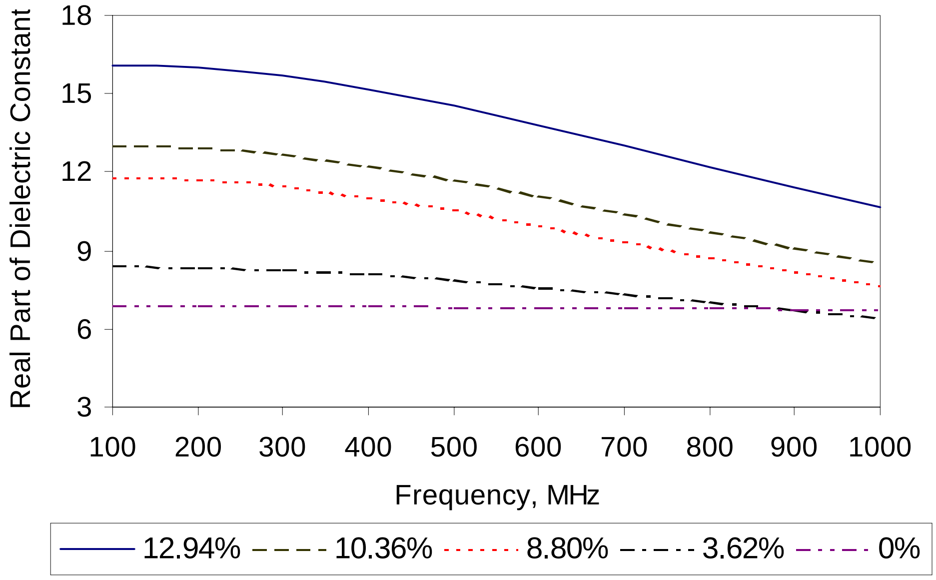


Figure F.35. Effect of frequency on the real part of the dielectric constant for L4C42 for five levels of volumetric moisture content (1 ns gating).

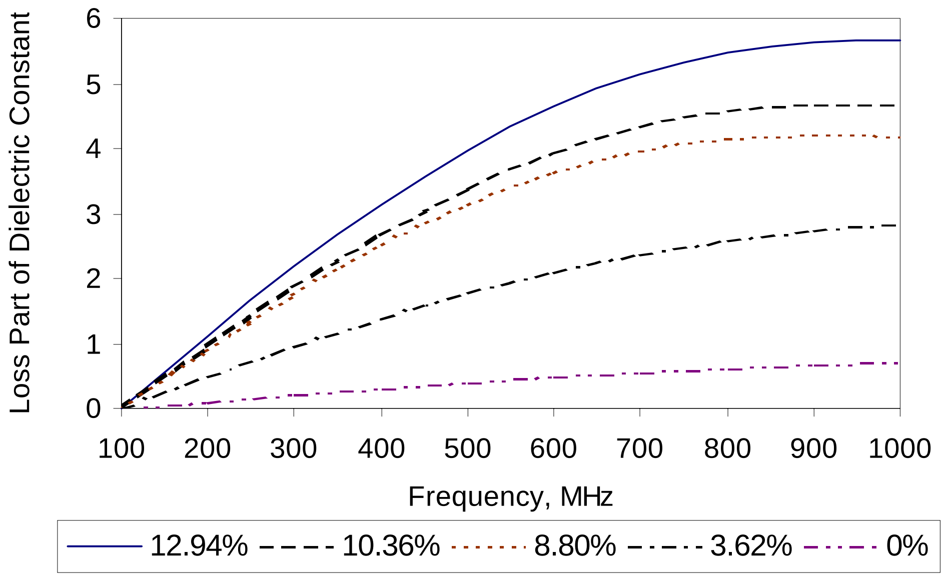


Figure F.36. Effect of frequency on the loss part of the dielectric constant for L4C42 for five levels of volumetric moisture content (1 ns gating).

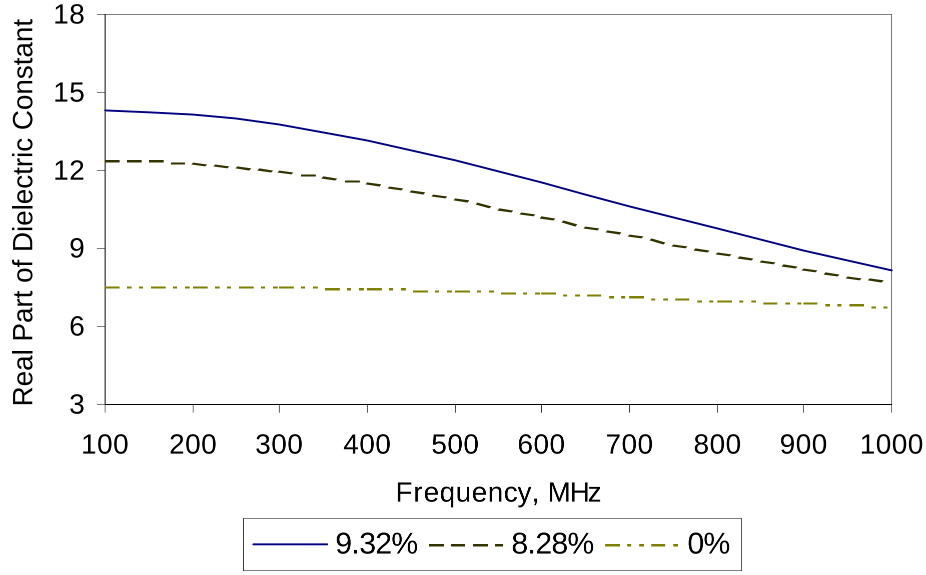


Figure F.37. Effect of frequency on the real part of the dielectric constant for L4C81 for five levels of volumetric moisture content (1 ns gating).

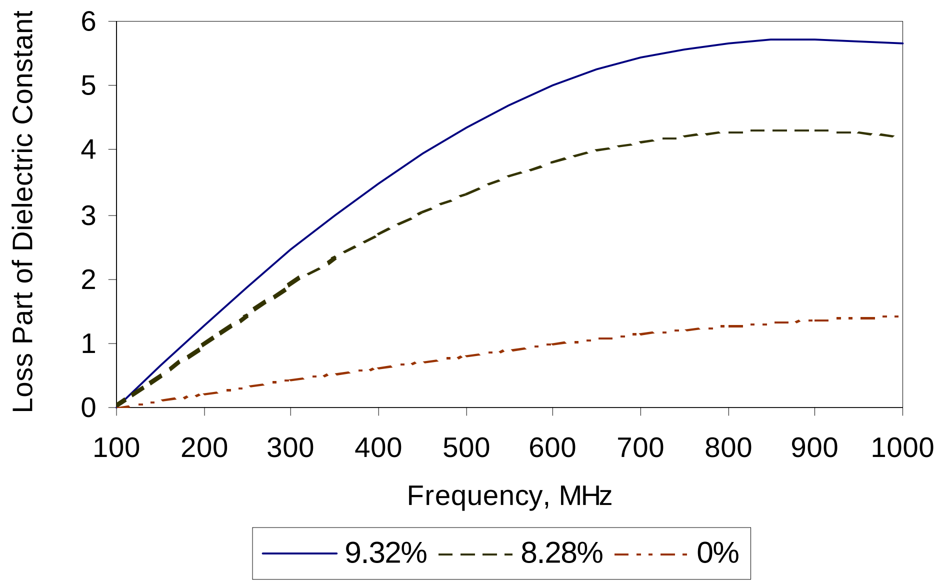


Figure F.38. Effect of frequency on the loss part of the dielectric constant for L4C81 for five levels of volumetric moisture content (1 ns gating).

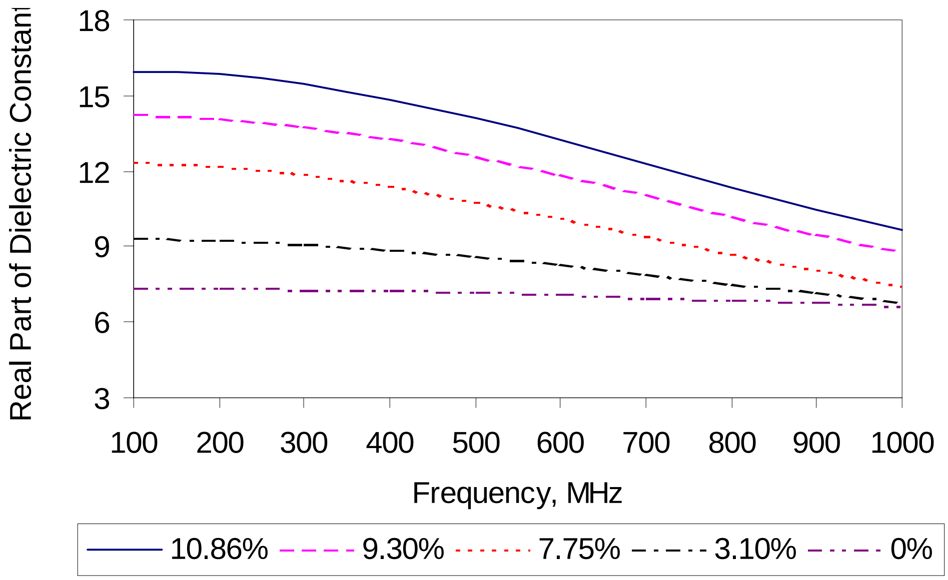


Figure F.39. Effect of frequency on the real part of the dielectric constant for L4C82 for five levels of volumetric moisture content (1 ns gating).

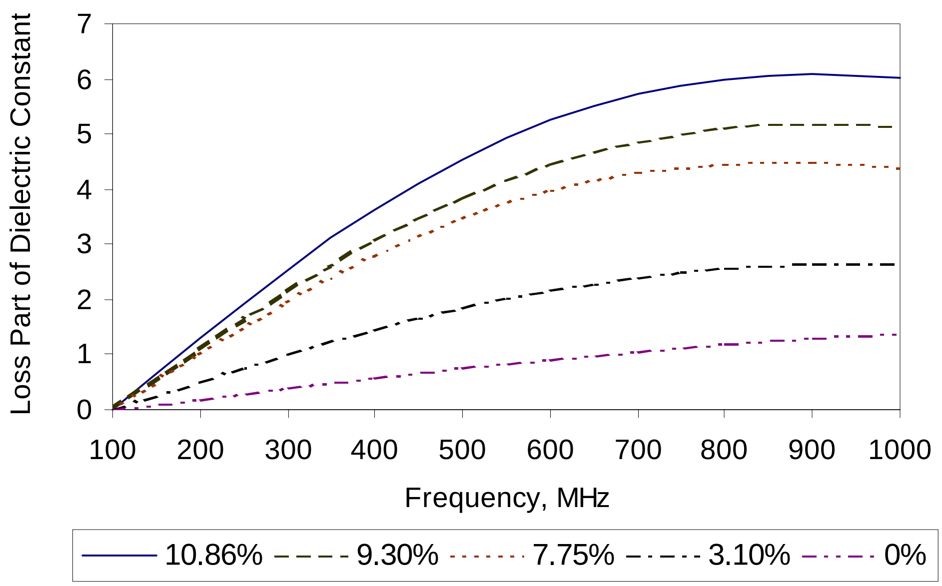


Figure F.40. Effect of frequency on the loss part of the dielectric constant for L4C82 for five levels of volumetric moisture content (1 ns gating).

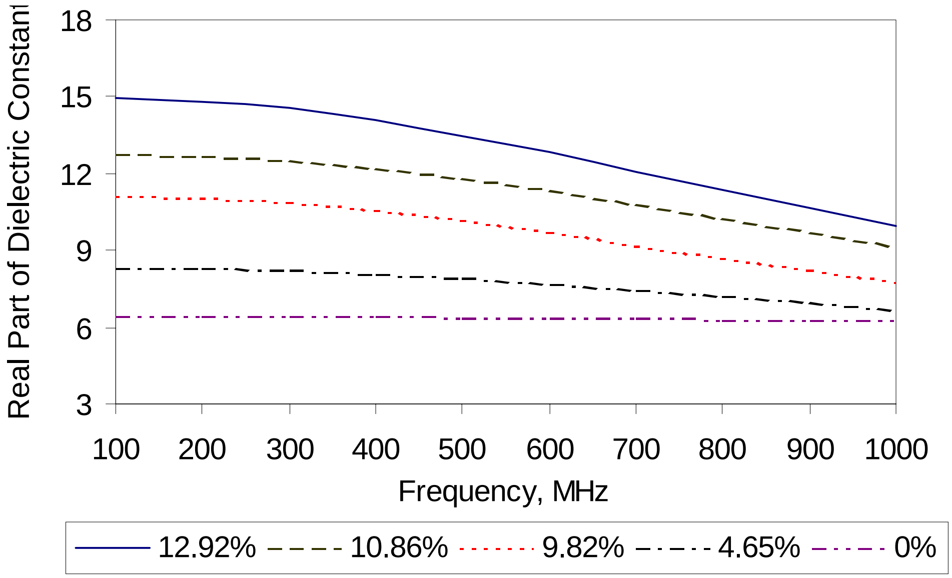


Figure F.41. Effect of frequency on the real part of the dielectric constant for L4M1 for five levels of volumetric moisture content (1 ns gating).

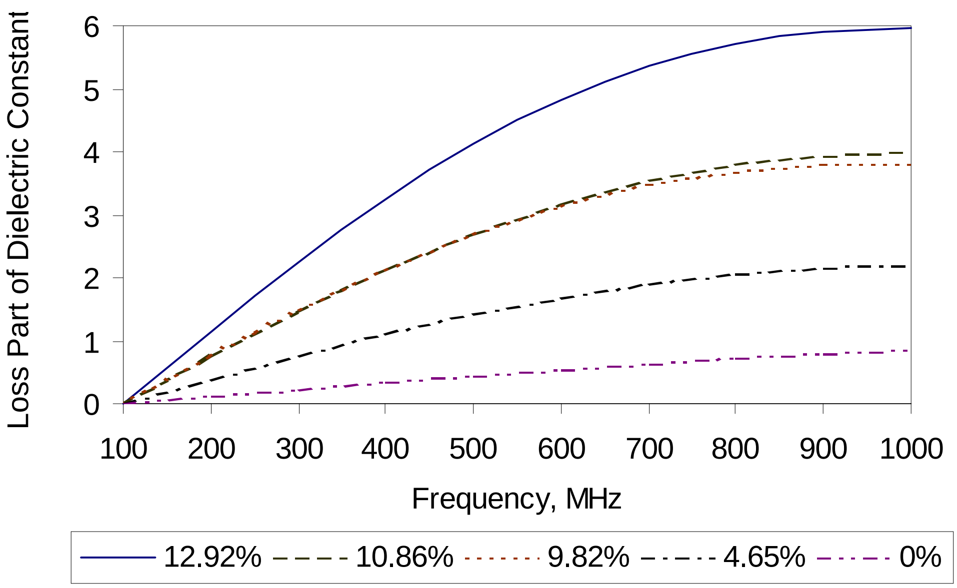


Figure F.42. Effect of frequency on the loss part of the dielectric constant for L4M1 for five levels of volumetric moisture content (1 ns gating).

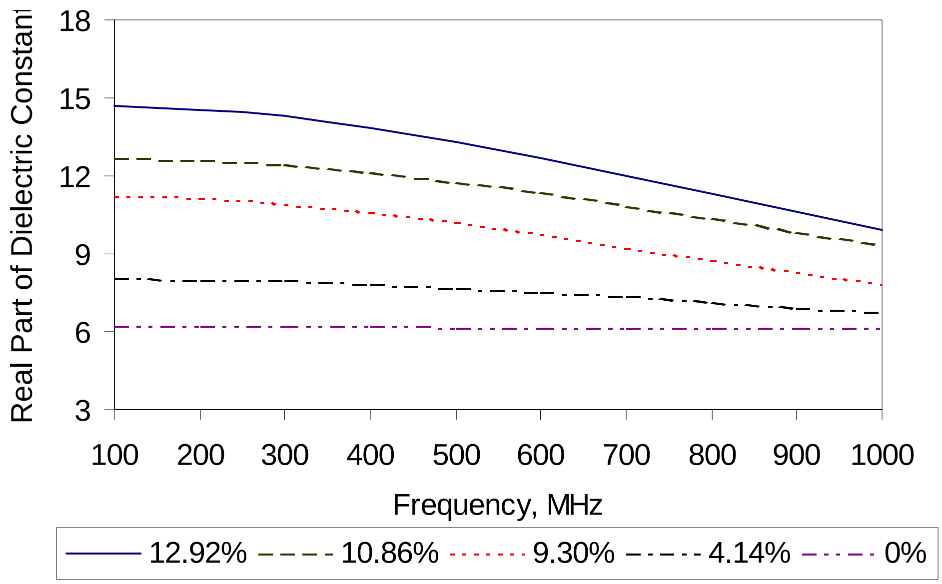


Figure F.43. Effect of frequency on the real part of the dielectric constant for L4M2 for five levels of volumetric moisture content (1 ns gating).

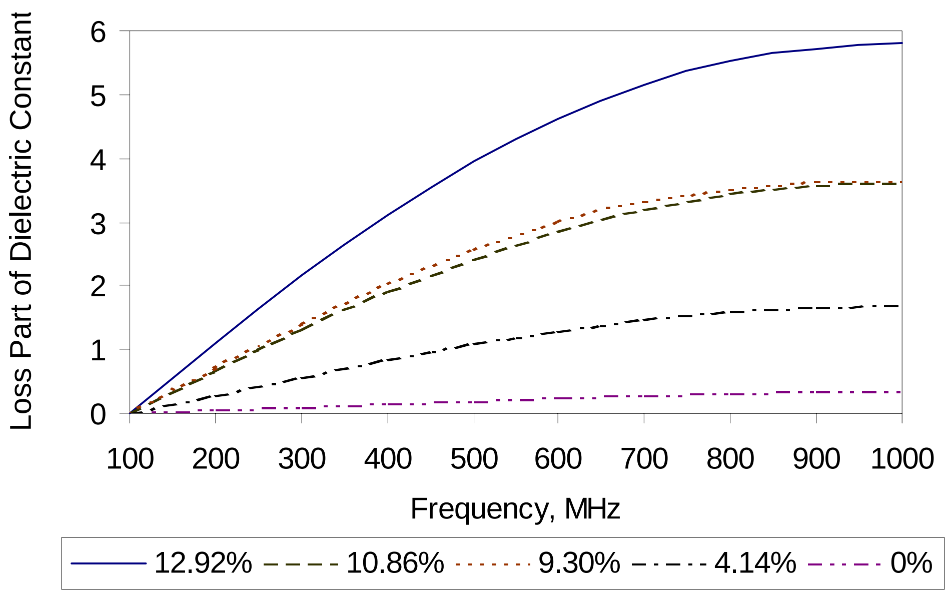


Figure F.44. Effect of frequency on the loss part of the dielectric constant for L4M2 for five levels of volumetric moisture content (1 ns gating).

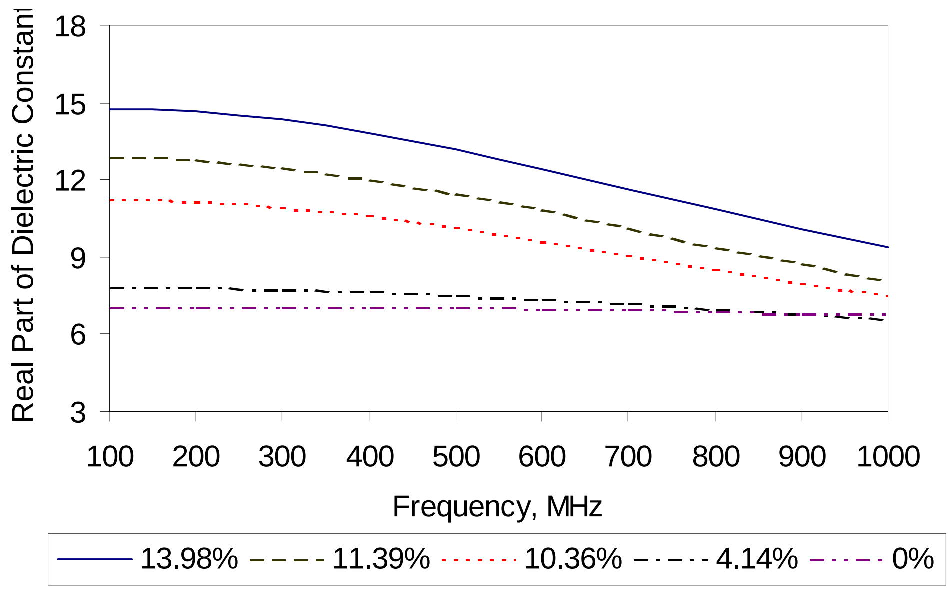


Figure F.45. Effect of frequency on the real part of the dielectric constant for L5M1 for five levels of volumetric moisture content (1 ns gating).

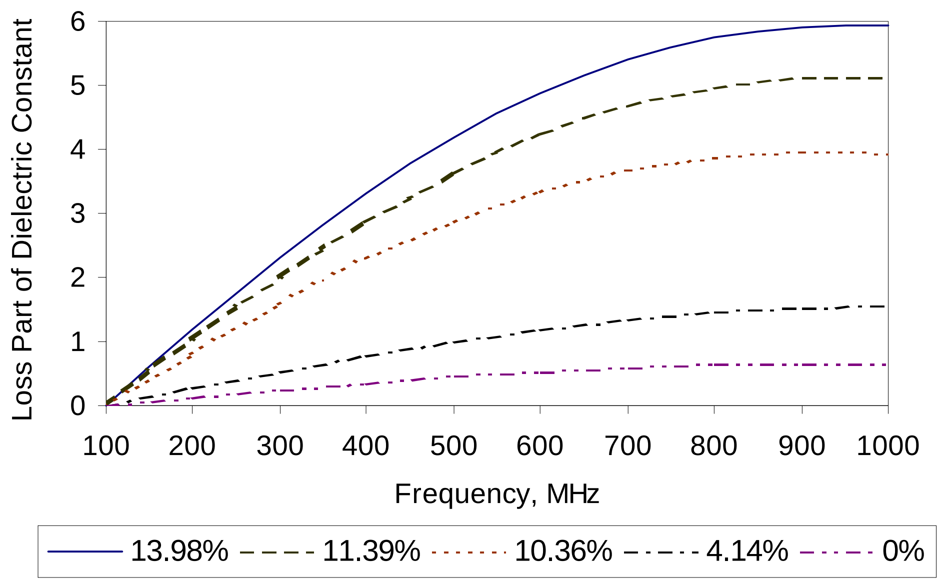


Figure F.46. Effect of frequency on the loss part of the dielectric constant for L5M1 for five levels of volumetric moisture content (1 ns gating).

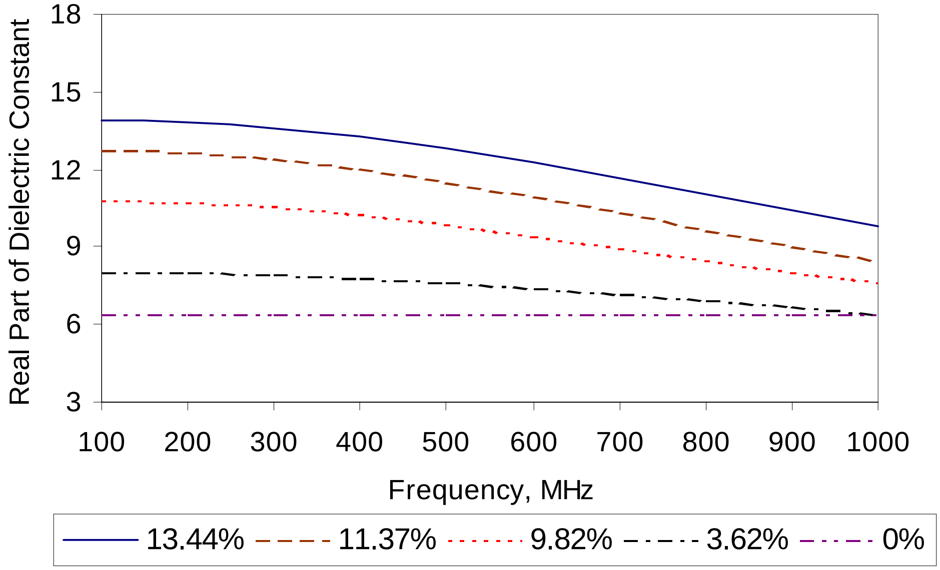


Figure F.47. Effect of frequency on the real part of the dielectric constant for L5M2 for five levels of volumetric moisture content (1 ns gating).

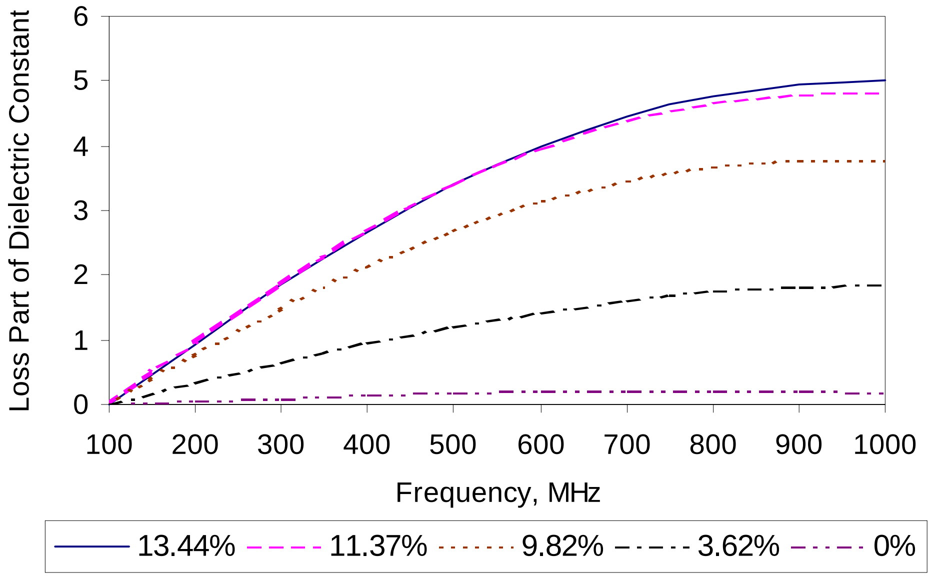


Figure F.48. Effect of frequency on the loss part of the dielectric constant for L5M2 for five levels of volumetric moisture content (1 ns gating).

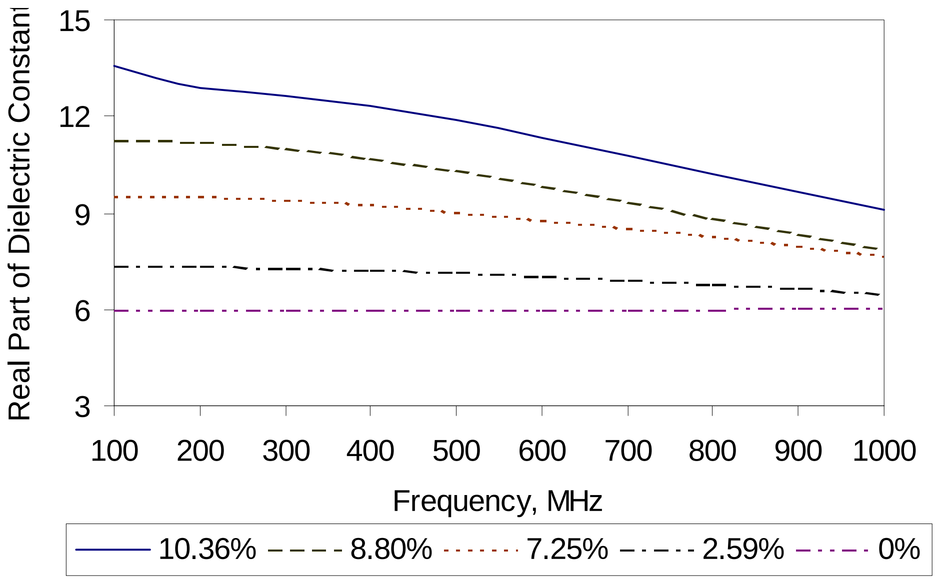


Figure F.49. Effect of frequency on the real part of the dielectric constant for G3N1 for five levels of volumetric moisture content (1 ns gating).

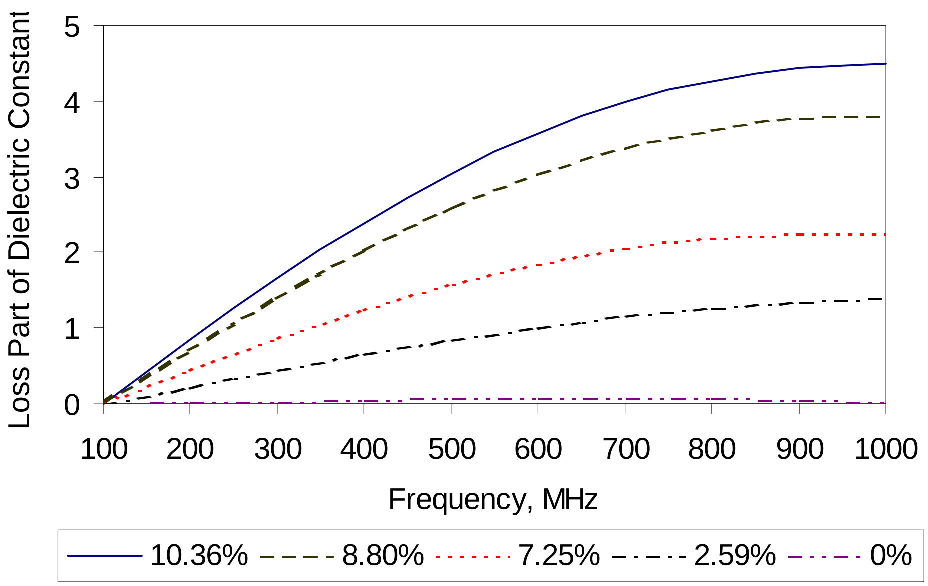


Figure F.50. Effect of frequency on the loss part of the dielectric constant for G3N1 for five levels of volumetric moisture content (1 ns gating).

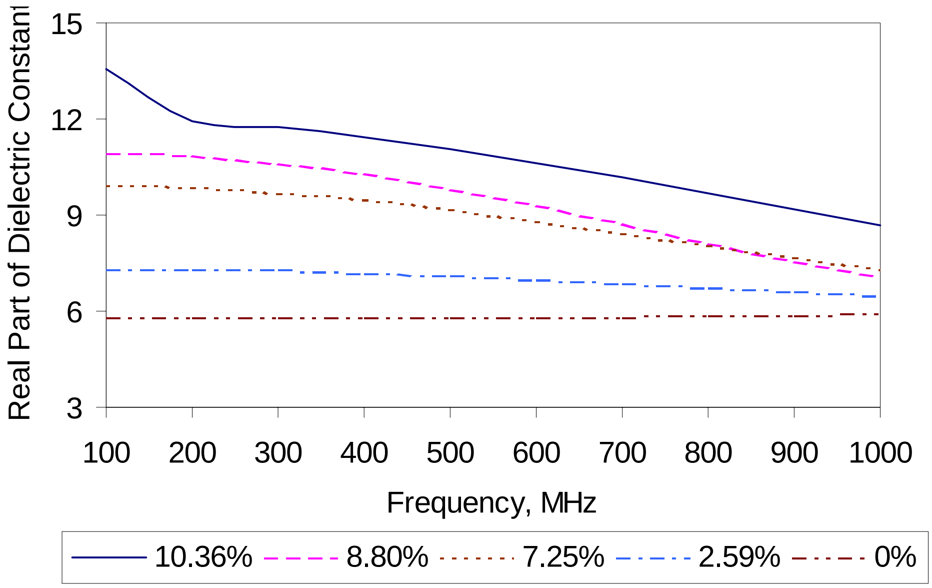


Figure F.51. Effect of frequency on the real part of the dielectric constant for G3N2 for five levels of volumetric moisture content (1 ns gating).

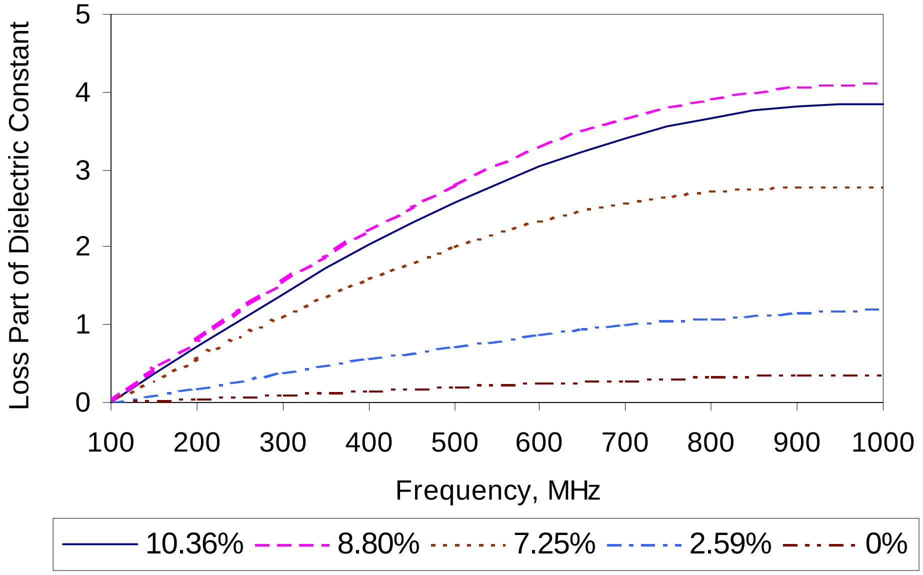


Figure F.52. Effect of frequency on the loss part of the dielectric constant for G3N2 for five levels of volumetric moisture content (1 ns gating).

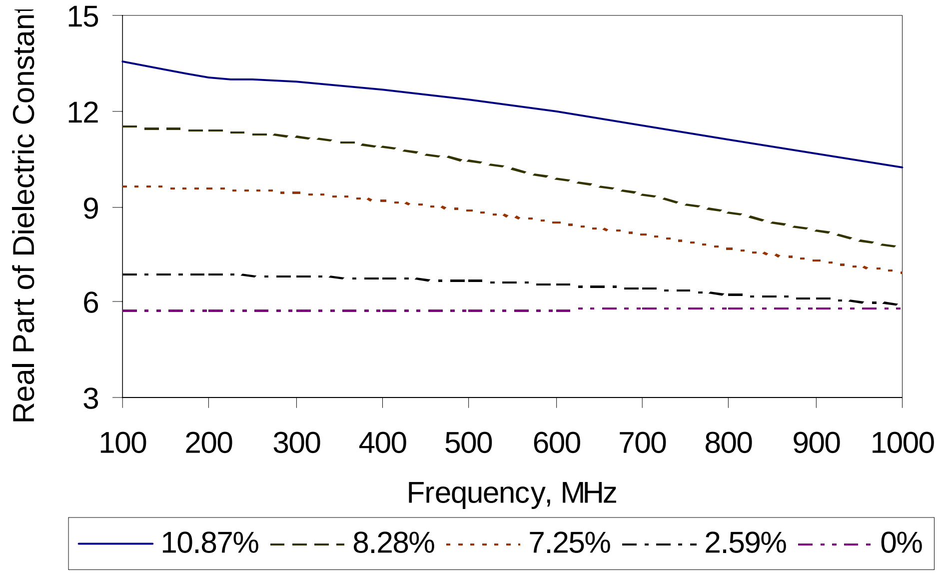


Figure F.53. Effect of frequency on the real part of the dielectric constant for G4N1 for five levels of volumetric moisture content (1 ns gating).

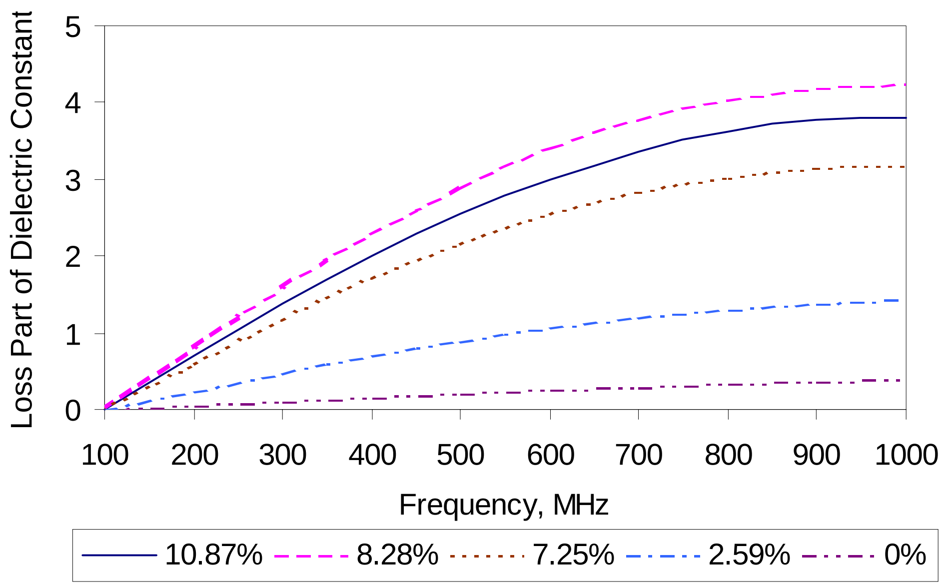


Figure F.54. Effect of frequency on the loss part of the dielectric constant for G4N1 for five levels of volumetric moisture content (1 ns gating).

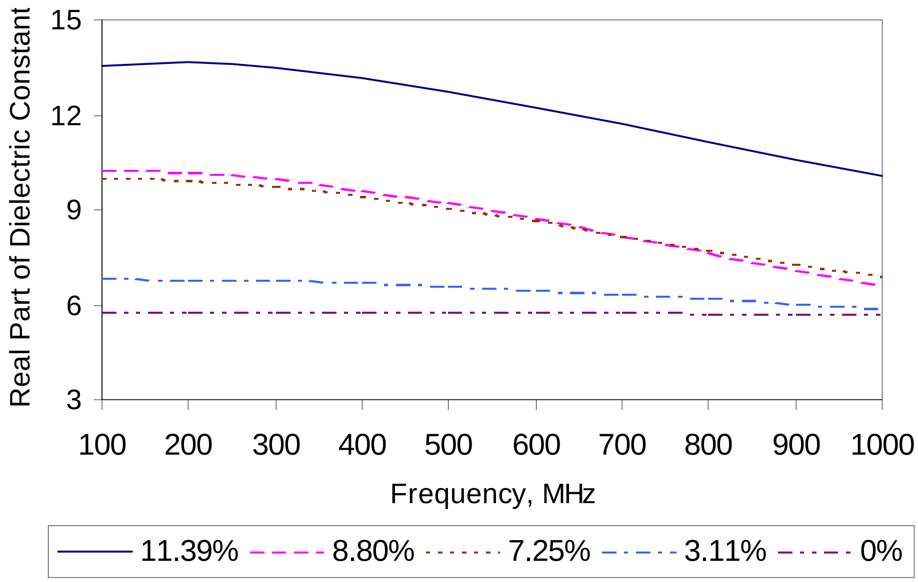


Figure F.55. Effect of frequency on the real part of the dielectric constant for G4N2 for five levels of volumetric moisture content (1 ns gating).

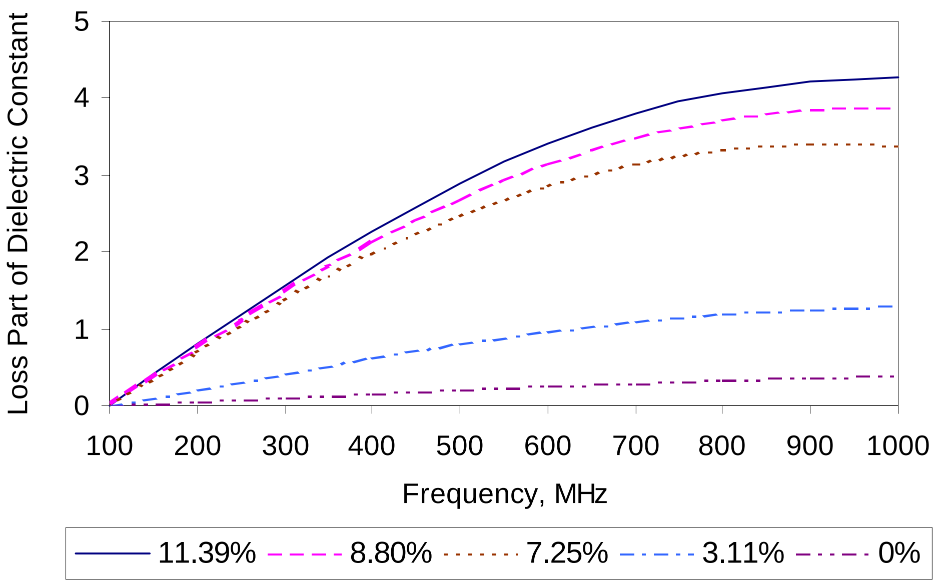


Figure F.56. Effect of frequency on the loss part of the dielectric constant for G4N2 for five levels of volumetric moisture content (1 ns gating).

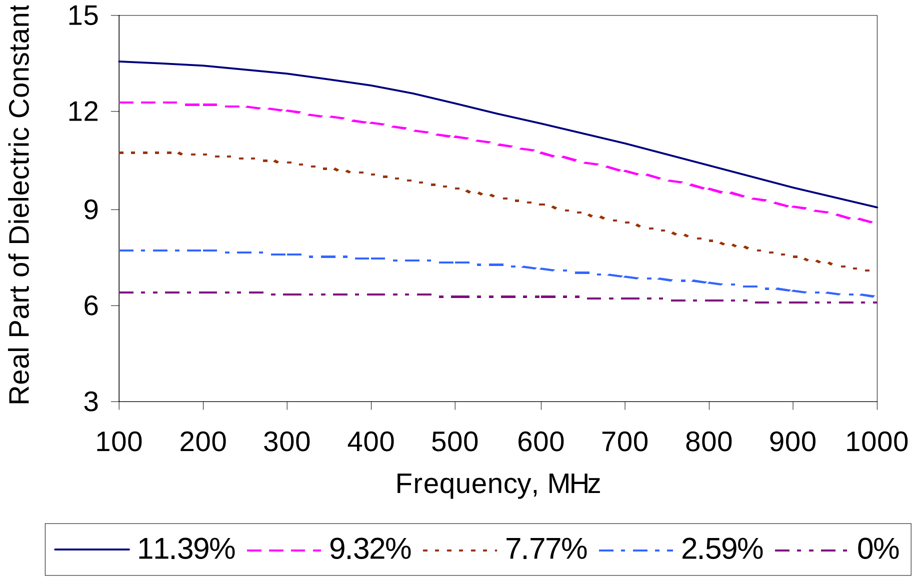


Figure F.57. Effect of frequency on the real part of the dielectric constant for G4C41 for five levels of volumetric moisture content (1 ns gating).

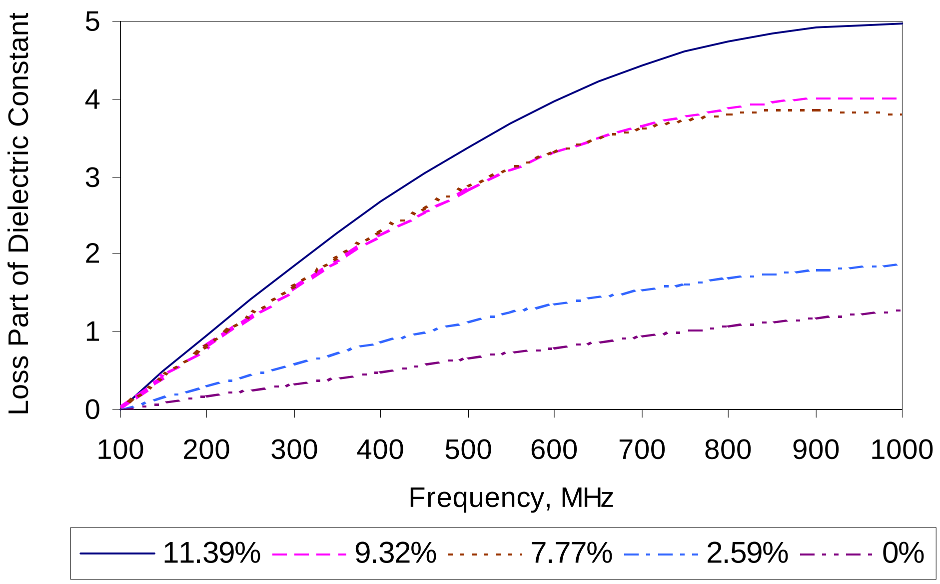


Figure F.58. Effect of frequency on the loss part of the dielectric constant for G4C41 for five levels of volumetric moisture content (1 ns gating).

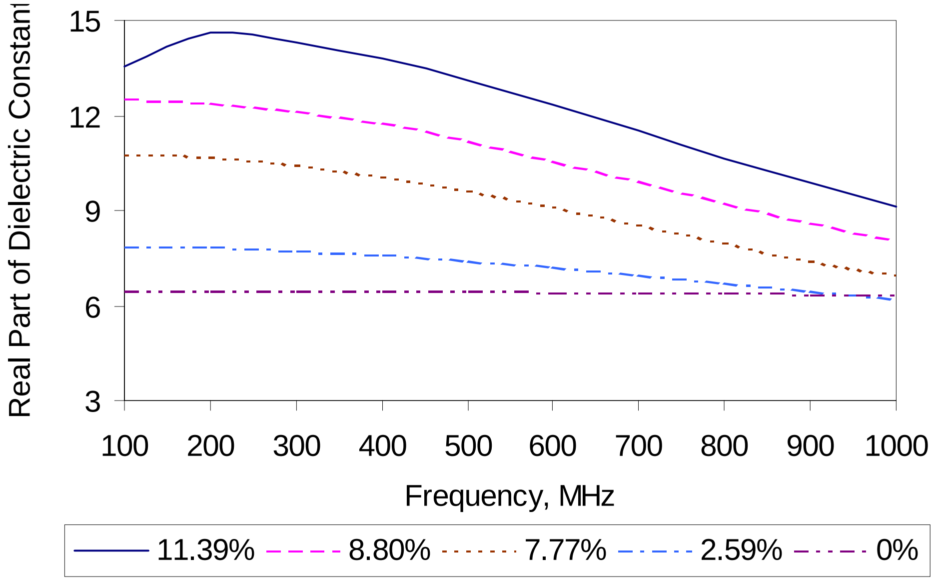


Figure F.59. Effect of frequency on the real part of the dielectric constant for G4C42 for five levels of volumetric moisture content (1 ns gating).

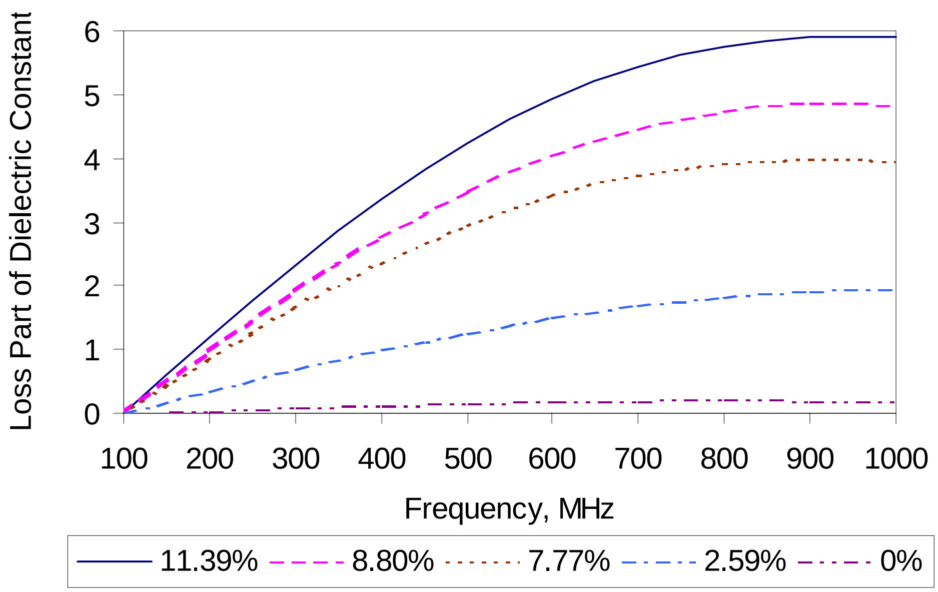


Figure F.60. Effect of frequency on the loss part of the dielectric constant for G4C42 for five levels of volumetric moisture content (1 ns gating).

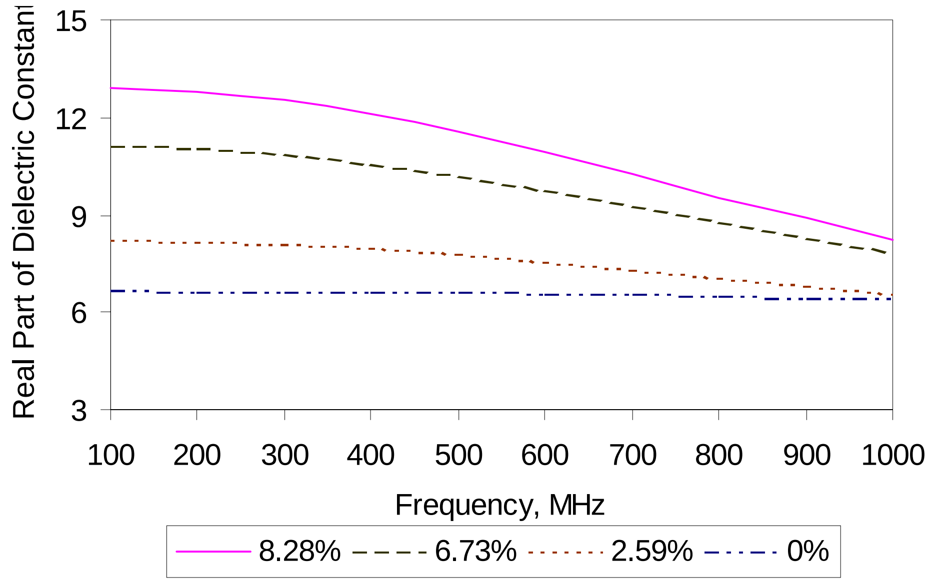


Figure F.61. Effect of frequency on the real part of the dielectric constant for G4C81 for five levels of volumetric moisture content (1 ns gating).

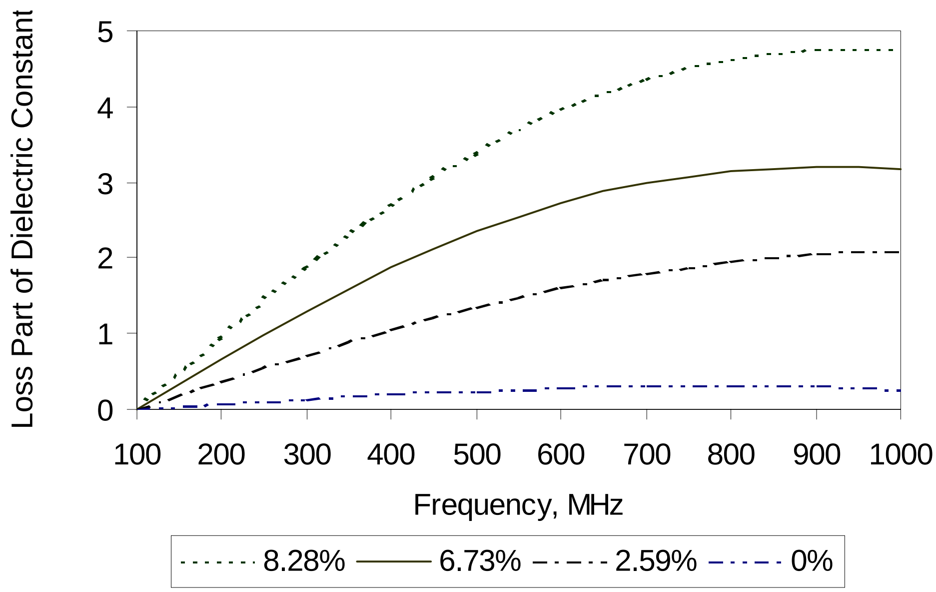


Figure F.62. Effect of frequency on the loss part of the dielectric constant for G4C81 for five levels of volumetric moisture content (1 ns gating).

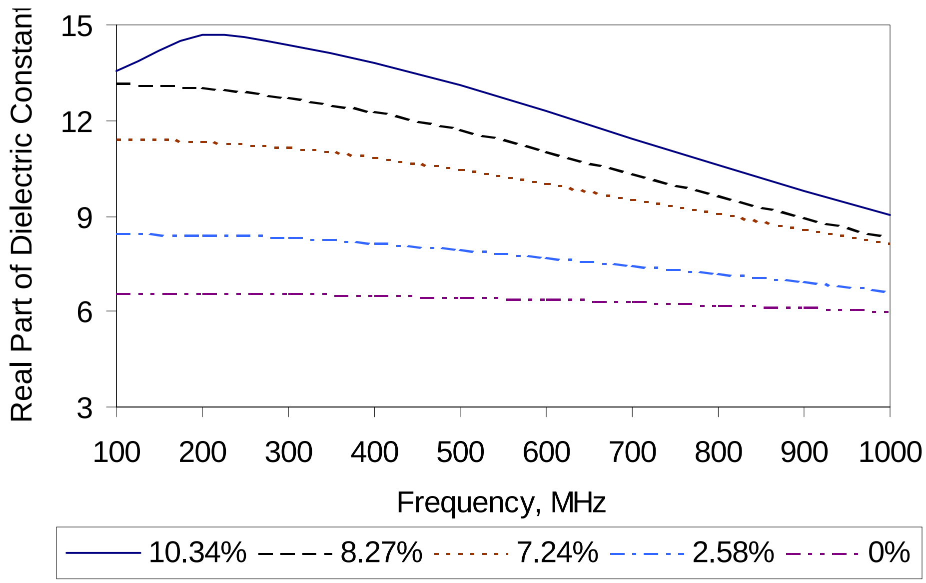


Figure F.63. Effect of frequency on the real part of the dielectric constant for G4C82 for five levels of volumetric moisture content (1 ns gating).

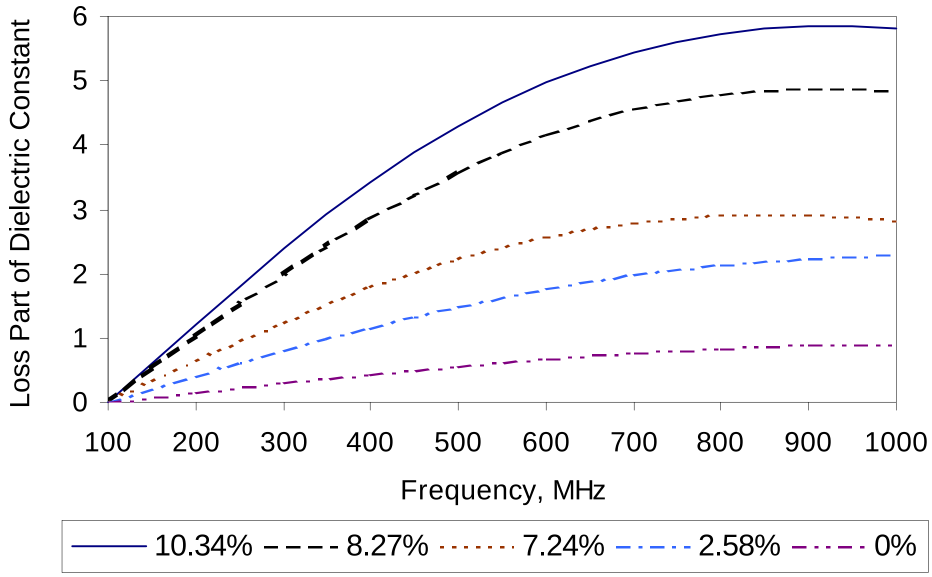


Figure F.64. Effect of frequency on the loss part of the dielectric constant for G4C82 for five levels of volumetric moisture content (1 ns gating).

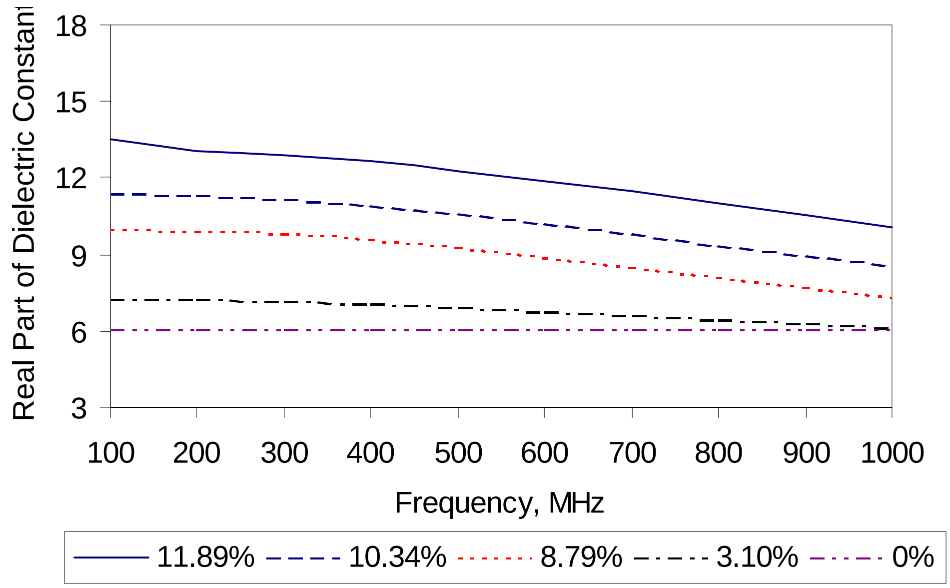


Figure F.65. Effect of frequency on the real part of the dielectric constant for G4M1 for five levels of volumetric moisture content (1 ns gating).

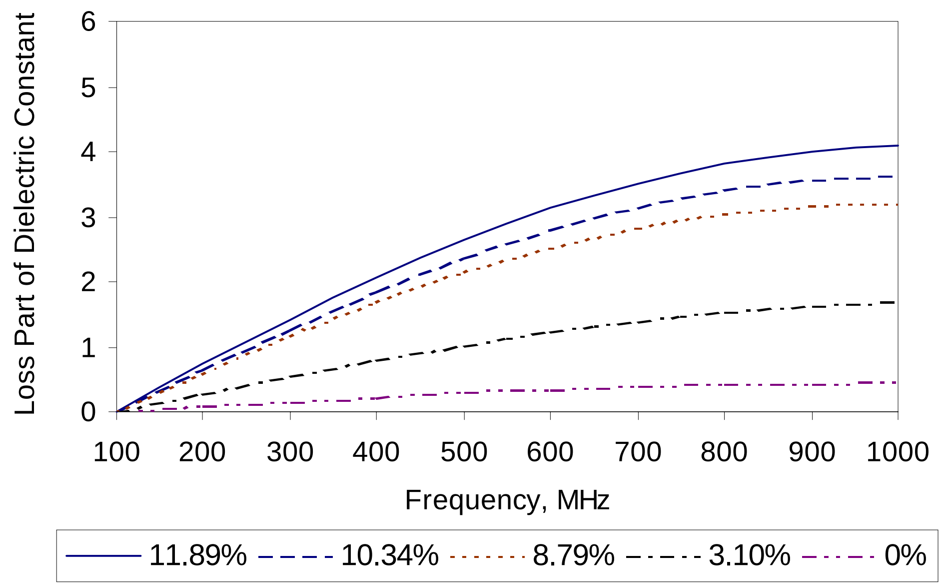


Figure F.66. Effect of frequency on the loss part of the dielectric constant for G4M1 for five levels of volumetric moisture content (1 ns gating).

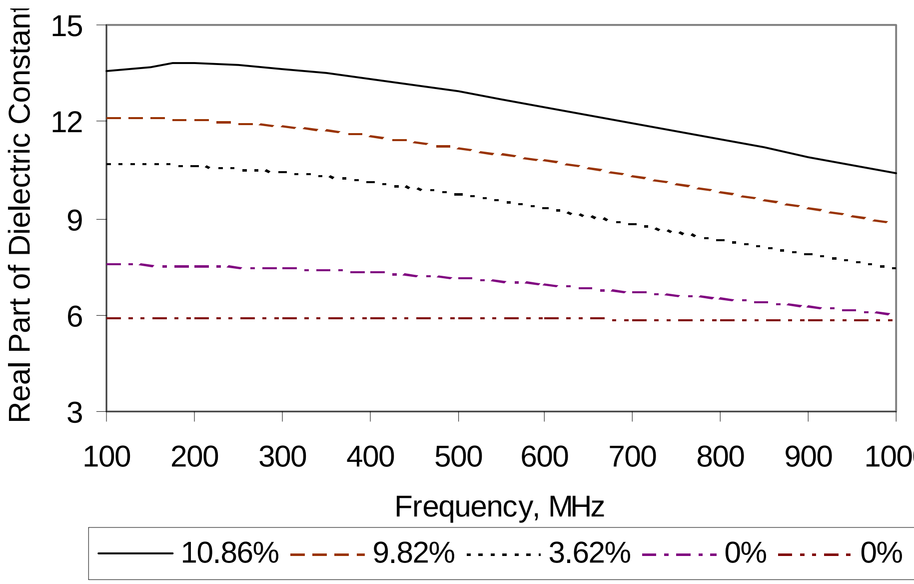


Figure F.67. Effect of frequency on the real part of the dielectric constant for G4M2 for five levels of volumetric moisture content (1 ns gating).

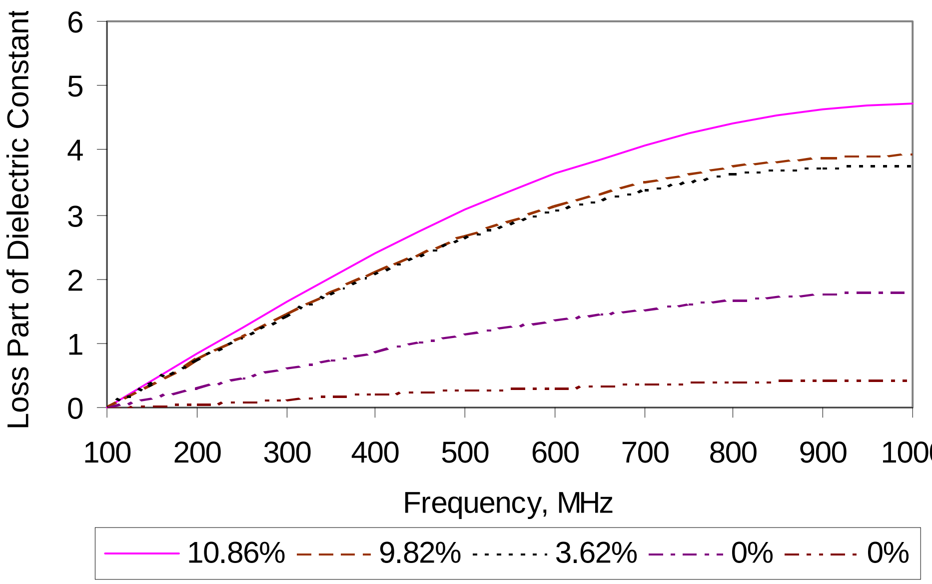


Figure F.68. Effect of frequency on the loss part of the dielectric constant for G4M2 for five levels of volumetric moisture content (1 ns gating).

# VITA

Kiran Satya Pokkuluri was born on March 27th, 1975 at Bhilai, India. He completed his high school at Kakatiya Vidya Niketan, Hyderabad, India. He received his Bachelor of Engineering degree in Civil Engineering in June 1996 from Osmania University, Hyderabad, India. He joined the Masters Program in Civil Engineering at Virginia Tech in January 1997. During his study there, he was a research assistant in The Civil Engineering Materials Program where he conducted research in nondestructive evaluation of civil infrastructure.